PHOTOGRAPH THIS SHEET

AD A995025

DTIC ACCESSION NUMBER

LEVEL

INVENTORY

AEC

WT-365

DOCUMENT IDENTIFICATION

Dtd Oct.-Nov 1951

DISTRIBUTION STATEMENT A
Approved for public release;
Distribution Unlimited

DISTRIBUTION STATEMENT

ACCESSION FOR
NTIS GRA&I [X]
DTIC TAB [ ]
UNANNOUNCED [ ]
JUSTIFICATION

Per Ltr. on File
(Nov. 1951)

BY
DISTRIBUTION /
AVAILABILITY CODES

DIST	AVAIL AND/OR SPECIAL	
A		

DISTRIBUTION STAMP

Release

DTIC
ELECTE
S OCT 8 1980 D
D

DATE ACCESSIONED

UNANNOUNCED

80 8 28 051

DATE RECEIVED IN DTIC

PHOTOGRAPH THIS SHEET AND RETURN TO DTIC-DDA-2

DTIC FORM OCT 79 70A

DOCUMENT PROCESSING SHEET

[redacted]

UNCLASSIFIED

WT-365
Copy 182 B

[redacted]

Operation

JANGLE

NEVADA PROVING GROUNDS
OCTOBER-NOVEMBER 1951

HIGH EXPLOSIVE TESTS

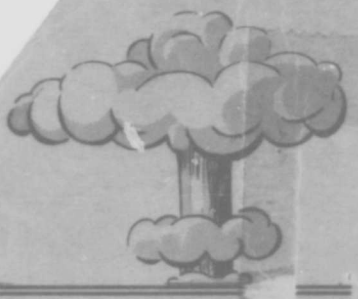

[redacted]

ARMED FORCES SPECIAL WEAPONS PROJECT
WASHINGTON, D.C.

[redacted]

RESTRICTED DATA

This document contains restricted data as defined in the Atomic Energy Act of 1946. Its transmittal or the disclosure of its contents in any manner to an unauthorized person is prohibited.

This document contains information affecting the national defense of the United States within the meaning of the Espionage Laws, Title 18 U. S. C. Sections 793 and 794. The transmission or the revelation of its contents in any manner to an unauthorized person is prohibited by law.

SWC 9 S54428

UNCLASSIFIED [redacted]

WT-365

This document consists of 319 plus 4 pages (counting all preliminary pages in all reports and all unnumbered blanks)

No. 182 of 243 copies, Series B

OPERATION JANGLE

HIGH EXPLOSIVE TESTS

Project 1(9)-1 Scaled HE Tests (WT-377)

Project 1(9)-2 Composition of Clouds Formed by TNT Explosions (WT-349)

Project 1(9)-3 Tests and Observations on Craters and Base Surges (WT-410)

Project 1(9)-4 Base Surge Analysis for HE Tests (WT-339)

Classification cancelled (or changed to Un) by authority of Sandia Ltr 12/2/58 Rf Copy by E B Moncini 30 Mar 62
Name & Grade of Officer making change Date

file copy 180

UNCLASSIFIED

UNCLASSIFIED

[redacted] [redacted]

OPERATION JANGLE

PROJECT 1(9)-1

SCALED HE TESTS

By

E. B. Doll and V. Salmon

April, 1952

STANFORD RESEARCH INSTITUTE
STANFORD, CALIFORNIA

[redacted]

CONTENTS

[redacted]

[redacted]

ILLUSTRATIONS

TABLES

ABSTRACT

This series of four HE tests at the Nevada Test Site was conducted to provide information for scaled predictions for the shallow underground and surface nuclear tests. The results of the HE tests were quite satisfactory, and predictions were made only if justified by the demonstrated adherence to scaling laws within the HE test series. In addition, correlation with results from 1951 Dugway tests in dry clay was obtained.

In general, the air blast scaled as predicted in both duration and amplitude. Acceleration scaling was good for the amplitude of the first smoothed pulse, but the durations did not scale. The sharp and highly damped oscillation acceleration due to air blast scaled as did air-blast pressure, but its period, as expected, increased less rapidly than the scale factor. Some preliminary particle velocity and permanent displacement information was obtained, but proved not to scale suitably to permit predictions.

Air-coupled phenomena were prominent due to the relatively shallow scaled charge depths, and appeared to predominate in earth accelerations at large distances. Analytical work on this topic should aid in explaining many of the effects observed.

A comparison with Dugway results (for dry clay) from similar tests indicates that the earth-acceleration amplitudes and durations were approximately inverse to each other for the two soils, with the Dugway amplitudes considerably less than for the HE program. This cannot be explained by a simple soil constant, and probably indicates that much depends on details of the transfer of energy from the expanding gas bubble to the soil. The assumption of considerable cohesion in Dugway soil gave a qualitative explanation to many of the observations.

[redacted]

CHAPTER 1

INTRODUCTION

1.1 OBJECTIVE

The four high explosive tests at the Nevada Test Site during August and September 1951 were conducted for the following principal purposes:

1. To establish a better basis for the prediction of corresponding phenomena from anticipated larger explosions under similar conditions at the same test site. In particular, predictions for the surface and underground nuclear tests were required.

2. To establish correlation between future explosion tests at this site with similar tests conducted at the Dugway Proving Ground.

3. To obtain additional information on air-earth coupling as a function of the charge depth.

4. To obtain additional information in the general field of underground explosion phenomena with respect to such items as attenuation characteristics, wave forms, and scale and model laws.

1.2 HISTORICAL

In planning the underground nuclear test at the Nevada Test Site, several differences were anticipated between it and previous underground explosion tests. Important differences were considered to be (1) the type of explosion (2) the relatively shallow scaled depth of burial, and (3) the characteristics of the soil. For purposes of more properly estimating the behavior and magnitude of the phenomena to be expected from the underground nuclear test, a scaled high explosive (HE) test of 40,000 pounds of TNT was planned at the same location. Later designated as HE-2, this test was intended to provide gage setting information for the underground nuclear test and to give some basis for correlation with the large HE underground tests at other locations. However, because of uncertainty as to the phenomena even in this case, it was decided to add a smaller test, later designated as HE-1, of 2560 pounds of TNT. Moreover, these two tests were planned on a scaled basis so that the applicability of the model law could be estimated. These two HE tests utilized the same charge sizes and constructions as were employed in the 1951 underground explosion test program at the Dugway Proving Ground.[1,2,3]*

*Superscript numbers refer to references given in the Bibliography at the end of this report.

[redacted] [redacted]

To this basic HE program was next added a 2560-pound surface shot, to provide predictions for the surface nuclear test. This was designated as HE-4; it also served to indicate the difference between just-above and just-below surface detonations. Finally, a fourth test, designated as HE-3, was added to the HE program. This 2560-pound test was chosen to be identical to Dugway Round 312, which was representative of the principal Dugway program using a considerably greater scaled charge depth than that contemplated for the underground nuclear test.

Thus the Scaled HE Tests were evolved. The four tests permitted the possibility of a variety of correlations and comparisons. Table 1.1 outlines these comparisons between any two tests, designated as Test A and Test B.

TABLE 1.1

Correlation of Tests

Test A	Test B	Correlation
Dugway Round 312	HE-3	Soil type
HE-3	HE-1	Scaled depth of charge (λ_c)
HE-1	HE-2	Scale factor (S = 2.5)
HE-2	Underground nuclear	Scale factor (S = 3.68 for 1 KT and S = 10.0 for 20 KT)
HE-2	Underground nuclear	Explosive type (HE vs. nuclear)
HE-1	HE-4	Scaled depth of charge (λ_c)
HE-4	Surface nuclear	Scale factor (S = 9.2 for 1 KT and S = 25.0 for 20 KT)
HE-2	Dugway Round 315	Soil type - for 40,000 lb. of TNT (using HE-3 : HE-1 correlation for effect of scaled depth of charge)

This report is concerned with these four HE tests. As a group they can be considered as part of a continuing experimental program devoted to the study of underground explosion phenomena. Extensive pioneer work performed during World War II has been reported by Lampson.[4] Lampson's work involved several different soil types and

was concerned principally with the effects of small charges, mostly below 100 pounds of TNT; a few tests were made up to 1000 pounds. A later series of tests was conducted under the sponsorship of the Office of the Chief of Engineers, U. S. Army, in a program entitled "Underground Explosion Tests."[1,2,3] This program included measurements in soils of several types at the Dugway Proving Grounds in Utah. However, no measurements were made in a soil type of characteristics sufficiently close to those at the Nevada Test Site to permit valid enough predictions.

1.3 THEORETICAL

A simplified discussion of the model law as normally applied to explosion phenomena is presented here principally to familiarize the reader with the nomenclature that will be used in the main body of this report. If all dimensions of an experiment are increased by a factor S, where S is designated as the scale factor, and if it is assumed that all times describing the experiment are increased by this same factor S, the model law or scale relations for the various phenomena concerned can be derived by simple dimensional analysis. The model law is known to be invalid under some conditions, such as when the velocity of propagation is a function of the rate of application of stress, when viscosity effects exist, when the effects of gravity are important, etc. However, extensive scale tests using small TNT charges have indicated good model law behavior for underground explosion phenomena, particularly for reasonable scaled charge depths, where the effects of venting into a completely different medium are reduced or eliminated.

If all dimensions of an explosive charge are changed by a factor S, the scale factor is then equal to

$$(W_2/W_1)^{1/3},$$

the cube root of the ratio between the explosive charge weights. As a consequence, the cube root of the charge weight in pounds is a convenient quantity to use in describing the scale of an experiment, and the ratio of the cube root of the weights of two charges is generally considered to be the scale factor between the two tests. It is convenient to use the symbol λ in describing the dimensions of an experiment wherein λ is designated as follows:

$$\lambda = R/W^{1/3},$$

where R is a length in feet and W is the charge weight in pounds of TNT of equivalent energy release. In this report, λ refers specifically

to horizontal distances measured from ground zero. The term λ_c describes the charge depth, and the term λ_g describes the gage depth. To obtain distances in feet, λ is multiplied by the cube root of the explosive charge weight in pounds of equivalent TNT.

When the dimensional analysis referred to above is applied to the various phenomena of interest, it is found that at scaled distances (corresponding values of λ) and at scaled times, the pressure and particle velocity are independent of charge size or scale factor, S; impulse is proportional to S; particle acceleration is inversely proportional to S; and particle displacement is proportional to S. In this report, model law behavior is considered in accordance with these relationships. No attempt has been made to derive empirical scale laws, since inadequate experimental data were available for such a derivation, and no adequate theory was available to support conclusions which might be reached in this manner.

Every effort was made to conduct the HE tests under proper scaled or model law conditions. However, the vagaries of nature make it impossible to find a homogeneous earth medium for the experiments. For small charges, a slowly changing irregularity such as increase of seismic velocity with depth will have little effect. This is because in the region of military interest the transmission of earth motion is along a near-surface path with practically constant velocity. For large charges, however, the path embraces a considerable variation in seismic velocity, with consequent change of transmitting properties, direction of arrival, and the like. This difficulty could be even more pronounced in the presence of faults, reflecting layers, hard rock boundaries, and water tables at distances comparable to those used for describing the experiments. Of course, these deviations from homogeneity make it necessary to modify the simple method of application of the normal model law except for small charges. An important fact which a carefully controlled test program should reveal is the charge size and depth of burial above which these effects become significant.

When the statement is made that a certain phenomenon follows the scaling laws, it must be noted that this refers to the total phenomenon, and not merely to selected aspects of it. Thus if the earth acceleration is known as a function of time and position, in true scaling the acceleration function for a similar scaled experiment can be predicted directly. As applied to HE-1 and HE-2, if a comparison of amplitude and time variables indicates the same scale factor for a variety of aspects of the acceleration, then there is reinforced justification for extrapolation of results. But if the scale factors for amplitude and time differ from each other, or are markedly different from the known value (here 2.5), then confidence in extrapolation must decrease. If

empirical scaling laws are derived, then the test of their validity is the universality of their application to all aspects of the phenomena in the class for which they are intended. In this report, departures from normal scaling will be used only to estimate rough upper or lower limits.

Since the principal purpose of these scaled high explosive tests was to permit an estimate of corresponding phenomena from anticipated nuclear explosions, some consideration should be given to the different explosive characteristics. A direct application of the model law between high explosive tests and nuclear tests having yields described in equivalent pounds of TNT must assume an explosive configuration equivalent to that of TNT. It is at once obvious that the explosive source characteristics of a nuclear charge are not equivalent to those of a TNT charge. In other words, in a strict sense, the dimensions of the experiment do not obey the assumed model law relationship. The hydrodynamics and thermodynamics of the expanding gas bubbles are obviously different for the two types of explosives.[5] It is suspected that the effect of these differences is even more pronounced for the relatively shallow charge depths involved, since the energy relations in the venting processes can readily be affected by the thermodynamic conditions in the gas bubbles. Furthermore, there is no reason to assume that all physical output characteristics of a nuclear explosion can be expected to be described by a single equivalent energy release. It is quite conceivable that the equivalent yield of a nuclear explosion can be a function of the phenomenon that is used to judge this yield; for instance, the equivalent yield for thermal and radiation effects will obviously be different from the equivalent yield for such mechanical effects as pressure and acceleration.

In this report, no consideration has been given to the inherent differences between nuclear and TNT explosives. All estimates herein obtained for nuclear explosives by upward scaling of TNT tests are, in fact, in terms of a charge of one KT of TNT.

The experiments described in this report were intended only to investigate the ground motions, ground pressures, and air pressures produced by the underground explosions. This report is not concerned with cratering, throwout, rupture zones, etc. Ground motion can be described in terms of either displacement, particle velocity, or acceleration as functions of time. If one of these phenomena is known precisely, the other two may be determined by integration or differentiation. On the other hand, such processes are subject to large errors and are lengthy, laborious, and expensive.

Given a choice, it would probably be most desirable to measure particle velocity as a function of time, with particle displacement a

satisfactory alternative. The choice of the quantity measured depends essentially upon the ratio of the characteristic period of the earth motion to that of a typical structure being attacked. For small charges, this ratio is considerably less than unity, and a simple analysis indicates that earth displacement is the principal factor determining structure deformation. As this ratio approaches unity for progressively larger charges, earth particle velocity becomes the principal factor that determines structure deformation. Finally, for very large charges the ratio of earth motion to structure period will increase considerably beyond unity. Earth acceleration then becomes the quantity from which structure deformations may be most readily estimated. For these tests, practical considerations of availability and reliability led to the use of accelerometers. Hence, this report is concerned principally with earth motion as it can be described by acceleration. In due course of time, adequate study, including integration of the acceleration records, will permit a better evaluation of the military effects of the ground motions.[3]

A considerable uncertainty exists with respect to the mechanism to be used to measure "free earth pressure". It is probably improper to describe earth pressure as hydrostatic, since the phenomena must necessarily be tensorial in nature, and be a function of direction. On the other hand, extensive previous experiments (references 2, 3, and 4) have been conducted using a simplified hydrostatic technique for earth pressure measurements. Principally for correlation purposes, these same techniques were adopted for the experiments described herein.

In the small charge work of Lampson,[4] the earth pressure gage depths were usually greater than

$$3W^{1/3}/2.$$

This gage depth, $\lambda_g = 1.5$, would require holes 190 feet deep for a 1 KT test and 510 feet deep for a 20 KT test. Such gage depths were completely impractical, and consequently the earth pressure measurements reported herein were obtained in holes that were very shallow on a scaled basis as compared with those used by Lampson. Furthermore, the scaled charge depths used for these experiments were very much less than those used by Lampson, and the direct effect of air blast on the open-hole earth pressure measurements could be expected to be more pronounced. At this time, the authors know of no adequate theoretical background supporting the techniques used for the earth pressure measurements and correlation methods by which these earth pressure measurements can be converted to directly useful military effects.

[redacted]

CHAPTER 2

TEST DESCRIPTION

2.1 SITE

The HE test site was located between the sites chosen for the later surface and underground nuclear tests. Except for local variations, the site was chosen to be representative of the specific localities to be used for the underground and surface nuclear tests. For all practical purposes, the test area was flat. The soil appeared to consist of extremely fine, powder-like sand mixed with some gravel. Below the surface there were one or more streaks of localized "caliche" deposits (caliche is a hard cemented conglomerate of geologically recent origin). The sub-surface soil was tightly packed, very dry, and extremely porous. There was no water table, and bedrock was said to be at a depth of greater than 1,000 feet. Preliminary seismic survey data gave the following results for the seismic velocity and soil constant.[4]

Depth ft	Seismic Velocity fps	Soil Constant[4] lb/sq in
0 - 100	3,000	8,400
100 - 350	4,000 - 4,500	15,000 - 19,000
350 - 1,000	5,000 - 5,500	23,000 - 28,000

Complete geological surveys of the test site have been conducted. The results are published in the series of JANGLE reports as Project 1(8)a Report, "Geologic, Hydrologic and Thermal Features of the Site", U. S. Geological Survey; and Project 1(8)a-1 Report, "Seismic Refraction Survey", by United Geophysical Co., Inc.

2.2 EXPLOSIVE CHARGES

The four explosions with which this report is concerned were as follows:

[redacted] [redacted]

Test Number	Pounds of TNT W	$W^{1/3}$	Depth of Charge ft	λ_c	Date
HE-1	2,560	13.7	1.9	0.150	August 25, 1951
HE-2	40,000	34.2	4.7	0.150	September 3, 1951
HE-3	2,560	13.7	6.9	0.5	September 15, 1951
HE-4	2,560	13.7	-1.9	-0.150	September 9, 1951

The explosive charges were composed of 100-pound TNT blocks stacked to approximate a sphere. The gage lines were perpendicular to one of the flatter sides of the stack. On HE-1 and HE-2 the charge depth was such that the top of the charge was essentially flush with the ground surface. On HE-4 no excavation was made for the charge, and the bottom of the TNT sphere was flush with the ground surface (surface shot). The charge depth was measured to the center of the charge, and λ_c represents the ratio of the charge depth in feet to the cube root of the charge weight in pounds of TNT.

Tests HE-1 and HE-2 were designed to be direct scaled experiments of the underground nuclear test. Test HE-3 was designed to be similar on a scaled basis to the majority of the OCE Underground Explosion Tests,[1,2,3] and to be identical to Round 312 of the Dugway dry clay portions of that program. Test HE-4 was designed to be a scaled experiment of the surface nuclear explosion. In this case, the scaled height of the charge center was greater than that ultimately used for the surface nuclear test, because of the different geometry of the two explosive types.

Figure 2.1 shows the explosive charge positions with respect to the ground surface for each test, where the charges are idealized in the form of equivalent spheres of TNT. At the charge depth of 17 feet chosen for the 1.0 KT underground test, the equivalent TNT sphere would be approximately tangent to the earth's surface, as shown for HE-1 and HE-2.

2.3 GAGE LINE

The HE-2 gage line was arranged to be parallel to the major gage lines to be used for the underground and surface nuclear tests. The gage line used for HE-1, HE-3, and HE-4 made an angle of approximately 30° with the HE-2 line. Figure 2.2 illustrates the general test area and gage line layout in the four tests.

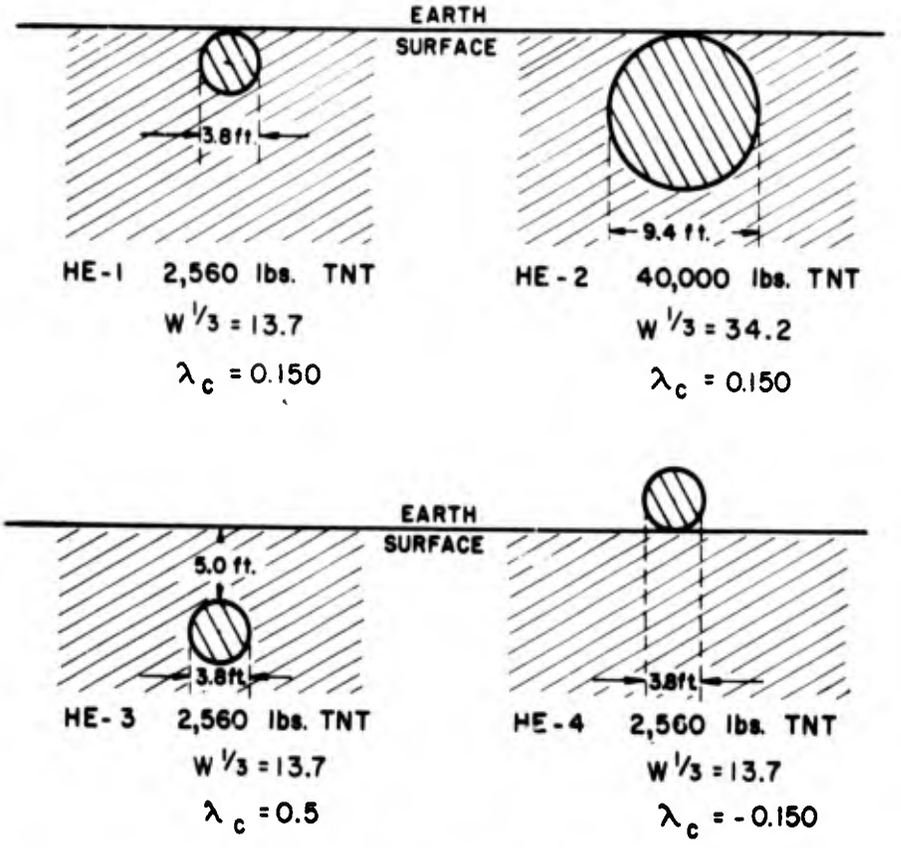

Fig. 2.1 Charge Geometry

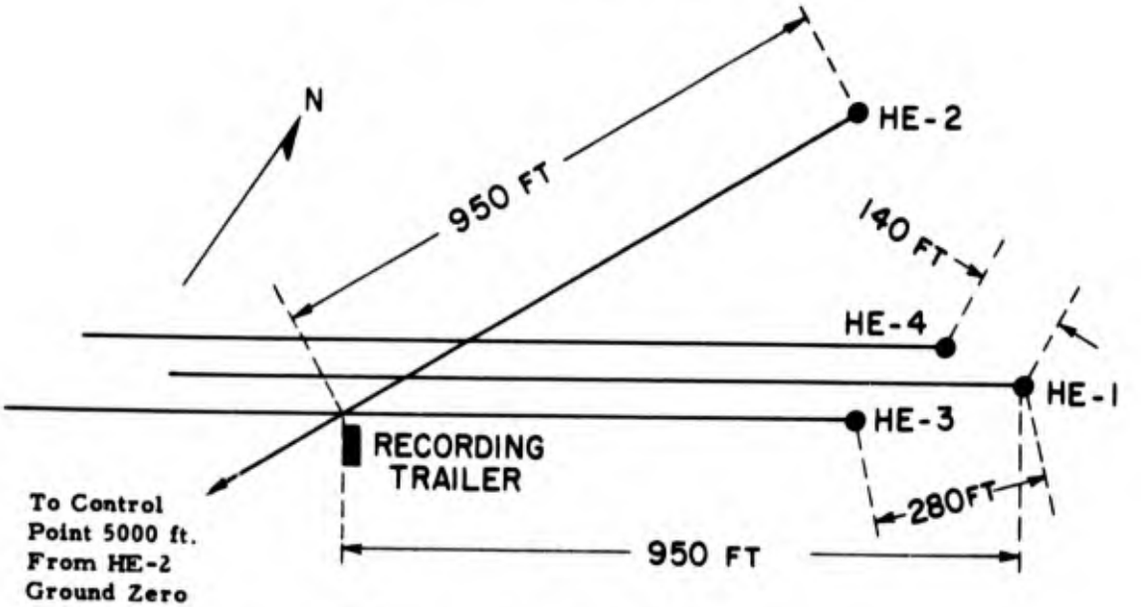

Fig. 2.2 Blast Line Layout

PROJECT 1(9)-1

The principal earth acceleration measurements were made at a gage depth of five feet. Two components of acceleration were measured, the horizontal radial component and the vertical component. Earth acceleration measurements were made at ranges varying in λ-values from 2.08 to 108, with the principal concentration of instruments in the region less than 12. The region of direct military interest is undoubtedly less than this, but the experiment incorporated the larger ranges to investigate transmission effects over distances in feet which correspond to $\lambda = 5$ for an equivalent charge of 20 KT. In addition, two-component earth accelerometers were included at gage depths of 17, 34, and 68 feet at λ-values of 3.0, 11.1, and 30.0 on the HE-2 test.

Earth pressure measurements were made at a gage depth of five feet at λ-values ranging from 1.72 to 40, with the principal concentration in the region λ less than 10. In addition, earth pressure gages at depths of 17 and 34 feet were included at $\lambda = 1.72$ for HE-2 and at depths of 17 feet, 34 feet, and 68 feet for λ-values of 3.0 and 11.1 for test HE-2.

Air pressure measurements were made at a height of 14 inches above the ground surface at distances ranging from $\lambda = 2.5$ to 75. Previous measurements at Dugway[2,3] indicated no significant difference in pressure as a function of height above the ground up to a scaled gage height of $\lambda_g = -0.3$ (10 feet for HE-2, 38 feet for 1 KT, and 100 feet for 20 KT).

The five-foot deep accelerometers were on a radial line for each test, and the remaining instruments were located as close as possible to this same line.

The detailed gage pattern is clearly evident in the tables of test results found in Chapter 4.

[redacted]

CHAPTER 3

INSTRUMENTATION

3.1 VARIABLE-RELUCTANCE GAGES

The gages used to measure earth acceleration, earth pressure, and air pressure all contain the same variable-reluctance transducer element (Figure 3.1), differing only in the mechanism used to actuate the movable unbalance between the two coils, which have equal inductance when the armature is in its neutral position. Each coil has a nominal inductance of 20 millihenries, and the two in series have an impedance of about 500 ohms at the 3000 cps carrier frequency, since they are connected in opposing polarity.

Figure 3.2 illustrates one complete variable-reluctance gage channel. The gage is connected to its coupling unit by a shielded three-conductor microphone cable, up to 1,000 feet in length. The 3000-cps carrier power is supplied at a level of 20 volts from an oscillator of very low source impedance. Gage unbalance produces a signal at the input to the ring demodulator, which rectifies the signal while preserving the polarity (or sense) of the gage unbalance. The carrier filter removes the residual carrier voltage and its harmonics from the input, producing a current which is a true reproduction of the gage unbalance modulation from zero frequency to about 1000 cps.

For calibration a known voltage may be injected across the capacitor C. The galvanometer calibration deflection recorded thus includes effects due to oscillator voltage variation, as well as attenuation, gage impedance, and so forth.

At rated mechanical input to the gage, the rectified output current is 7 ma. A balanced 85-ohm attenuator terminates the coupling unit, permitting the adjustment of the recording current level. The over-all variable-reluctance gage system is essentially linear up to an output current of 10 ma, or about 150 per cent of gage rating. The large linear unbalance permitted by this gage system eliminates the use of signal amplifiers and produces an excellent signal to background ratio. Under the actual field conditions of the explosion tests, including cable agitation due to air blast and ground motion, the background or noise level was at least 60 db below rated output.

[redacted]

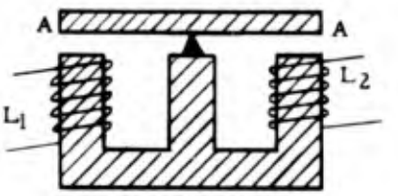

Fig. 3.1 Basic Variable-Reluctance Element

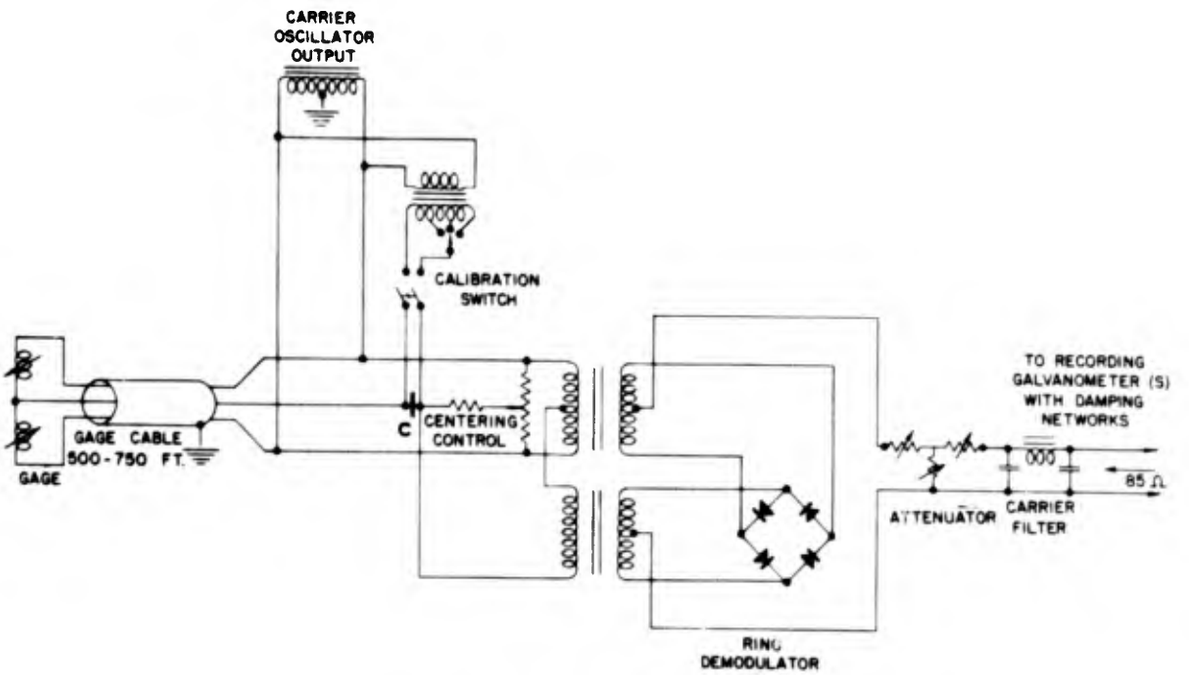

Fig. 3.2 Typical Gage Channel

[redacted]

Fig. 3.3 Interior of Instrument Trailer

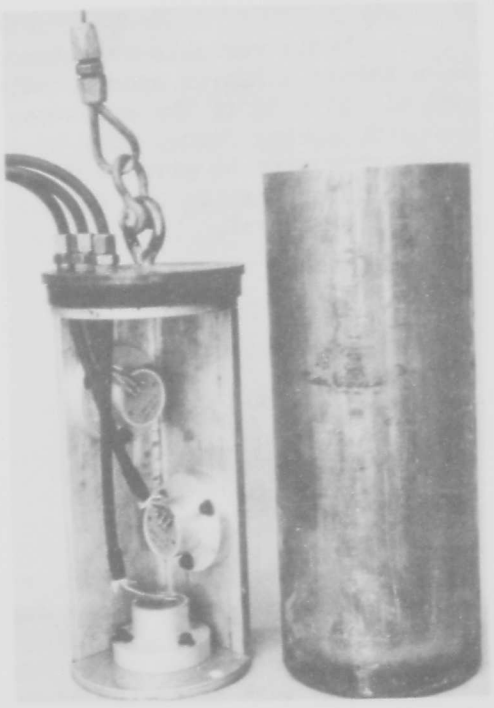

Fig. 3.4 Accelerometers Mounted in Canister

A single power oscillator was used to supply 12 gage channels. The upper section of the right-hand relay rack in Figure 3.3 is a complete 12-channel system. The upper panel contains the individual centering controls to balance the gages under static conditions. The second panel is the 12-channel coupling unit, including a tap switch for adjusting the calibration voltage and the 12 attenuators to set the recording level independently for each channel. The third panel is the power oscillator which supplies carrier voltage for 12 gages. Six such assemblies were used, giving a total of 72 variable-reluctance gage channels. The two oscillograph cameras in the foreground are described later.

3.2 EARTH ACCELERATION

The basic variable-reluctance transducer element of Figure 3.1 is converted to a linear accelerometer by the addition of a concentrated mass to one side of the armature, with the armature support giving the restoring spring force. The case is filled with silicone oil of the proper viscosity to give 60 to 70 per cent of critical damping. Accelerometers having the following rated outputs and natural frequencies were used.

Rated Output (G units)	Natural Frequency (filled with damping oil) (cycles per second)
30	190
5	80
1	45
0.5	26

In all cases the recording system was chosen so that the upper limit of uniform frequency response was determined by the accelerometer used and was about 70 per cent of the accelerometer natural frequency. An examination of the gage records obtained from the explosion tests shows that in most cases the highest significant frequencies were well below the high frequency limits of the gages; the frequencies of interest are in the low frequency region. Since the gage system is responsive to zero frequency (DC) signals, no low frequency cut-off is encountered, a feature of great importance when such acceleration records are to be integrated to obtain transient velocities and displacements. Low frequency amplitude and phase errors are difficult to correct before or after recording, and will therefore introduce large errors upon integrating low frequency accelerations.

For the measurement of earth acceleration, two mutually perpendicular gages were mounted in a single canister as shown in Figure 3.4. Suitable damping was provided by wooden blocks inside the canister to eliminate ringing upon shock excitation. The average canister density was adjusted to be approximately equal to the soil in which it was placed.

The excellent linearity and the zero-frequency response characteristic of the accelerometers permitted direct field calibration by manual rotation in the earth's gravitational field. This calibration was performed for each gage at the time of installation for each test, using the gage cable, coupling unit, and recording element as connected

for the test. At the same time the output due to the calibration voltage was noted for subsequent comparison with the automatic calibration records obtained during each explosion test. Laboratory spin-table tests established the validity of the earth's field calibration technique. The short armature makes the accelerometer relatively insensitive to the angular accelerations produced by the explosion forces.

Each canister was installed and oriented at the bottom of a hole in the ground six inches in diameter, at a nominal gage depth of five feet. On the HE-1 and HE-2 tests the canisters were cemented in the holes with Calseal, a quick-setting gypsum cement. Some holes were then filled and packed with dirt and others were left open. No difference between filled and open holes was detected in the accelerometer output attributed to air blast. In some cases gage holes having depths of 17, 34, and 68 feet were used.

Because of the very extensive effort involved in the recovery of the cemented canisters, as well as unavoidable damage to them, a single additional test canister was installed by careful tamping with damp earth on HE-2. There were no significant differences between the records obtained from this unit and those obtained from a cemented canister located alongside. Hence it was decided that tamped damp earth could be used for the accelerometer installations on HE-3 and HE-4. After the earth around the canister was tamped, the gage holes were filled and tamped with additional earth. On both HE-3 and HE-4 a single canister was cemented for control purposes; again, no significant differences were observed.

3.3 EARTH PRESSURE

The basic variable-reluctance transducer element of Figure 3.1 is converted to a hydrostatic-pressure gage by fastening the armature to a slightly twisted Bourdon tube. The gage is filled with oil to give 60 to 70 per cent of critical damping at 70° F; the gage is intended for use immersed in similar oil. Behind the Bourdon tube is a controlled "air bubble", followed by a "porous plug" having a time constant of 15 minutes to two hours, which permits the relief of a very slowly changing ambient pressure.

An earth-pressure gage is shown in Figure 3.5. The pressure gage is placed in a five-inch diameter, flexible Neoprene bag which is filled with oil having the proper viscosity for damping at the operating temperature. This gage then measures the hydrostatic pressure of the oil contained in the closed Neoprene bag.

Fig. 3.5 Earth-Pressure Gage, Shown with the Neoprene Oil Bag

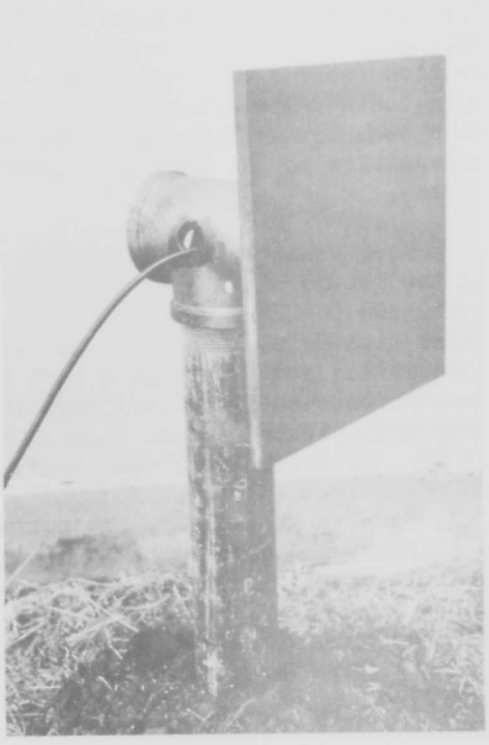

Fig. 3.6 Air-Blast Gage Mounting

Hydrostatic pressure gages having nominal ratings of 100, 10, and 1 psi were utilized. The rise times of the gages were such that the ultimate high-frequency response was determined by the particular recording galvanometers used. All recording galvanometers were adjusted to 70 to 80 per cent of critical damping, and galvanometers having natural frequencies of 120, 230, and 340 cps were included. Examination of the pressure records shows very few instances of frequency components approaching 70 cps.

Most of the ground-pressure data included in this report were obtained with the oil bag located near the bottom of a five-foot hole six inches in diameter. Each hole was filled to the top with a thin solution of Aquagel. The Aquagel solution was adjusted to minimize the loss of liquid into the surrounding porous earth. The holes were examined immediately after each test, and in no case had the liquid level dropped more than a few inches. When deeper gage holes were used, they were also filled to the top with the Aquagel solution.

3.4 AIR-BLAST PRESSURE

The basic variable-reluctance transducer element is converted to an air-pressure gage by fastening the armature to a slightly twisted Bourdon tube. A porous plug having a time constant of 30 to 90 seconds is used for static equilibrium. Silicone grease in the armature gap along with acoustic damping gives a net damping of 60 to 70 per cent of critical. The rise time of the gages used was less than 0.0003 second, and hence the over-all rise time of each air-blast channel was determined by the single 315-cps recording galvanometer used for all air-blast measurements. At 70 per cent of critical damping about 0.0015 second was required to attain 90 per cent response.

As with the accelerometers, the final calibration was performed for each pressure gage after installation. The zero-frequency response of the gage system permitted the connection of a measured static air pressure line directly to the gage inlet following installation.

Each air-pressure gage was mounted at the center of a 12-inch by 12-inch by 0.5-inch steel plate, with the gage inlet flush with the baffle surface. This baffle plate was then mounted vertically in a radial plane passing through ground zero as shown in Figure 3.6. The gage center was approximately 14 inches above the ground surface.

3.5 RECORDERS

For recording, five battery-powered William Miller Model J optical oscillographs were used, two of which are illustrated in the foreground of Figure 3.3. Each recorder contains provisions for 30 recording galvanometers, producing records on photosensitive paper 12 inches wide. To assist in trace identification, no more than 28 recording elements were used in a single recorder. An interesting feature of these oscillographs is the inclusion of a stand-by recording lamp in each unit, which is automatically placed in operation in the event of lamp failure.

A separate tuning fork and amplifier are included in each recorder to produce timing lines at 0.010-second intervals, with every tenth line accentuated. In addition, the output of one timing amplifier was recorded simultaneously on all five recorders to permit an accurate time-base in the event of tuning fork or timing amplifier failure. A common zero-time marker, along with subsequent time-reference markers, was recorded on each oscillograph to permit exact synchronization of the five records obtained on each explosion test. Zero

time was recorded by the interruption of the blasting cap current due to its detonation. A paper speed of approximately 18 inches per second was used for each test.

In most cases the output of a single gage channel was connected to two recording galvanometers. These dual-galvanometer channels used a recording ratio of about six to one. If the signal to be recorded is considerably higher than anticipated, the low sensitivity trace produces a usable record, whereas for low signals the high sensitivity trace is useful. This extension of the dynamic recording range is of particular value in underground explosion tests, where the predicted magnitudes are quite uncertain. The excellent signal-to-noise ratio of the variable-reluctance gage system permitted the realization of the full value of such an expanded dynamic recording range. Sixty such dual-galvanometer channels and 12 single galvanometer channels were used.

Before a test each recording channel was adjusted to give an expected deflection of plus or minus 0.75 inch for the single trace gages and an expected deflection of plus or minus 1.8 inches on the high sensitivity trace (plus or minus 0.3 inch on the low sensitivity trace) for the gages connected to dual galvanometers. The damping of each recording galvanometer was adjusted to be 60 to 70 per cent of critical. Recording galvanometers having natural frequencies of 120, 230, and 315 cps were used, with coil-current deflection sensitivities of 0.06, 0.2, and 0.5 ma per inch, respectively.

A typical developed record is shown in Figure 3.7, reduced in size from the original width of 12 inches. The outer traces are for reference and record identification, and the sinusoidal trace records a common time base between recorders, with the breaks providing exact synchronization. The dual-galvanometer traces are easily identified. For accurate measurements amplitudes are read directly from the records, while direct tracing of individual curves facilitates wave form studies. Trace identification is generally not too difficult, and the low sensitivity record of dual traces is frequently of considerable assistance in this regard. However, there are cases, especially in the early part of the records, where the simultaneous high activity of several beams results in overlapping which is difficult to differentiate. Such cases occur only two or three per cent of the time but often involve important sections of the traces. Several techniques have been evolved for dealing with this problem. One uses a comparison of the uncertain trace with another that can be expected to be similar. The "trace identifiers" incorporated in the recorders, which interrupt each trace periodically and in sequence, were not used, since trace interruption during a period of rapid deflection greatly complicates trace identification on the kind of records obtained from these explosion tests.

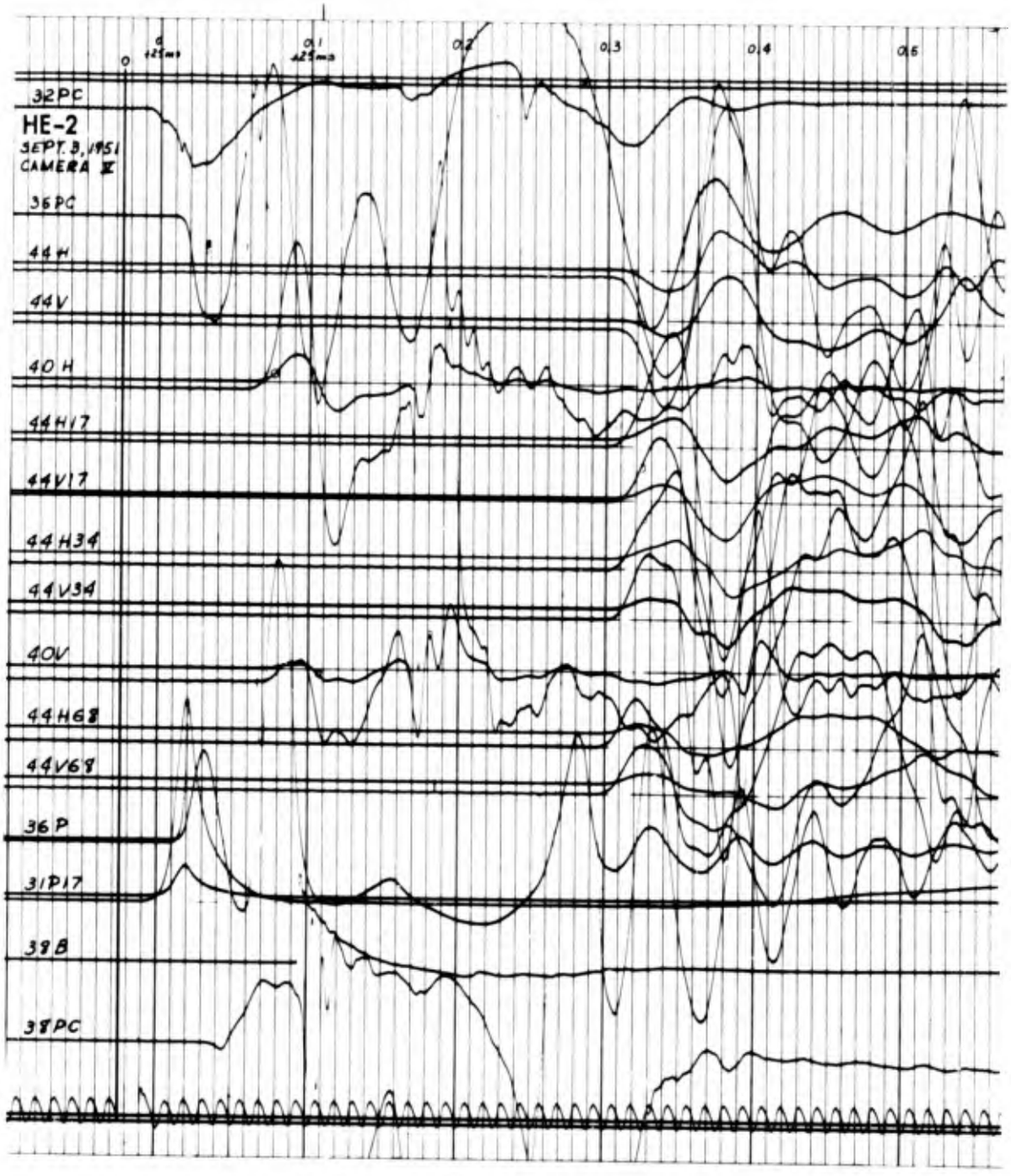

Fig. 3.7 Reduction of Typical Oscillograph Record (Height of original record 12 inches)

3.6 RECORDING STATION

The six 12-channel variable-reluctance gage coupling units with their associated carrier power oscillators, the five recording oscillographs with their individual battery power supplies, and the associated control equipment were noused in a modified type K-19 Army communications trailer. A small darkroom was included in the rear of the trailer for loading recorder magazines and for processing test records.

The recording trailer was designed for unattended remote operation. The trailer was connected to the remote-control point by a single nine-conductor cable which carried indicator circuits plus the control circuit for the recorder paper transport motors. In practice, all carrier oscillators and recorder stand-by circuits were turned on manually and the trailer abandoned about one-half hour prior to the scheduled detonation times. By the indicator circuits the operator at the remote-control point, about one mile from the recording trailer, was able to detect a malfunction of the carrier power oscillators or a defect in recorder stand-by operation. About 15 seconds prior to the detonation the recording paper transport mechanisms were initiated from the remote-control position with monitoring to indicate actual paper transport and recording lamp operation in all recorders. Assuming proper equipment operation, the detonation followed. On no test was it necessary to interrupt the firing sequence due to equipment failure indications, and on no test did equipment failure occur. Because of the number of individual equipment units involved, it is probable that the automatic monitoring and control have a greater assurance of successful operation than would have been obtained by direct visual observations of personnel at the recording station.

The recording trailer was placed in a simple shelter, Figure 3.8, located from 500 to 900 feet from the shot points. Such close proximity to the shot points required unattended operation for personnel safety. A recording station at the closest point permitted for personnel (one mile) would have greatly increased the gage cable cost in both material and labor, while also seriously impairing the gage performance.

Immediately following the initiation of paper transport, stepping switches automatically started which applied a calibration signal to each gage channel in sequence. A typical automatic calibration record is shown in Figure 3.9.

A geophone was mounted in the trailer and connected to a recorder to indicate trailer motion due to ground shock and air blast. On no test were any spurious signals or deflections recorded that could be attributed to trailer motions.

Fig. 3.8 Recording Trailer in Shelter. Portable generators shown at right

(See page 22 for Fig. 3.9)

Fig. 3.10 Cable Truck

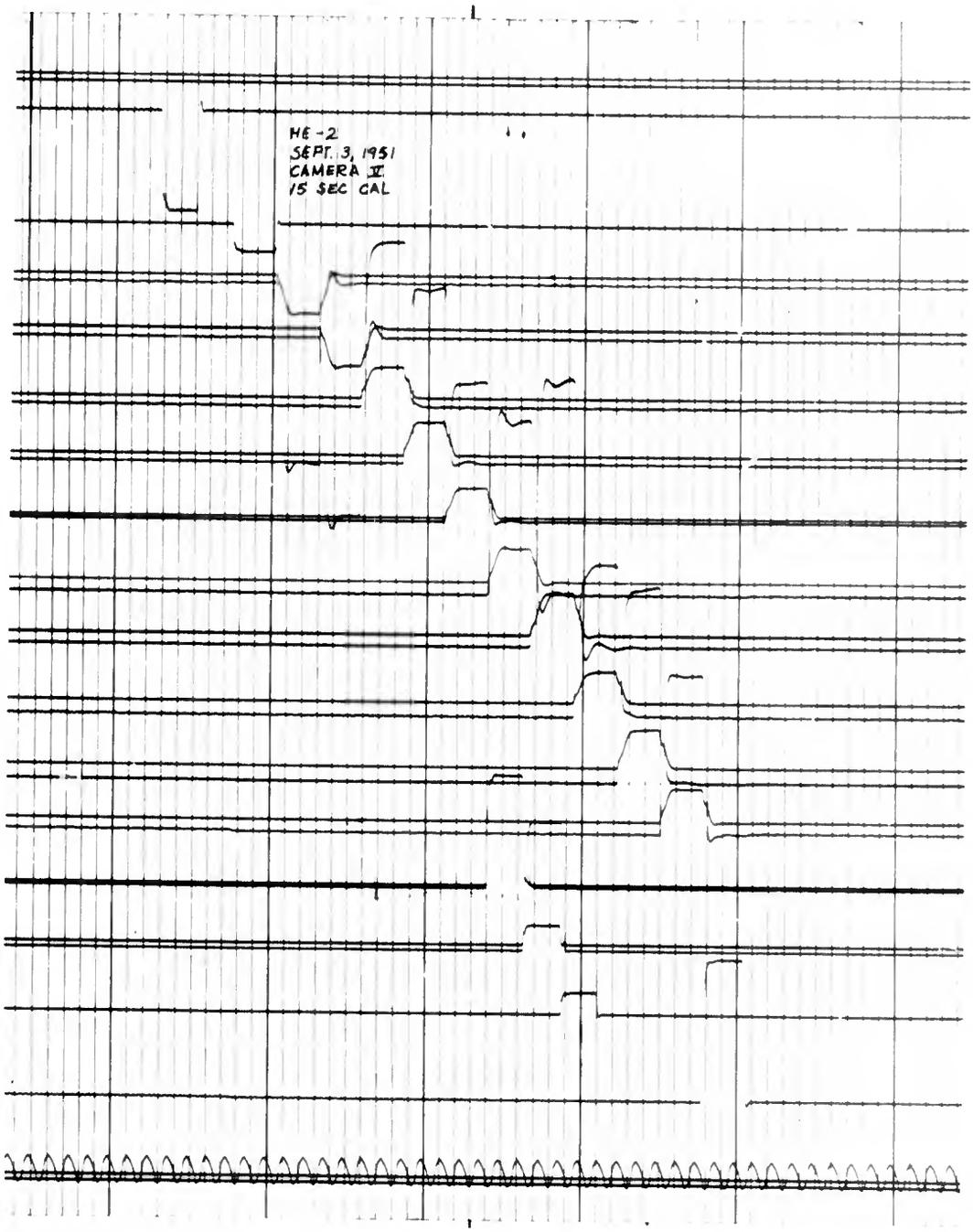

Fig. 3.9 Reduction of Typical Calibration Record
(Height of original record 12 inches)

3.7 POWER SUPPLIES

Each recorder was operated by a separate storage battery. The AC power for the carrier oscillators and amplifiers was supplied by a five-kilowatt portable gasoline-engine generator located adjacent to the recording trailer. A second similar generator was available and connected into an appropriate dummy load. An automatic transfer panel was located in the recording trailer to provide connection to the stand-by generator in the event of failure of the first generator. Transfer was sufficiently rapid to prevent serious interruption in the gage records. In no test was there a generator failure.

3.8 CABLE

Conventional two-conductor and three-conductor shielded microphone cable was used to connect the gages to the recording trailer. Each cable was moved between tests. It is estimated that the close-in recording trailer location permitted a saving of about 350,000 feet of gage cable (which could not have been procured in time for the tests), to say nothing of the saving in labor for the installation and recovery of the gage cable for each test. A one-half ton pickup truck was modified to serve as a cable laying and pickup vehicle (Figure 3.10). Batteries under constant charge from the truck engine supplied the motors used for winding in the cable. The cable was laid in trenches which were later filled with dirt for protection against air blast and throwout material.

[redacted]

CHAPTER 4

RESULTS

4.1 INSTRUMENT PERFORMANCE

From the 264 channels connected for the four tests, 264 useful records were obtained. Of these, 212 supplied data for this report. No gage failures occurred, although the two nearest air pressure gages on HE-4 were damaged by the blast wave and did not give complete records.

4.2 DATA REPORTED

The standard data reported and discussed at length include the five-foot earth accelerations and pressures plus the near surface air-blast pressures. Also presented in the form of functions of time are some data for deep earth accelerations and pressures, but the records for the pressures in 34-foot and 68-foot holes are not reported. There is good evidence that these uncased holes collapsed prior to the test, so that the coupling to the soil was not as in the other installations. The effect of various methods of coupling accelerometers and pressure gages forms another series of records unreported here. However, these records were invaluable for selecting and testing the techniques reported in Chapter 3.

Some earth pressures were measured for the Sandia Corporation, using their Carlson-Wiancko diaphragm-type gages. The records have been transmitted directly to Sandia. Finally, some geophones were placed at large distances from ground zero. Neither of these sets of data is reported here. Where pertinent, these unreported data will receive full discussion in the final report to be prepared for the Office of the Chief of Engineers. Project 1(9)-1 was conducted by the Stanford Research Institute under Contract DA-49-129-eng-119 with the Office of the Chief of Engineers, Washington, D. C.

4.3 ORGANIZATION OF DATA

The primary data are, of course, the original oscillograph records (Figure 3.7 shows a sample of the initial portion of one oscillograph record from the HE-2 test). The individual transient gage records, copied with no smoothing or editing whatsoever, have

[redacted] [redacted]

been published in the Appendix to the Interim Report.[6] Here only sample transient records are presented. Figures 4.1 through 4.9 portray the air blast, five-foot earth acceleration and the five-foot earth pressure. The wave form of the air-blast-induced "slap" in vertical acceleration is shown in Figure 4.10; the horizontal earth particle velocity (obtained by integration) is portrayed in Figure 4.11. Figures 4.12 through 4.16 show the effect of gage depth on earth acceleration and pressure.

From the transient records certain amplitudes and times have been measured. Figure 4.17 illustrates quantities of interest that are tabulated in Tables 4.1 through 4.14. Owing to the effect of air blast on earth motion, it is necessary to define certain of the quantities somewhat more closely than suggested by Figure 4.17. For close-in stations the air blast often arrives during the first acceleration or earth pressure pulse. The amplitudes and durations tabulated for the first pulse are those existing after the first pulse has been smoothed to remove air-blast effects. Similarly, in measuring the slap in vertical acceleration due to air blast, measurements are made from this smoothed base line, shown dotted at the top of Figure 4.17. Because the slap is highly damped, the first peak, which is negative (downward), is chosen to characterize its amplitude.

The particle velocity is obtained by integration of acceleration records (machine for HE-2, manual for HE-1). The cycle having the maximum peak-to-peak swing is chosen to describe the velocity; the amplitude tabulated is half this peak-to-peak swing.

The air blast for HE-3 is typified by the third curve on Figure 4.17. For the other tests the "front porch" was absent. On HE-3 the duration of the front porch decreased with increasing distance from ground zero until only a single shock was observed. Table 4.10 indicates that this disappearance of the front porch occurred at a value of λ between 6.25 and 10.8. The positive impulse has been evaluated for the whole positive phase, since the time (and impulse) added by the front porch is small compared with these quantities for the remainder of the positive phase.

A note on the polarity of the records is in order. Radially outward horizontal acceleration, upward vertical acceleration, and positive over-pressures correspond to positive (upward) ordinates. Some records near the upper end of the recording galvanometer array were reversed to keep them on the paper, but these were reversed again to the standard presentation during the tracing process.

[redacted]

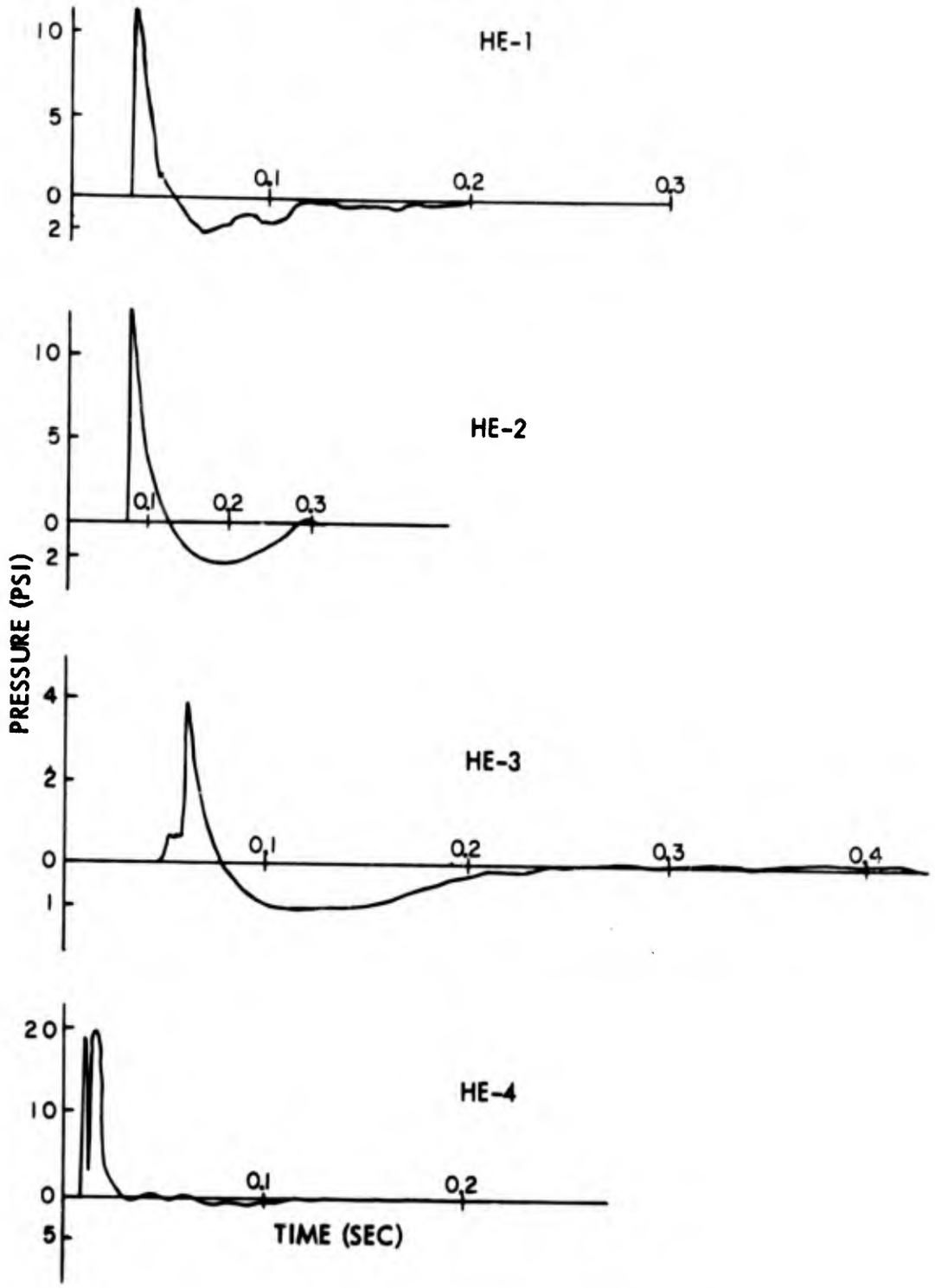

Fig. 4.1 Air-Blast Pressure vs. Time at $\lambda = 4.3$.
Note scaling of time on HE-2

[redacted]

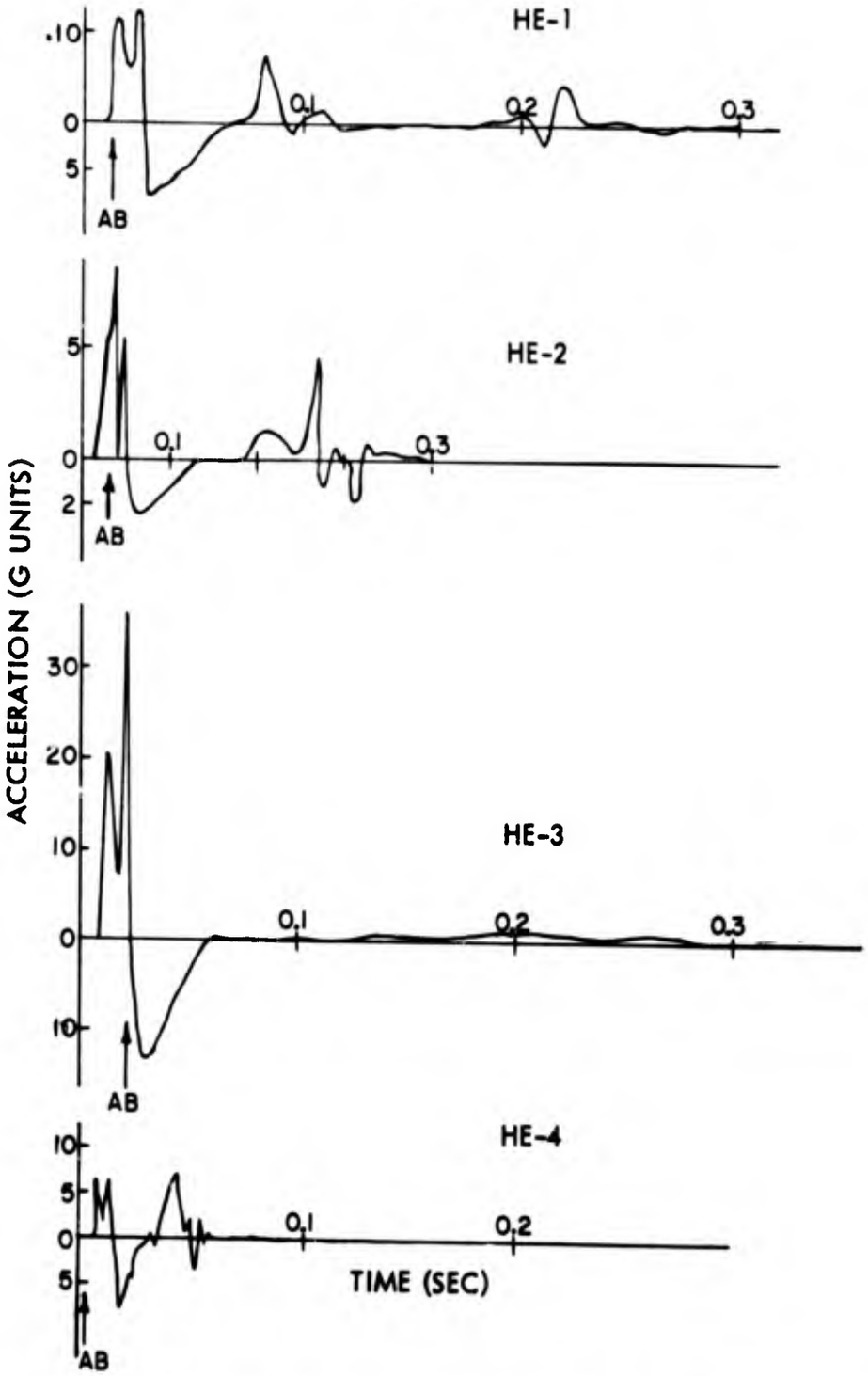

Fig. 4.2 Horizontal Earth Acceleration vs. Time at $\lambda = 2.08$. Note scaling of time and acceleration scales for HE-2. AB denotes arrival of air blast

[redacted]

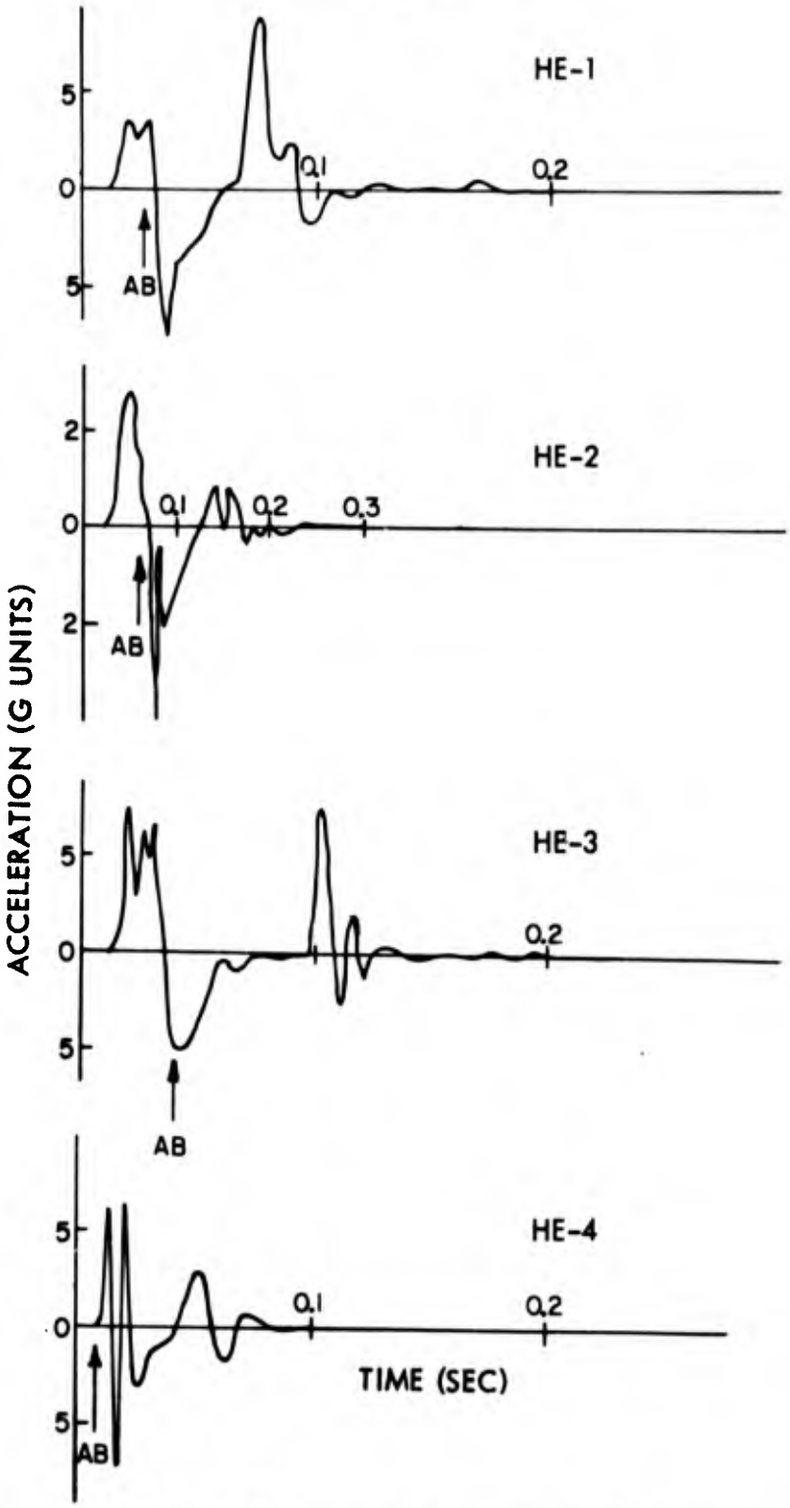

Fig. 4.3 Horizontal Earth Acceleration vs. Time at $\lambda = 3.62$. Note scaling of time and acceleration scales for HE-2. AB denotes arrival of air blast

[redacted]

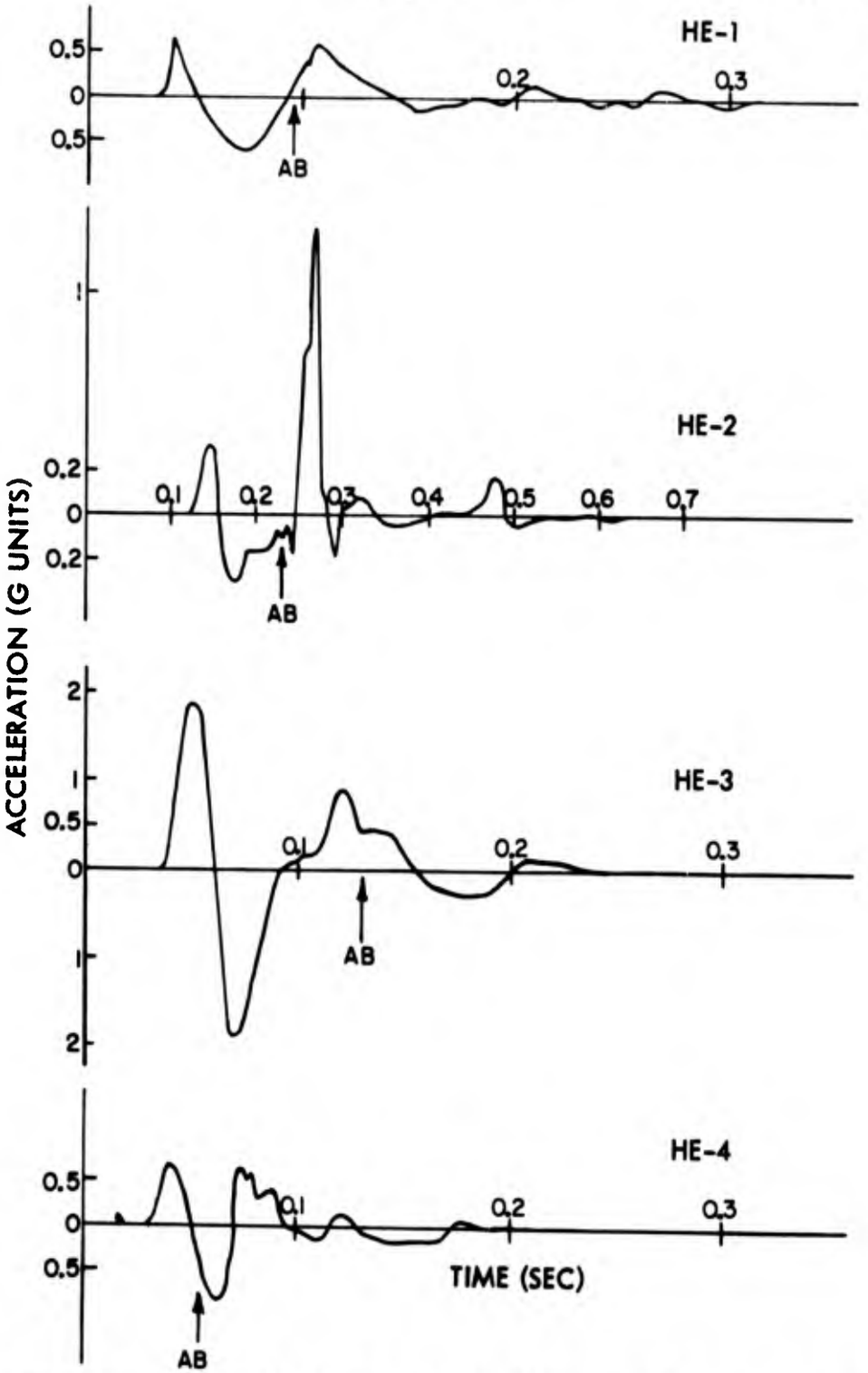

Fig. 4.4 Horizontal Earth Acceleration vs. Time at $\lambda = 11.1$. Note scaling of time and acceleration scales for HE-2. AB denotes arrival of air blast

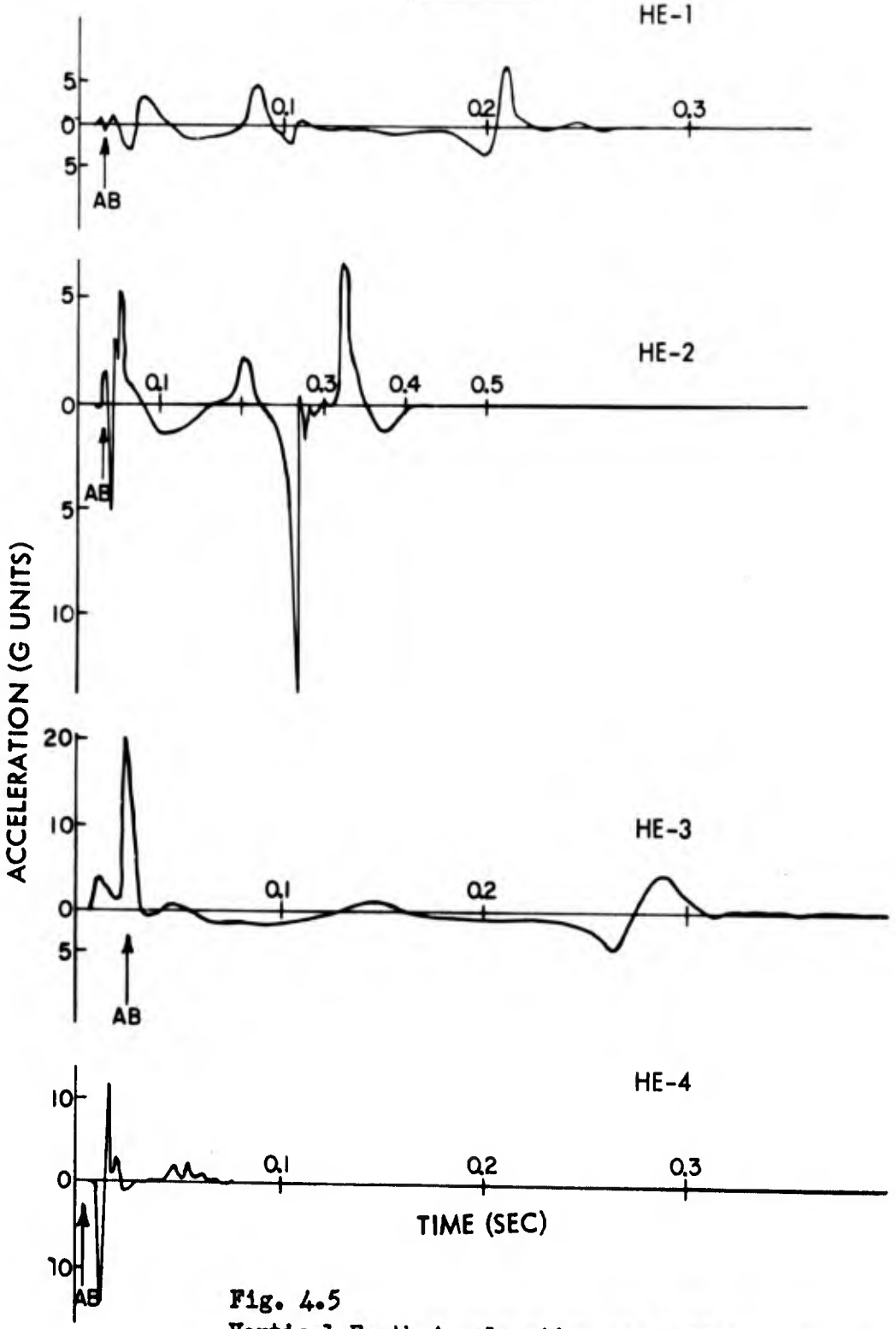

Fig. 4.5
Vertical Earth Acceleration vs. Time at $\lambda = 2.08$. Note scaling of time and acceleration scales for HE-2. AB denotes arrival of air blast

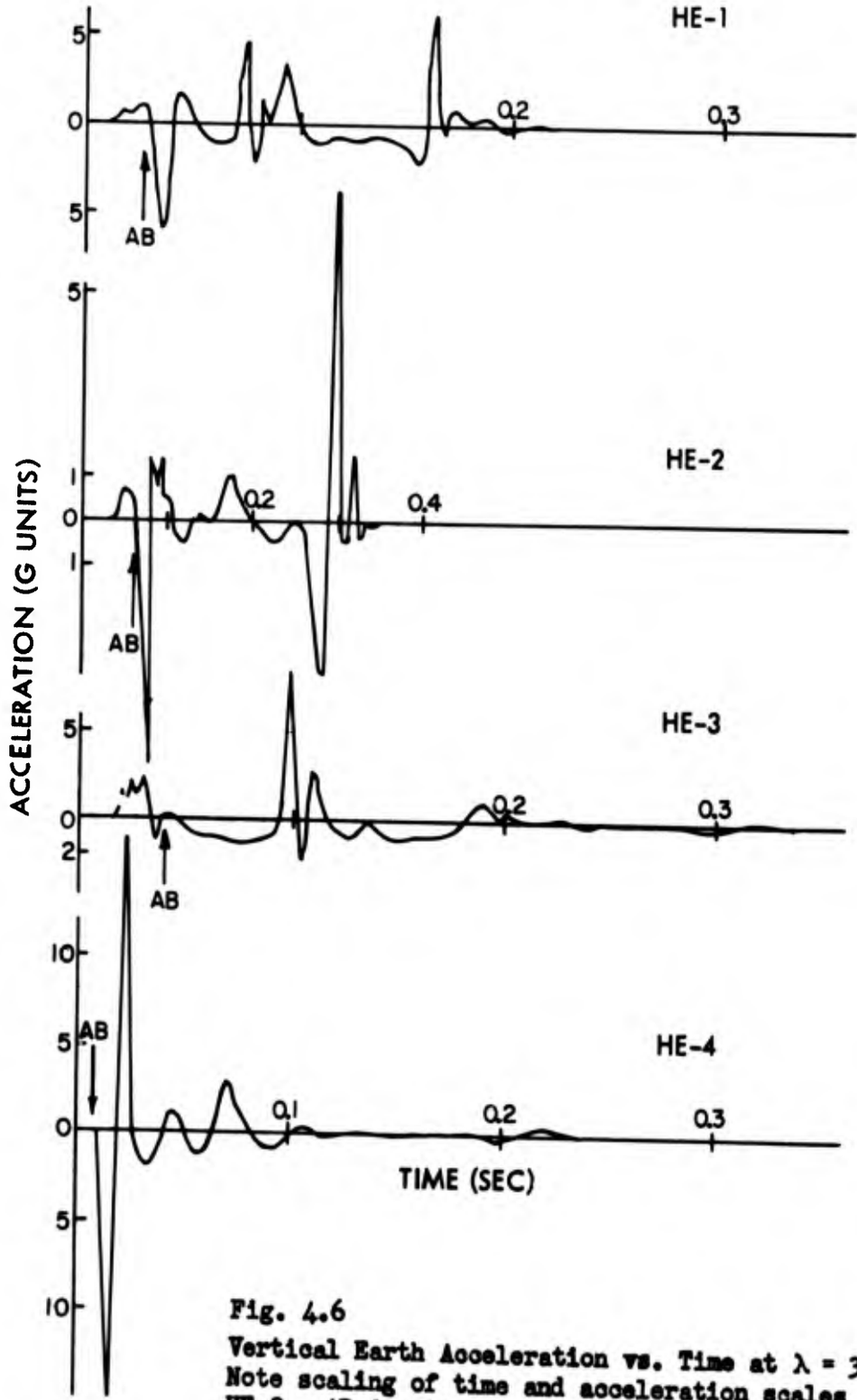

Fig. 4.6
Vertical Earth Acceleration vs. Time at $\lambda = 3.62$. Note scaling of time and acceleration scales for HE-2. AB denotes arrival of air blast

[redacted]

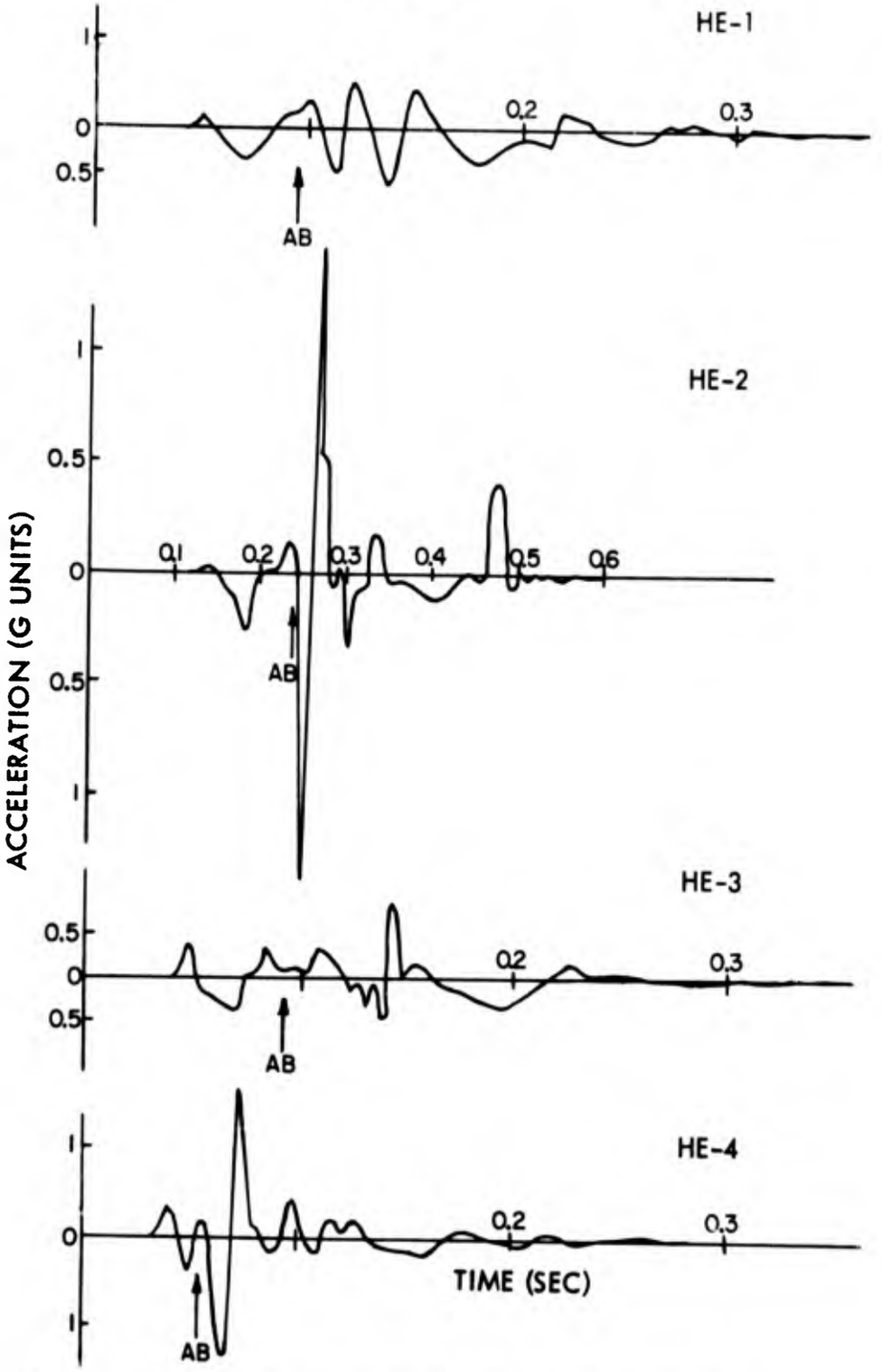

Fig. 4.7 Vertical Earth Acceleration vs. Time at λ = 11.1. Note scaling of time and acceleration scales for HE-2. AB denotes arrival of air blast

[redacted]

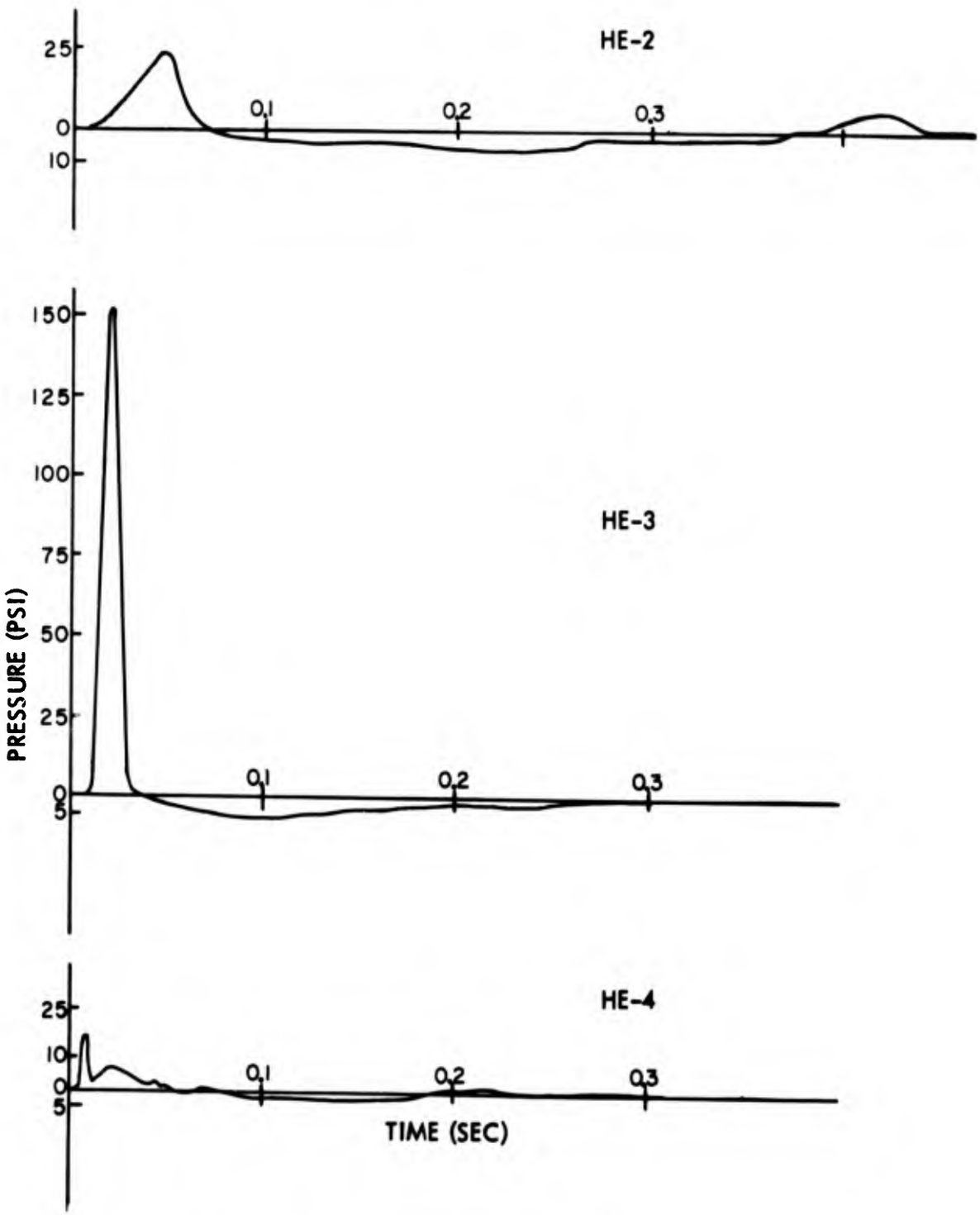

Fig. 4.8 Earth Pressure vs. Time at $\lambda = 1.72$.

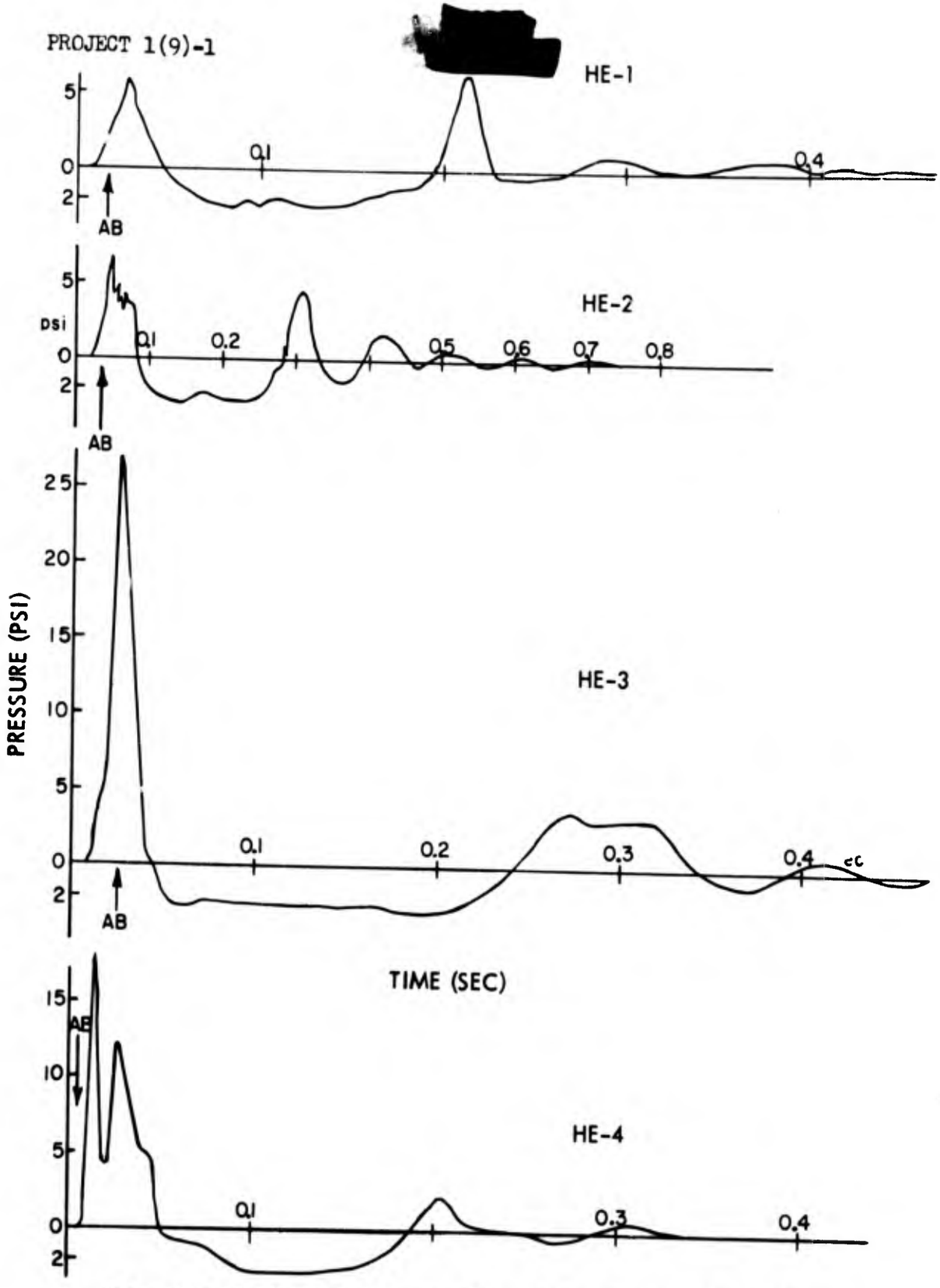

Fig. 4.9 Earth Pressure vs. Time at $\lambda = 2.49$. AB denotes arrival of air blast. Note scaling of time for HE-2

[redacted]

Fig. 4.10 Wave Form of Air-Blast Slap in Vertical Earth Acceleration. HE-2, $\lambda = 7.66$

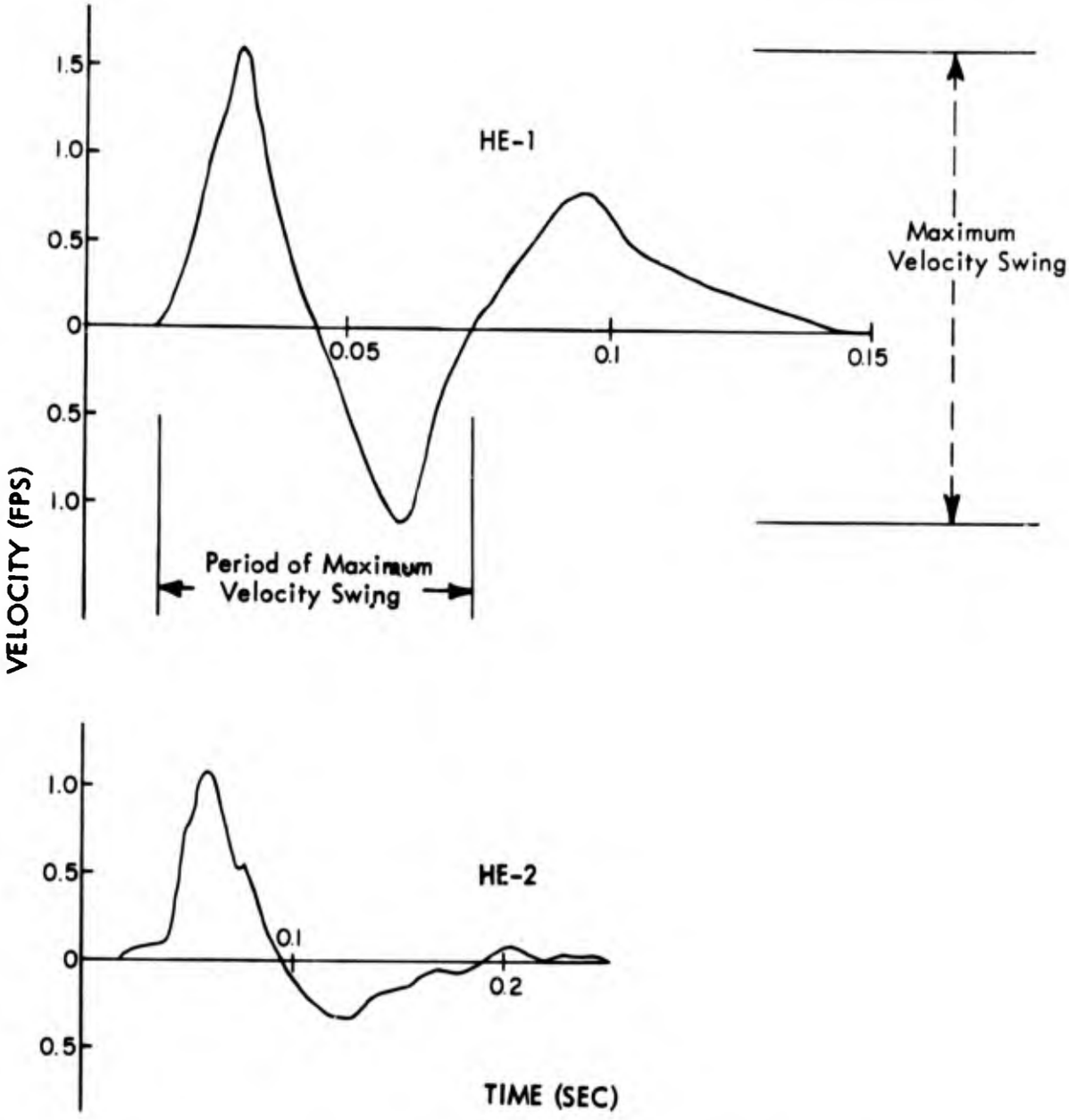

Fig. 4.11 Horizontal Velocity vs. Time at $\lambda = 3.62$ by Integration of Earth Acceleration. HE-1 by manual and HE-2 by machine integration. Amplitude is half of maximum swing

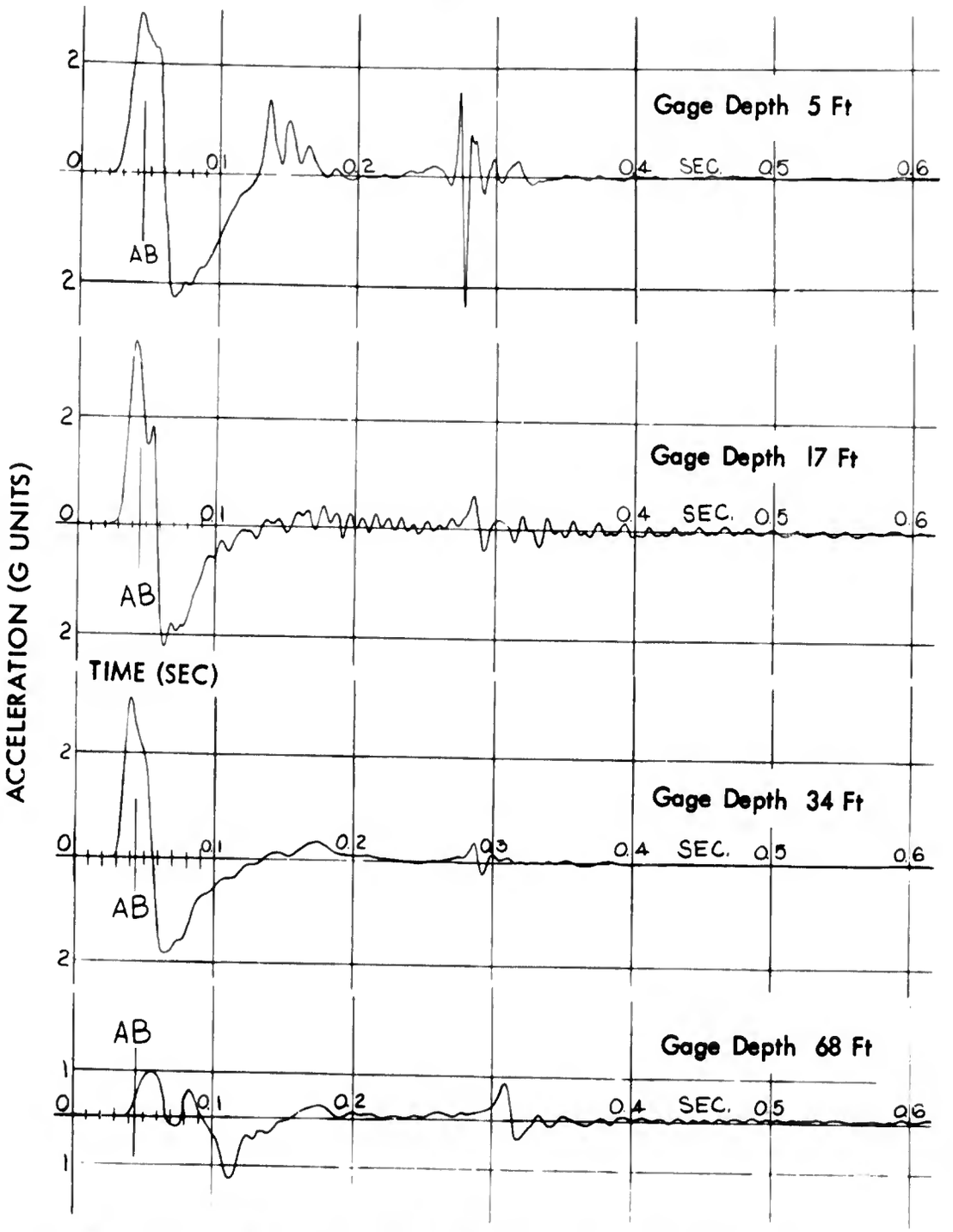

Fig. 4.12 HE-2, Horizontal Earth Acceleration vs. Time at Various Depths, $\lambda = 3.0$

[redacted]

PROJECT 1(9)-1

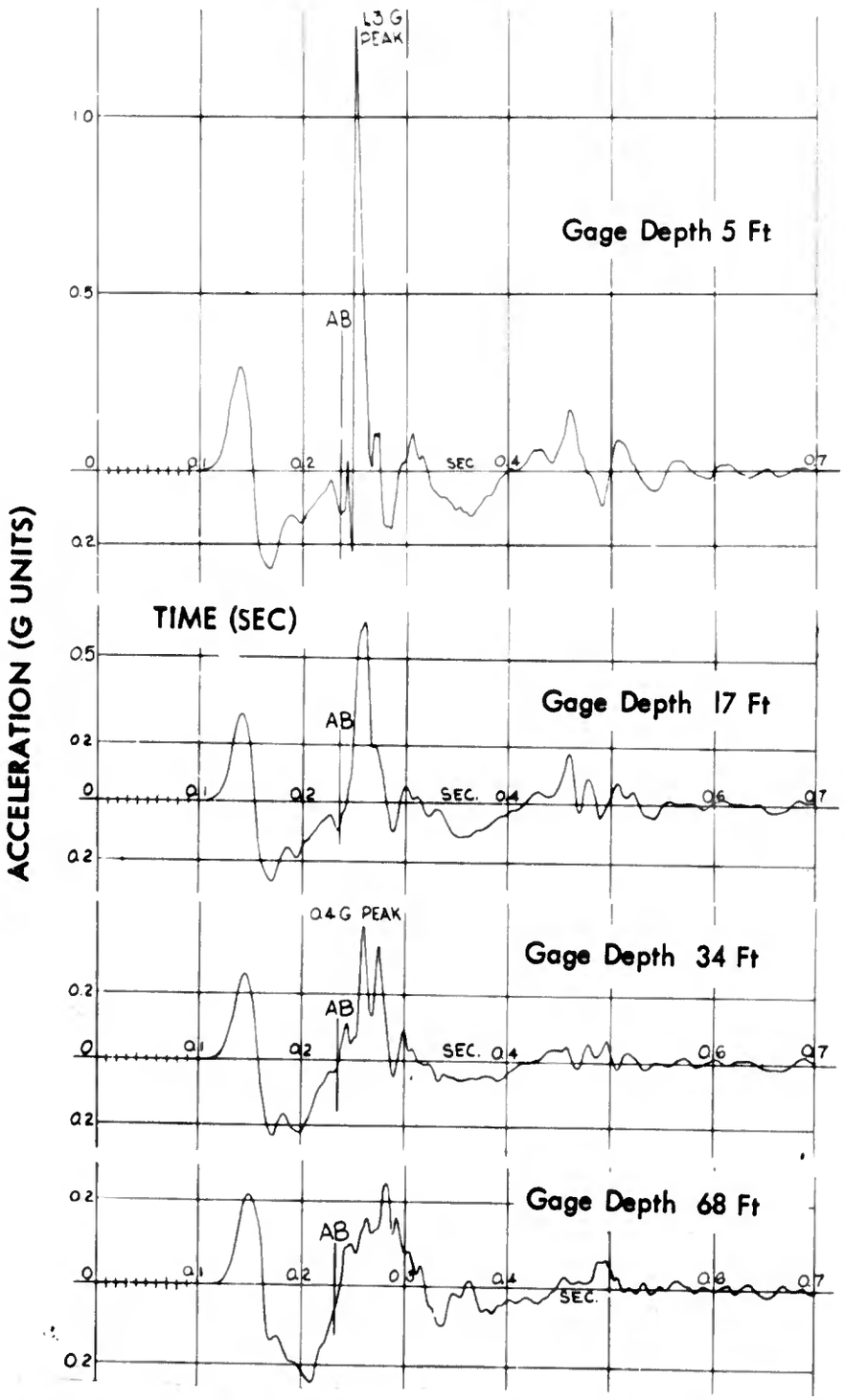

Fig. 4.13 HE-2, Horizontal Earth Acceleration vs. Time at Various Depths, λ = 11.1

[redacted]

[redacted]

PROJECT 1(9)-1

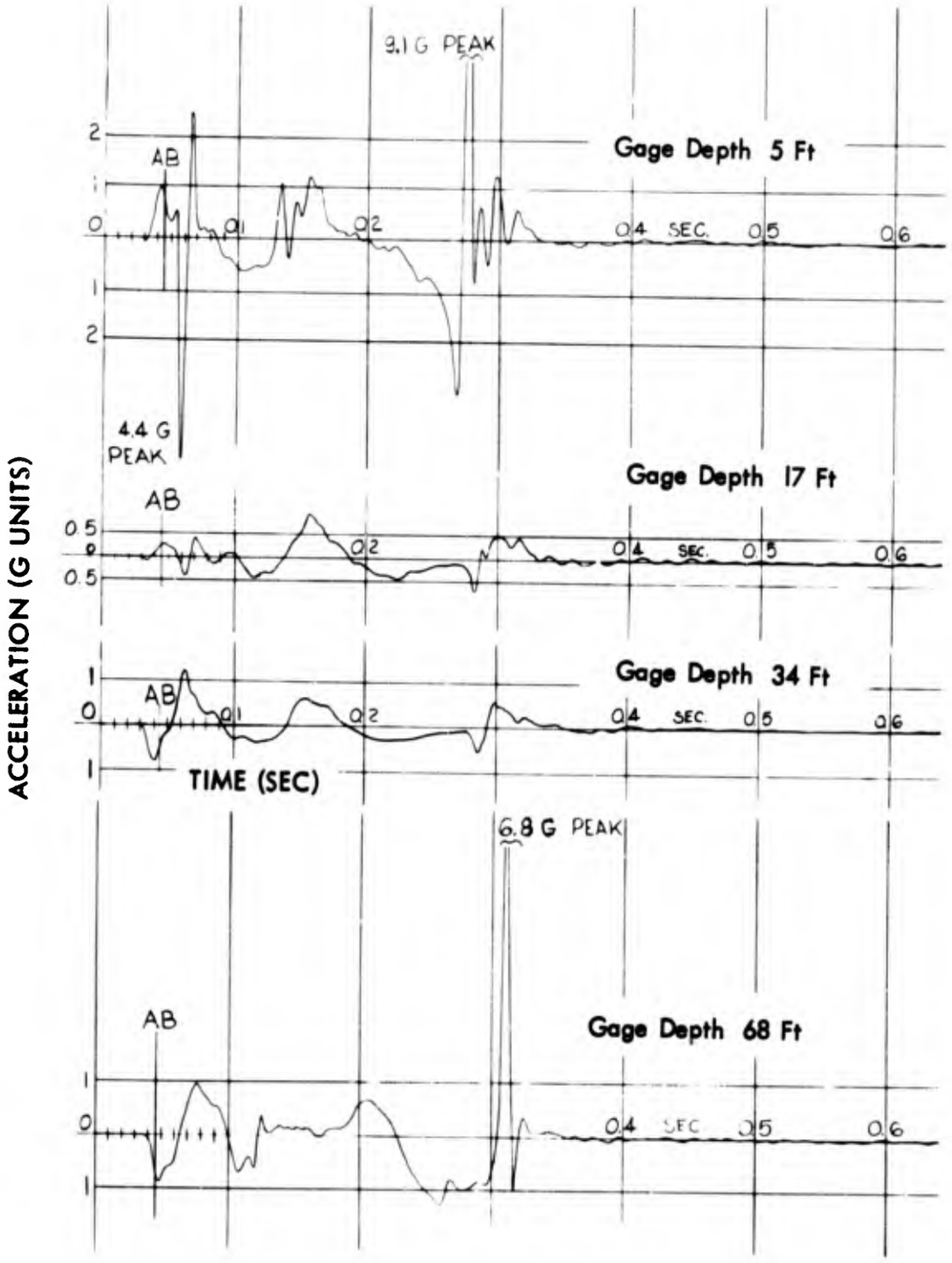

Fig. 4.14 HE-2, Vertical Earth Acceleration vs. Time at Various Depths, $\lambda = 3.0$

[redacted]

[redacted]

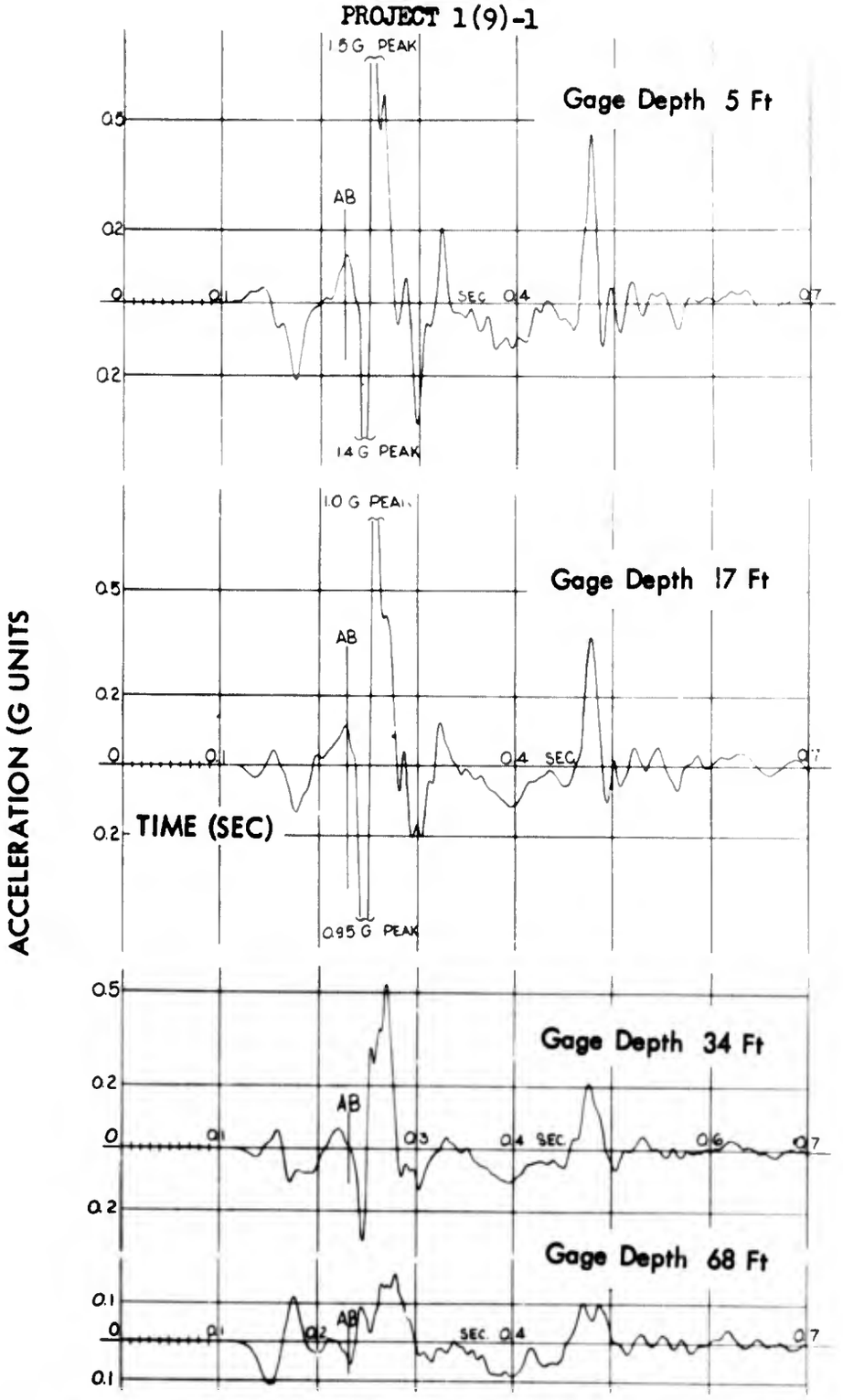

Fig. 4.15 HE-2, Vertical Earth Acceleration vs. Time at Various Depths, λ = 11.1

[redacted]

[redacted]

PROJECT 1(9)-1

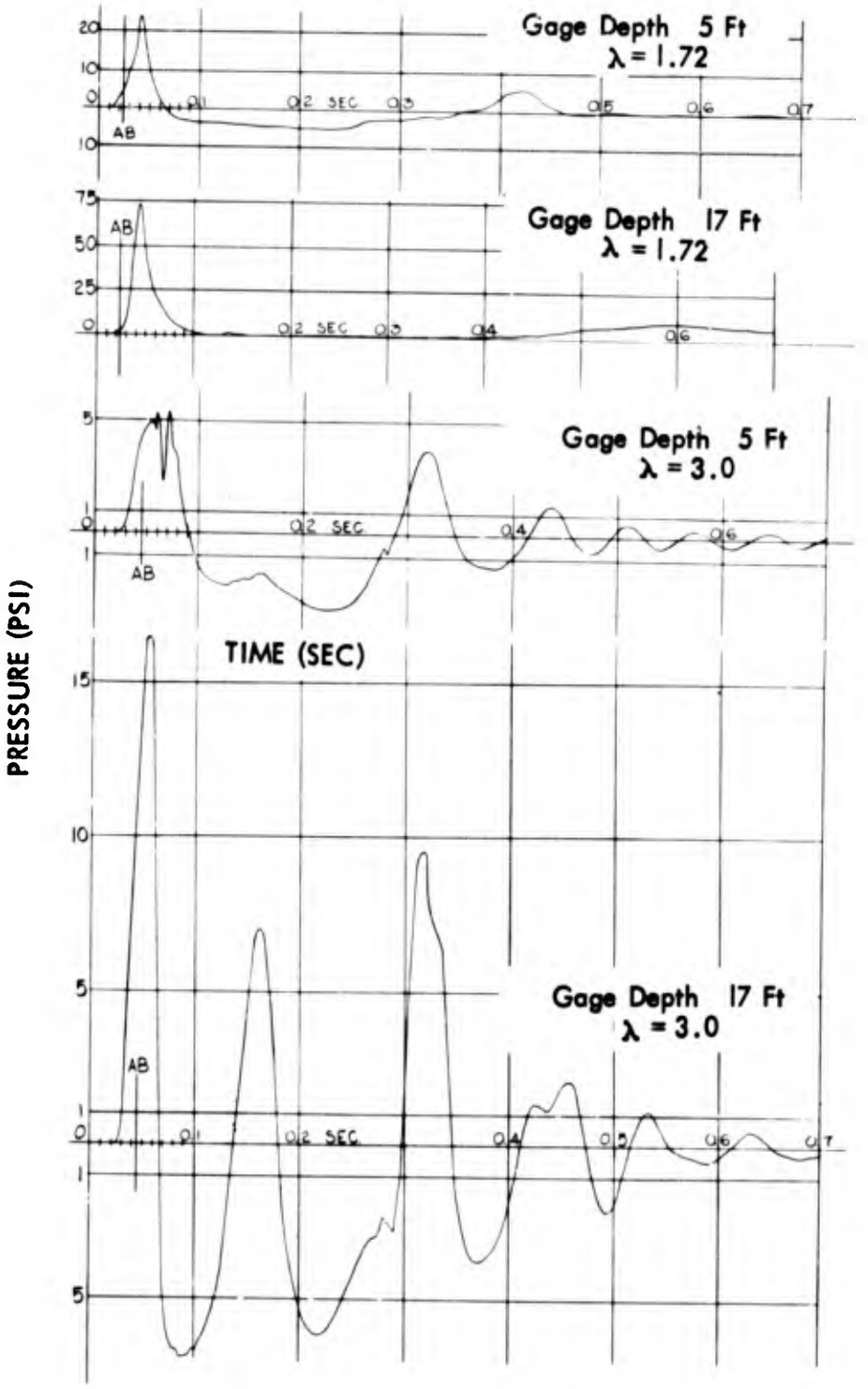

Fig. 4.16 HE-2, Earth Pressure vs. Time at Various Depths

[redacted]

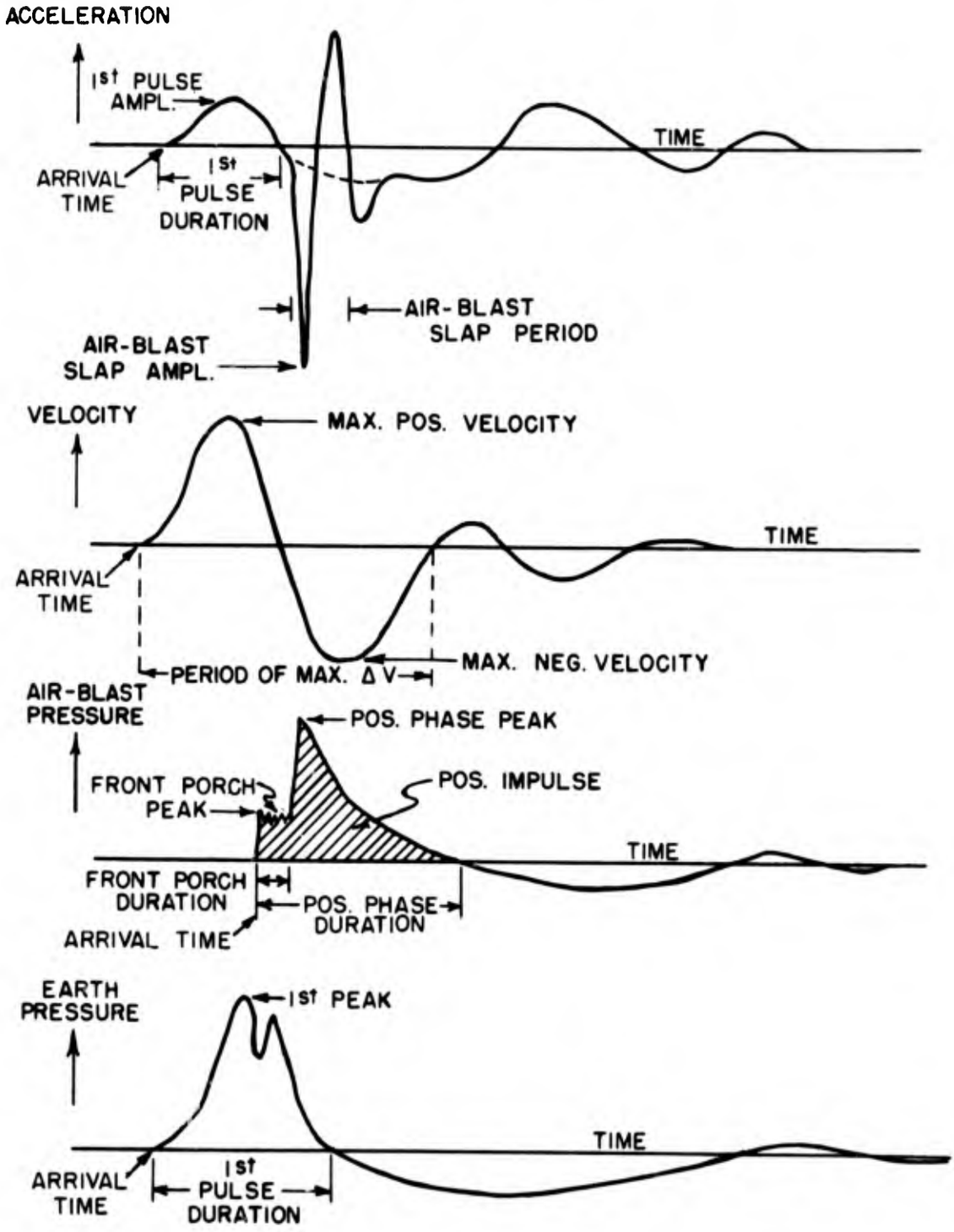

Fig. 4.17 Quantities Measured from Transient Records

4.4 TABLES

Besides containing numerical data taken as indicated in Figure 4.17, Tables 4.1 through 4.14 give gage locations and type by the gage code number. The gage number describes the test by its general magnitude, while its particular value refers to the gage station at the given distance. The succeeding letter is coded to each one of the four measurements—Horizontal or Vertical acceleration, earth Pressure, and air Blast. With no numbers following, the accelerometer or earth-pressure gage depth is five feet; deeper gages can be signified by adding to the code number the depth in feet. For example, 56H refers to a horizontal accelerometer at Station 56 in Test HE-3 (Stations 50 - 69). All air-blast gages were 14 inches above the ground surface.

TABLE 4.1

HE-1 Earth Acceleration - Horizontal
(Gage Depth = 5 Feet)

Gage Code No.	Gage Rating (G)	Horizontal Radius		Arrival Time (sec)	First Pulse	
		(ft)	λ		Ampl. (G)	Durat'n (sec)
2H	30	28.4	2.08	0.008	9.2	0.016
3H	30	34.0	2.49	0.009	5.6	0.019
4H	30	41.0	3.0	0.010	4.3	0.017
5H	30	49.5	3.62	0.013	1.7	0.019
6H	5	58.8	4.3	0.014	2.9	0.023
7H	5	71.1	5.2	0.017	3.2	0.024
8H	5	85.5	6.25	0.020	2.3	0.021
9H	5	102.5	7.5	0.027	1.9	0.017
10H	1	123	9.0	0.032	1.3	0.018
11H	0.5	148	10.8	0.036	0.67	0.022
12H	0.5	178	13.0	0.041	0.50	0.019
13H	1	217	15.9	0.051	0.34	0.022
14H	1	262	19.2	0.061	0.24	0.031
15H	0.5	314	23.0	0.069	0.14	0.033
16H	0.5	378	27.6	0.088	0.062	0.024
17H	0.5	542	39.6	0.123	0.073	0.038
18H	0.5	788	57.5	0.186	0.044	0.046
19H	0.5	1025	75.0	0.255	0.043	0.050
20H	0.5	1480	108.0	0.383	0.025	0.052

TABLE 4.2

HE-1 Earth Acceleration - Vertical
(Gage Depth = 5 Feet)

Gage Code No.	Gage Rating (G)	Horizontal Radius (ft)	Horizontal Radius λ	Arrival Time (sec)	First Pulse Ampl. (G)	First Pulse Durat'n (sec)	Air-Blast Slap Ampl. (G)	Air-Blast Slap Period (sec)
2V	30	28.4	2.08	0.009	1.3	0.012	3.9	0.012
3V	30	34.0	2.49	0.009	2.6	0.017	3.6	0.014
4V	30	41.0	3.0	0.010	1.8	0.022	4.5	0.011
5V	30	49.5	3.62	0.013	0.92	0.018	5.2	0.011
6V	5	58.8	4.3	0.015	0.74	0.021	2.9	0.036
7V	5	71.1	5.2	0.018	0.49	0.016	3.8	0.016
8V	5	85.5	6.25	0.021	0.67	0.017	2.3	0.007
9V	5	102.5	7.5	0.026	0.32	0.015		
10V	1	123	9.0	0.033	0.25	0.017		
11V	0.5	148	10.8	0.036	0.10	0.021		
12V	0.5	178	13.0	0.043	0.13	0.019		
13V	1	217	15.9	0.051	0.079	0.019		
14V	1	262	19.2	0.061	0.080	0.024		
15V	0.5	314	23.0	0.071	0.030	0.027		
16V	0.5	378	27.6	0.085	0.016	0.029		
17V	0.5	542	39.6	0.128	0.0084	0.034		
18V	0.5	788	57.5	0.186	0.0097	0.038		
19V	0.5	1025	75.0	0.265	0.012	0.043		
20V	0.5	1480	108.0	0.388	0.010	0.044		

[redacted]

TABLE 4.3

HE-1 Earth Pressure
(Gage Depth = 5 Feet)

Gage Code No.	Gage Rating (psi)	Horizontal Radius (ft)	Horizontal Radius λ	Arrival Time (sec)	First Pulse Ampl. (psi)	First Pulse Durat'n (sec)
3PF	100	34.0	2.49	0.011	5.7	0.036
6PF	10	58.8	4.3	0.016	1.5	0.026

TABLE 4.4

HE-1 Air-Blast Pressure
(Gage Height = 14 Inches)

Gage Code No.	Gage Rating (psi)	Horizontal Radius (ft)	Horizontal Radius λ	Arrival Time (sec)	Positive Phase Peak (psi)	Positive Phase Durat'n (sec)	Positive Impulse (psi-sec)
3B	10	34.0	2.49	0.018	13.3	0.012	0.0726
6B	10	58.8	4.3	0.032	11.4	0.019	0.0798
9B	10	102.5	7.5	0.061	6.4	0.024	0.0651
12B	10	178	13.0	0.118	4.2	0.036	0.0520
15B	10	314	23.0	0.225	2.0	0.040	0.0300
17B	10	542	39.6	0.413	0.89	0.054	0.0207
19B	10	1025	75.0	0.824	0.36	0.056	0.0107

[redacted]

PROJECT 1(9)-1

TABLE 4.5

HE-2 Earth Acceleration
(Gage Depth = 5 Feet)

Gage Code No.	Gage Rating (G)	Horizontal Radius (ft)	Horizontal Radius λ	Arrival Time (sec)	First Pulse Ampl. (G)	First Pulse Durat'n (sec)	Air-Blast Slap Ampl. (G)	Air-Blast Slap Period (sec)
Horizontal								
32H	30	71.1	2.08	0.015	4.5	0.037		
33H	30	85.5	2.49	0.019	3.5	0.034		
34H	5	102.5	3.0	0.024	2.9	0.035		
35H	5	123	3.62	0.031	2.5	0.038		
36H	5	148	4.3	0.038	2.0	0.037		
37H	5	178	5.2	0.046	1.3	0.038		
38H	5	217	6.35	0.058	0.90	0.040		
39H	5	262	7.66	0.070	0.60	0.041		
40H	5	314	9.2	0.088	0.45	0.045		
41H	5	378	11.1	0.106	0.31	0.046		
42H	1	512	15.0	0.145	0.18	0.057		
43H	1	788	23.0	0.252	0.12	0.052		
44H	1	1025	30.0	0.327	0.050	0.056		
45H	0.5	1480	43.3	0.456	0.036	0.053		
Vertical								
32V	30	71.1	2.08	0.016	1.3	0.024	5.2	0.008
33V	30	85.5	2.49	0.021	1.3	0.028	6.4	0.009
34V	5	102.5	3.0	0.025	1.0	0.030	4.9	0.012
35V	5	123	3.62	0.035	0.63	0.032	5.4	0.015
36V	5	148	4.3	0.041	0.39	0.030	6.0	0.012
37V	5	178	5.2	0.050	0.34	0.031	3.5	0.013
38V	5	217	6.35	0.062	0.13	0.030	3.0	0.014
39V	5	262	7.66	0.080	0.080	0.027	2.4	0.017
40V	5	314	9.2	0.095	0.063	0.032	1.1	0.022
41V	5	378	11.1	0.115	0.040	0.037	1.4	0.017
42V	1	512	15.0	0.155	0.043	0.033	0.73	0.014
43V	1	788	23.0	0.257	0.035	0.047		
44V	1	1025	30.0	0.330	0.038	0.050		
45V	0.5	1480	43.3	0.456	0.040	0.050		

[redacted]

TABLE 4.6

HE-2 Earth Pressure
(Gage Depth = 5 Feet)

Gage Code No.	Gage Rating (psi)	Horizontal Radius (ft)	Horizontal Radius λ	Arrival Time (sec)	First Pulse Ampl. (psi)	First Pulse Durat'n (sec)
31P	100	58.8	1.72	0.014	24.2	0.053
32P	100	71.1	2.08	0.017	14.2	0.068
33P	100	85.5	2.49	0.019	6.5	0.062
34P	10	102.5	3.0	0.024	5.4	0.068
36P	10	148	4.3	0.037	2.9	0.032
38P	1	217	6.35	0.057	1.1	0.033
41P	1	378	11.1	0.104	0.13	0.042

TABLE 4.7

HE-2 Air-Blast Pressure
(Gage Height = 14 Inches)

Gage Code No.	Gage Rating (psi)	Horizontal Radius (ft)	Horizontal Radius λ	Arrival Time (sec)	Positive Phase Peak (psi)	Positive Phase Durat'n (sec)	Positive Impulse (psi-sec)
33B	100	85.5	2.49	0.037	21.4	0.034	0.226
36B	10	148	4.3	0.075	13.4	0.053	0.199
38B	10	217	6.35	0.119	10.1	0.062	0.198
41B	10	378	11.1	0.237	5.1	0.082	0.149
42B	10	512	15.0	0.342	3.3	0.095	0.123
44B	10	1025	30.0	0.763	1.35	0.124	0.0790

TABLE 4.8

HE-3 Earth Acceleration
(Gage Depth = 5 Feet)

Gage Code No.	Gage Rating (G)	Horizontal Radius (ft)	Horizontal Radius λ	Arrival Time (sec)	First Pulse Ampl. (G)	First Pulse Durat'n (sec)
Horizontal						
52H	30	28.4	2.08	0.007	26.2	0.015
53H	30	34.0	2.49	0.009	9.9	0.018
54H	30	41.0	3.0	0.010	6.9	0.019
55H	30	49.5	3.62	0.013	5.4	0.019
56H	30	58.8	4.3	0.015	4.2	0.019
57H	30	71.1	5.2	0.018	4.1	0.017
58H	5	85.5	6.25	0.022	4.0	0.018
59H	5	102.5	7.5	0.025	4.3	0.018
60H	5	148	10.8	0.034	1.7	0.022
61H	5	178	15.9	0.041	1.1	0.025
62H	5	314	23.0	0.071	0.38	0.021
63H	1	542	39.6	0.127	0.12	0.036
64H	0.5	1340	98.2	0.342	0.037	0.050
Vertical						
52V	30	28.4	2.08	0.008	10	0.022
53V	30	34.0	2.49	0.008	2.8	0.020
54V	30	41.0	3.0	0.010	3.4	0.018
55V	30	49.5	3.62	0.014	1.2	0.018
56V	30	58.8	4.3	0.015	1.5	0.019
57V	30	71.1	5.2	0.018	1.6	0.017
58V	5	85.5	6.25	0.020	1.5	0.019
59V	5	102.5	7.5	0.025	0.80	0.018
60V	5	148	10.8	0.035	0.35	0.016
61V	5	178	15.9	0.042	0.25	0.018
62V	5	314	23.0	0.071	0.084	0.024
63V	1	542	39.6	0.127	0.0089	0.036
64V	0.5	1340	98.2	0.355	0.012	0.044

[redacted] [redacted]

TABLE 4.9

HE-3 Earth Pressure
(Gage Depth = 5 Feet)

Gage Code No.	Gage Rating (psi)	Horizontal Radius (ft)	Horizontal Radius λ	Arrival Time (sec)	First Pulse Ampl. (psi)	First Pulse Durat'n (sec)
51P	100	23.5	1.72	0.006	146	0.028
52P	100	28.4	2.08	0.007	44	0.030
53P	100	34.0	2.49	0.009	26.6	0.028
54P	100	41.0	3.0	0.010	8.3	0.026
55P	100	49.5	3.62	0.013	8.0	0.028
56P	10	58.8	4.3	0.014	3.3	0.021
57P	10	71.1	5.2	0.018	3.4	0.017
58P	10	85.5	6.25	0.020	3.0	0.020
59P	10	102.5	7.5	0.026	1.3	0.020
60P	10	148	10.8	0.034	1.1	0.021
61P	1	178	15.9	0.040	1.1	0.020
62P	1	314	23.0	0.068	0.36	0.029
63P	1	542	39.6	0.122	0.056	0.038

TABLE 4.10

HE-3 Air-Blast Pressure
(Gage Height = 14 Inches)

Gage Code No.	Gage Rtng. (psi)	Horizontal Radius (ft)	Horizontal Radius λ	Arrival Time (sec)	Front Porch Peak (psi)	Front Porch Dur. (sec)	Positive Phase Peak (psi)	Positive Phase Durat'n (sec)	Positive Impulse (psi-sec)
52B	10	28.4	2.08	0.022	1.2	0.011	4.2	0.027	0.0484
54B	10	41.0	3.0	0.033	0.82	0.008	4.2	0.029	0.0440
56B	10	58.8	4.3	0.047	0.57	0.009	3.8	0.029	0.0396
58B	10	85.5	6.25	0.070	0.41	0.005	3.1	0.029	0.0326
60B	10	148	10.8	0.124	none		2.0	0.030	0.0222
61B	10	178	15.9	0.148	none		1.4	0.031	0.0185
62B	10	314	23.0	0.260	none		0.73	0.032	0.0110
63B	10	542	39.6	0.453	none		0.43	0.039	0.0070

[redacted]

[redacted]

PROJECT 1(9)-1

TABLE 4.11

HE-4 Earth Acceleration
(Gage Depth = 5 Feet)

Gage Code No.	Gage Rating (G)	Horizontal Radius (ft)	Horizontal Radius λ	Arrival Time (sec)	First Pulse Ampl. (G)	First Pulse Durat'n (sec)	Air-Blast Slap Ampl. (G)	Air-Blast Slap Period (sec)
Horizontal								
72H	30	28.4	2.08	0.007	4.6	0.009		
73H	30	34.0	2.49	0.008	5.2	0.010		
74H	30	41.0	3.0	0.009	3.2	0.011		
75H	30	49.5	3.62	0.010	2.1	0.014		
76H	5	58.8	4.3	0.012	1.0	0.016		
77H	5	71.1	5.2	0.015	0.86	0.017		
78H	5	85.5	6.25	0.018	0.56	0.018		
79H	5	102.5	7.5	0.023	0.52	0.019		
80H	5	148	10.8	0.034	0.69	0.015		
81H	5	178	15.9	0.041	0.50	0.016		
82H	5	314	23.0	0.068	0.12	0.024		
83H	1	542	39.6	0.125	0.030	0.039		
84H	0.5	1480	108	0.380	0.015	0.039		
Vertical								
72V	30	28.4	2.08	0.007			-28.5	0.008
73V	30	34.0	2.49	0.008			-26.3	0.008
74V	30	41.0	3.0	0.010			-23.3	0.010
75V	30	49.5	3.62	0.011			-15.3	0.018
76V	5	58.8	4.3	0.012			-10.0	0.011
77V	5	71.1	5.2	0.016			- 5.7	0.013
78V	5	85.5	6.25	0.019			- 5.6	0.011
79V	5	102.5	7.5	0.024	0.24	0.006	- 4.0	0.012
80V	5	148	10.8	0.034	0.49	0.013	- 1.5	0.023
81V	5	178	15.9	0.040	0.14	0.011	- 1.2	0.025
82V	5	314	23.0	0.067	0.019	0.018		
83V	1	542	39.6	0.125	0.0045	0.027		
84V	0.5	1480	108	0.388	0.006	0.042		

[redacted] [redacted]

[redacted]

PROJECT 1(9)-1

TABLE 4.12

HE-4 Earth Pressure
(Gage Depth = 5 Feet)

Gage Code No.	Gage Rating (psi)	Horizontal Radius (ft)	Horizontal Radius λ	Arrival Time (sec)	First Pulse Ampl. (psi)	First Pulse Durat'n (sec)
71P	100	23.5	1.72	0.005	19.7	0.049
72P	100	28.4	2.08	0.006	27.4	0.060
73P	10	34.0	2.49	0.007	17.0	0.041
74P	10	41.0	3.0	0.008	15.2	0.041
75P	10	49.5	3.62	0.010	12.9	0.044
76P	10	58.8	4.3	0.012	7.4	0.045
77P	10	71.1	5.2	0.014	13.3	0.044
78P	10	85.5	6.25	0.018	1.9	0.044
79P	1	102.5	7.5	0.022	1.4	0.046
80P	1	148	10.8	0.034	0.56	0.014
81P	1	178	15.9	0.040	0.64	0.014
82P	1	314	23.0	0.068	0.094	0.021
83P	1	542	39.6	0.124	0.015	0.035

TABLE 4.13

HE-4 Air-Blast Pressure
(Gage Height = 14 Inches)

Gage Code No.	Gage Rating (psi)	Horizontal Radius (ft)	Horizontal Radius λ	Arrival Time (sec)	Positive Phase Peak (psi)	Positive Phase Durat'n (sec)	Positive Impulse (psi-sec)
72B	100	28.4	2.08	0.003	106*	*	*
74B	100	41.0	3.0	0.006	85**	**	**
76B	100	58.8	4.3	0.011	19.0	0.020	0.167
78B	100	85.5	6.25	0.019	13.4	0.032	0.0739
80B	10	148	10.8	0.056	6.2	0.040	0.109
81B	10	178	15.9	0.077	3.9	0.043	0.0790
82B	10	314	23.0	0.184	1.8	0.049	0.0458
83B	10	542	39.6	0.369	1.0	0.056	0.0260

* Questionable. Cable torn loose from gage shortly after air-blast arrival.

**Questionable. Gage record failed to return to zero following passage of air blast.

[redacted]

[redacted]

TABLE 4.14

Horizontal Earth Velocity

Gage Code No.	Horizontal Radius (ft)	Horizontal Radius λ	Peak Vel. (fps) Max. Pos.	Peak Vel. (fps) Max. Neg.	Aver. Ampl. (fps)	Period (sec)
HE-1						
5H	49.5	3.62	1.6	1.2	1.4	0.062
6H	58.8	4.3	1.35	0.95	1.15	0.068
HE-2						
32H	71.1	2.08	2.75	0.90	1.83	0.190
33H	85.5	2.49	2.1	1.0	1.55	0.170
34H	102.5	3.0	1.3	0.57	0.94	0.180
35H	123	3.62	0.97	0.48	0.73	0.170
36H	148	4.3	0.79	0.40	0.60	0.180
37H	178	5.2	0.71	0.23	0.47	0.155
38H	217	6.35	0.62	0.36	0.49	0.175
39H	262	7.66	0.35	0.30	0.33	0.200
40H	314	9.2	0.27	0.17	0.22	0.135
41H	378	11.1	0.20	0.21	0.21	0.155
42H	512	15.0	0.17	0.05	0.11	0.215
43H	788	23.0	0.07	0.08	0.08	0.235
44H	1025	30.0	0.05	0.04	0.05	0.300
45H	1480	43.3	0.03	0.03	0.03	0.285

[redacted] [redacted]

[redacted]

CHAPTER 5

DISCUSSION

5.1 GENERAL

The discussion will be presented in terms of five topics: air blast, earth acceleration, time of arrival, earth pressure, and comparison with Dugway results. The general point of view will be that of making specific predictions for the underground nuclear test and, where possible, for the surface nuclear test. Apart from serving to help set the gage channel sensitivities, such predictions will be valuable in that both their success and their failure will give greater insight into the behavior of large underground explosions.

Because of the influence of air-coupled effects upon earth motion, certain aspects of this motion do not always scale as predicted in the absence of such feedback of energy. Since analysis and experience both indicate that some of the air-coupled effects should increase with the size of charge, a better understanding of them is needed if predictions are to be made with confidence for an operational, penetrating nuclear weapon. This report is confined to suggesting some of the possible explanations and to presenting whatever evidence is available to indicate how scaling should be effected.

In general, Tests HE-1 and HE-2 will be examined for consistent scaling of each phenomenon. If the expected scaling is observed, then predictions will be made for the underground nuclear test and usually also for the surface nuclear test. Where scaling fails in either magnitude or consistency, predictions will sometimes be made to indicate upper or lower limits.

5.2 AIR BLAST

Figure 4.1 indicates typical transient air-blast wave forms, and in Tables 4.4, 4.7, 4.10, and 4.13 are listed the time of arrival and the peak overpressure and duration, for both the front porch (HE-3 only) and the total positive phase. Figures 5.1 through 5.4 show the peak overpressure and positive phase duration as a function of λ. These results are summarized in the composite pressure curves of Figure 5.5 and the duration curves of Figure 5.6. In this report the term "pressure" is used for overpressure; total or absolute pressure will be used specifically where needed. The pressures tabulated

[redacted]

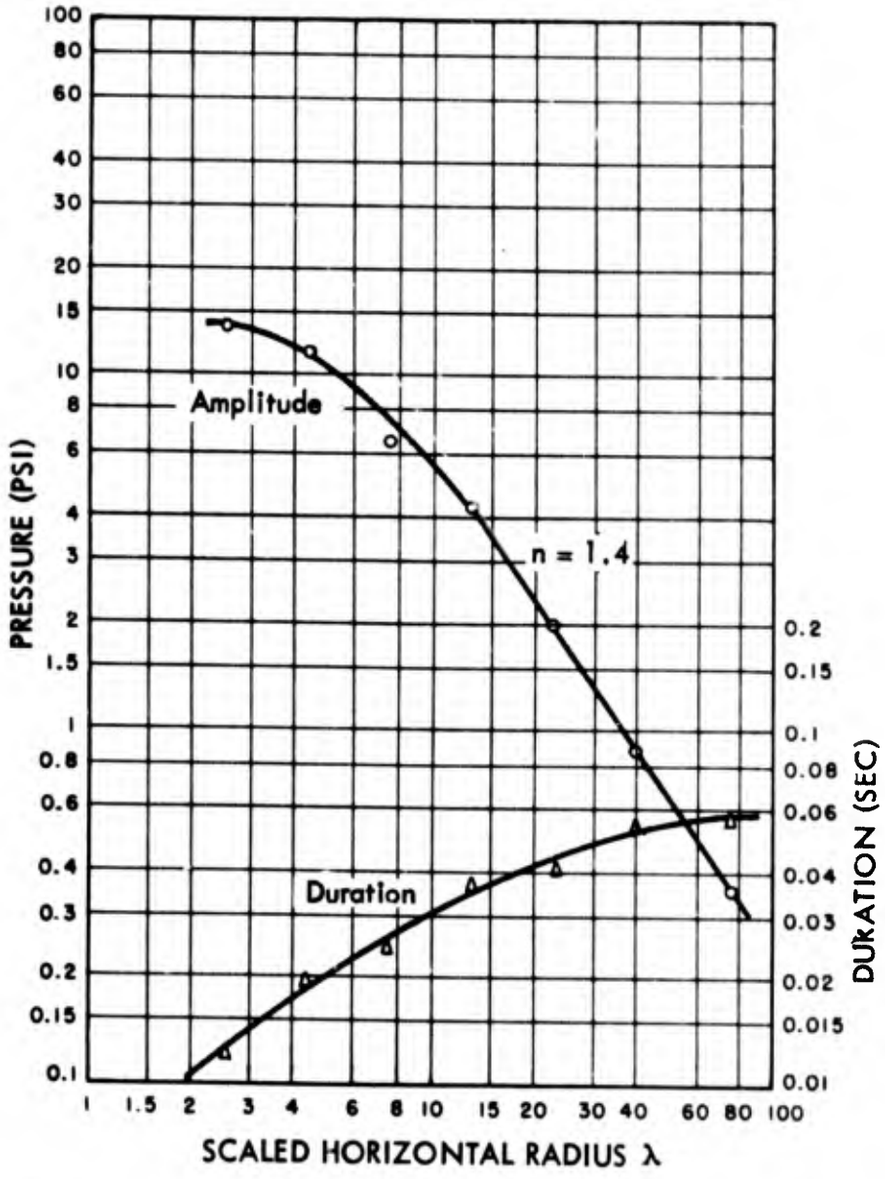

Fig. 5.1 HE-1 Air-Blast Maximum Peak and Positive Duration

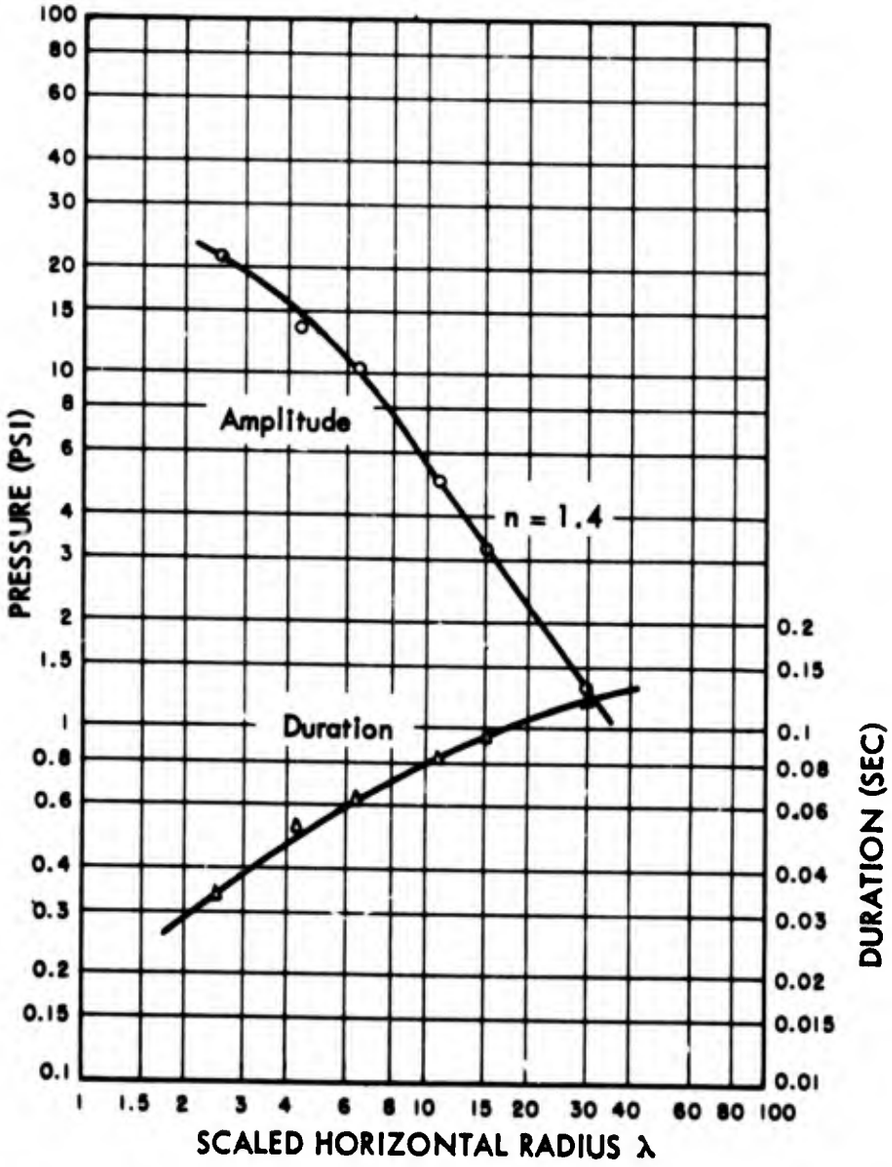

Fig. 5.2 HE-2 Air-Blast Maximum Peak and Positive Duration

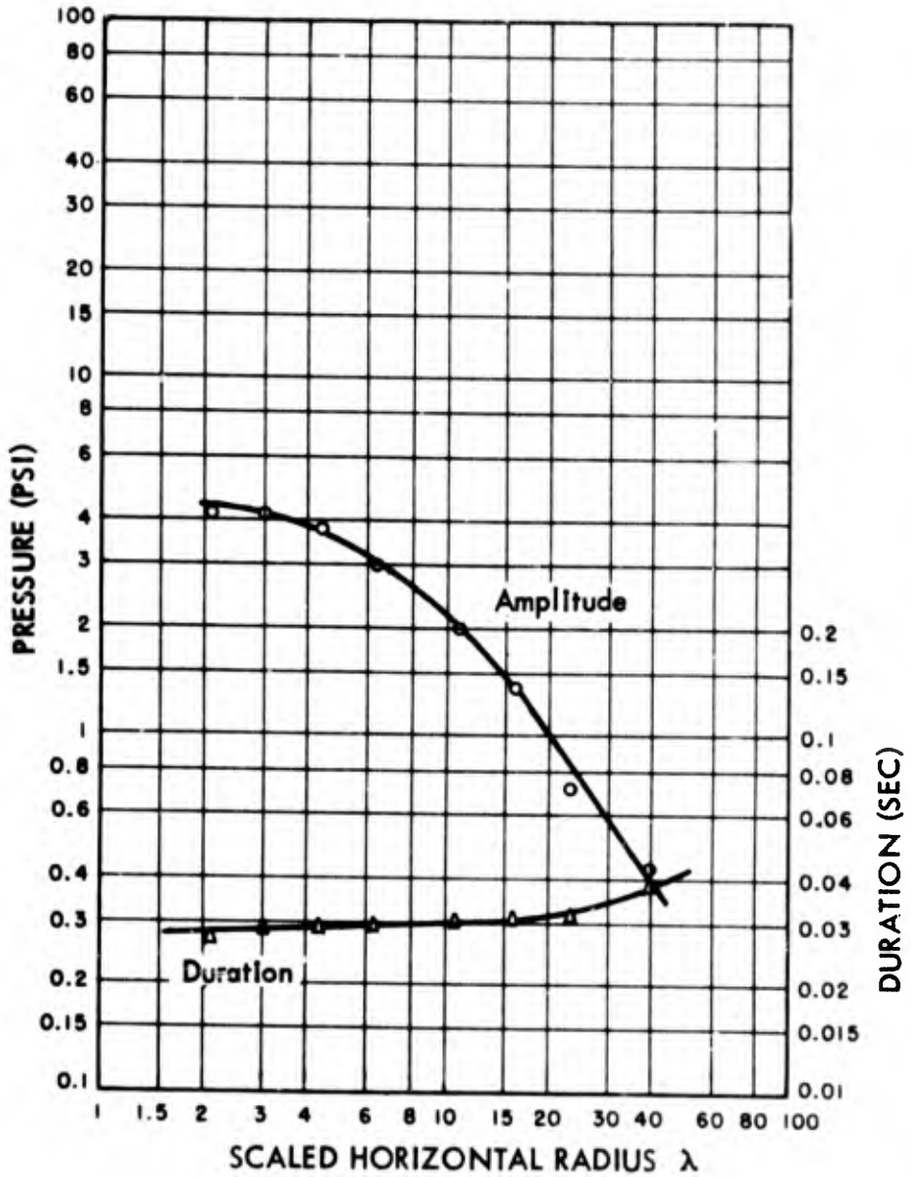

Fig. 5.3 HE-3 Air-Blast Maximum Peak and Positive Duration

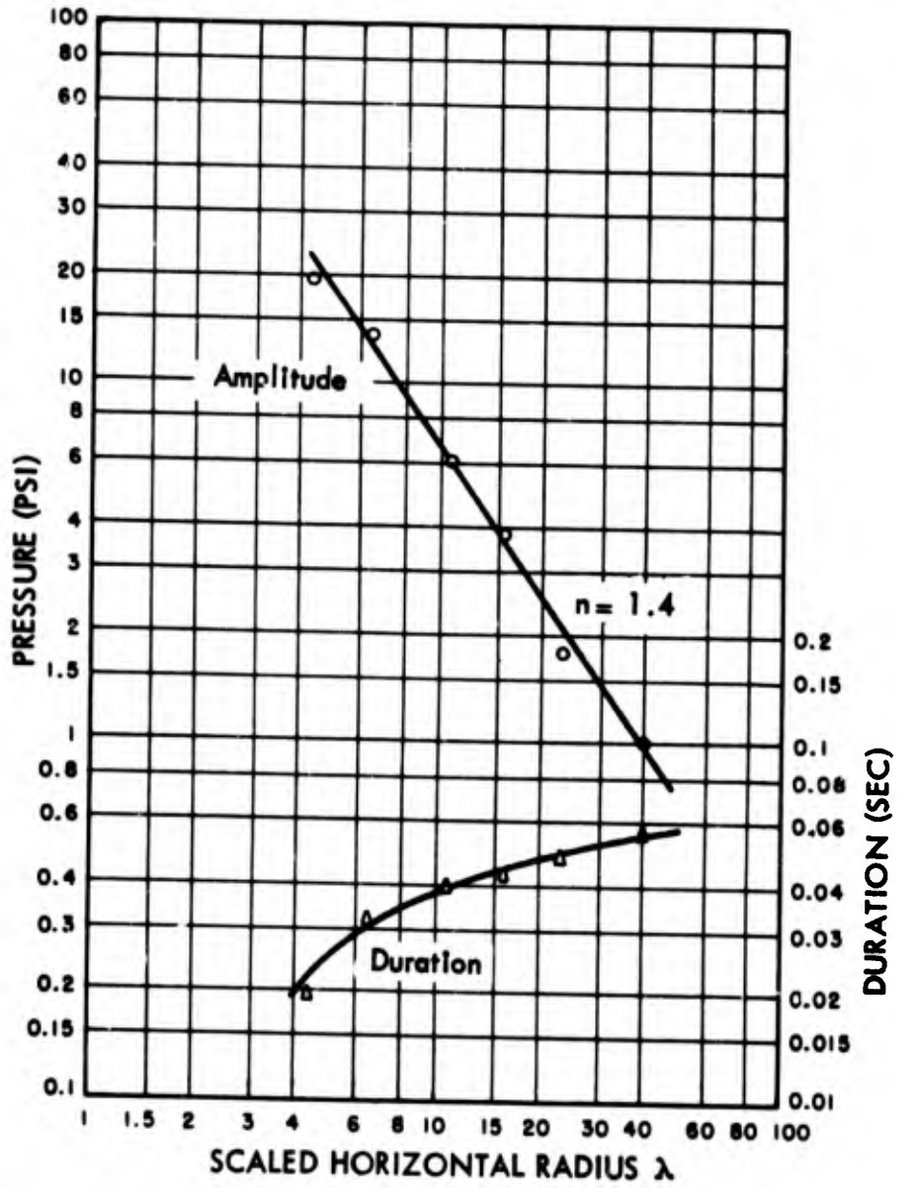

Fig. 5.4 HE-4 Air-Blast Maximum Peak and Positive Duration

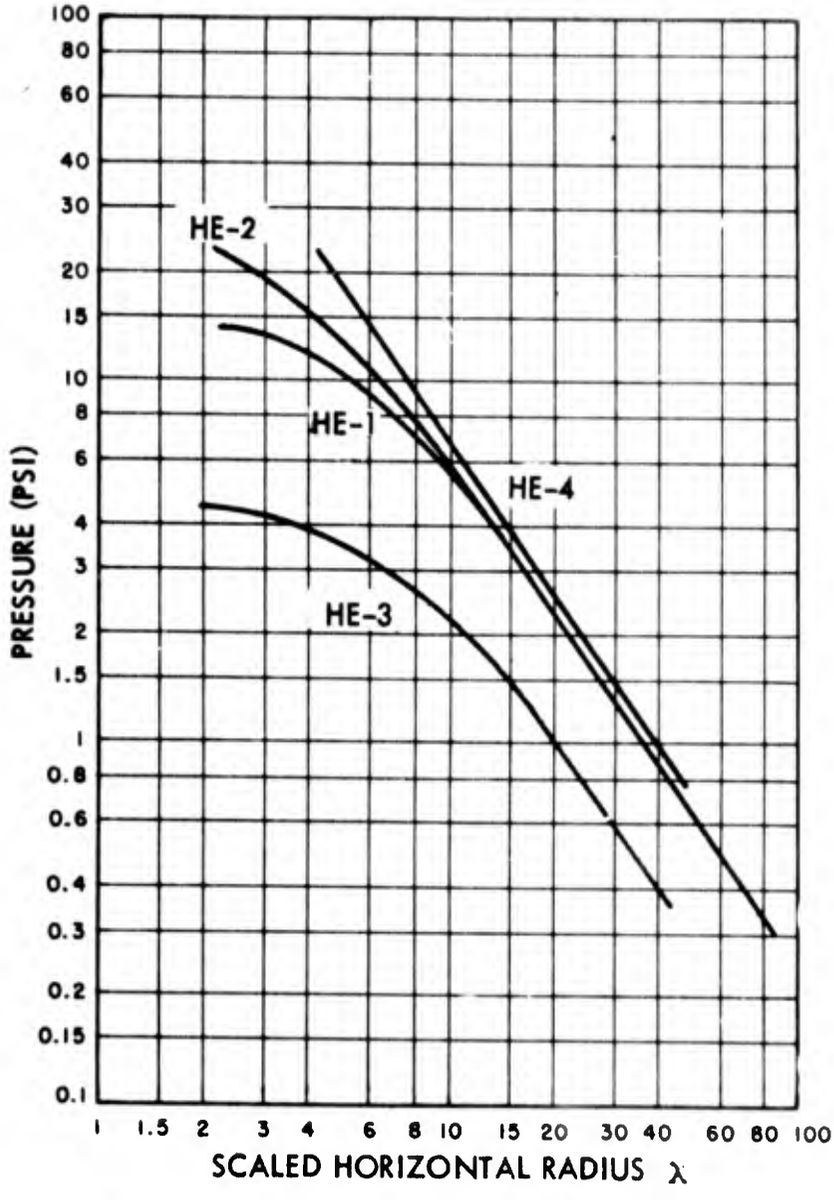

Fig. 5.5 Air-Blast Maximum Peak Pressure, All Tests

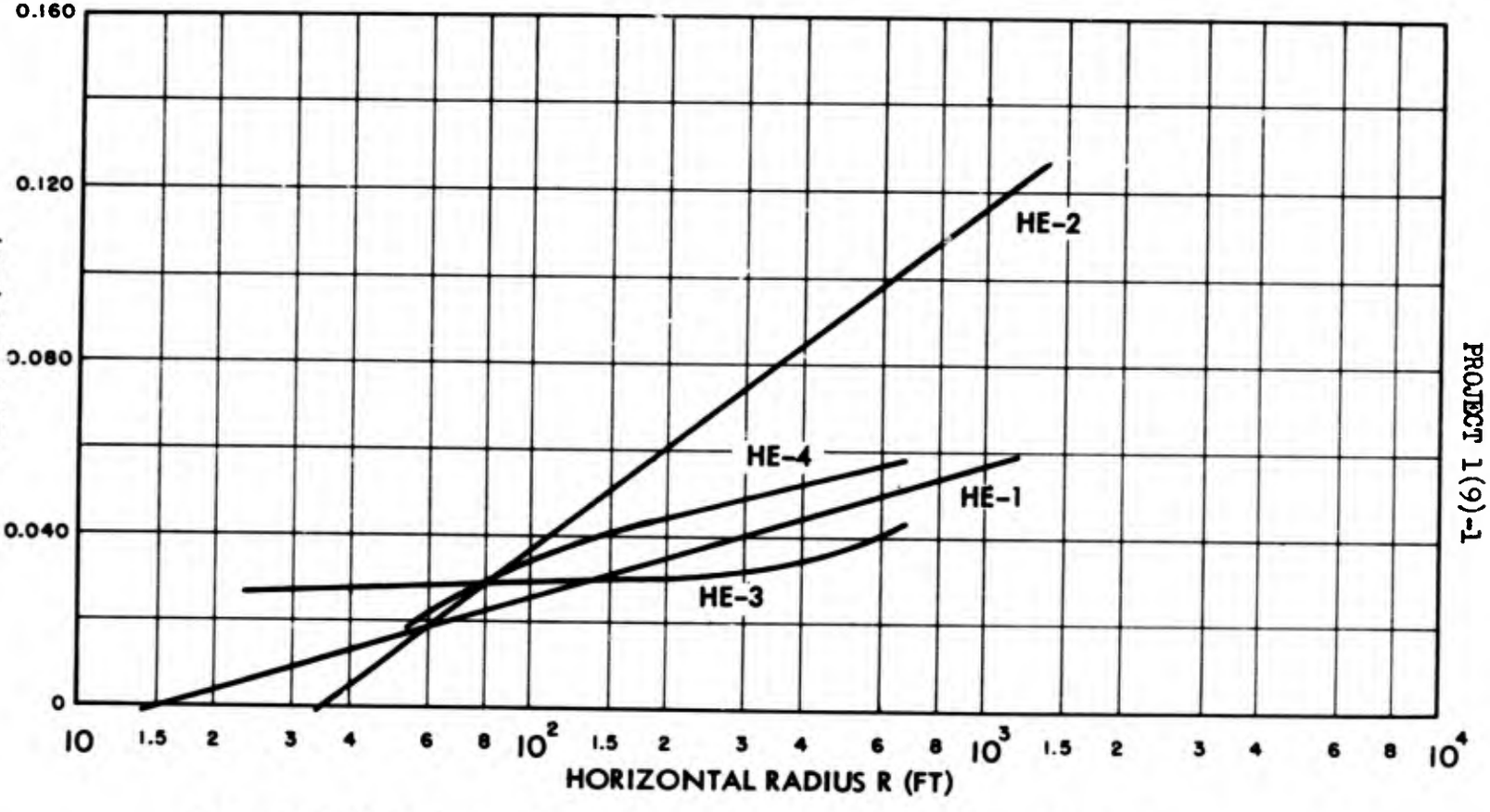

Fig. 5.6 Air Blast, Duration of Total Positive Phase, All Tests

have not been reduced to the values to be expected at sea level. This reduction was not necessary, since the nuclear tests for which these HE tests provided preliminary information were also conducted at the same site. It may be noted that the ambient pressure was about 12.6 psi.

Several features may be noted on the peak pressure curves. First, at large λ the negative slope on all tests is asymptotically 1.4. Since the plots are on log-log paper, this number is also the exponent n in an inverse power law of the form

$$P = \frac{A}{R^n}, \qquad (5.1)$$

where R is the horizontal distance from the gage to ground zero. Second, in the composite peak pressure curves of Figure 5.5 it is seen that for $\lambda > 10$, the peaks in HE-1 and HE-2 scale as predicted ($S = 2.5$). Third, the air blast from the surface test, HE-4, is only about 15 per cent greater than that from the shallow buried charges, HE-1 and HE-2. Fourth, the air blast from HE-3, at a scaled charge depth of 0.5, is less than 40 per cent of that from the surface burst. Finally, for $\lambda < 10$ the curves show various degrees of divergence. This is apparently not due to instrumental error, since substantially the same phenomenon was present in the pressures obtained from the time of arrival (velocity) method employed on HE-1 and HE-2 by a group from the Ballistic Research Laboratories.

It was noted above that at large λ the air-blast peak pressures for HE-1 and HE-2 scaled as predicted. The graphical comparison in Figure 5.5 is quite simple, since the curves for scaled tests should coincide. However, when the positive phase duration is considered, the situation is slightly more complicated. In Figure 5.6 the positive phase duration for HE-1 and HE-2 plots as a straight line against log R (on semi-log paper). This affords the opportunity for using two separate analytical comparisons for calculating the scale factor, S. First, the curves intersect the abscissa axis at different points corresponding to different horizontal distances from ground zero. The ratio of these distances should be the known scale factor, 2.5; the observed ratio is $35/14.5 = 2.4$. Another quantity that should scale is the slope dt/d (log R). The slope will not depend on the units of R, because log R is simply changed by a constant, when R is multiplied or divided by a constant. Thus the ratio of the slopes should be the scale factor, since time alone contributes dimensions. The observed slope ratio is $80/31 = 2.6$; together with the intercept ratio, the resultant average scale factor is 2.5. This agreement for the amplitude and time aspects of the air blast is further reinforced by examining the transient records of Figure 4.1. Except for small

details, the appearance is quite similar. Note that in Figure 4.1 the time scale for HE-2 has been changed by the scale factor (S = 2.5) to make the comparison direct.

The results for HE-2 may now be scaled up to 1 KT of TNT for the underground nuclear test. This is shown in Figure 5.7 for the peak pressure and Figure 5.8 for the positive phase duration. Peak pressure for the surface nuclear test is also predicted from HE-4 in Figure 5.7, but no predicted duration for the surface nuclear test appears on Figure 5.8. This is because the shape of the HE-4 duration curve (see Figure 5.4) is quite different from the others, and the close-in air-blast data were not conclusive. For an estimate, however, the duration of the positive phase at 1000 feet for the surface nuclear test may be near 0.3 second.

The predicted peak pressure curve for the underground nuclear test is shown with the same droop at small λ as for HE-2. It is anticipated that the actual pressures will be greater than those predicted from HE-2 in this region. This conclusion is suggested by the behavior of HE-1 and HE-2 for $\lambda < 10$: as the charge size increases, the departure from the asymptotic straight line becomes less at a given value of λ. However, with only two tests on which to base the trend, this conclusion must be regarded as tentative.

The integral of the positive phase of the air blast pressure-time curve represents the positive impulse, which is tabulated in Chapter 4. The variation of impulse with scaled horizontal radius is shown in Figures 5.9 and 5.10; Figure 5.11 summarizes the results from all four tests. In the last figure the values of impulse for HE-2 have been divided by the scale factor of 2.5, and are shown as points near the curve for HE-1. The closeness of fit indicates satisfactory model law behavior and lends further support to the validity of scaling air-blast phenomena. Predictions of the impulse for the underground and surface nuclear tests, using the scale factor for 1 KT of TNT, are shown in Figure 5.12. The dotted portions indicate extrapolation from values in the λ-range covered by HE-2 and HE-4.

It is possible to express the peak air-blast pressure in terms of a fraction α of the weight W of the underground charge, where α is so chosen that if αW is detonated at the surface, the same blast pressure p is observed at the same radial distance R. In general, α is a function of the matching pressure chosen; α is constant only if the air blast vs. distance curves for buried and surface charges can be matched for all pressures by translation in the direction of the R-axis only on a log-log presentation. Figure 5.13 graphically illustrates what is involved in obtaining α; Figures 5.13a and 5.13b indicate the charge geometry involved. Figure 5.13c shows the reference surface pressure,

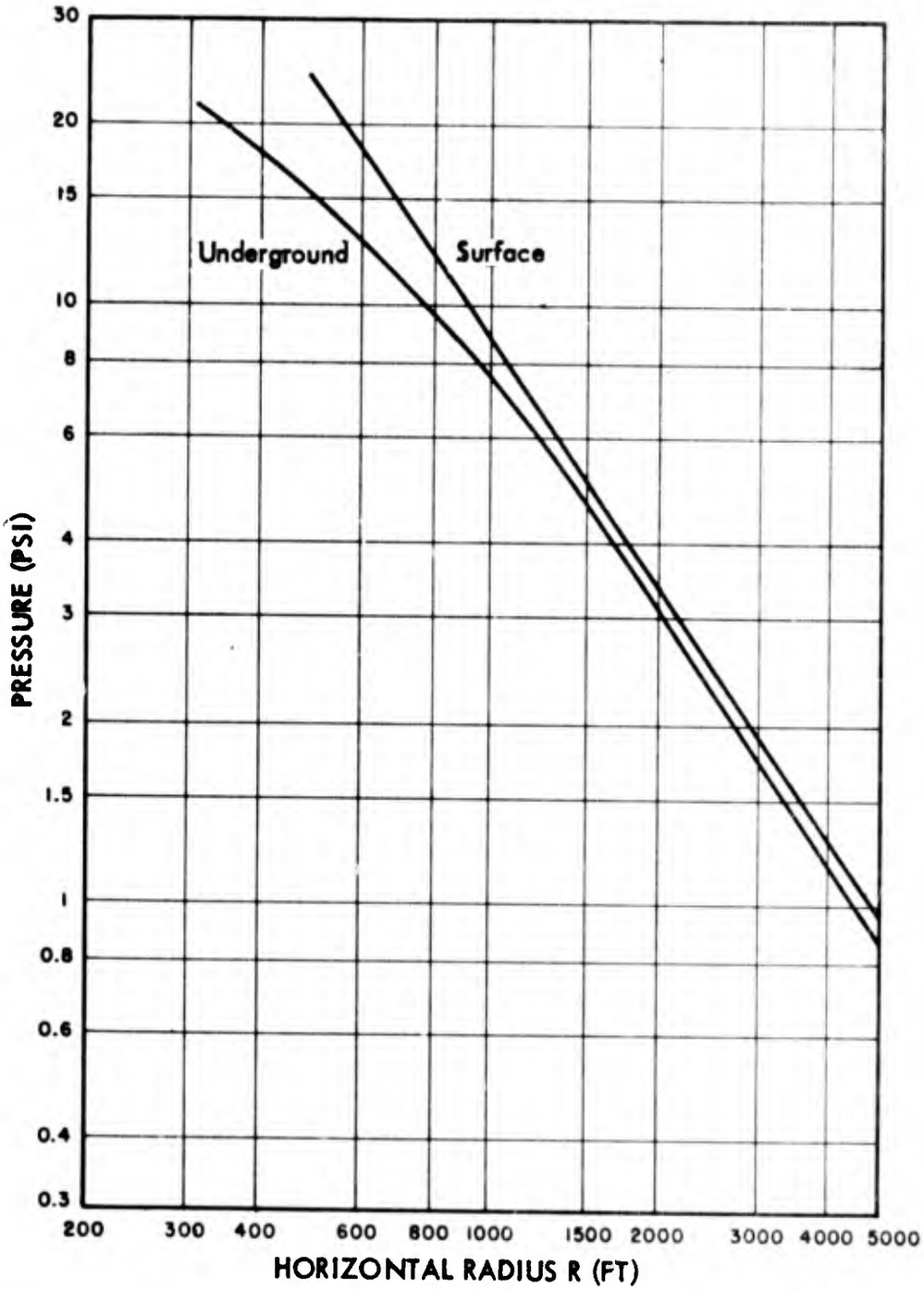

Fig. 5.7 Predicted Maximum Air-Blast Pressure, Underground and Surface Tests

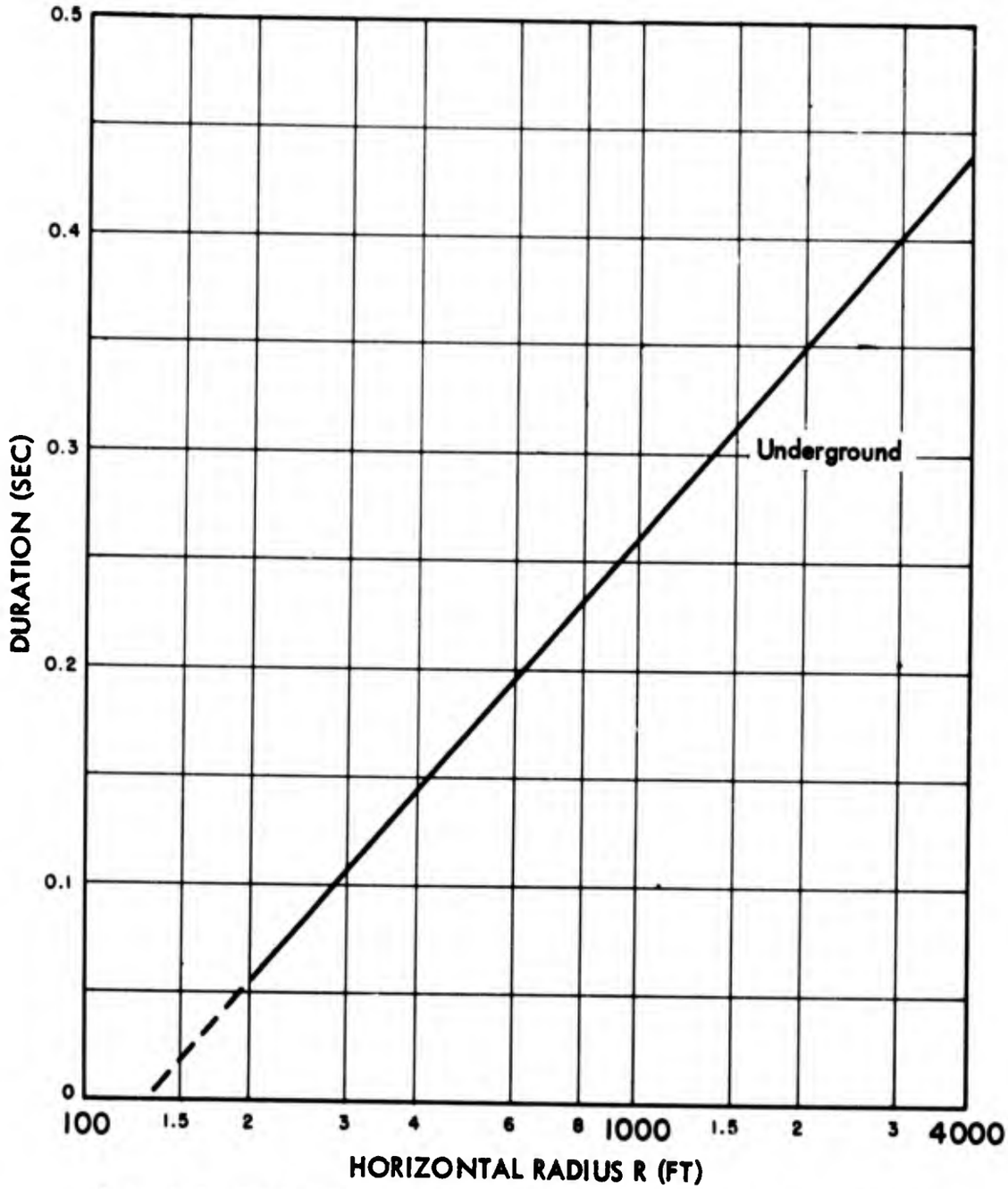

Fig. 5.8 Predicted Duration of Positive Phase of Air Blast, Underground Test

[redacted]

PROJECT 1(9)-1

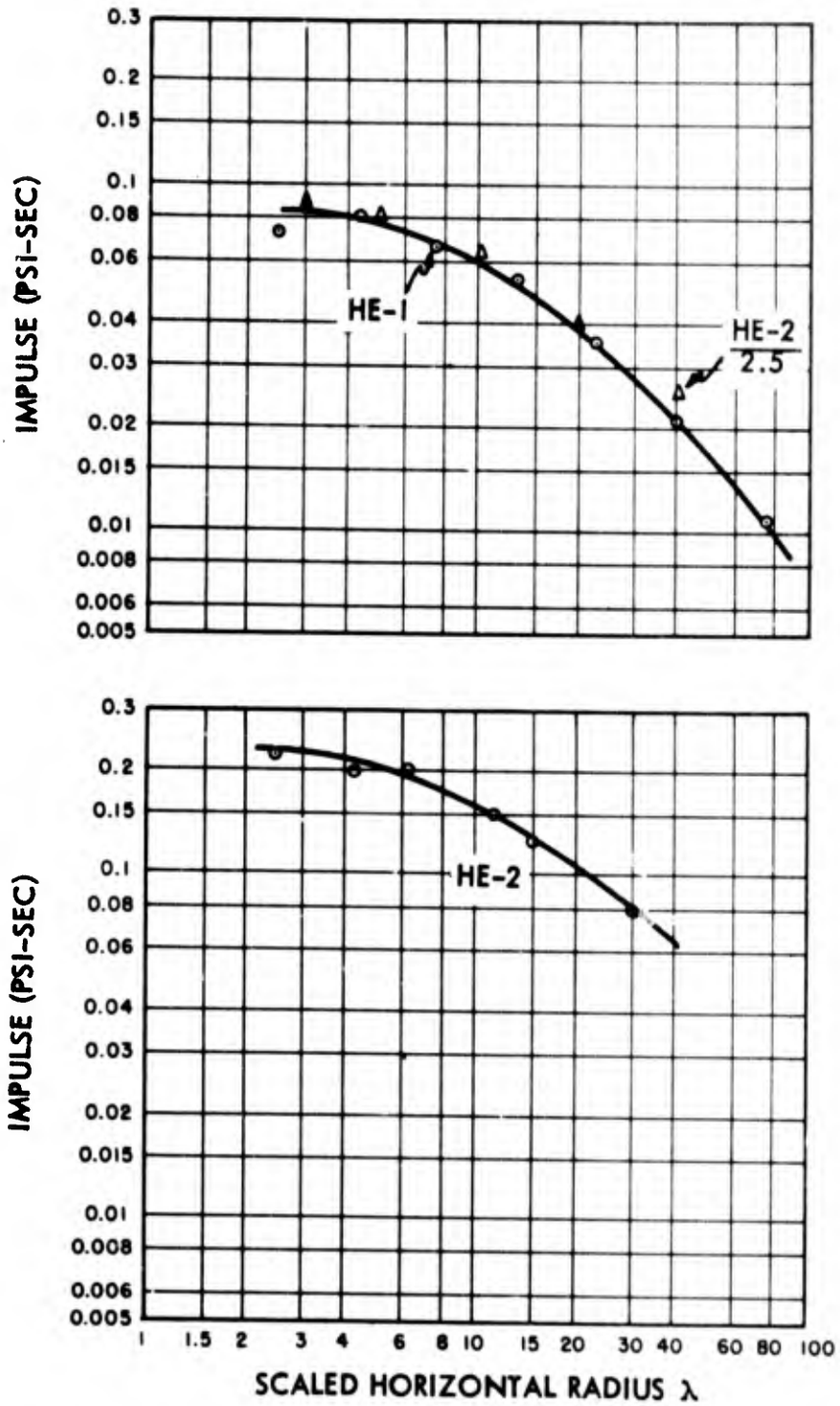

Fig. 5.9 Air-Blast Positive Impulse, HE-1 and HE-2

[redacted]

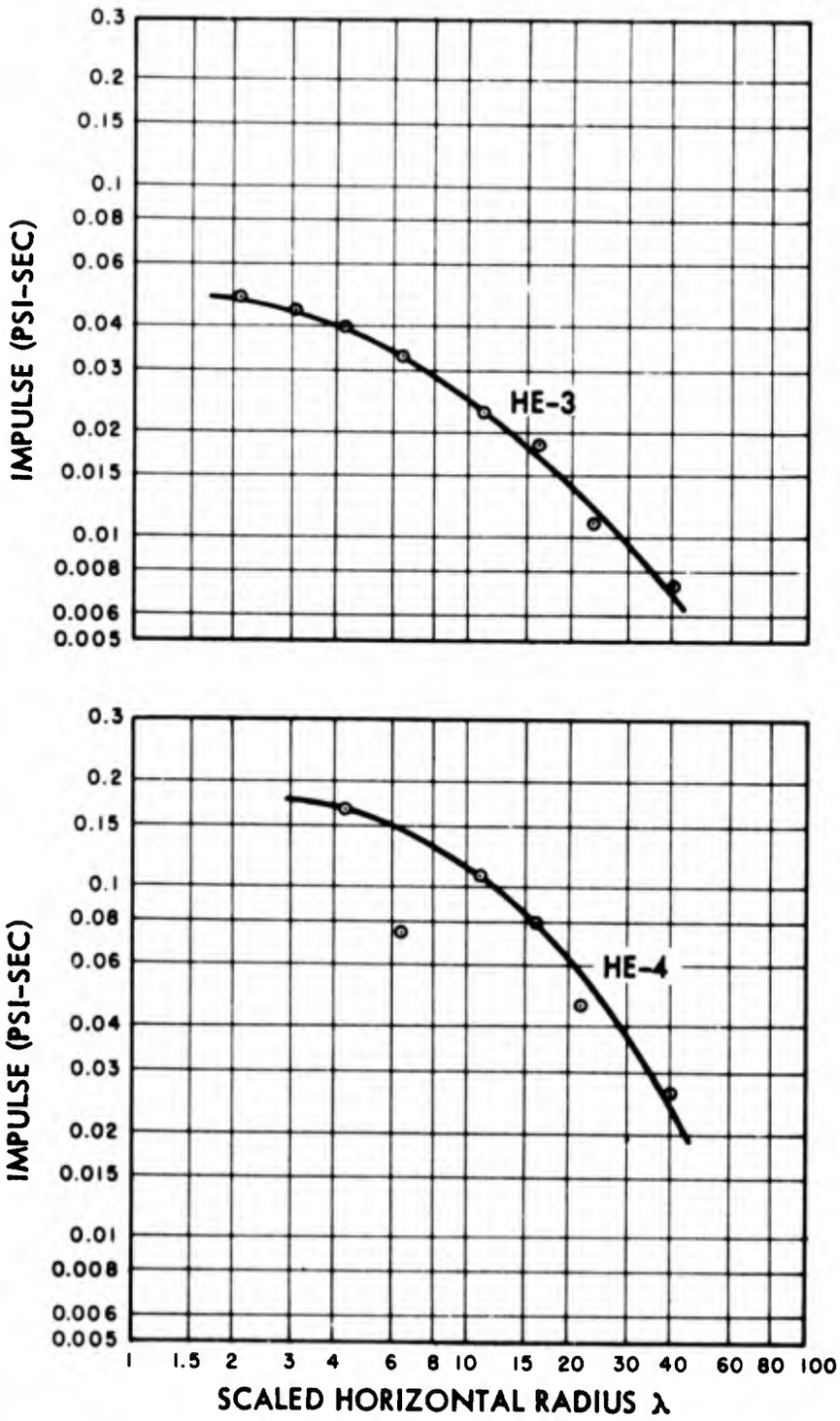

Fig. 5.10 Air-Blast Positive Impulse, HE-3 and HE-4

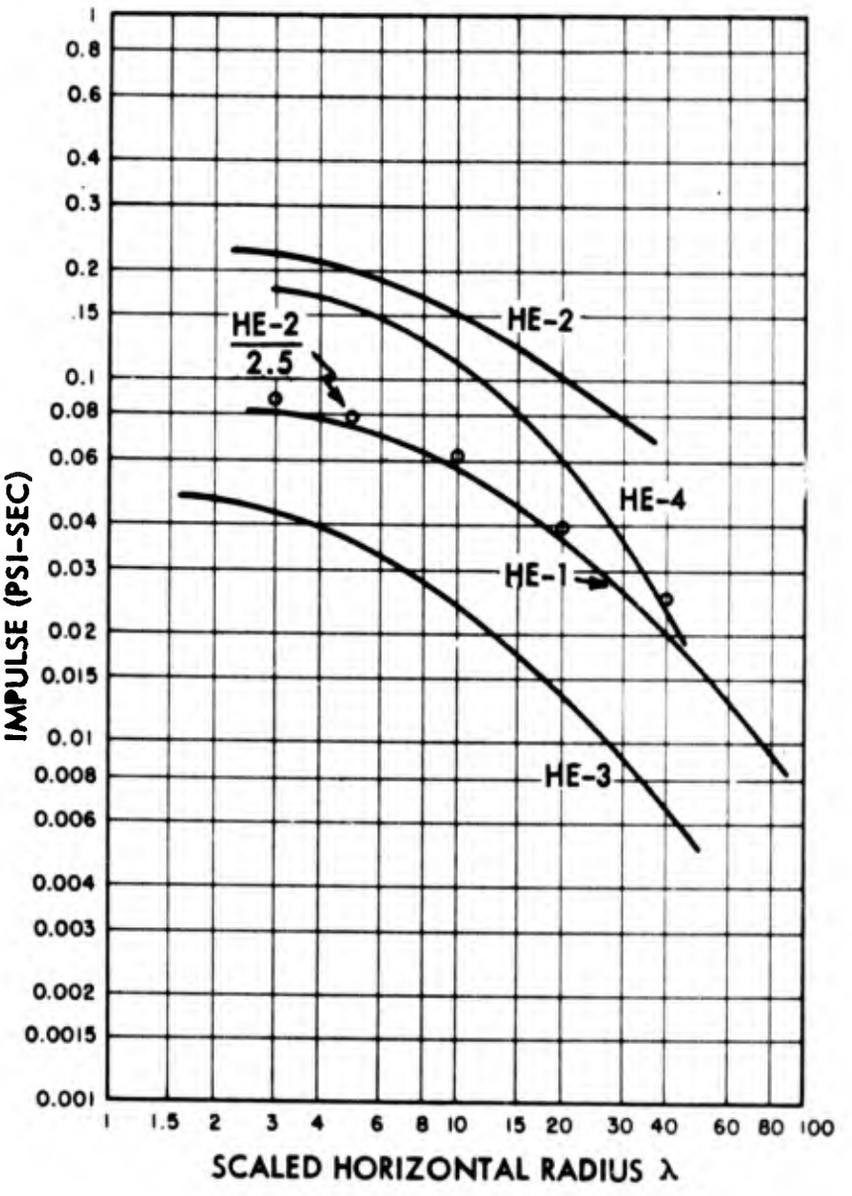

Fig. 5.11 Air-Blast Positive Impulse, All Tests

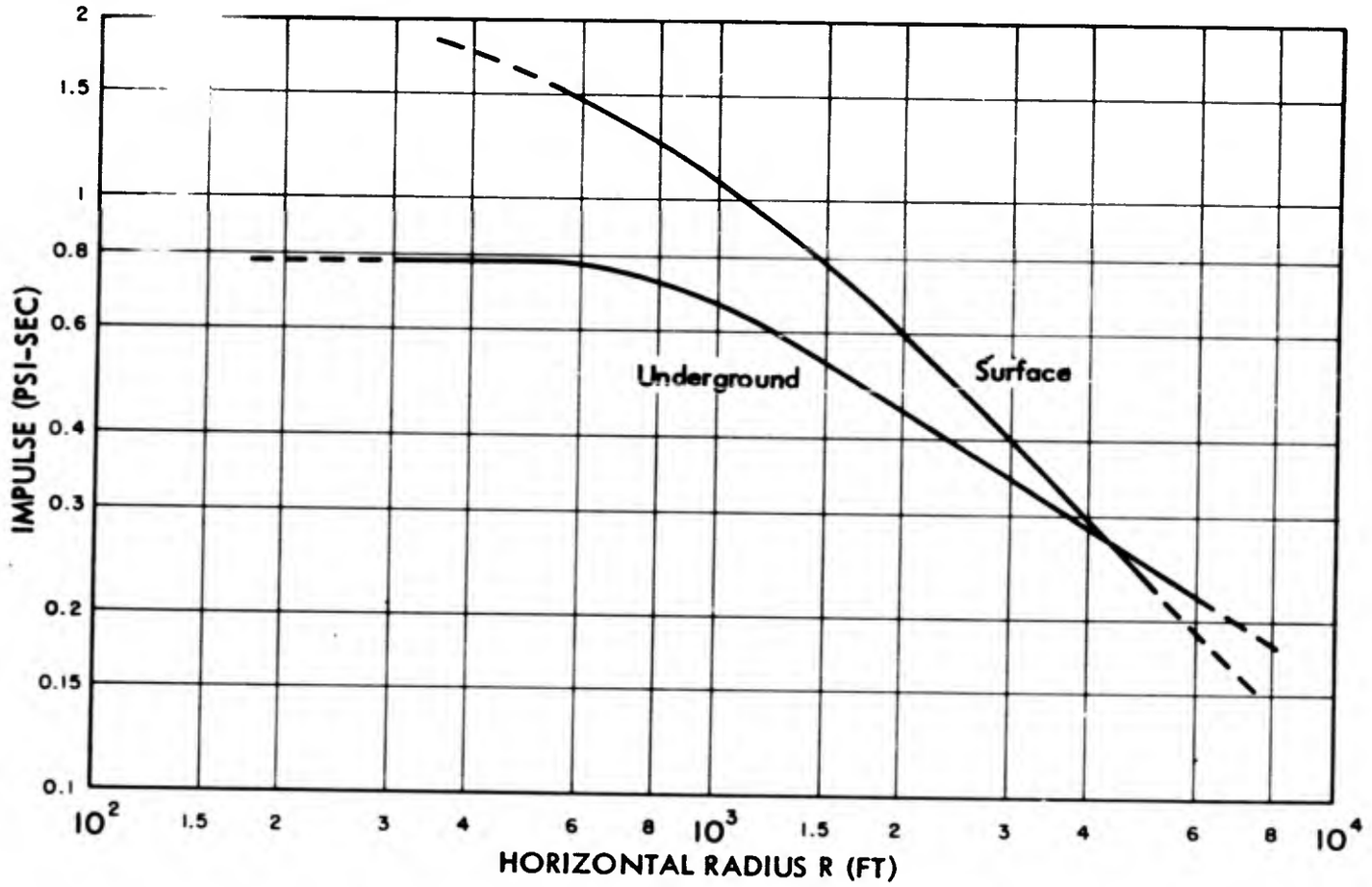

Fig. 5.12 Predicted Air-Blast Positive Impulse, Underground and Surface Tests

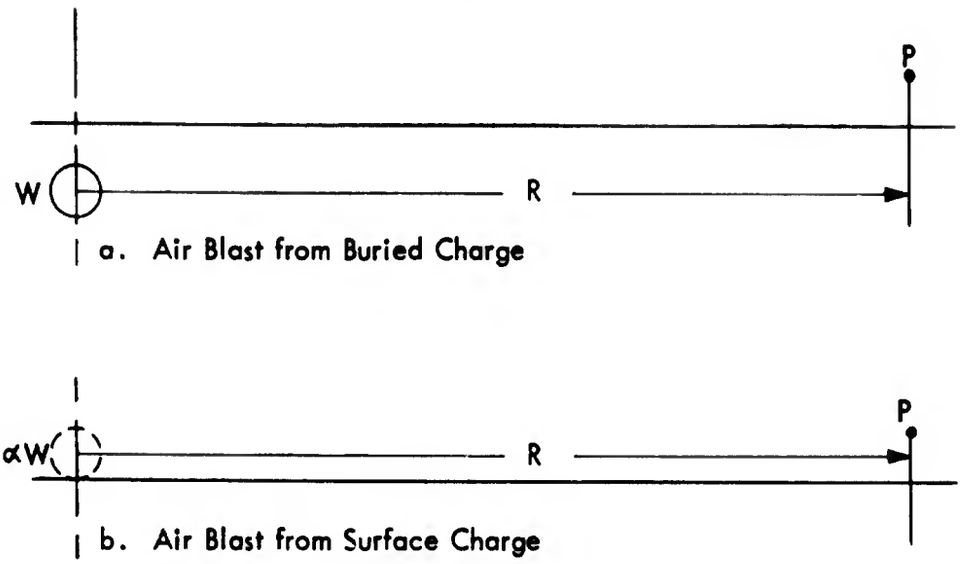

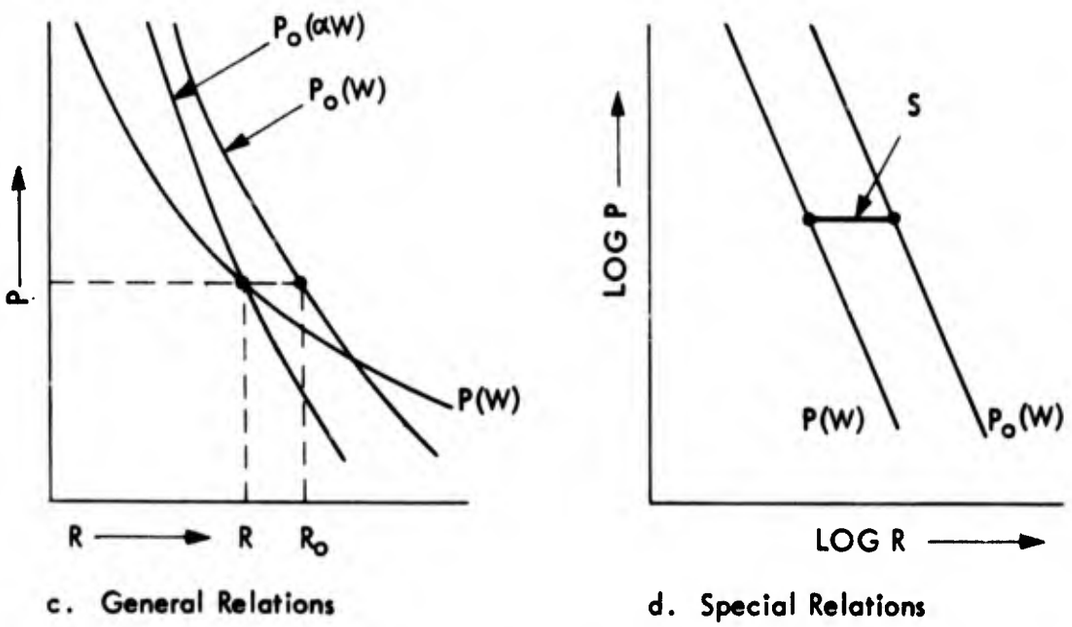

Fig. 5.13 Equivalent Surface Charge for Air Blast

p_o (with charge weight W as the parameter), and the pressure, p, for a buried charge of the same weight. It can be seen in this figure that the shapes of these two curves may differ widely. However, if scaling laws hold at each position of the charge, then there exists an α such that for a given pressure p(W), $p(w) = p_o(\alpha W)$. Graphically, if given the curves p(W) and $p_o(W)$ of Figure 5.13c, one first draws a horizontal line for the given value of p at which matching is desired. Then the ratio of the radii corresponding to the R-shift of the points is R/R_o. Since scaling laws are assumed to hold, the radius ratio is the scale factor S. Then, since α is a charge-weight ratio,

$$\frac{\alpha W}{W} = S^3 = \left\{\frac{R}{R_o}\right\}^3, \quad \text{or} \quad \alpha = \left\{\frac{R}{R_o}\right\}^3. \tag{5.2}$$

In the simple case when both pressure functions are parallel lines on a log-log grid, the horizontal separation is constant and corresponds to the scale factor S. Alternatively, if the vertical separation p_o/p (at given R) and the slope exponent n are known for the parallel curves, then

$$\alpha = \left\{\frac{p}{p_o}\right\}^{3/n}. \tag{5.3}$$

By the above procedure it is found that for peak air-blast pressure the equivalent surface values of α are: HE-4, 100 per cent; HE-3, 12 per cent; and HE-1, HE-2, 75 per cent. This holds only for $\lambda > 10$; for smaller λ there is no longer a single value for the equivalent charge ratio, and any comparison in this region must state the pressure that is being matched. Note that if the equivalent surface charge is determined for positive phase duration or positive impulse, the values of α will in general not be the same. The above discussion applies specifically to the peak pressure; different geometrical and analytical operations for duration and impulse are required.

The front porch observed on HE-3 (see Figure 4.1) was also present in the 1951 tests at the same scaled charge depth (0.5) at the Dugway Proving Ground, Dry Clay Site. In the report covering certain aspects of this program,[3] explanations were advanced to explain this shape of shock wave. Briefly, it is assumed that first the earth rises relatively slowly but steadily; this is supported by measurements taken from high-speed motion pictures. The resultant air shock from this "earth piston" should thus be of small but relatively constant amplitude. However, the explosion gases soon pierce the curtain of rising earth. Since the velocity of this gas jet is considerably greater than that of the rising earth, the air shock resulting from this "gas

jet piston" is stronger than that from the earth rise. However, the jet is decelerated much faster than the earth, so the air-blast pressure decays from the peak much more rapidly than does the pressure from the earth rise alone. Now, the jet shock is traveling through a medium already shocked by the earth rise. Hence the jet shock will start later, but will eventually overtake the "earth piston" shock and merge to produce a single shock; in HE-3 the point of catch-up[7] occurred at a value of λ in the region of 6.25 to 10.8.

To summarize, this discussion of the air blast indicates that the model law behavior is quite satisfactory, and air-blast predictions for HE tests may be made from it with considerable confidence. Air blast scales completely in peak pressure, positive duration and positive impulse. Stated in other terms, air-blast phenomena expressed as a function of time and horizontal distance scale well in both these variables. In the next section it will be demonstrated that earth motion shows no such over-all adherence to the model laws, which is necessary to permit reliable predictions.

5.3 EARTH MOTION

As indicated earlier in this report, the choice of acceleration for earth motion measurements was determined principally by the reliability and availability of instruments, rather than by damage considerations. Hence particle velocities and displacements must be obtained by integration of the acceleration records. Some preliminary cross-checked results on velocity from the machine integration of HE-2, plus a few points obtained for HE-1, are discussed here. A complete presentation will be reserved for the final contract report to be prepared for the Office of the Chief of Engineers, U. S. Army, for whom this work was done under Contract DA-49-129-eng-119 with Stanford Research Institute. Again, the general point of view will be that of examining the propriety of applying scaling laws; predictions for the underground and surface nuclear bursts, based on 1 KT of TNT, will be made whenever justified.

Reference should be made to the sample transient earth acceleration records in Figures 4.2 through 4.7 for five-foot gage depth. These records have been replotted so that the time and acceleration scales for HE-2 contain the scale factor of 2.5. Thus the records may be compared directly for similarity of wave form, particularly HE-1 and HE-2. The arrival of the air blast at the gage station is denoted by the arrow and the symbol AB. These records are but a small portion of those that have been published in the Interim Report.[6] They do, however, illustrate all the quantities of interest, as specified in Figure 4.17.

On a casual qualitative basis, the comparison of HE-1 and HE-2 records reveals a general similarity, but with considerable difference in details. The scaled pulse durations for HE-2 appear slightly less than those predicted from HE-1; the amplitudes are erratic but fairly similar. In the vertical accelerations the arrival of the air blast at the gage station is evinced a few milliseconds later by a sharp, initially negative, damped oscillation (the slap) superimposed on the longer-period pulses obtaining before the air blast arrives. The prominence of this first (negative) peak above the low-frequency pulses also increases from HE-1 to HE-2, suggesting that for still larger charges this effect of air blast would be still greater. A measure of this effect may be obtained by first smoothing the vertical acceleration curve as shown dotted in Figure 4.17. Then the high-frequency deviations from this lower-frequency base line are a measure of the air-blast slap. Figure 4.10 shows the approximate wave form of the slap in the vertical acceleration from Test HE-2, at $\lambda = 7.66$. Of course, this implicit assumption that superposition holds is probably not justified, owing to the complex nature of the interaction. This slap is almost certainly the direct effect of the air blast, and interferes with the scaling of other phenomena. For this reason the smoothing referred to above has been carried out to separate the long- and short-period phenomena, particularly for the first pulse and the slap reported in the tables of Chapter 4.

On comparing the vertical acceleration records for HE-1 and HE-3, it is evident that there is very little effect of air blast upon the acceleration for HE-3. This is in agreement with the smaller air blast of HE-3 (Figure 5.5) as well as with the increased earth acceleration normally to be expected from the better coupling afforded by the deeper scaled charge depth of the HE-3 test. Both horizontal and vertical smoothed first acceleration pulse components for HE-3 are roughly two to three times those for HE-1.

In a sense, earth acceleration from HE-4 is induced entirely by the air blast, but in appearance these records are not too dissimilar to the others. There appear to be consistently more high-frequency components in the HE-4 records than in the others.

A convenient measure of the magnitude of the earth acceleration is the maximum value of the smoothed first half cycle, or pulse. This measure is significant only if (1) the peak acceleration is a quantity of interest, and (2) if the amplitude of the first pulse is the largest. Peak acceleration is a useful quantity for damage calculations only if the pulse duration is considerably greater than the period of the structure being attacked. Hence if the peak acceleration is used at all, only low-frequency pulses need to be considered. This

[redacted]

justifies the smoothing which first removes the high-frequency slap peaks. The second requirement of significance is not fulfilled throughout all the acceleration records. However, it is followed with reasonable consistency in the close-in horizontal accelerations, which represent the earth motion of prime military interest. The amplitude and duration of the first smoothed pulse of the horizontal earth acceleration as a function of scaled hoirzontal radius are shown in Figures 5.14 through 5.17 for each of the four tests; the air-blast slap has been edited out. The curves are quite similar to those reported earlier,[6] except Figure 5.17 for HE-4; the smoothing necessary makes the new curve about 40 per cent of the previous one. A similar series for the vertical components is presented in Figures 5.19 through 5.22. Figure 5.18 is a summary for the first pulse horizontal acceleration amplitudes, and Figure 5.23 presents the vertical summary. In both summaries the acceleration has been scaled by reduction to one pound of TNT; for any charge weight W (pounds of TNT) in the range of applicability, the acceleration at a given λ is the graphical value divided by $W^{1/3}$. It is seen that the scaling of acceleration first pulse magnitude from HE-1 and HE-2 is acceptable when $\lambda > 4$, for both components.

When the durations of the smoothed first pulse are compared for HE-1 and HE-2, the picture is different. For the horizontal component the time ratio is about 2 : 1, whereas it is only 1.6 : 1 for the vertical. The scale factor, S, between these two tests was 2.5. Thus the first pulse of acceleration does not follow the model law as a complete phenomenon. If the amplitudes only are considered, then the expected values for the underground and surface nuclear tests may be estimated. However, since the whole acceleration function does not scale, the model law can be applied to acceleration with considerably less confidence than to air blast. As an empirical fact, it may be noted that for the first horizontal pulse the duration varies as $W^{1/4}$. On this basis, the estimated duration of the smoothed first horizontal acceleration pulse for the underground nuclear test should be about 110 milliseconds near 1000 feet. Of course, this scaling can have no significance unless all aspects of the phenomenon being considered scale in a manner consistent with this relation. Since consistent scaling on this basis is not followed (peaks appear to scale as $W^{1/3}$), the predicted time is nothing more than a rough empirical estimate. A similar procedure provides an estimate of 50 milliseconds for the first vertical pulse duration near 1000 feet for the underground nuclear test, exclusive of air-blast induced effects.

Scaling of the amplitude of the first pulse may be applied only on the basis that the results are not as firm as for air blast. Figure 5.24 indicates the predicted horizontal amplitudes for both underground and surface nuclear tests (the latter scaled from HE-4);

[redacted] [redacted]

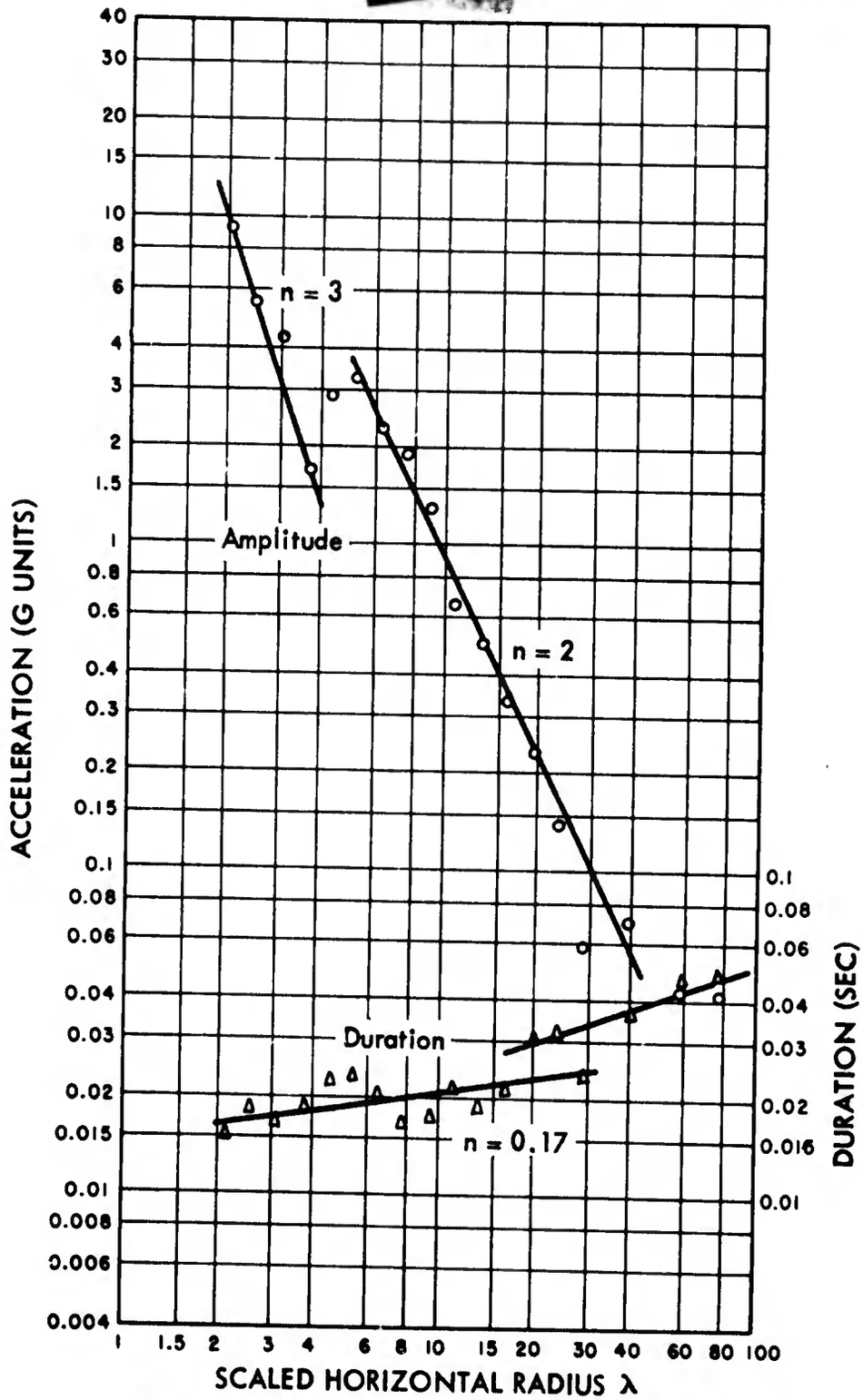

Fig. 5.14 HE-1 Horizontal Earth Acceleration, Maximum and Duration in Smoothed First Pulse

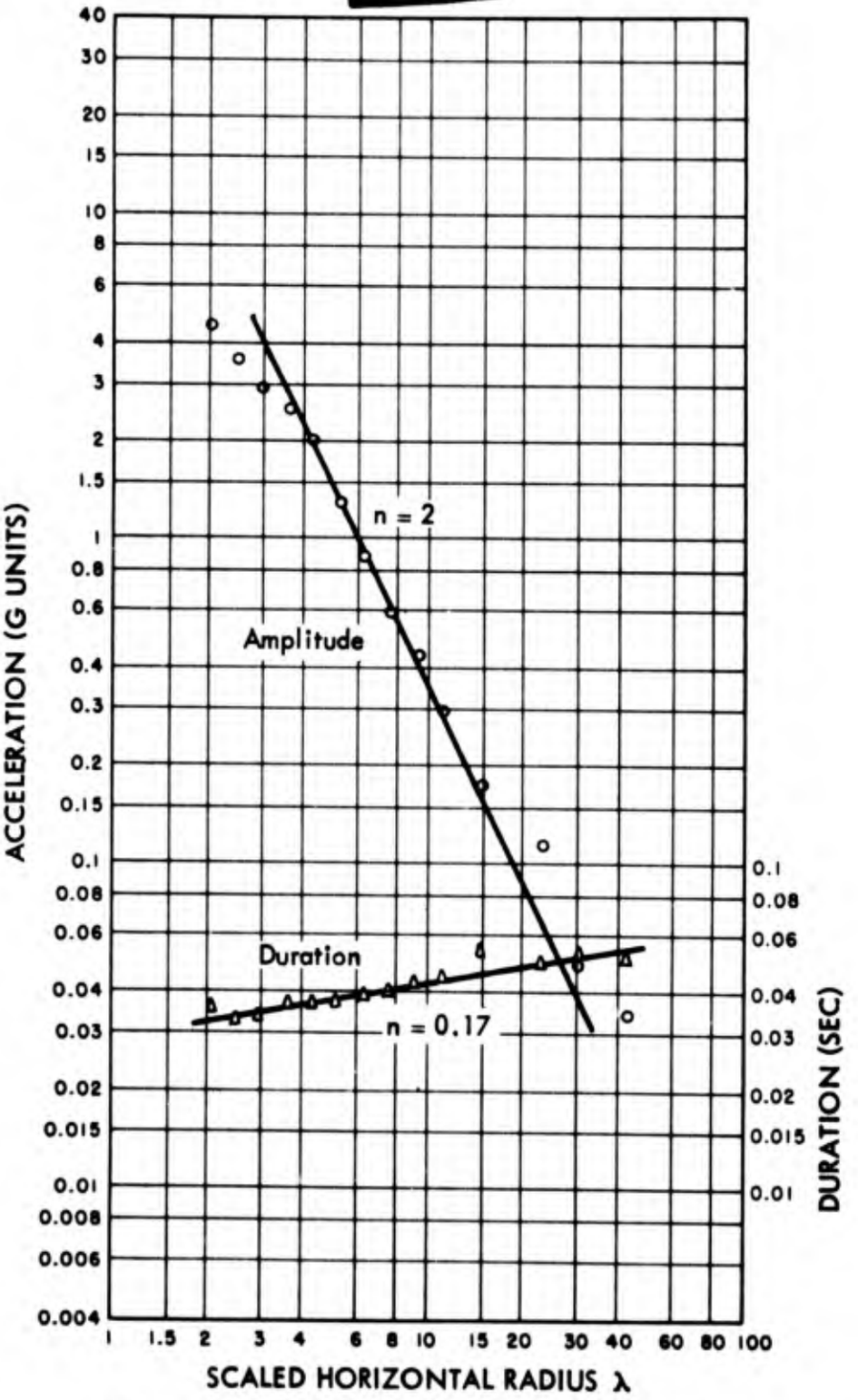

Fig. 5.15 HE-2 Horizontal Earth Acceleration, Maximum and Duration in Smoothed First Pulse

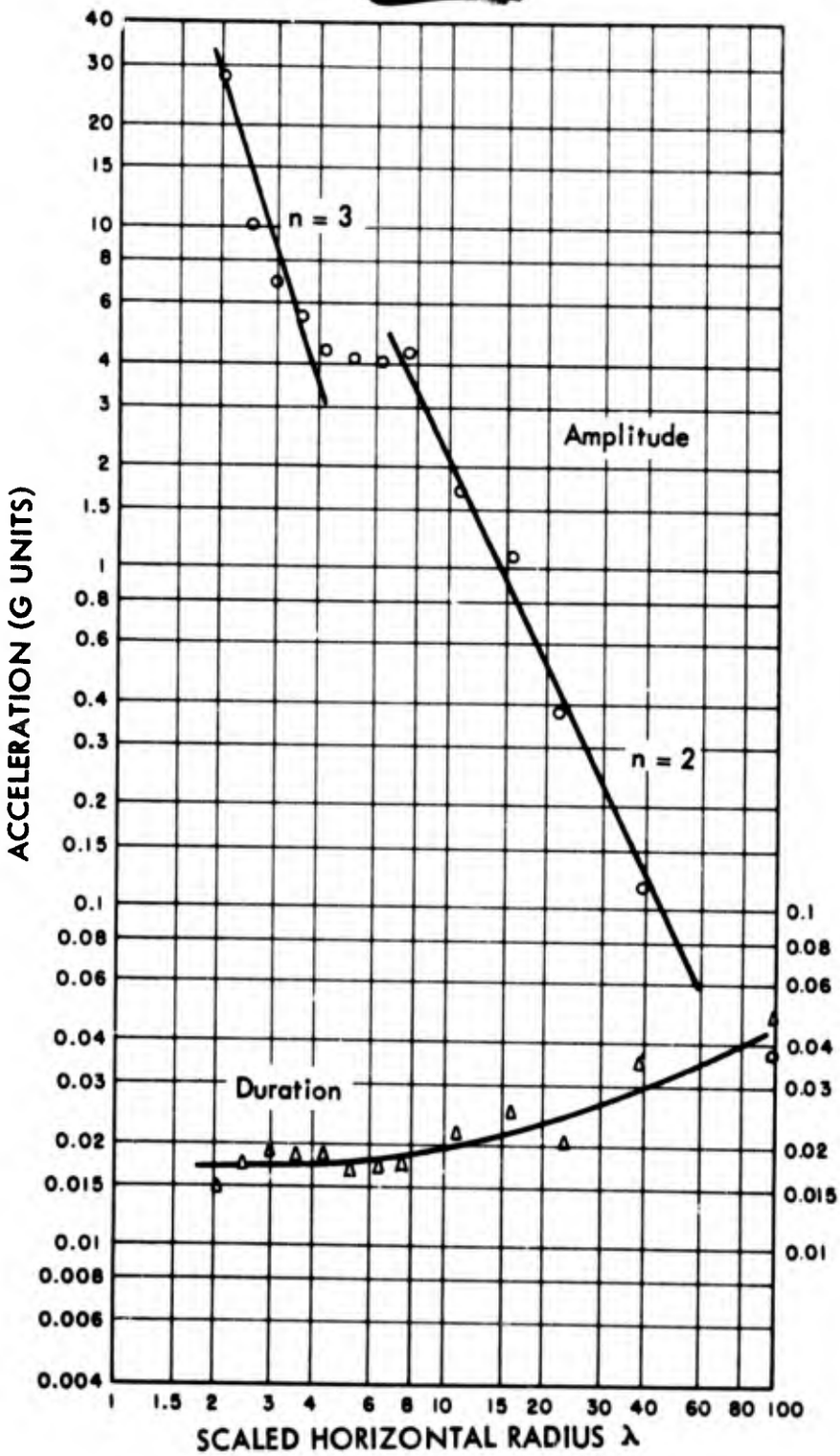

Fig. 5.16 HE-3 Horizontal Earth Acceleration, Maximum and Duration in Smoothed First Pulse

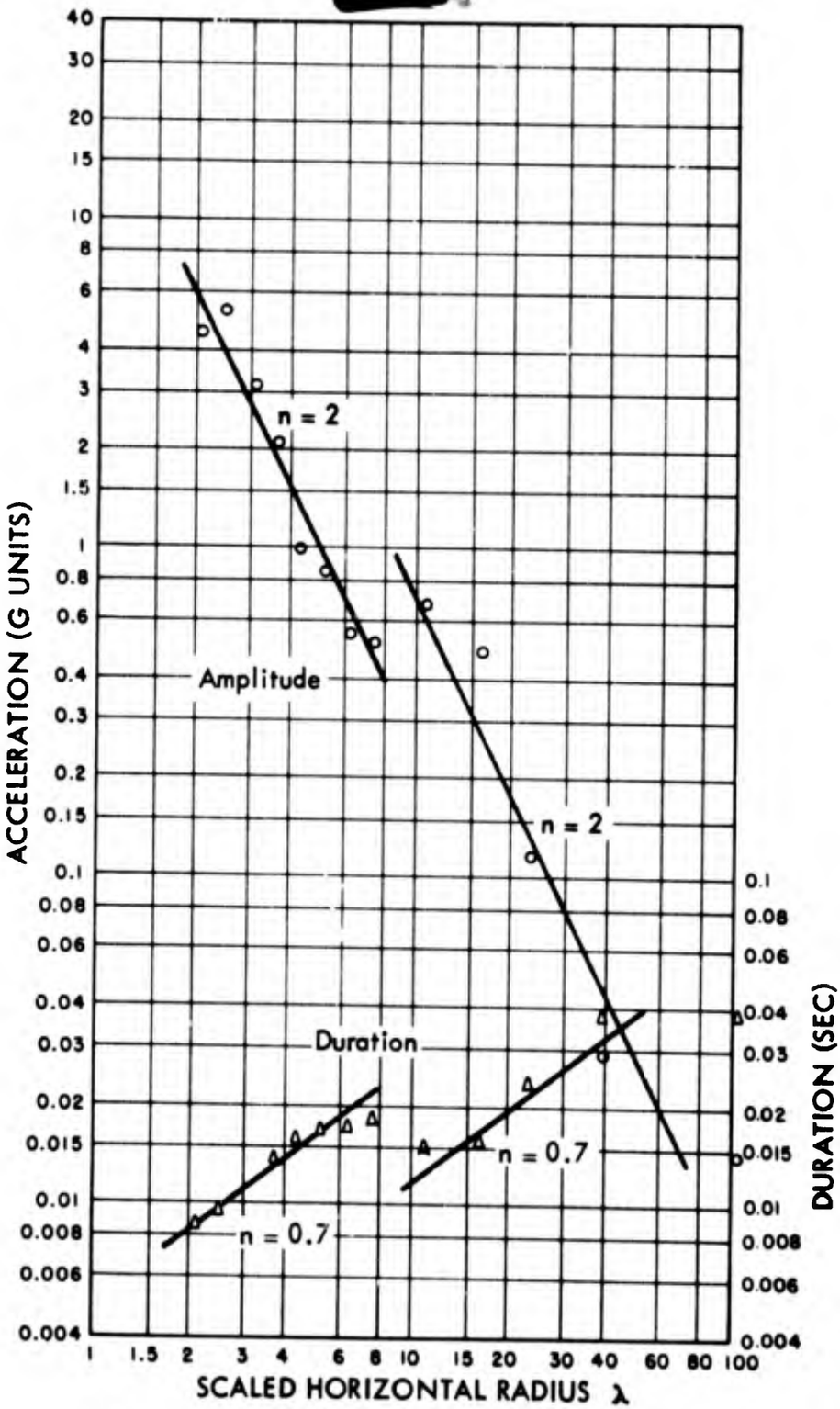

Fig. 5.17 HE-4 Horizontal Earth Acceleration, Maximum and Duration in Smoothed First Pulse

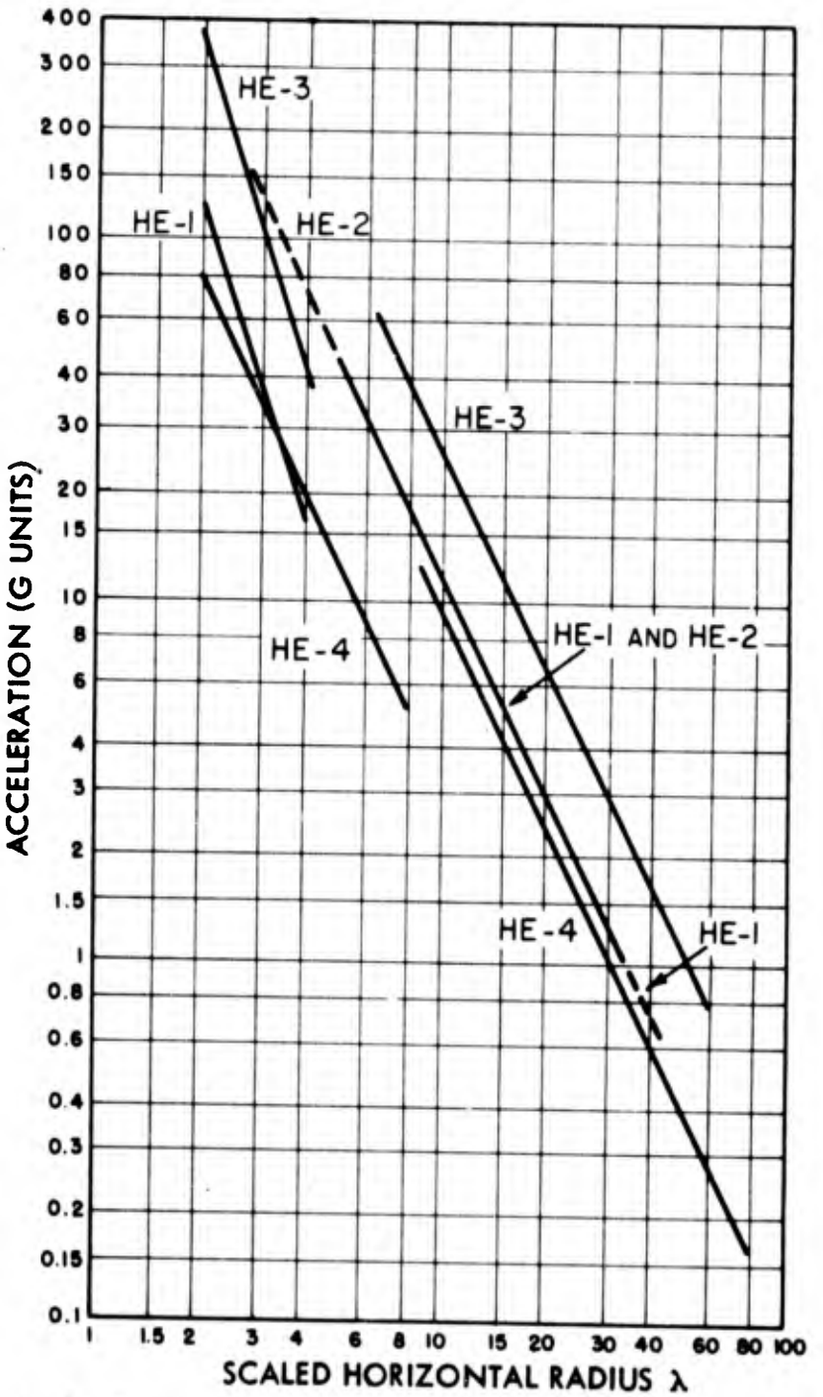

Fig. 5.18 Horizontal Earth Acceleration, Maximum in Smoothed First Pulse, All Tests. Equivalent for one pound of TNT. For charge weight W pounds of TNT, divide by $W^{1/3}$

[redacted]

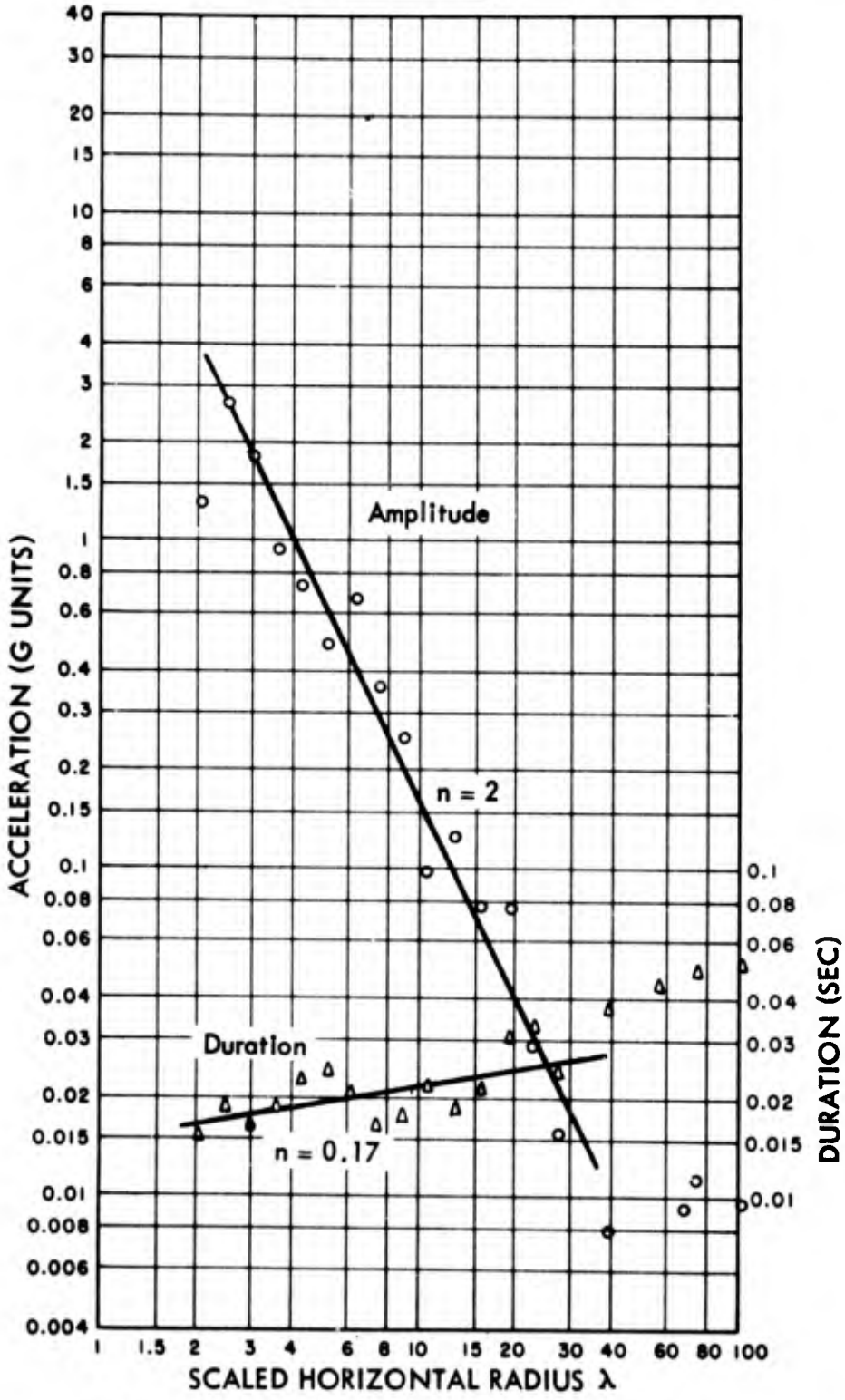

Fig. 5.19 HE-1 Vertical Earth Acceleration Maximum and Duration in Smoothed First Pulse

[redacted]

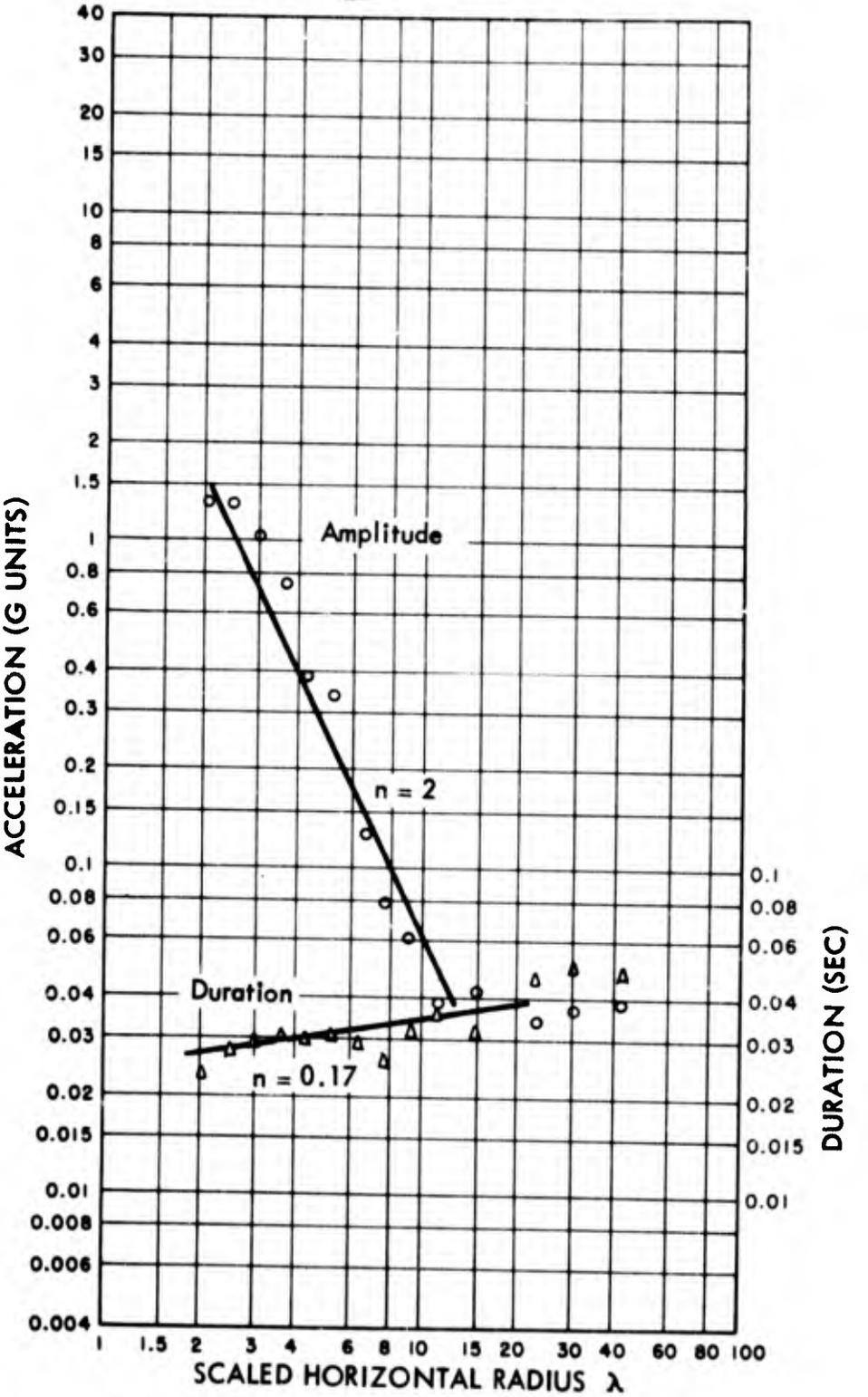

Fig. 5.20 HE-2 Vertical Earth Acceleration Maximum and Duration in Smoothed First Pulse

[redacted]

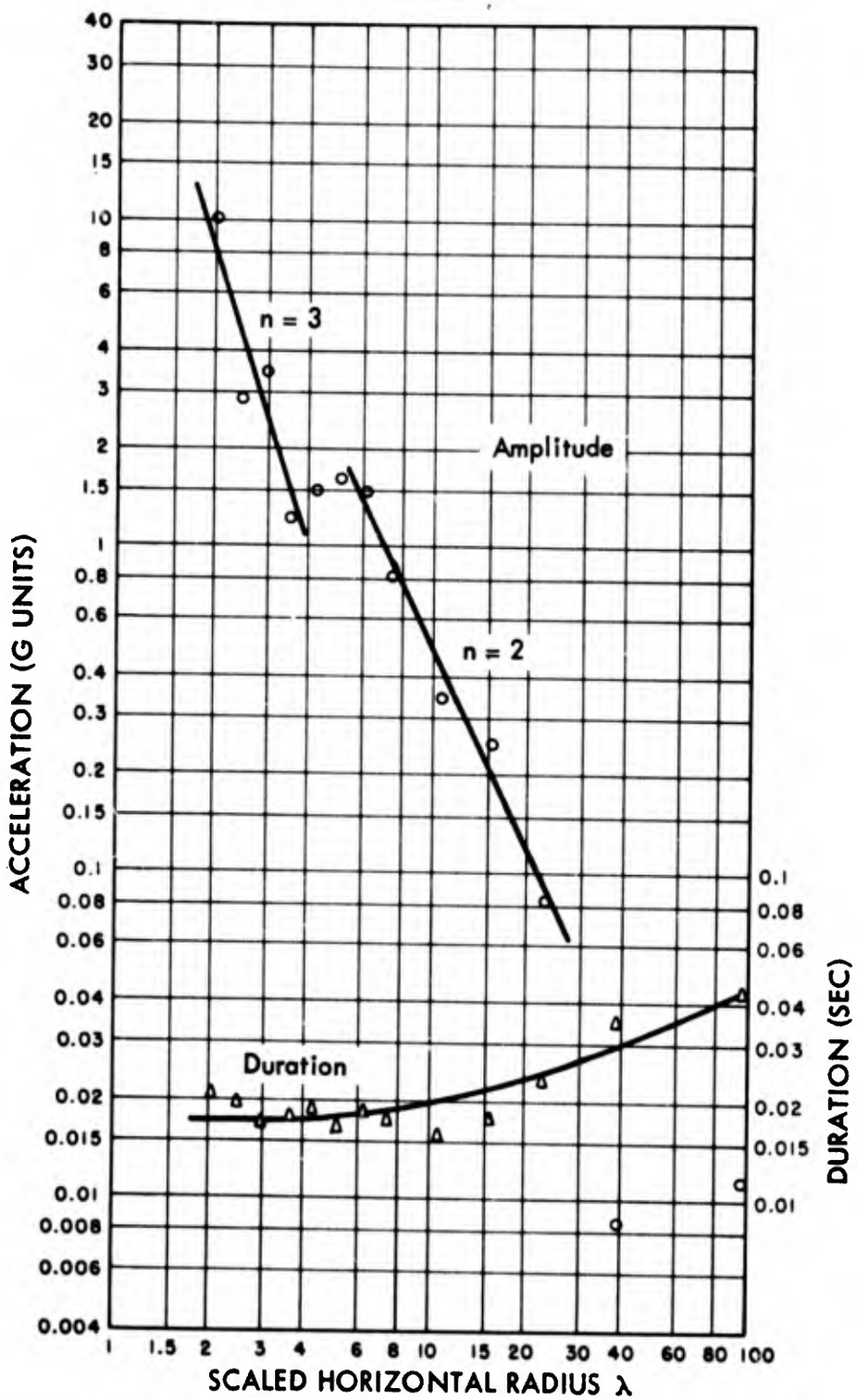

Fig. 5.21 HE-3 Vertical Earth Acceleration Maximum and Duration in Smoothed First Pulse

[redacted]

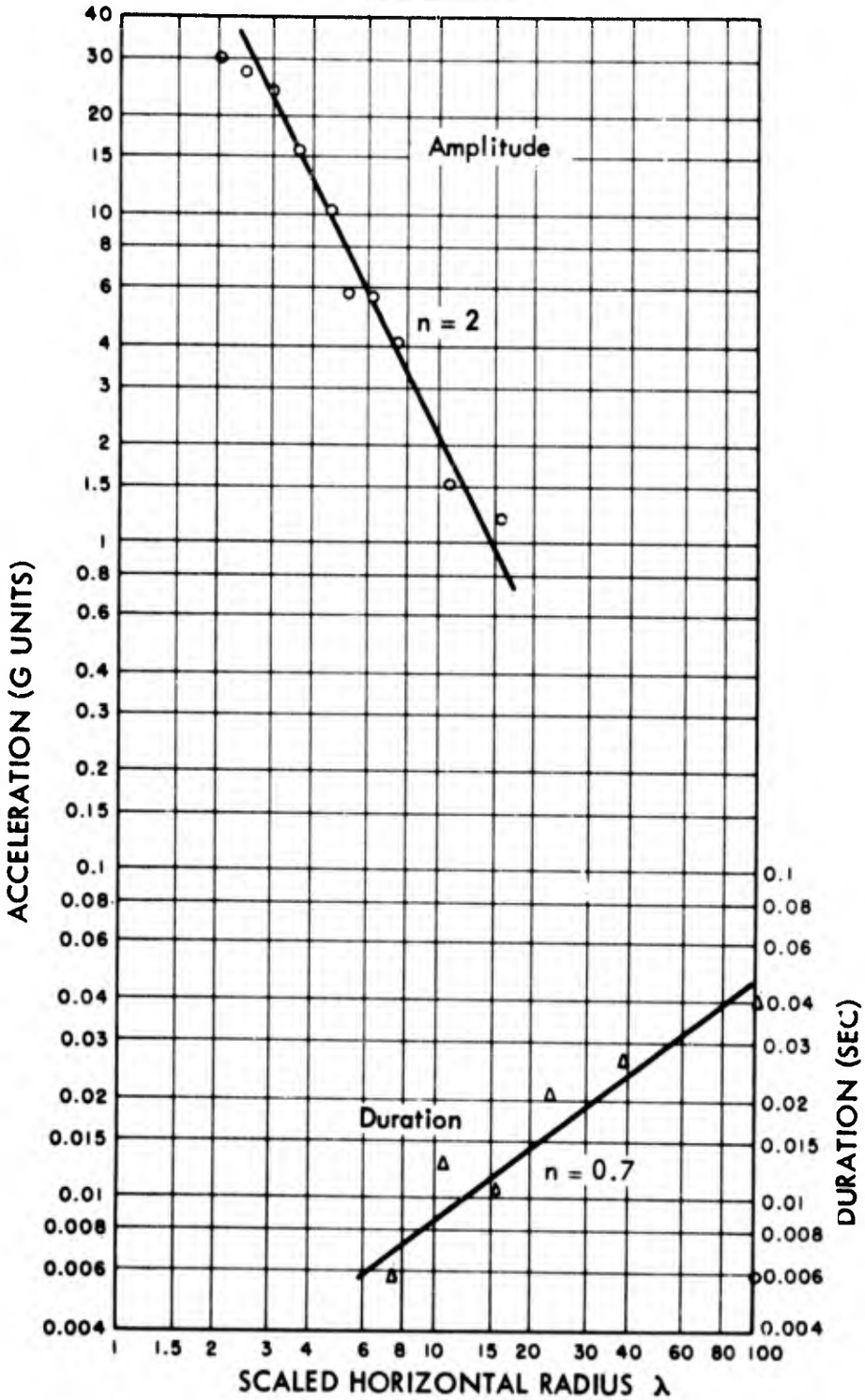

Fig. 5.22 HE-4 Vertical Earth Acceleration, Maximum and Duration in First Negative Pulse

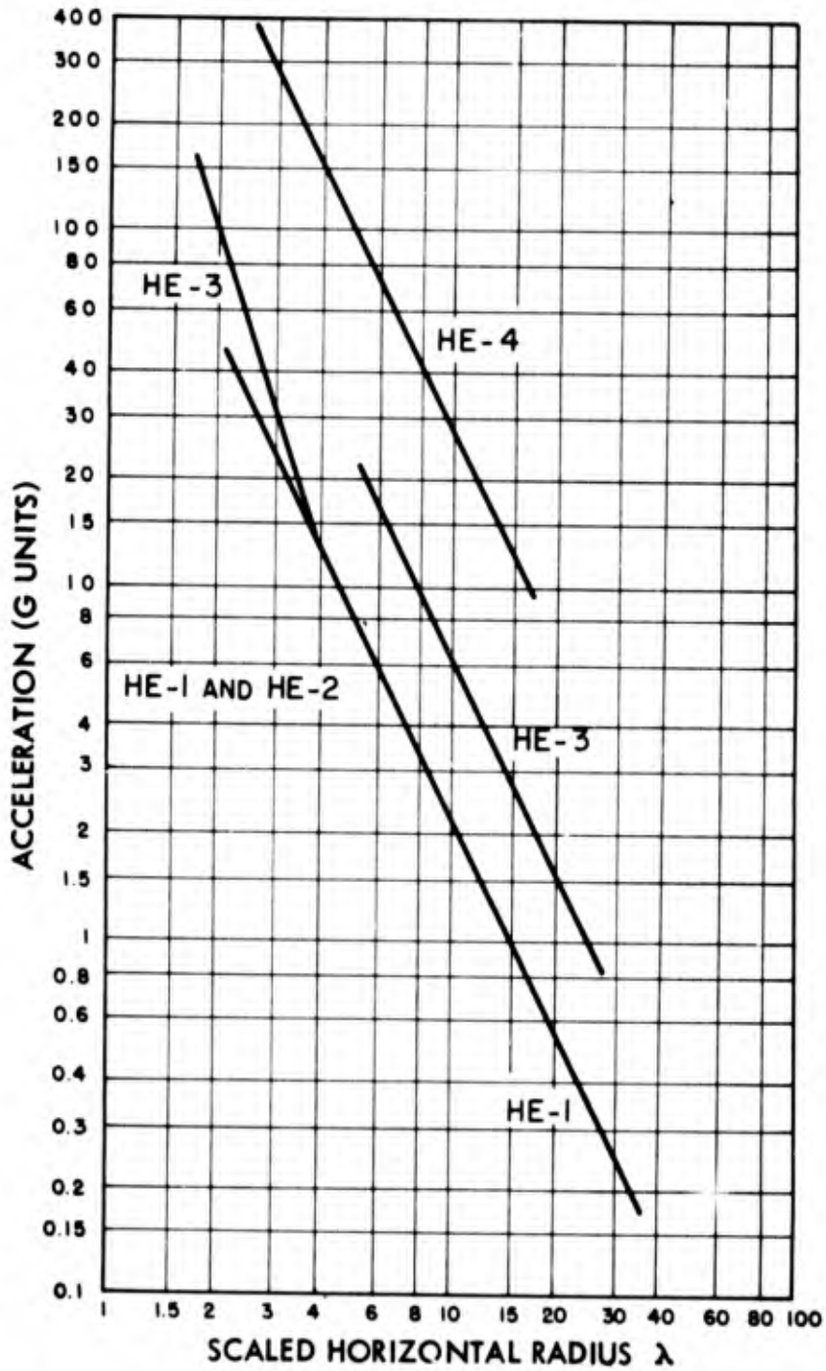

Fig. 5.23 Vertical Earth Acceleration, Maximum in Smoothed First Pulse, All Tests. Equivalent for one pound of TNT. For charge weight W pounds of TNT, divide by $W^{1/3}$

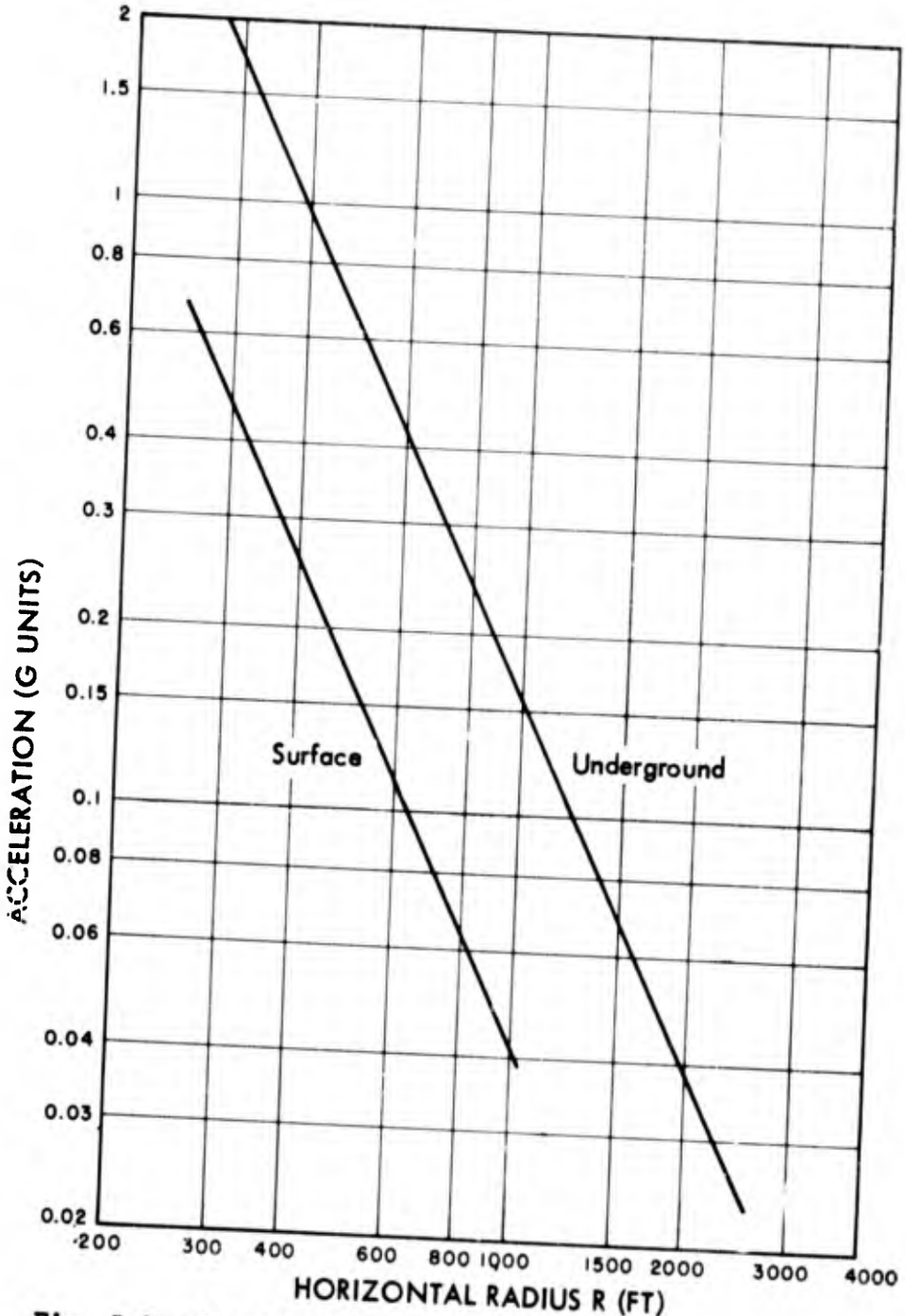

Fig. 5.24 Predicted Maximum Horizontal Earth Acceleration in Smoothed First Pulse, Underground and Surface Tests. Assumed energy release, 1 KT

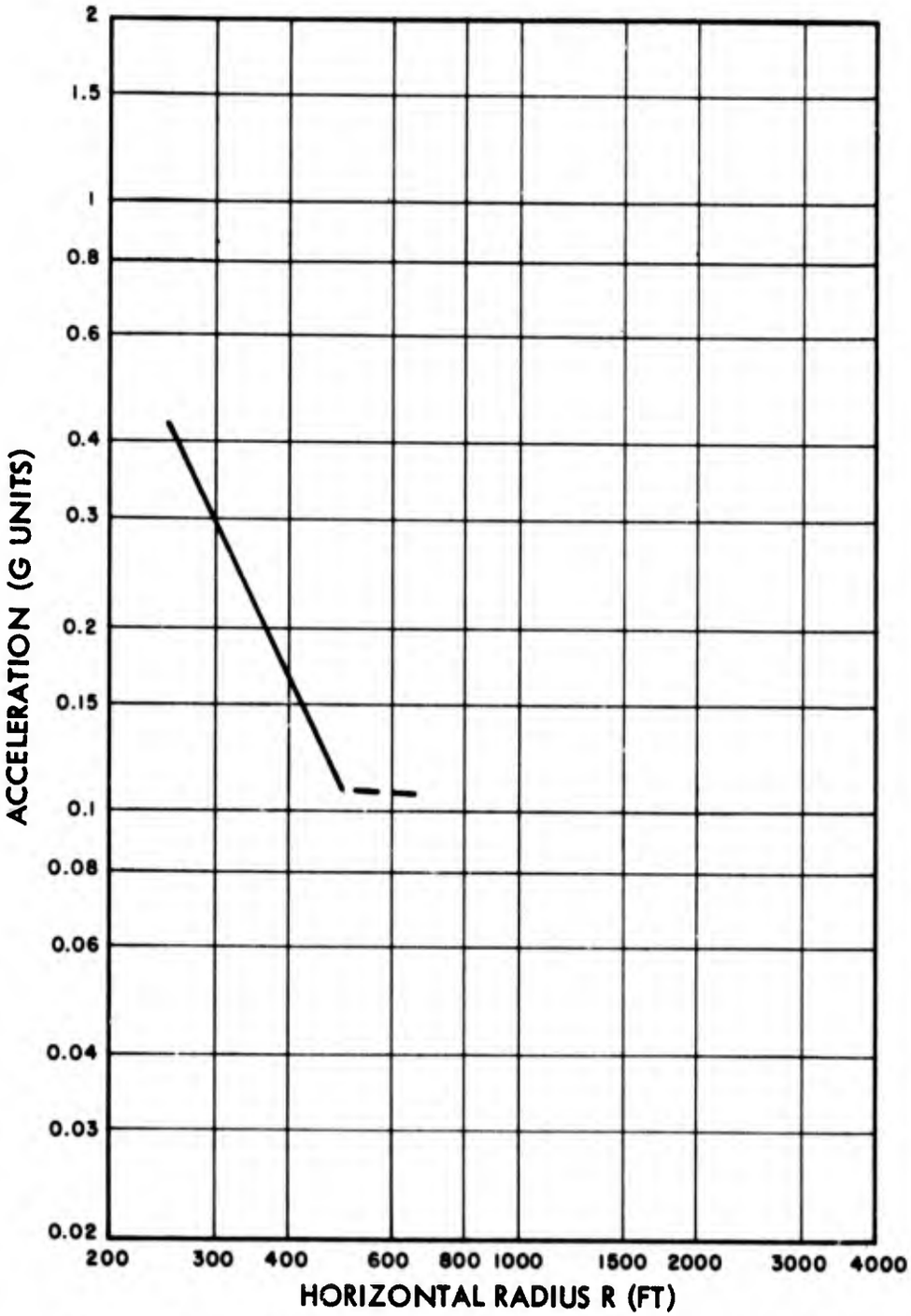

Fig. 5.25 Predicted Maximum Vertical Earth Acceleration in Smoothed First Pulse, Underground Test. Assumed energy release, 1 KT. Dashed portion especially uncertain

Figure 5.25 makes the prediction of vertical amplitude for the underground nuclear test only. No surface nuclear test prediction was made here from HE-4 because the contribution of air blast to the vertical component of acceleration predominates over direct earth effects and makes scaling uncertain. The first pulse of vertical earth acceleration from HE-4 is usually negative and is associated with the direct "slap" of the air blast passing over the gage location. This phenomenon is considered later in this section. The slap is more unmistakable and often more intense in the vertical component, especially at a large distance from ground zero. Thus in a surface explosion, where air-coupled effects may be expected to predominate, near-surface underground scaling laws are uncertain, to say the least.

A feature of both horizontal and vertical components is a break in most amplitude-distance curves. For the vertical component this is presumed to be due to the refraction of seismic energy from a deep high-velocity layer, leading to more nearly vertical arrivals beyond a calculable distance from ground zero. Previous calculations[5] have estimated this turn-over distance to be at about 450 feet. Estimates may be made from the three tests from the vertical components plotted in Figures 5.19 through 5.21. The values of λ and R for the turn-over distance are then estimated as below:

HE-1	$\lambda \doteq 40$	R ≐ 550 ft
HE-2	$\lambda \doteq 14$	R ≐ 480 ft
HE-3	$\lambda \doteq 38$	R ≐ 520 ft

No estimate is made for HE-4, owing to masking by air-blast induced effects. The average value of 510 feet is in good agreement with that predicted. Since this distance will not scale, the step portion beyond 500 feet of the prediction in Figure 5.25 for the vertical component is dotted to indicate the uncertainty. The radial extent in feet of the step should likewise not scale, since it depends on site geometry, not explosion scaling laws.

A break in the curves for the horizontal component appears to occur near $\lambda = 4.5$ for HE-1 and near $\lambda = 3.5$ for HE-2. A discussion of the possible significance of this break will be given in Section 5.4.

We now turn to a consideration of the slap. The vertical component of the slap is much more definite than the horizontal. Admittedly, its military importance is slight, for, although the amplitudes are large, the periods are smaller than those for the phenomena on which it is superimposed (see Figures 4.5, 4.6, and 4.7). Predictions of

the slap amplitude will be important, however, in setting gages. If the dynamic range of the system is limited, it is important to avoid overloading which may persist and thus affect later portions of the record until the system recovers. For short-period earth motion pulses, the effect on structures is best described by the earth displacement. For similar acceleration wave forms, the displacement is proportional to AT^2, where A and T characterize respectively the amplitude and period of the slap in earth acceleration. The discussion will be confined to the relation between the air blast and the slap; damage effects will be considered later.

From Figure 4.10, the wave form of the slap is seen to resemble a damped sinusoid. For the particular wave shown, the amplitude of each of the first three half cycles is on the average about 45 per cent of the previous one. Thus the amplitude of the first pulse may be used to characterize the wave. Figures 5.26, 5.27, and 5.28 show this amplitude as a function of λ for HE-1, HE-2, and HE-4 respectively. No curve is presented for HE-3, since the air blast was too weak to produce a slap that could be determined reliably from the transient records.

If the slap is due to air blast, its amplitude should be proportional to that of the air blast. This statement requires several qualifications to be valid. First, when subjected to a step function of air pressure, the reaction of the soil has a fairly well defined period which depends on the elastic properties of the soil. If, however, the pressure pulse has a finite duration, the effect on the earth will also depend on the ratio of its duration to the period of earth motion expected from a step function. Hence, as air-blast duration increases well beyond the period of earth motion, the effect of the air blast should approach that of a step function of pressure. By examining the transient records of Figures 4.5, 4.6, and 4.7 and comparing Tests HE-1 and HE-2, it is seen that for HE-1 the slap and "direct earth acceleration" periods are comparable. Thus for HE-1 separation of the slap effects is not readily accomplished. For HE-2 this separation may be effected with much greater certainty. It appears that for charges larger than HE-2, and at the same scaled depth of burial at this test site, the effect of the air blast will be almost entirely determined by the peak air pressure. The period plotted in Figure 5.27 for HE-2 should not be much less than that for much larger charges. Note that this leveling-off of slap period is a direct violation of the underground scaling laws, indicating that air-coupled effects cannot be scaled without a detailed examination of the processes involved.

A second factor affecting the proportionality between air blast and slap is the depth of gage. The attenuation of the slap will

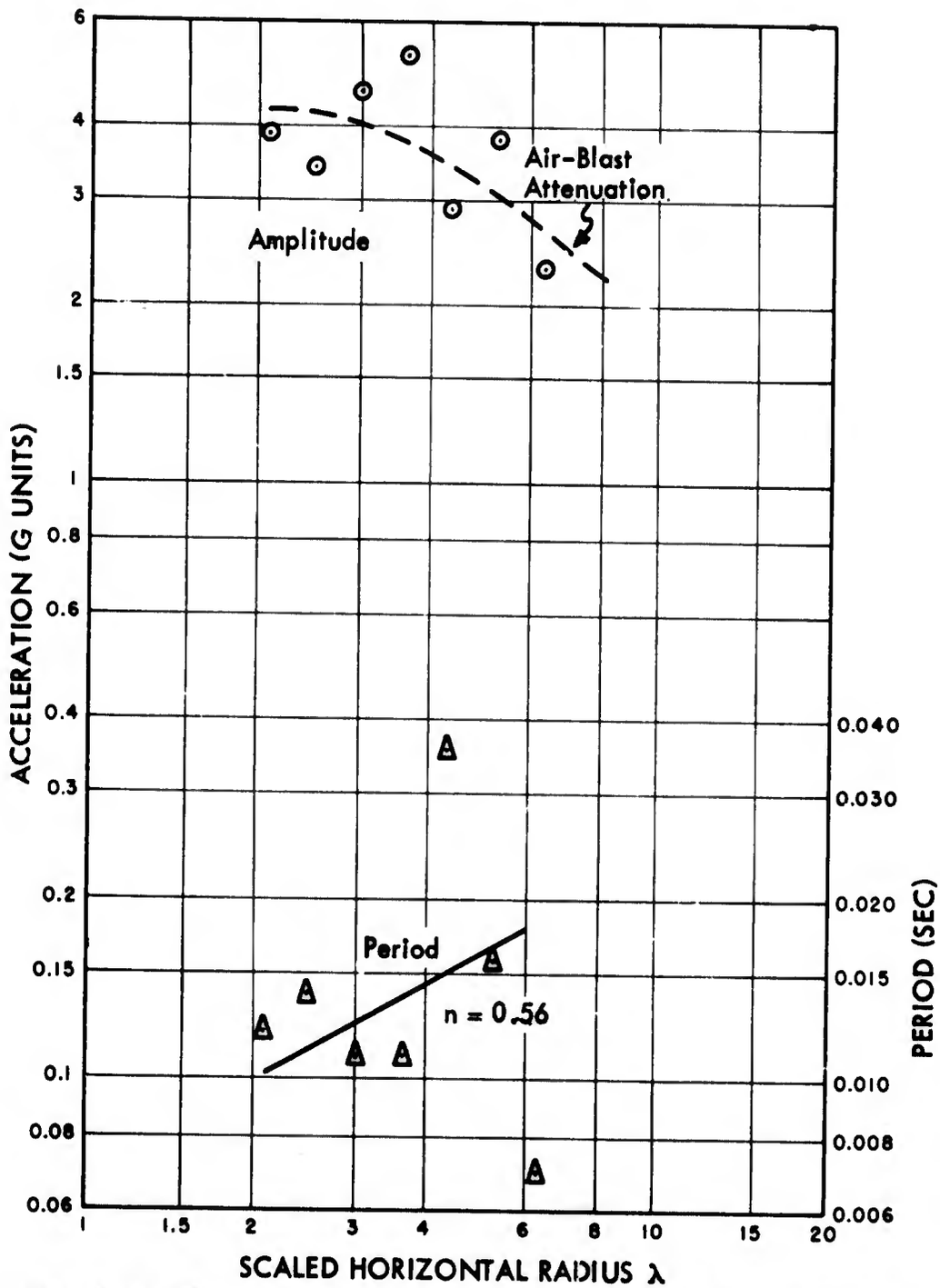

Fig. 5.26 HE-1, Negative Peak in Vertical Earth Acceleration Due to Air-Blast Slap, Maximum Value and Estimated Period

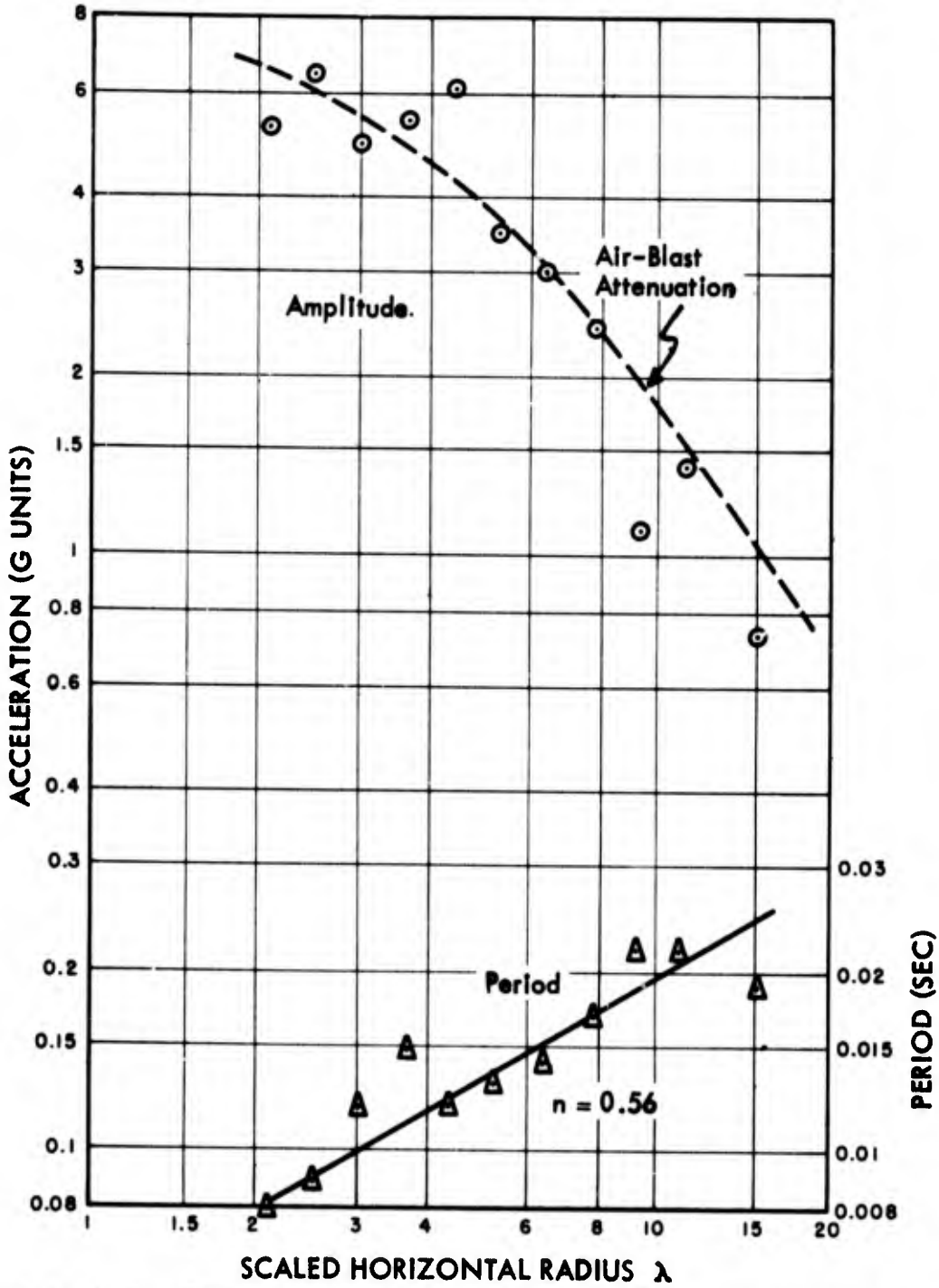

Fig. 5.27 HE-2, Negative Peak in Vertical Earth Acceleration Due to Air-Blast Slap. Maximum value and estimated period

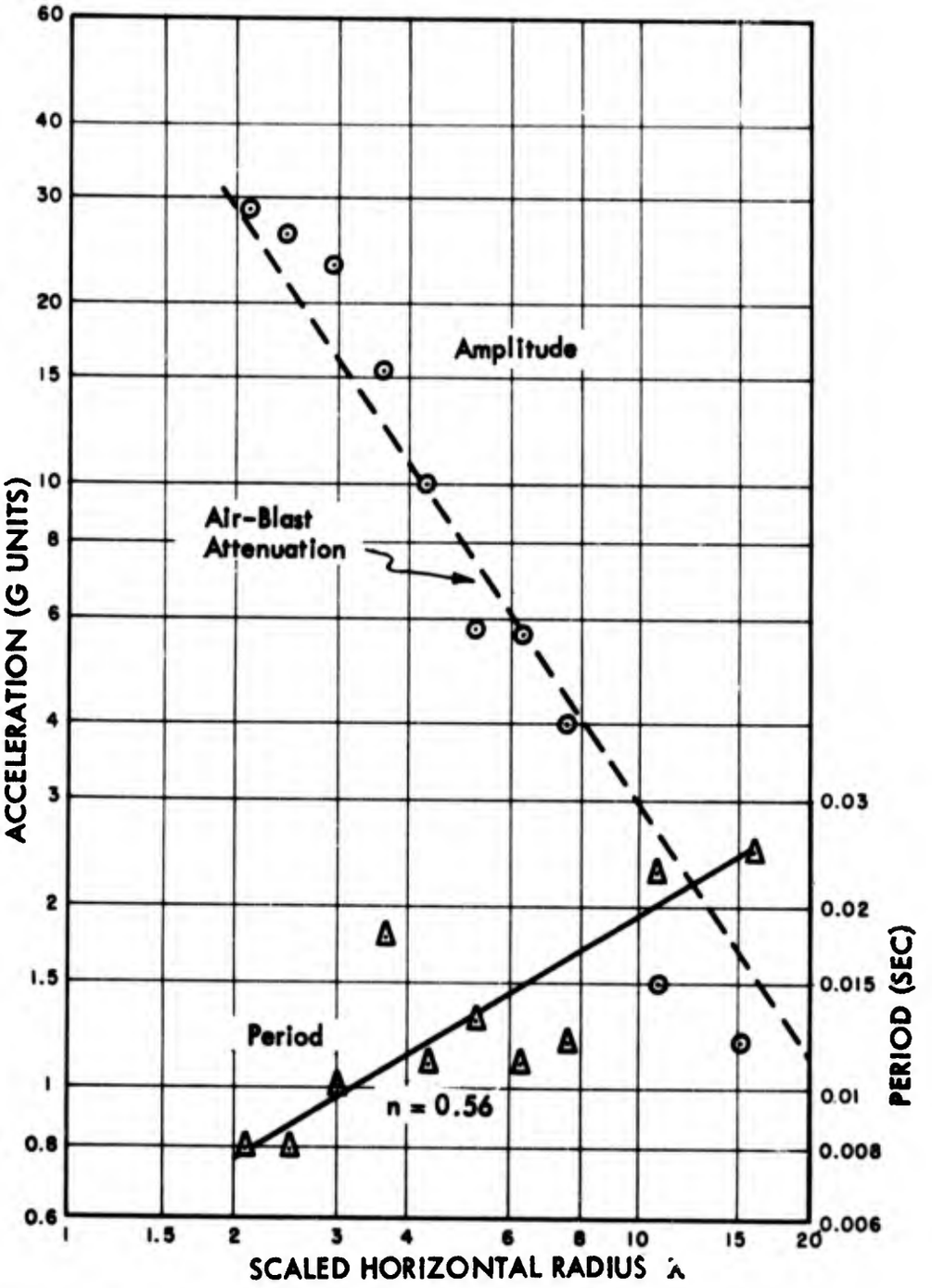

Fig. 5.28 HE-4, Negative Peak in Vertical Earth Acceleration Due to Air-Blast Slap. Maximum value and estimated period

obviously depend on the amount of soil through which it has passed from the surface to the gage. A third factor is the possible non-linearity of the proportionality. The importance of these three factors can now be assessed by considering the curves of Figures 5.26 through 5.28.

As regards periods, that of the slap from HE-1 is about 25 per cent larger than that from HE-2, and the scatter of the points is considerably greater. This reversal of direction of expected variation probably reflects the fact that the slap and direct earth acceleration periods are roughly equal in HE-1, with consequent severe interference effects. For a 1 KT explosion the slap period should be but little greater than that for HE-2. The available evidence is insufficient to make a reliable estimate.

Since all standard gages were at the same depth (five feet), the slap attenuation due to earth is constant for all tests. Note that this depth has not been scaled; the effect of depth is discussed later in this section.

The constancy of the proportionality of the air blast and slap is tested in Figures 5.26 through 5.28 by plotting the air-blast attenuation curve for best fit among the points. Although the points show considerable scatter, particularly for HE-1, the agreement is fair. On the basis of the curve positions shown, the ratio of peak slap acceleration (G units) to air-blast peak pressure (psi) has the following values:

HE-1	0.3
HE-2	0.3
HE-4	0.43

It is difficult to reconcile the departure of the HE-4 ratio from the others, for the curve fit is as good as for HE-2. Hence in the prediction of the peak slap for 1 KT tests in Figure 5.29 two curves are shown for the surface nuclear test. The upper curve is based on the (slap/blast) ratio of 0.43 for HE-4, whereas the central curve uses the 0.3 ratio obtaining for HE-1 and HE-2. The curves probably define reasonable limits for the phenomenon to be expected. The prediction for the underground nuclear test departs from a straight line at small λ. As was noted in the section on air blast, the blast attenuation for this test will probably show less deviation from a straight line than that for HE-2 and thus the slap amplitudes may be greater than predicted at small values of λ. Again, note that these predictions are for a constant gage depth of five feet.

[redacted] [redacted]

[redacted]

PROJECT 1(9)-1

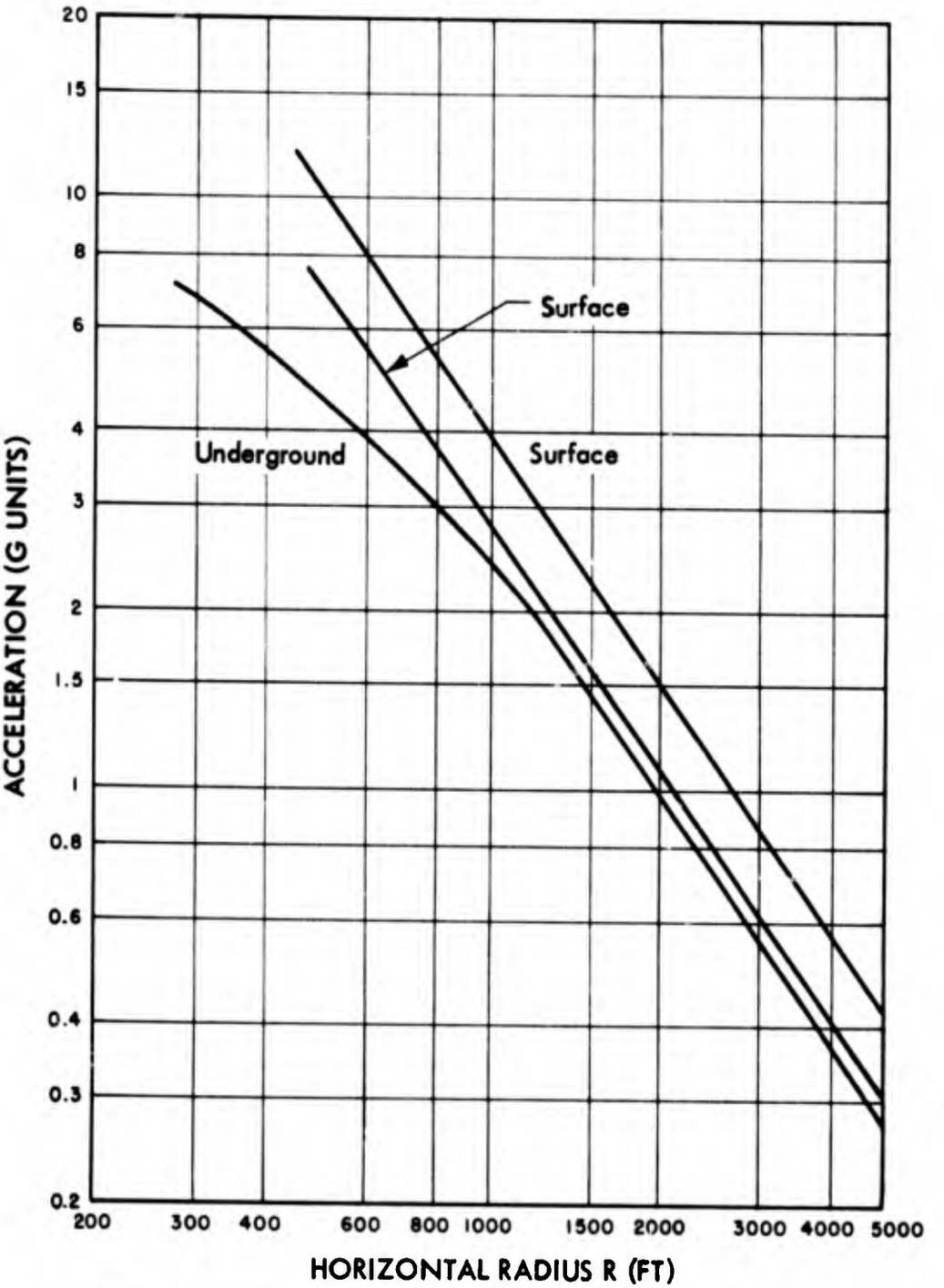

Fig. 5.29 Predicted Negative Peak in Vertical Earth Acceleration Due to Air-Blast Slap, Underground and Surface Tests. See text for explanation of the two surface test curves shown

[redacted]

The earth acceleration records for HE-2 have been integrated mechanically but all the results have not yet been completely checked. However, the horizontal velocity integrations were checked and data were tabulated as depicted in Figure 4.17. The average amplitudes of the cycle showing the maximum swing, as well as the associated periods, are shown in Figure 5.30 as a function of scaled radius. By manual integration, two points were obtained for HE-1 also, and are shown in the same figure. Note that they lie <u>above</u> those for HE-2 by a ratio of about two to one, indicating such a departure from scaling that no velocity prediction appears justified. The periods, however, show a ratio of 2.7, and thus scale well; nevertheless, the total phenomenon cannot be said to scale satisfactorily.

The dashed curves are the air-blast attenuations for the two tests. The fit for HE-2 suggests that continuous air-coupled effects may play a large part in the velocity attained. However, no firm conclusion is justified from such meager data. A thorough analytical treatment is needed as the background for an interpretation of such data.

The importance of the velocity arises from damage considerations. From a knowledge of the periods involved, it appears that for an operational penetrating nuclear weapon detonated at a scaled depth of 0.150 in the Nevada Test Site soil used for this HE test series, the expected period of earth motion may be of the same order of magnitude as that of a one- or two-story steel-framed structure.[3] Thus earth velocity becomes the quantity to which the relative displacements within a structure should be approximately proportional, for the operational weapon.

To indicate the effect of gage depth upon earth acceleration, at some gage stations on the HE-2 test, accelerometers were located at depths of 5, 17, 34, and 68 feet. The horizontal components at $\lambda = 3.0$ and 11.1 are shown in Figures 4.12 and 4.13; Figures 4.14 and 4.15 similarly present the vertical components. From Figure 4.12 the amplitudes of the smoothed first pulse, close-in ($\lambda = 3.0$), horizontal accelerations at 5 feet, 17 feet, 34 feet, and 68 feet are respectively 2.9, 3.4, 3.0, and 1.0 G. At $\lambda = 11.1$ the similar horizontal peaks are 0.29, 0.30, 0.26, and 0.22 G respectively. Thus the smoothed horizontal first pulse acceleration amplitude at these stations is relatively constant at least to 34 feet, under the conditions of the HE-2 test.

The variation of the smoothed first pulse of the vertical acceleration with depth cannot be described by any such simple numerical means. By reference to Figures 4.14 and 4.15, it is seen that the first half-cycle starts near the surface as upward or very slightly downward. With increasing depth, the acceleration becomes increasingly downward. The first positive half-cycle at first decreases, then approaches what appears to be a relatively constant value. Thus there

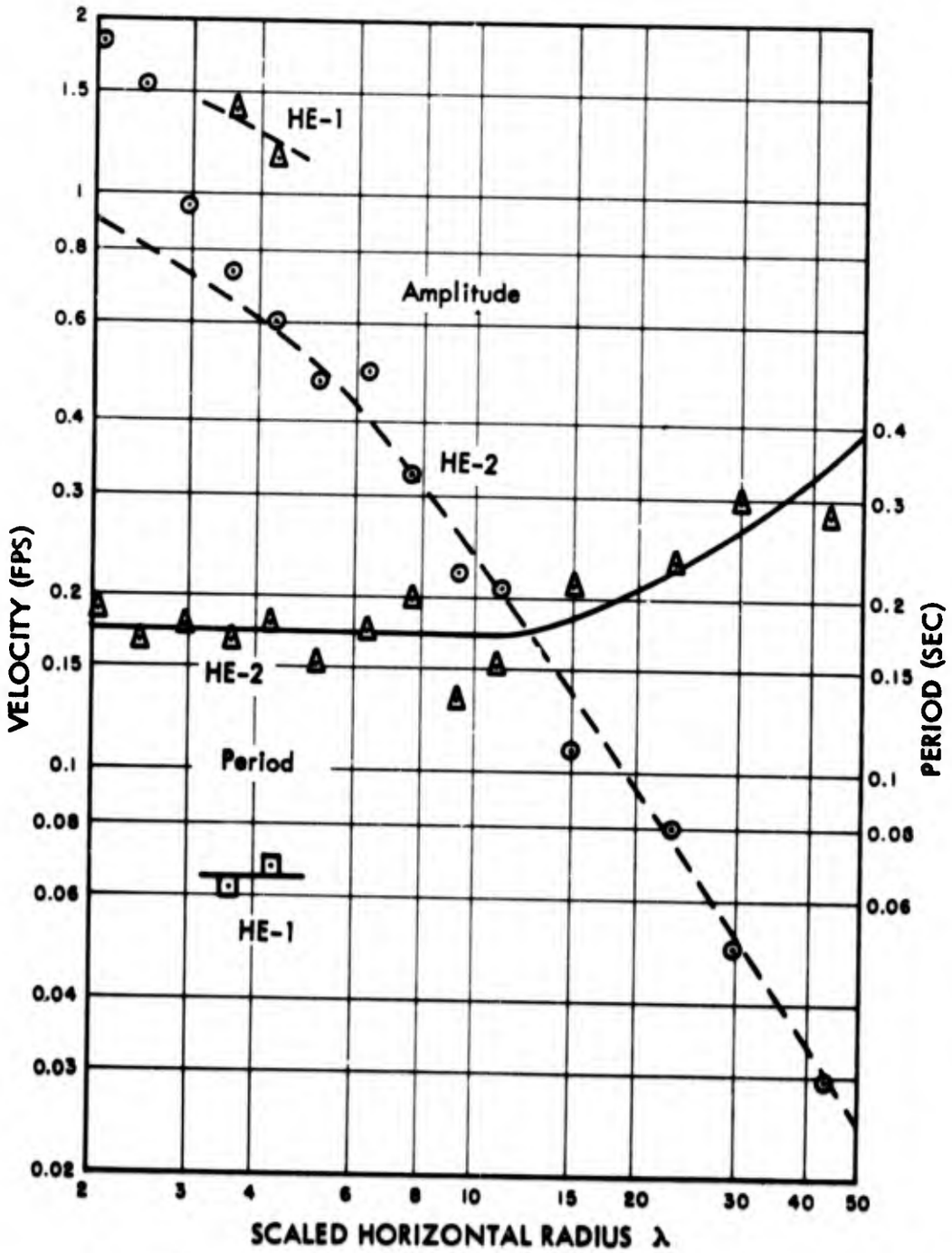

Fig. 5.30 Horizontal Earth Velocity Amplitude and Period, HE-1 and HE-2. Dotted lines indicate air-blast attenuation

is not too much regularity in the behavior of the vertical component. The horizontal component predominates in the early stages of each record.

With respect to the relatively high-frequency slap (direct effect of the air blast passing over a gage location), the station at $\lambda = 11.1$ provides more clear-cut information than do the close-in stations. A possible reason for this will be discussed under time of arrival. By smoothing the region of the curve about the slap, the slap amplitudes from this adjusted base line may be measured. From Figure 4.13, the horizontal slap is outward, and at the four depths is 1.3, 0.62, 0.25, and 0.10 G. Likewise from Figure 4.15, the vertical slap is downward, with values of 1.4, 0.95, 0.30, and 0.05 G. If the slap peak acceleration is plotted against gage depth on log-log paper, the initial attenuation with depth is small. From 17 to 68 feet the attenuation exponent appears to be about 1.3 for the horizontal and 2 for the vertical components of the slap in the acceleration. Although the data are insufficient to justify firm conclusions, it appears that the horizontal and vertical components of the acceleration slap are almost equal at the surface but the vertical component is attenuated more rapidly with depth. In general, the horizontal slap is not as well defined as is the vertical, so that the latter component should be weighted more heavily if conclusions are to be drawn from changes of wave form, damping, or attenuation with depth.

To summarize this discussion of earth motion, the earth acceleration does not follow the scaling laws as a complete phenomenon. Because of this, the apparent scaling of smoothed first pulse amplitudes should be taken as an empirical fact. The special (air-blast) scaling that the slap amplitude apparently follows indicates the need for further study of air-coupled effects and their scaling laws.

5.4 TIME OF ARRIVAL AND AIR-COUPLED EFFECTS

Figures 5.31 and 5.32 give the time of earliest arrival for air blast and earth motion respectively. For HE-3 the air blast was weak enough so that its velocity (reciprocal of the slope) was constant along most of the path. This asymptotic velocity was about 1200 fps, which appears somewhat high.

When idealized, the time of arrival diagrams appears as in Figure 5.33a, where both air and earth curves are shown passing through the origin. Because of chaotic conditions at ground zero, and the possibility of an elevated equivalent source for air blast, this congruence may not actually exist. However, the usefulness of the diagram is not thereby appreciably impaired. Note also that the earth motion arrival

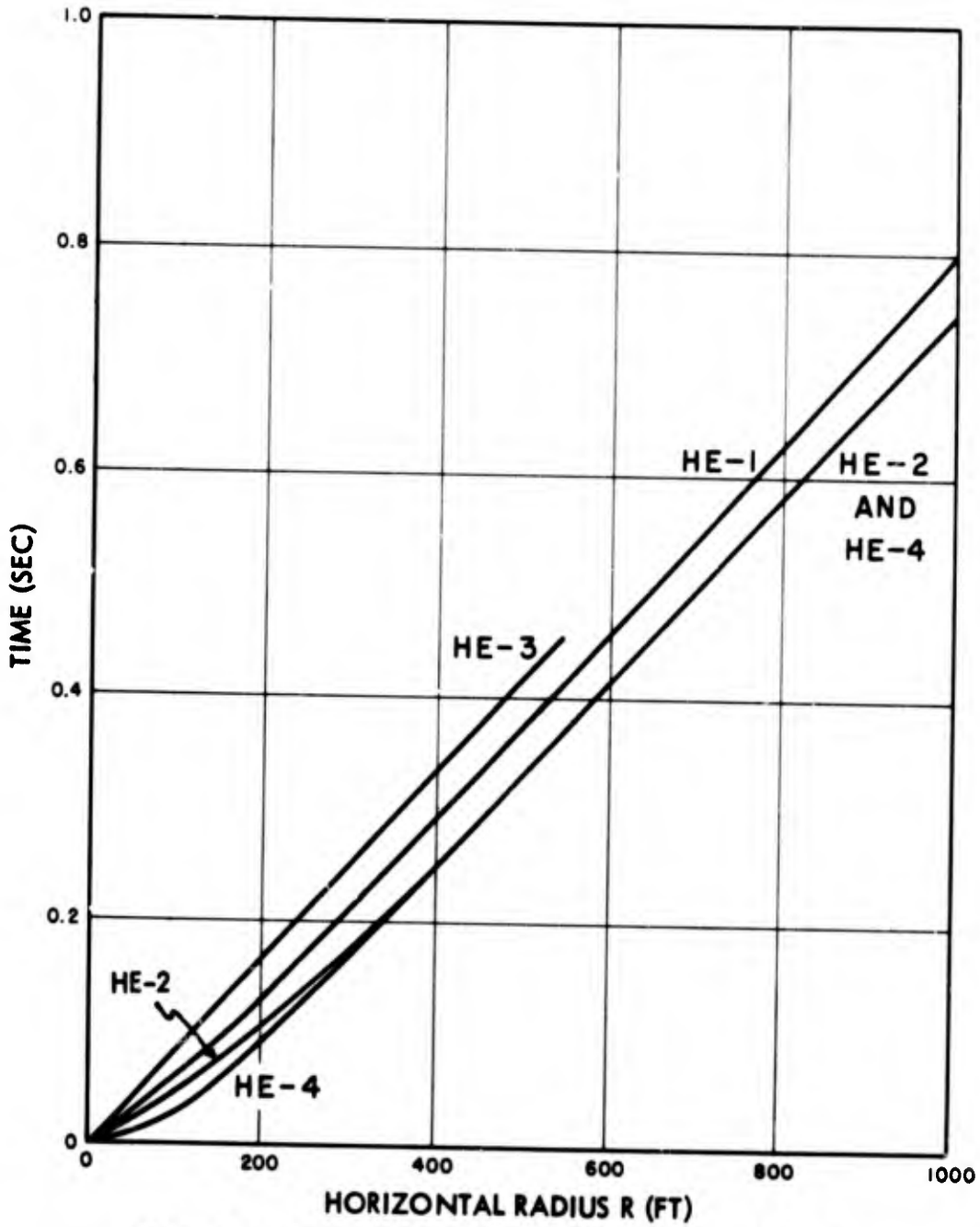

Fig. 5.31 Time of Arrival of Air Blast, All Tests

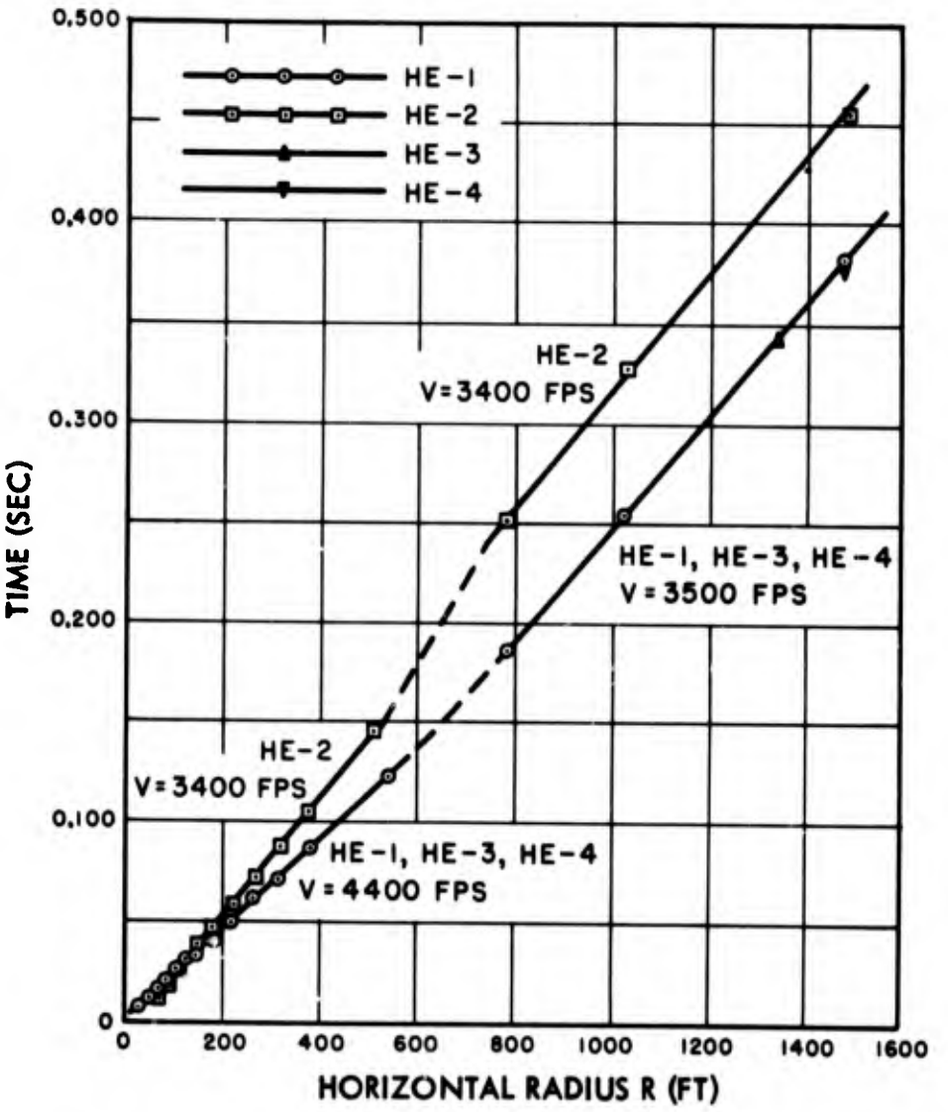

Fig. 5.32 Time of Arrival of Earth Acceleration, All Tests

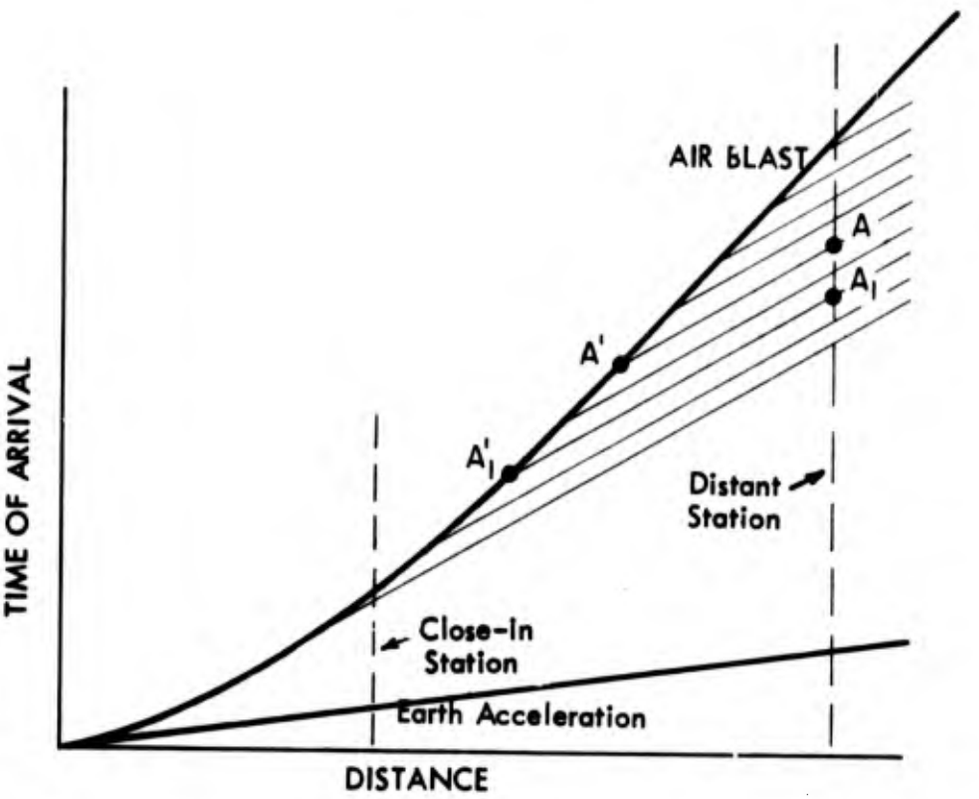

a. Composite Time of Arrival and Air Coupling

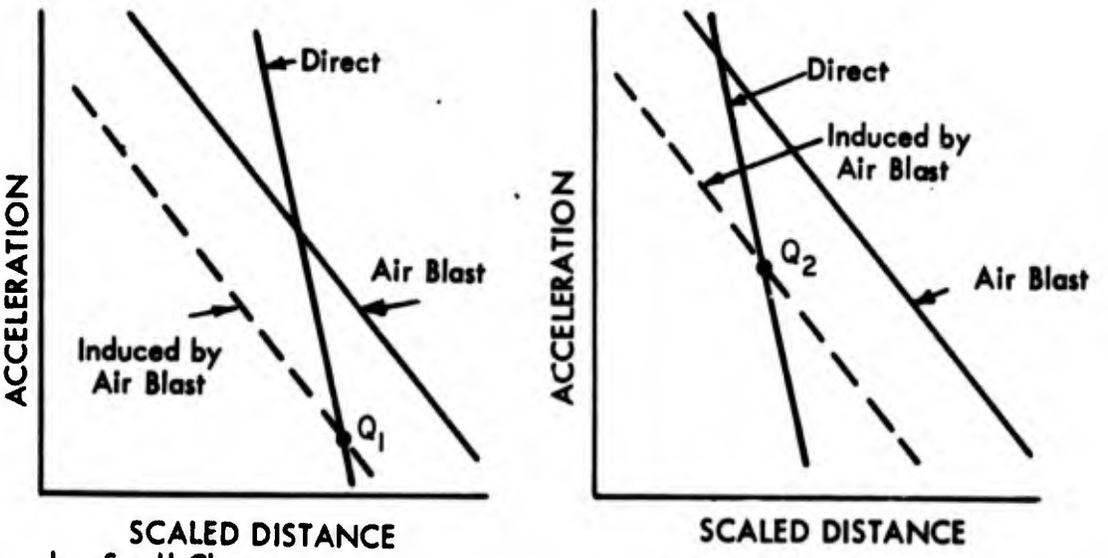

b. Small Charge

c. Large Charge

Fig. 5.33 Dependence of Air-Coupled Earth Acceleration Effects on Time of Arrival and Charge Size

is shown as a straight line, implying an ideal constant-velocity earth. This diagram may be used as a framework on which to base some preliminary observations of continuous air-coupled effects. It is obvious that it is no substitute for a complete analytical treatment, but some general inferences can be obtained.

The work of Press and Ewing[8] on flexural waves in ice on water, from air blast in the air above, supplies a few general conclusions that are applicable here. If in underground explosions the air blast similarly excites dispersive flexural waves in the surface layers of the earth, then the predominant frequency of surface earth motion may with some justification be expected to be that of the flexural wave in the earth having a phase velocity equal to that of the air blast. In a sense, this corresponds to the frequency of the slap. The formulation of the actual problem is complicated by the three-dimensional nature of the waves, the varying velocity of air blast, and the imperfect elastic nature of the earth. Scaling is certain to be different from the model laws used as the basis of this report. If gravity waves form the important mode of energy transmission, then dimensional analysis leads to scaling in which lengths vary as $W^{1/4}$ and times as $W^{1/8}$. Thus velocity will then scale as $W^{1/8}$ and acceleration will be unchanged. These statements, while independent of the analytical work, should of course be confirmed by it if gravity waves are the important type arising from air coupling.

To return to the diagram of Figure 5.33a, note the lightly-drawn parallel lines. They represent the initiation of air-coupled motion in the elemental spatial region at distances from ground zero corresponding to their intersection with the air-blast curve. The lines are then the time trajectories of these induced motions; the common slope signifies waves of a constant velocity. Also, with the slope shown as less than that for direct earth motion, the wave velocity is less than that for this latter motion. This is consistent with the fact that the first arrivals for direct earth motion are due to compressional (P) waves, which have the highest velocity; flexural waves travel more slowly.

The magnitude of the net earth motion at a given distance and time, say at A, then consists of two principal components: the direct earth motion and the integrated effect of all air-coupled wave motion initiated at distances up to that corresponding to the point A' in Figure 5.33a. These air-coupled effects will be attenuated first by the amount corresponding to a path along the air-blast curve, then by an amount corresponding to waves of the air-coupled type propagated in earth from the point of excitation (as A') up to the vertical line (as at A_1), which represents the position at which measurements are made. For example, the incremental effect at A due to air-coupled

waves initiated at A_1' will roughly depend on the air-blast attenuation up to A_1', earth attenuation up to A_1, then time (or phase) variation from A_1 to A. At the close-in station shown on Figure 5.33a, very little air-coupled energy should be received.

It is seen that the details of the integrated air-coupled effect cannot be predicted by any such crude analysis as this, but some broad inferences may be safely drawn. First, since the air blast attenuation is less than that for earth acceleration, at a sufficiently distant station the earth acceleration will be determined more by air-coupled effects than by directly transmitted earth effects. Also because of this relation between air and earth attenuation, air-coupled information from A' will be less attenuated than that from a closer-in position such as A_1'. Thus a second aspect of the general behavior can be inferred: at sufficiently distant stations the phenomenon will probably initially show oscillations of increasing amplitude, decreasing after the air blast has passed by. The details of this behavior will be obscured both by interference effects and by the direct slap from the air blast, but the envelope of the smoothed curve should show a fairly smooth rise and fall. If there are enough cycles in the envelope, an analytical consequence is that the attenuation of maximum envelope acceleration, velocity, and displacement should be the same.

A third inference as to the general behavior is the effect of charge size. Consider Figure 5.33b, showing direct earth acceleration (steep solid) and air-coupled earth acceleration (dashed) magnitudes as a function of scaled distance. Beyond the turnover point Q_1 (left-hand sketch) air-coupled effects predominate. For a larger charge, the air-blast pressure (as a function of scaled distance) will remain fixed, whereas the acceleration curve will be shifted as in the right-hand sketch. Thus the turnover point Q_2 now occurs at a smaller scaled distance. When the charge size is increased more and more, eventually earth accelerations at all positions at which measurement is possible may consist principally of air-coupled wave motion, since the scaled turnover distance may become too small for safe instrumenting. A partial test for the reasonableness of this assumption is to examine attenuation curves for the amplitude of the first smoothed horizontal acceleration pulse for HE-1 and HE-2 (Figures 5.14 and 5.15). For HE-1, a break in the curve occurs at a value of slightly less than four.

In this region the exponent n (negative of the slope) changes from three to two. It is to be expected that air-coupled effects will suffer less attenuation than directly transmitted effects in the earth. Hence the break in the smoothed first horizontal acceleration pulse curve is tentatively identified with the turnover point, which is the point Q in Figures 5.33b and 5.33c. Since directly transmitted earth

effects should predominate close in, the exponent three is tentatively identified with this direct transmission as characteristic of earth alone. On log-log paper, the acceleration vs. scaled distance λ curves may be taken as straight lines within the accuracy justified by the scatter of points. A simple analysis indicates that a, the λ-shift-ratio in the turnover point, should be given by

$$\log a = \frac{\log S}{n_e - n_a} \tag{5.4}$$

where S is the scale factor between two scaled experiments, and the exponents n_e and n_a characterize the acceleration attenuation due to directly transmitted earth acceleration and air blast respectively. Thus for HE-2 (Figure 5.16) the turnover shift a is given by

$$\log a = \frac{\log 2.5}{3 - 0.8} = 0.181 \tag{5.5}$$

where the value $n_a = 0.8$ is that for HE-2 near $\lambda = 4$. Thus $a = 1.5$, and the turnover should thus occur near $\lambda = 4/1.5 = 2.7$. Since this is at the edge of the region in which measurements were made, a clear-cut comparison between theory and experiment is impossible. However, if the horizontal acceleration curves for HE-1 and HE-2 (Figures 5.14 and 5.15) are compared by superimposing with a λ-shift of 1.5, the apparent turnover region observed for HE-2 is near $\lambda = 3$, which is not inconsistent with this prediction. For the underground nuclear test the turnover, using the above reasoning, should be near $\lambda = 0.6$, which presumably will be unobservable.

When the vertical components (Figures 5.19, 5.20) for HE-1 and HE-2 are compared, the exponent is two for both, with little indication of any turnover. This suggests that perhaps air-coupled effects are already predominant, and is consistent with the presumption that the principal effect of air coupling is in the vertical direction. Indeed, in the transient curves, the slap was most clean-cut in the vertical component; see Figures 4.2 through 4.7.

For the HE-3 test, with better earth coupling and less air blast than HE-1, the turnover in the horizontal component attenuation should occur at a value of λ larger than four; a value of about five for the break in the curve may be seen in Figure 5.16 for the amplitude of the smoothed first pulse. Thus the meager data available suggest that air coupling may have been important even in the first acceleration pulse at large distances. Under conditions of these tests, time of arrival alters phase conditions so that details of the resultant amplitude cannot be estimated by this qualitative analysis.

5.5 EARTH PRESSURE

Because of uncertainty concerning the significance of the quantity measured as "earth pressure", this discussion will be confined to noting a few general features of the data. The transient records of Figure 4.8, taken at $\lambda = 1.72$, do not include HE-1, while those for Figure 4.9 ($\lambda = 2.49$) include all four tests. Since the first pulse is almost always the largest in the region of interest (λ less than 4.3), we may justifiably use the first pulse as a measure of the pressure.

In Figure 4.9, the first pulse wave forms for HE-1 and HE-2 are not too different; the peak values are roughly the same, as are the durations. However, the scaling of durations is very bad for succeeding pulses. Between HE-2 and HE-3, the effect of a deeper charge shows as a six-fold ratio of peak pressures, with but slightly decreased duration. Since the air blast on HE-3 was only 20 per cent of that from HE-2 at $\lambda = 2.5$, the increase observed here should be due almost completely to the better earth coupling afforded by the greater depth of charge in HE-3. This conclusion is further reinforced by a similar six-fold ratio observed from HE-2 to HE-3 in Figure 4.8, at $\lambda = 1.72$. The greater simplicity of the wave forms is also noteworthy. This ratio of six to one may be compared with the three to one ratio obtaining in first acceleration pulses.

The transient records for the surface detonation of HE-4 should depend almost entirely on air-coupled effects. In fact, if the maximum positive peak (not just the first maximum) is plotted, the upper branch of the HE-4 curve in Figure 5.34 continues at an average exponent of 1.4 to $\lambda = 15$. This is also the air-blast exponent, so it may be tentatively concluded that air blast accounts for the earth pressure maximum peaks. The double-peaked first pulse is a feature for which no consistent explanation is yet available. Interference phenomena probably play a large part, but this is not borne out by the relatively simple behavior of HE-1, detonated just under the surface, with little difference in air-blast pressure.

The amplitude of the first positive pulse is a fairly consistent quantity. A composite presentation of the amplitude as a function of scaled horizontal distance for all tests is shown in Figure 5.34. On Test HE-1 a variety of coupling procedures were tried; the method finally proving the most reliable and reproducible has been described in Chapter 3. On HE-1, only two points, at $\lambda = 2.4$ and 4.3, were instrumented by this technique, which was later used on HE-2, HE-3, and HE-4. The points lie somewhat below those for HE-2, on a scaled basis. This probably reflects the increasing importance of air-coupled

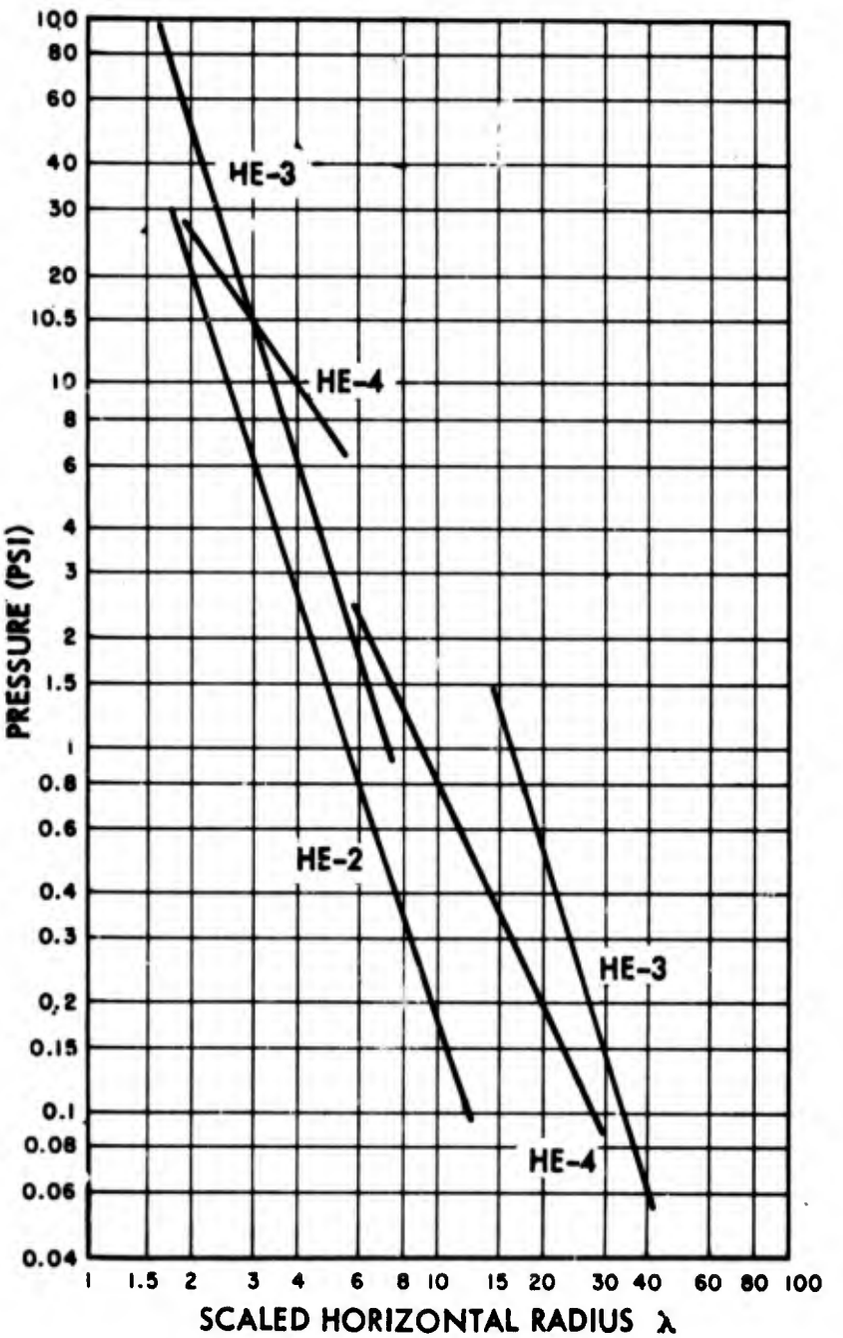

Fig. 5.34 Earth Pressure, First Maximum, All Tests

effects for larger charges. The portion of the HE-4 curve for small λ has an attenuation exponent about 1.4 (the same as for the air blast), whereas the remainder of the curve fits n = 2. For the other tests, n = 3 is a reasonable fit.

In the hydrodynamics of loss-free fluids, pressure and acceleration are related by

$$A_r = - \frac{1}{\rho} \frac{\partial p}{\partial r} . \qquad (5.6)$$

If both pressure and acceleration have similar wave shapes, then this relation implies that the exponent for acceleration should be that for pressure, plus one. If the fluid has appreciable losses and follows the Navier-Stokes relation, to the above equation is added a viscosity term involving the velocity gradient. In actuality the earth cannot be idealized in any such simple manner, but the actual results should be roughly parallel to those obtained from the idealization, especially at small λ values. A comparison of pressure and acceleration attenuation exponents does not show the expected behavior; in fact, the observed acceleration attenuation exponent was less than that for earth pressure. In this regard it appears that the quantity measured as earth pressure should not be used for correlation with other phenomena.

From Figure 4.16 a few general statements may be made about the effect of depth on earth pressure on Test HE-2. This figure does not include the measurements in the 34-foot and 68-foot holes. As was noted earlier, these holes collapsed prior to the test, making the coupling uncertain. The transient curves show pressure measurements obtained at depths of 5 feet and 17 feet and λ-values of 1.72 and 3.

The most striking contrast with the acceleration curves is in the threefold increase of peak pressure from the 5-foot to the 17-foot depth, at each value of λ. The actual first peak values are: at λ = 1.72, 24 psi and 73 psi, at 5 feet and 17 feet respectively; at λ = 3, 5.3 and 16.6 psi, at 5 and 17 feet. Since no such effect of depth was observed in earth acceleration it is difficult to conceive of an earth characteristic that offers a consistent explanation of both effects of depth.

5.5 COMPARISON WITH DUGWAY RESULTS

In Section 1.2 was tabulated the chain of comparisons between these HE tests and those conducted in 1951 at the Dry Clay Site of the Dugway Proving Ground, Utah.[3, 9, 10, 11] Some salient features of these comparisons will now be discussed.

Dugway Round 312 and HE-3 differed only in soil type; both used 2560 pounds of TNT at a scaled charge depth of 0.5. The air-blast comparison of Table 5.1 indicates that the "front porch" pressure is

TABLE 5.1

Double Air-Shock Pressures and Durations

Test	Scaled Radius λ	Pressure (psi)		Duration (sec)	
		Front Porch	Peak	Front Porch	Positive Phase
HE-3	3.0	0.82	4.[illegible]	0.008	0.029
312	3.0	0.8	2	0.016	0.041
HE-3	4.3	0.57	3.8	0.009	0.029
312	4.5	0.5	1.4	0.013	0.046
HE-3	6.25	0.41	3.1	0.005	0.029
312	6.0	0.4	1.4	0.012	0.042

substantially the same for both shots, but on the average the HE-3 peak air blast is about twice that for Round 312. On the other hand, the ratio of the positive phase duration for HE-3 to that for 312 at $\lambda = 3.0$ is 0.029/0.041 or about 0.7. Hence the impulses will probably not be too different, as may be judged visually from the air blast transient records ($\lambda = 3.0$) of Figure 5.35. Also note in this figure that the front porch for the Dugway test showed increasing pressure rather than a constant or decaying portion after the first sharp rise. The constancy of this plateau probably depends on the constancy of earth rise velocity after the shock wave reaches the surface at ground zero. Thus the rising plateau possibly indicates that the earth was cohesive enough to hold together and to be accelerated by the continued pressure of the gas bubble beneath. This hypothesis is consistent with the decreased value of the peak pressure for Round 312 as compared to HE-3, presumed to be due to a lower jet velocity. This would be the case if the gases expended part of their energy in continued work against the surrounding earth before final venting.

Further supporting evidence for this view is available from Figure 5.36, showing the horizontal earth acceleration at $\lambda = 4.5$ for Dugway Round 312 and for Tests HE-3 and HE-1. The ratio of peaks

[redacted]

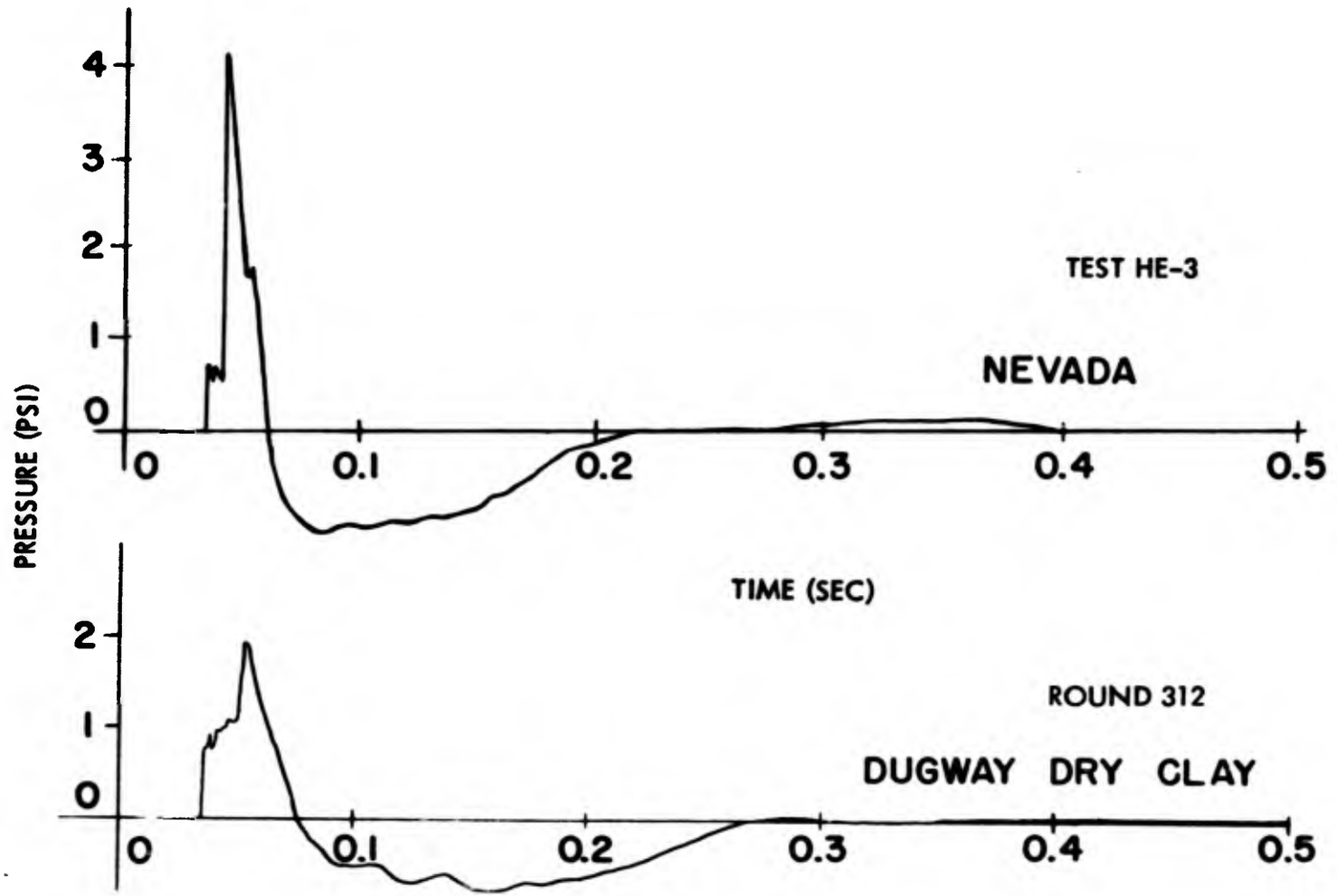

Fig. 5.35 Air Blast from 2560 Lb TNT, $\lambda = 3.0$, $\lambda_o = 0.5$

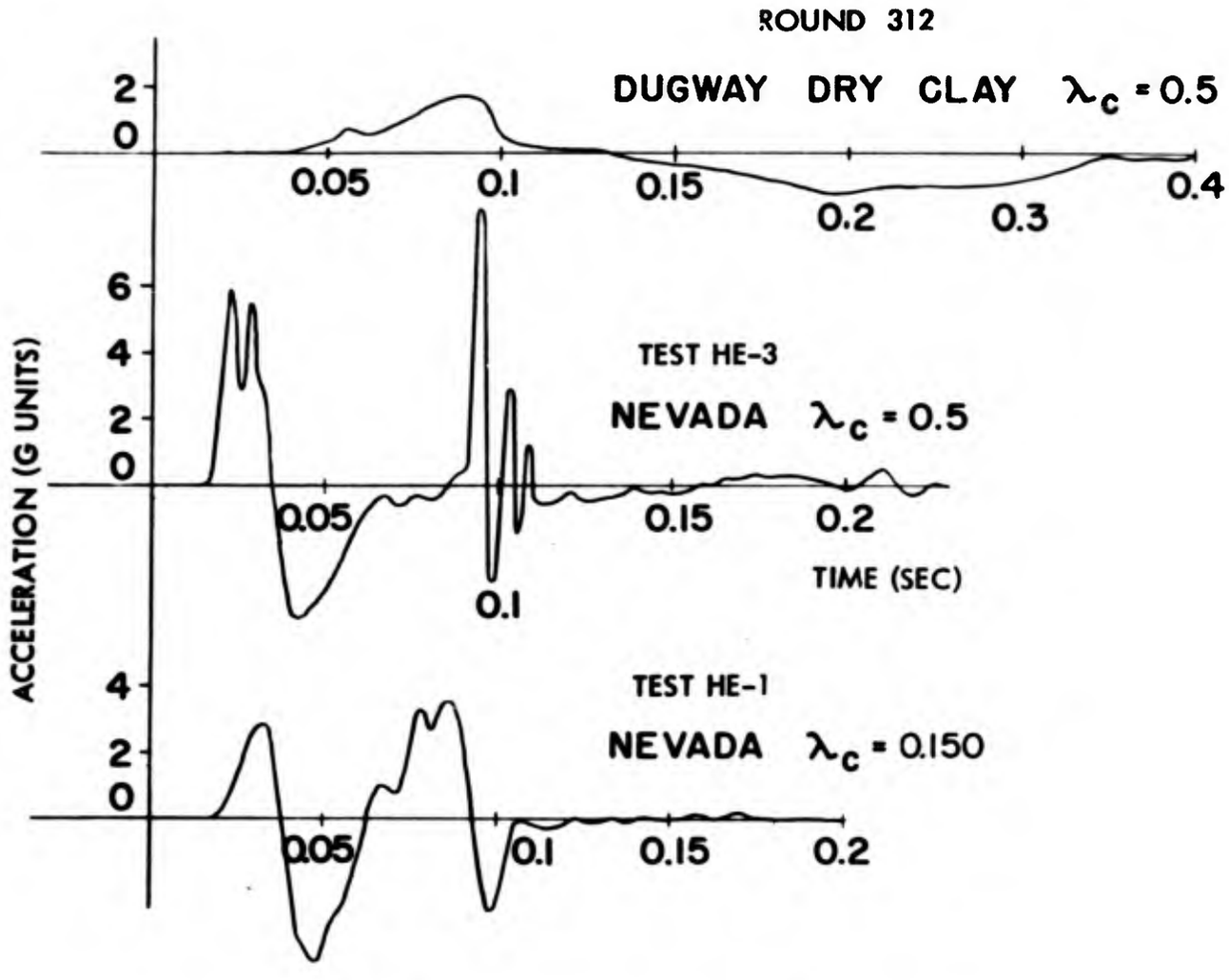

Fig. 5.36 Horizontal Earth Acceleration from 2560 Lb TNT, λ = 4.5

for the first pulse of Round 312 to that of HE-3 (identical tests except for soil types) is 1.7/5.9, or about 0.3. On the other hand, the pulse duration ratio is about 0.095/0.020, or 5. Note that the integrals (the velocities) will probably not be too different. For the shallow burial of HE-1, the pulse amplitude is reduced to about 2.8 G, as compared to HE-3, but the pulse duration is the same as for HE-3, 0.020 second. Thus the expanding gases were apparently able to act upon the Dugway Dry Clay Site soil for a much longer time than on the Nevada Test Site soil. This would tend to lengthen periods; it is difficult to see how this would reduce peak accelerations. Possibly the rate at which the gas bubble supplies energy to the soil decreases as the size increases, so the average intensity decreases for long pulses.

From the above it is seen that between the two depths of burial represented by HE-1 and HE-3, the principal difference in the first pulse of horizontal earth acceleration is in the amplitude rather than the duration. Hence the next comparison of Figure 5.37 may be considered. Here the horizontal earth acceleration (at $\lambda = 3.5$) for Dugway Round 315 and HE-2 are shown; both tests used 40,000 pounds of TNT. Although these were at different scaled depths, the above HE-1 to HE-3 acceleration comparison indicates that the pulse durations for HE-2 will not be appreciably affected by this difference in charge depth ($\lambda_c = 0.5$ to 0.150). Thus the HE-2 acceleration can be extrapolated with some confidence to a similar charge at a scaled depth of 0.5 to permit comparison with Dugway Round 315, which was detonated at this scaled charge depth. The pulse duration ratio of Dugway Round 315 to a similar test at the Nevada Site would then be about 0.274/0.034, or 8. The amplitude ratio (using the factor of 2.8 from HE-1 to HE-3, in Section 5.3), is then approximately 1.0/(2.6 x 2.8) = 0.14. Note that in this as well as in the previous comparisons the pulse amplitude and duration ratios are approximately inverse to each other. For Round 312 to HE-3, the product of the ratios is (0.3) (5) = 1.5; for 315 to (extrapolated HE-2), it is (0.14) (8.0) = 1.1. This may be interpreted to indicate that the first velocity peak (first integral) perhaps is approximately constant between the tests compared.

Another striking difference between the Dugway and Nevada tests is the permanent displacements as observed by surveying monuments (hubs). Table 5.2 summarizes this information at three scaled distances.

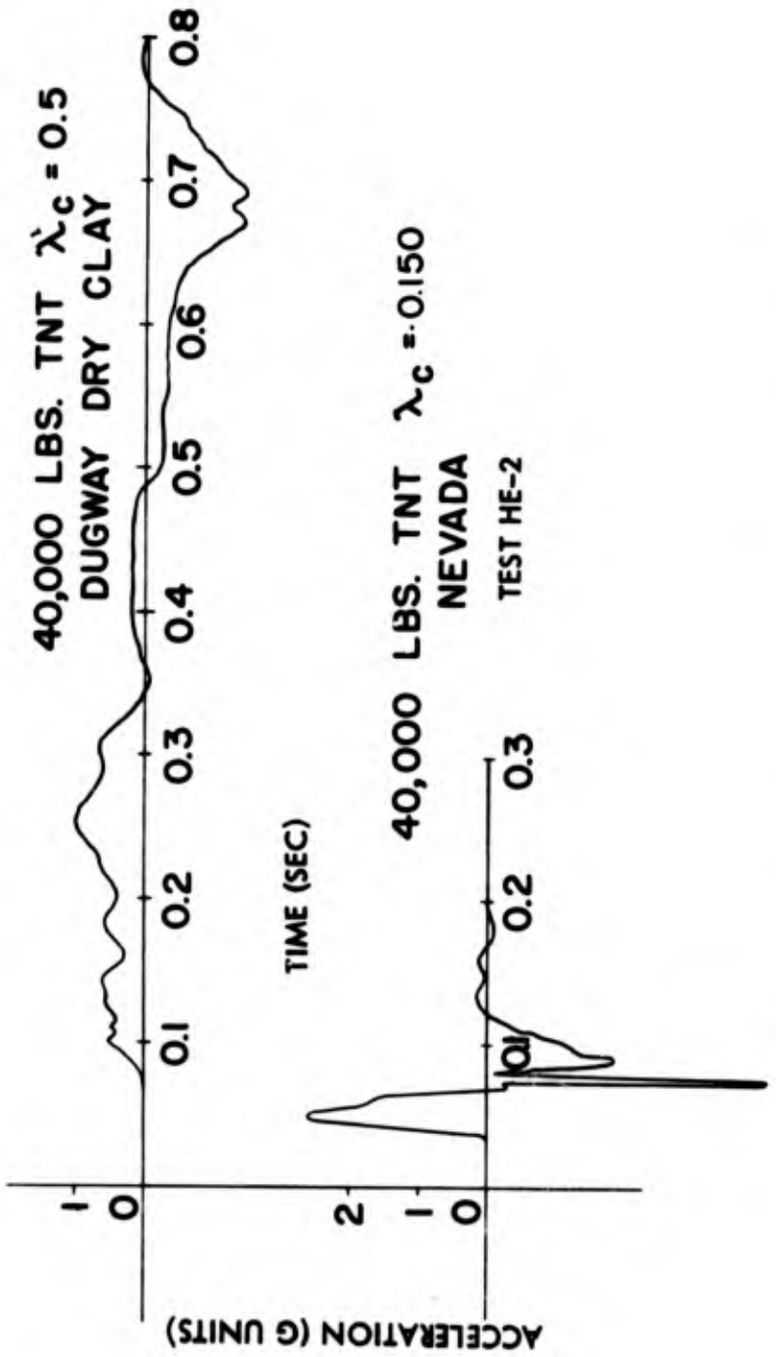

Fig. 5.37 Horizontal Earth Acceleration, 40,000 Lb TNT, λ = 3.5

TABLE 5.2

Permanent Displacements by Survey (ft)

Dugway Round 312			Nevada HE-3		
λ	Radial	Vertical	λ	Radial	Vertical
3	0.720	0.414	3	0.04	0.07
4.5	0.143	0.039	4.3	0.03	0.04
6	0.034	0.013	6.25	0.03	0.01

The Nevada displacements were much less than those at the Dugway Site. If the first pulse velocities are approximately the same, then the peak displacement should depend directly on the durations. Assume that velocity pulse durations are in the ratio of acceleration pulse durations. This would then indicate a ratio of Dugway to Nevada peak displacement in the range of four times to ten times. However, the permanent displacements, as judged from the table, are in ratios in the range of ten to fifty times. This possibly may mean that the Nevada soil recovered from its maximum displacement to a greater extent than did the Dugway dry clay. This, again, is in keeping with the assumption of a much more cohesive soil at Dugway.

This discussion indicates the difficulty of using results for one soil for extrapolation to another. These results probably cannot be explained by a simple soil constant that depends exclusively on what might be termed propagation scaling. A closer look is needed at details of the transfer of energy from the gas bubble to the soil. In addition, the influence of soil cohesiveness (or similar characteristic) on the duration of gas bubble, acceleration of earth rise, jet velocity, and similar source phenomena needs investigation. A carefully planned program of scaled tests in a variety of soils and at a controlled series of depths of charge will do much toward providing experimental data on which to construct a unified analysis. The present tests have emphasized the dangers of underestimating the need for such information, particularly when military effects must be predicted.

[redacted]

CHAPTER 6

CONCLUSIONS AND RECOMMENDATIONS

6.1 CONCLUSIONS

The general conclusion which the preceding discussion supports is that prediction of the results of one test from another of different scale cannot be undertaken with certainty for all aspects of all underground explosion phenomena. In particular, often the ordinary scaling laws do not apply with equal confidence to both the amplitude and time variables of the phenomenon considered. The change of one factor at a time - soil type, depth of burial, charge size and charge type - aids in more closely delineating the region of applicability of the scaling laws. In all these various test conditions, it appears that only the air blast may be said to obey the scaling laws in a true and complete sense, when viewed as a function of two independent variables, distance and time.

For non-scaling phenomena the changes in the conditions of experiments being compared lead to relations which may be interpreted as a change in the type of scaling. However, it is best to regard these relations as empirical means of limited extrapolation. The following listing summarizes this and other empirical information developed in the discussion. It applies specifically to scaling from HE-1 to HE-2 and thence to the underground nuclear test. In general, scaling from HE-4 to the surface nuclear test is much less certain.

1. To repeat, air-blast peak pressure, duration of positive phase, and positive impulse follow the normal scaling laws.

2. If placed on the surface (as HE-4), the following fractions of the test charges would give (at large distances) the same peak air-blast pressure as actually observed at the given distances: HE-1 and HE-2, 75 per cent; HE-3, 12 per cent; and HE-4, 100 per cent.

3. The amplitude of the smoothed first pulse of horizontal and vertical earth acceleration for $\lambda > 4$ scales as normally expected.

4. For the close-in horizontal accelerations, the peak of the first smoothed pulse is the maximum peak.

[redacted] [redacted]

5. The corresponding acceleration durations do not scale; for the horizontal component the HE-2/HE-1 duration ratio is 2, whereas for the vertical component it is 1.6. The scale factor was 2.5.

6. The vertical first pulse acceleration amplitude vs. λ curve shows a step which occurs at a distance constant at from 400 to 500 feet. This appears to be due to a discontinuity in the seismic velocity, and should occur at the same absolute distance in the nuclear tests.

7. The horizontal acceleration shows a discontinuity close-in which is tentatively identified with the increasing predominance of air-coupled effects as the distance increases. The shift in the discontinuity from HE-1 to HE-2 is not inconsistent with this assumption.

8. The smoothed first acceleration pulse for HE-1 is noticeably less than for HE-3; the ratio for the horizontal component is about 40 per cent, and 30 per cent for the vertical. On the other hand, the HE-3 air blast is but 40 per cent of that from HE-1. These facts reflect the better coupling to the earth of the more deeply buried HE-3 charge, with consequent effects on the energy partition between air blast and earth motion (effect of charge depth).

9. The passage of the air blast over a gage station results in a sharp, highly-damped oscillation in earth acceleration, particularly in the vertical component. This oscillation is termed the "slap". The first slap peak in the vertical acceleration is negative (downward), and appears to be proportional to the air-blast pressure at that station. The ratio of first vertical peak of the slap acceleration (in G-units) to the air-blast peak pressure (in psi) was 0.3 for HE-1 and HE-2, and 0.43 for HE-4. These ratios should be the same, and the difference observed above remains unexplained.

10. The behavior of the slap period with charge size is contradictory. However, it is expected that a constant value will be reached for very large charges. No estimate is made of this value.

11. Preliminary results on particle velocities for HE-1 and HE-2 show poor scaling for amplitudes. The amplitude of the maximum oscillation in velocity appears to be proportional to peak air-blast pressure, indicating that air-coupled effects may be involved.

12. The horizontal earth acceleration does not change much with depth down to 34 feet for stations at $\lambda = 3$ and $\lambda = 11$. The smoothed first pulse of the vertical component shows a change of sign from positive to increasing negative, down to 68 feet. However, the

horizontal components predominate at most depths at the stations instrumented.

13. The effect of depth on the slap in acceleration shows an attenuation exponent of 1.3 for the horizontal and 2.0 for the vertical component. Near the surface both components are approximately equal.

14. Time of arrival and attenuation data can be used to infer some of the behavior of air-coupled effects. In general, air-coupled acceleration may predominate increasingly as the distance from ground zero increases.

15. "Earth pressure" data do not correlate well with other information. The measured value increases with depth, at 17 feet being about three times the value at 5 feet. Note that the corresponding acceleration values are practically unchanged.

16. Comparison of HE-1, HE-2 and HE-3 with Dugway Rounds 312 and 315 (dry clay) indicates that no simple soil constant will explain the acceleration results. The amplitude and duration ratios for earth acceleration are approximately inverse to each other, when the tests being compared differ only in soil type.

17. The longer acceleration durations observed at Dugway are consistent with the assumption that the Dugway dry clay was much more cohesive than the soil for the Nevada Site HE program. This property is also useful in indicating why the Nevada peak air-blast pressures were greater than those for the corresponding Dugway tests.

18. It appears that predictions of results from one soil to another will require more knowledge of the details of transferring energy from the gas bubble to the soil.

19. Decreased cohesiveness of the soil for the HE tests may also be inferred by comparing permanent displacements. Apparently much more slide back or recovery occurred with soil at the Nevada Test Site than for Dugway dry clay.

6.2 RECOMMENDATIONS

As a program designed specifically to provide results for scaling up to tests involving much larger energy releases, the HE tests covered in this report represent about the minimum effort needed to correlate both past and future programs. It would be most desirable to have more pairs of correlations (see Section 1.2) than were possible. Serious

consideration of this point would enhance the value of such tests with relatively little added cost.

The present report contains only a portion of the data available from the original records. Further analysis is intended, and will be included in a final report to the Office of the Chief of Engineers, under whose sponsorship this program was conducted. In particular, extensive integration of acceleration records has begun.

Continued analytical work is recommended on air-coupled effects from air blast above earth. The data available from these tests should provide valuable means of determining the validity of any theory developed.

Work should be continued on analysis of the transfer of energy from the expanding gas bubble to the surrounding soil. It would be highly desirable to develop a simple criterion, using an appropriate soil characteristic, for indicating the general effect of differing soil types on amplitudes and period of earth motion.

Future underground test programs, whenever possible, should include tests to collect further data on effects of air coupling, type of soil, depth of burial, and local seismic inhomogeneities.

[redacted]

PROJECT 1(9)-1

APPENDIX A

PERSONNEL

Project 1(9)-1 of OPERATION JANGLE was performed by Stanford Research Institute under Contract No. DA-49-129-eng-119 with the Office of the Chief of Engineers, Washington. Mr. T. O. Stark served as Project Officer for OCE.

All Stanford Research Institute activities on Project 1(9)-1 were under the direction of Dr. E. B. Doll. Dr. Doll supervised the initial planning for the test program and directed the field activities, with Mr. L. M. Swift serving as field party chief. Additional members of the field party were L. H. Inman, V. E. Krakow, C. C. Hughes, S. C. Ashton, W. M. Stewart, and D. C. Sachs. This report was prepared by Dr. Doll and Dr. V. Salmon, with typing and drafting assistance from Miss Blanche Shoemake and Mrs. Jane Simons, respectively.

LT. W. R. Brooks, USN, was responsible for handling, placing and priming the explosive charges. The Haddock Engineers Ltd. furnished the construction contractor facilities required. LCDR. D. C. Campbell, USN, and CAPT. R. McBride, USA, of Program One coordinated the activities of this project with the remainder of OPERATION JANGLE.

[redacted] [redacted]

[redacted]

PROJECT 1(9)-1

BIBLIOGRAPHY

1. Office, Chief of Engineers, Protective Construction Branch, Engineering Division, "Underground Explosion Tests; Program "A", Tests in Soils", Revised, November, 1950. RESTRICTED

2. Stanford Research Institute, "Underground Explosion Tests at Dugway", Interim Report, July, 1951. Prepared for Sacramento District Office, Corps of Engineers, U. S. Army, Contract DA-04-167-eng-379. CONFIDENTIAL

3. Stanford Research Institute, "Underground Explosion Tests at Dugway, Surface Structure Program", Final Report, March, 1952. Prepared for Sacramento District Office, Corps of Engineers, U. S. Army, Contract DA-04-167-eng-379. CONFIDENTIAL

4. C. W. Lampson, "Final Report on Effects of Underground Explosions", OSRD Report 6645, March, 1946. UNCLASSIFIED

5. Stanford Research Institute, "Predictions - U-Test - Operation JANGLE", Technical Report No. 4, November 8, 1951. Prepared for Office of Naval Research, Contract N7onr32104. SECRET RESTRICTED DATA

6. Stanford Research Institute, "HE tests - Operation JANGLE", Interim Report, October, 1951. Prepared for Office of the Chief of Engineers, Department of the Army, Contract DA-49-129-eng-119. CONFIDENTIAL

7. C. W. Lampson, "Resumé of the Theory of Plane Shock and Adiabatic Waves with Applications to the Theory of the Shock Tube", Ballistic Research Laboratories, Aberdeen Proving Ground; Technical Note No. 139, March, 1950. UNCLASSIFIED

8. F. Press and M. Ewing, "Theory of Air-Coupled Flexural Waves", Jour. Appl. Physics vol. 22, pp 892-899, July, 1951.

9. Engineering Research Associates, Inc., "Instrumentation of Underground Explosion Tests Program, Interim Technical Report No. 1, Dry Clay"; 1 August 1951. CONFIDENTIAL

[redacted] [redacted]

10. Engineering Research Associates, Inc., "Instrumentation of Underground Explosion Tests Program, Interim Technical Report No. 2, Dry Sand"; 1 October 1951. CONFIDENTIAL

11. Engineering Research Associates, Inc., "Instrumentation of Underground Explosion Tests Program, Interim Technical Report No. 3, Wet Clay"; 1 November 1951. CONFIDENTIAL

[redacted]

OPERATION JANGLE

PROJECT 1(9)-2

COMPOSITION OF CLOUD FORMED BY TNT EXPLOSIONS

by

R. D. Cadle
A. G. Wilder

3 October 1951

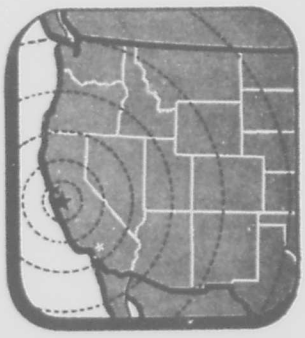

STANFORD RESEARCH INSTITUTE
STANFORD, CALIFORNIA

[redacted]

[redacted]

PROJECT 1(9)-2

CONTENTS

TABLES

[redacted]

[redacted]

PROJECT 1(9)-2

ABSTRACT

An investigation was made of particulate material in clouds produced by two explosions of 2560 pounds of TNT in dry soil at Yucca Valley (one of the Atomic Energy Commission's testing grounds) about 50 miles northwest of Indian Springs, Nevada. Sampling was effected by means of an airplane which made numerous passes through the dust clouds produced by the HE-3 and HE-4 tests of Operation JANGLE.

The following sampling devices were used: a molecular filter, an impactor, and a dust camera. These were arranged in a parallel manner between two manifolds. One manifold was connected to the sampling probe and the other to an air pump.

Most of the particles collected appeared to be unchanged soil and carbon. The carbon particles looked like minute fragments of coke and were probably decomposition products of TNT. There were a few small spheres which apparently were fused particles of soil.

The particle size distribution for material collected during each pass through the explosion clouds was determined. There were no particles greater than four microns in diameter collected by the impactor or the molecular filters and the majority of the particles were below one micron.

Particles as large as 50 microns in diameter were collected by filters mounted on the exterior of the plane. There was no evidence of fracturing of the ultimate particles of the soil.

The clouds had become quite stable with respect to composition and particle size distribution within two minutes after the explosion had occurred.

[redacted]

[redacted]

COMPOSITION OF CLOUDS FORMED BY TNT EXPLOSIONS (HE TESTS - OPERATION JANGLE)

1.1 INTRODUCTION

This report covers an experimental study of the cloud resulting from two underground HE explosions. The experiments reported here were undertaken as a part of the broad general study of explosion phenomena. A part of this general study is concerned with predictions in regard to the cloud of explosion products formed by an underground atomic explosion. To serve as a basis for such predictions, information regarding the cloud formed by HE explosions is of value.

Operation JANGLE is an extensive experimental program, consisting principally of two nuclear explosions planned at an early date for the Nevada Proving Ground of the Atomic Energy Commission (Yucca Flat - Site Mercury). Prior to the nuclear tests Operation JANGLE included four high explosive (HE - TNT) tests during August and September of 1951. These HE explosions occurred in the immediate vicinity of the sites to be used for the nuclear tests, and thus gave an excellent opportunity to obtain more information about the composition of underground TNT explosion clouds, with the possibility of later correlation with similar clouds resulting from underground nuclear explosions.

This report presents the results obtained from the airborne sampling of the explosion clouds resulting from tests HE-3 and HE-4 of Operation JANGLE. Each test used 2560 pounds of TNT (Dugway 0.2 scale). For HE-3 the charge center was 6.9 feet below the ground surface, while the charge rested on the ground surface for HE-4 (surface shot). HE-3 was fired 15 September 1951 and HE-4 was fired 9 September 1951.

The techniques, procedures, and equipment used for the work covered by this report have been fully described by Technical Report No. 2 of July, 1951 covering similar tests conducted on three underground TNT explosions at the Dugway Proving Ground in May, 1951.

The design, execution, and reporting of the dust cloud experiments have been the direct responsibility of Dr. R. D. Cadle and Mr. Arthur Wilder. Dr. R. B. Vaile, Jr. was responsible for planning the program and for coordination with the complex activities of Operation JANGLE.

1.2 SAMPLING EQUIPMENT AND TECHNIQUES

The sampling equipment consisted of molecular filters, a three-stage Sonkin impactor, and a dust camera.

The molecular filters are composed of a mixture of cellulose acetate and cellulose nitrate and were supplied by Professor Goetz of the California Institute of Technology. These filters are very efficient for particles of sub-micron size and permit a rapid flow of air with a very low pressure drop across the filter.

[redacted]

[redacted]

PROJECT 1(9)-2

The Sonkin impactor was used to collect particles to be studied by means of the electron microscope. The impactor has three stages, each one consisting of a narrow slit through which the air being sampled is drawn. A microscope slide, on which were mounted collodion-covered 200 mesh screens, was introduced opposite each jet so that the particles in the air stream were made to impinge against the collodion-covered screens. Later these screens were inserted in the electron microscope in order to study the particles below about 0.5 micron in diameter.

The dust camera is a device for determining the concentration, in situ, of the particles in an aerosol. The equipment consisted of a tube containing a focusing lens, a high speed photo-flash lamp, and a small aperture through which the light passed to a 35-mm camera.

A condenser lens, with a central dark field stop, focused the oblique light from the flash lamp on the aperture located between the condenser lens and the camera lens. The air sample to be studied was drawn slowly through the aperture and each particle in the field of focus diffracted the light so that it entered the camera and appeared as a small dot on the film. By using certain camera constants obtained from earlier calibration experiments it was possible to calculate the number of particles contained in each milliliter of air from the number of dots appearing on the film.

These three pieces of sampling equipment were mounted in parallel between two manifolds in an aluminum carrying box. Flowmeters were used in series with each instrument in order to control the air flow. The exhaust manifold was connected to an air pump driven by an electric motor and the intake manifold was connected by means of a flexible (Tygon) hose to an aluminum pipe which served as the "probe" through which the sample of air was drawn into the sampling devices.

This sampling apparatus was installed in an Air Force C-47 airplane supplied by the 2059th Air Weather Wing. The sampling equipment was mounted on a laboratory bench in the airplane and the aluminum probe extended about one foot above the top of the fusilage and was bent toward the front of the airplane.

A fourth dust sampler, designed to collect much larger quantities of particulate material than any of the above mentioned samplers, had previously been mounted on the airplane for other tests. This sampler was a filtering device which depended upon the speed of the airplane to force the air through the filters.

The airplane arrived at the site of the explosions before each test and had radio communication with the ground party. The plane circled the site at a distance of about 3 miles so that when the charge exploded the pilot turned and flew immediately into the body of the cloud. The pilot sounded a bell approximately 10 seconds before entering the cloud, upon entering the cloud, and upon leaving the cloud. Sampling was started at the 10 second bell and was continued for 20 seconds after leaving the cloud. A new molecular filter was used for each pass. The impactor samples were cumulative for all passes through each cloud. Six passes were made through the cloud from the HE-3 shot and four passes through that from the HE-4 shot.

[redacted]

The time required to leave the cloud, make a complete turn, and re-enter the cloud was about 2 minutes. When the sampling was complete the airplane was flown through clean air while "blanks" were obtained on the sampling devices. Practically no particulate matter was collected during these blank sampling runs.

During these sampling flights the co-pilot made a record of time in the clouds and the altitude of each pass. His records for the two shots are shown as Tables A.1 and A.2

1.3 GENERAL OBSERVATIONS CONCERNING FLIGHTS

Generally explosion clouds from charges such as these consist of essentially two parts: a central portion which is blown upward rapidly, and a later and roughly circular rolling lower cloud called the base surge. In these flights all of the sampling was carried out by passing through the central cloud.

Test HE-4, which was the surface charge, produced a characteristic cloud with a central column and a very small base surge.

Test HE-3, the buried charge, at first sent up a large column several hundred feet high. After about one-half minute the entire column seemed to draw back to earth, becoming almost entirely base surge which was about 50 feet high. The plane was 300 feet above the ground when the explosion occurred and it dropped down to about 75 feet, at which elevation it passed over most of the cloud. The pilot felt it was unsafe to pass through the body of the cloud during the first and second passes. About a minute after the explosion the cloud began to dissipate and to rise again so that subsequent passes through the cloud were made at 300 to 400 feet above the ground. A faint cloud of dust was still visible from the air about 20 minutes after the explosion. Observers on the ground reported that the cloud had almost completely disappeared only a few minutes after the explosion.

1.4 RESULTS

The molecular filters were rendered transparent by means of a solvent for the filters so that the particles collected could be studied on a microscope stage using transmitted illumination. These filters were also examined thoroughly at 500 X magnification using an "Ultropak" vertical illuminator. The use of incident light made it possible to distinguish between carbon particles and soil particles.

The concentrations of particulate material within the cloud are shown in Table A.7. Tables A.4 and A.5 give the particle size distribution of particles collected on molecular filters during tests HE-4 and HE-3, respectively. Concentrations indicated by the dust camera may represent the concentration near the edge of the clouds. The concentrations calculated from the number of particles collected with the molecular filter are an average concentration across the cloud. The figures given represent only the concentrations of particles larger than about 0.3

micron. Smaller particles could not be observed with the optical microscope and were not measured by means of the dust camera. The dust camera data for the sub-surface shot (HE-3) were considered unreliable and are omitted from Table A.7. As will be shown below, most of the particles are smaller than 0.3 micron and, therefore, are not included in these figures.

Table A.3 gives the particle size distribution for four samples of soil taken from several different depths at the site of these tests.[1] The last column in Table A.3 gives the particle distribution for the 1 foot deep sample after it had been blown into a large settling chamber to simulate conditions in an explosion cloud. This aerosol was then drawn through the same equipment that was used in the airplane and samples were caught on the molecular filter and on the first stage of the Sonkin impactor.

Most of the material from the explosion clouds collected on the molecular filter was either unchanged soil or black particles which appeared to be decomposition products of the TNT.

The material collected by impaction was examined by means of the electron microscope at a magnification of 5000 X. This material seemed to consist almost entirely of unchanged soil. Electron micrographs of the 1 foot deep soil sample from the site of HE-3 test were used for comparison. No significant differences in size or shape of particles were noted.

The particle size distribution of material collected by means of the impactors from the explosion clouds and from the laboratory dispersions is given in Table A.6. The particle size distribution mode for the sub-surface shot was about 0.2 to about 0.3 micron and was the same for the laboratory dispersed sample from site HE-3.[2] These data indicate that there were no significant differences between the size distributions of particles collected from the cloud and those collected from the dispersing apparatus in the laboratory. The particles shown by the electron micrographs appeared to be mostly ultimate particles, that is, there were very few aggregates.

The data in Tables A.4 and A.5 for the particle size distribution of particles caught on the molecular filters show that the clouds were quite stable at the time the airplane first entered them. Very little change in particle size distribution took place after the first pass. Carbon particles made up most of the large particles, and the proportion of carbon to soil particles decreased rapidly with decreasing particle size.

---

1. An aqueous suspension of this soil had a pH of about 9. This soil also effervesced violently when added to dilute hydrochloric acid and appears to be a mixture of limestone, sand, and some low grade clay.
2. Warpage of the plastic impactor, as a result of high temperatures inside of the airplane, caused contamination of the impactor slides during the surface shot (HE-4) and consequently no reliable impactor data are available for comparison with the sub-surface shot (HE-3).

Relatively few particles collected by the impactor or the molecular filters exceeded 4 microns in size. The filtering devices installed on the exterior of the airplane collected considerable quantities of particles as large as 50 microns. These filters sampled at a much faster rate than did the molecular filters or the impactor and the fibers constituting the filter material were very coarse. Therefore, no attempt was made to determine particle concentrations or size distributions of the material collected by these filters.

1.5 GENERAL CONCLUSIONS

1. The clouds from the TNT explosions consisted mainly of unchanged soil and decomposition products of TNT. Also present in both clouds were a very few spheres of fused soil.
2. The clouds had become quite stable with respect to particle size distribution and composition within 2 minutes following the explosions.
3. The composition of the 2 clouds was about the same, but the concentration of the cloud from the sub-surface (HE-3) explosion was slightly greater than that from the surface (HE-4) explosion.
4. There was little difference in particle size distribution between unexploded soil from the site and the material caught in the clouds. Most of the particles appeared to be discrete and very few aggregates were observed. Apparently the explosions produced little shattering of the ultimate particles in the soil.
5. The airplane filters caught particles as large as 50 microns but the majority of the particles caught on the molecular filters and in the impactor were less than 4 microns in diameter.

Meniskometer!

[redacted]

PROJECT 1(9)-2

APPENDIX A

TABLE A.1.
Flight Record of the HE-4 Test (Surface)
(9 September 1951)

Pass Number	Position with Respect to Cloud	Time	Altitude of Airplane above Ground (feet)[a]
—	Time of Explosion	10:40:00	--
1	(Entering Cloud) (Leaving Cloud)	10:41:36 10:41:40	700
2	(Entering Cloud) (Leaving Cloud)	10:43:47 10:43:51	650
3	(Entering Cloud) (Leaving Cloud)	10:46:00 10:46:17	1200
4	(Entering Cloud) (Leaving Cloud)	10:47:56 10:48:15	1400

a Elevation of shot site was about 4200 feet above mean sea level.

[redacted]

[redacted]

PROJECT 1(9)-2

TABLE A.2
Flight Record of the HE-3 Test (Sub-surface)
(15 September 1951)

Pass Number	Position with Respect to Cloud	Time	Altitude of Airplane above Ground (feet)[a]
—	Time of Explosion	9:45:00	—
1[b]	Entering top edge Leaving " "	9:46:05 ca. 9:46:09	75
2[b]	Entering " " Leaving " "	9:47:52 ca. 9:47:56	300
3	(Entering Cloud) (Leaving Cloud)	9:49:49 9:49:57	300
4	(Entering Cloud) (Leaving Cloud)	9:51:50 9:52:05	300
5	(Entering Cloud) (Leaving Cloud)	9:53:00 9:53:05	400
6	(Entering Cloud) (Leaving Cloud)	9:54:00 9:54:05	400

a Elevation of shot site was about 4200 feet above mean sea level.
b Missed body of cloud.

[redacted]

TABLE A.3
Particle Size Distribution of Soil taken from Several Sub-surface Levels at the Site of Test HE-3 (Sub-Surface Shot)

Size Range Microns	Percentage of Total Particles in Each Size Range at Different Depths				
	1 ft.	2 ft.	3 ft.	4 ft.	1 ft. Sample[a]
1	57.5	42.1	65.6	63.4	76.6
1-2	17.5	15.8	16.8	16.0	18.0
2-4	18.3	23.0	8.8	16.9	5.4
4-8	4.2	14.5	6.4	1.8	—
8-12	2.5	4.6	1.6	0.9	—
12-20	0	0	0.8	0.9	—

a This sample was blown into a large settling chamber and the effluent was drawn through the airborne sampler and caught in a molecular filter.

TABLE A.4
Particle Size Distribution of Particles Collected on Molecular Filters
HE-4 Test (Surface)

Size Range Microns	Percentage of Total Particles in Each Size Range			Percentage of Total Particles in Each Size Range Which are Carbon		
	Pass Number			Pass Number		
	1	2	3	1	2	3
1	90.5	91.0	98.0	6.3	4.7	5.9
1-2	4.8	3.2	0	60.0	54.5	—
2-4	4.4	5.2	2.0	78.0	44.5	33.3
4-8	0.5	0.6	0	100.0	50.0	—
8-12	0.3	0	0	100.0	—	—
				14.1[a]	8.7[a]	6.5[a]

a These figures represent the percentage of all particles counted which were carbon.

TABLE A.5
Particle Size Distribution of Particles Collected on Molecular Filters
HE-3 Test (Sub-surface)

Size Range Microns	Percentage of Total Particles in Each Size Range						Percentage of Total Particles in Each Size Range which are Carbon					
	Pass Number						Pass Number					
	1[a]	2[a]	3	4	5	6	1[a]	2[a]	3	4	5	6
1	80.7	81.2	92.9	86.8	76.0	78.2	0.1	4.3	4.5	5.8	0.1	5.4
1-2	12.7	15.3	3.6	11.9	19.0	15.5	9.5	13.6	66.7	5.2	11.4	0
2-4	6.6	3.5	3.5	1.3	5.0	6.3	18.2	20.0	50.0	50.0	22.2	11.1
							b	b	b	b	b	b
							3.0	6.2	8.3	6.3	3.8	4.9

a Passes 1 and 2 missed main body of cloud.

b These figures represent the percentage of all particles counted which were carbon.

PROJECT 1(9)-2

TABLE A.6
Particle Size Distribution for Particles Collected with the Impactor
From the Explosion Clouds and from Laboratory Dispersed Soil
From Site of Test HE-3
(From Electron Micrographs)

Size Range Microns	Percentage of Particles in Each Range (1st Stage Impactor Only)		
	HE-4 Surface	HE-3 Sub-Surface	Sample from Site HE-3[b]
	[a]		
0.05	—	0	1.4
0.05 - 0.1	—	6.3	12.6
0.1 - 0.2	—	19.1	14.0
0.2 - 0.3	—	30.2	17.5
0.3 - 0.4	—	12.7	10.5
0.4 - 0.5	—	7.9	8.3
0.5 - 1.0	—	15.8	27.3
1.0 - 2.0	—	7.9	7.6
2.0 - 3.0	—	0	0.8

a Warpage of the impactor as a result of high temperature inside the airplane resulted in contamination of the slides during this test.

b. This sample was blown into a large settling chamber and the effluent was drawn through the airborne sampler and caught on an electron microscope screen in an impactor.

TABLE A.7
Concentration of Particles Larger than About 0.3 Micron
In the Explosion Clouds

Shot	Pass through Cloud	Particle Concentration (Particles/ml.air)	
		Dust Camera	Molecular Filters
HE-4 (surface)	1	1332	5667
	2	—[a]	1428
	3	148	113
	4	222	--
	Blank	0	20
HE-3 (sub-surface)	1[b]	—	2272
	2[b]	—	1971
	3	—	6992
	4	—	2916
	5	--	2032
	6	--	1568
	Blank		20

a Dust camera misfired.

b Airplane missed main part of cloud

[redacted]

OPERATION JANGLE

Project 1(9) - 3

SOME HE TESTS AND OBSERVATIONS ON CRATERS AND BASE SURGES

BY

DONALD C. CAMPBELL
LCDR, U.S. Navy

1 November 1951

ARMED FORCES SPECIAL WEAPONS PROJECT

[redacted]

[redacted]

[redacted]

PROJECT 1(9)-3

CONTENTS

[redacted] [redacted]

[redacted]

PROJECT 1(9)-3

ILLUSTRATIONS

[redacted] [redacted]

[redacted]

PROJECT 1(9)-3

TABLES

[redacted]

[redacted]

PROJECT 1(9)-3

ABSTRACT

A series of HE Tests was planned at the Nevada Test Site preparatory to the nuclear explosions in Operation JANGLE. These HE shots were designed to obtain, under similar conditions, data to be used as a basis for making predictions concerning the phenomena to be studied during the nuclear explosions.

The HE program, as originally conceived, was expanded to permit further study of the base surge and crater phenomena.

Ten HE shots (a total of thirteen explosions) were conducted in the upper Yucca Flat and Frenchman Flat areas.

Practically all of the instrumentation by the various participating agencies was done on the first series (HE-1 through HE-4). With a few minor exceptions, all instrumentation performed in a satisfactory manner.

Shot HE-2 consisting of 40,000 pounds of TNT was fired with the c. g. 4.63 feet below the surface. There was a high order of detonation and the shot was completely successful. The following indications were noted as a result of this shot:

a. The ground acceleration phenomenon falls at a different attenuation factor than anticipated in the predictions from Lampson's work. This factor more nearly fits a square function than a fourth power law.

b. There is good agreement between the HE-1 and HE-2 results and it should be possible to extrapolate from HE to the nuclear.

c. Air blast has scaled from 1 pound of TNT to the large HE shots and should continue to the nuclear range. Air pressure measurements showed a true blast wave. Considerable underground shock can be anticipated from the air blast.

d. The various methods of measurement between different agencies were in excellent agreement. There should be no question concerning the measurement technique on the nuclear tests.

Meteorological data was carefully recorded for each shot in order to study the base surge and fall-out phenomena. Pie pan dust collectors were used on some of the shots for a simplified study of fall-out.

[redacted]

[redacted]

PROJECT 1(9)-3

The base surge formation in HE-7 was so slight that it was not considered necessary to fire additional shots to confirm the curve in Figure 1.1.

It was tentatively concluded that there is little difference in the above ground activity produced by TNT and Pentolite.

It is certain that some minimum density of soil is required in the plume in order to produce the downward sweep of dust which, at ground level, moves outward as a base surge. The density is produced by blowing a large volume of earth a relatively short distance up into the air. The closer the charge to the surface (smaller values of λ_c), the smaller the crater and greater the height of plume, hence, lower density and less base surge contribution.

Inasmuch as the phenomenology is so complex and only limited HE tests were conducted, it is very difficult to come to any clear-cut set of conclusions to use as a basis for predicting what will occur in the way of craters and base surges for the nuclear shots. However, on the basis of these limited tests, the following guesses are made:

a. For the surface nuclear shot, a base surge appears very unlikely. The crater radius should be 80-90 feet while the crater depth should be 25-30 feet. The maximum cloud height should be 12,000 feet.

b. For the underground nuclear shot, there will be a considerable amount of throw-out at the base of the plume which may be mistaken for a base surge. The probability of a base surge appears small. The crater radius should be 140-150 feet; its depth should be 50-60 feet. Maximum cloud height should be 6,000 feet.

Since it is an observed fact that the crater diameter is a readily scaled parameter for underground TNT explosions, the immediate observation (photographic or otherwise) of the underground crater diameter may be a simple and reliable method for determining equivalent TNT mechanical yield of the nuclear weapon.

Of course, if predictions were always right there would be no need for experimental programs and field tests.

[redacted] [redacted]

[redacted]

SECTION 1

INTRODUCTION

1.1 GENERAL

A series of large scale TNT explosions fired by the Army Corps of Engineers at the Dugway Proving Ground has indicated that a base surge formation was most probable at $\lambda_c = 0.5$ (λ_c = depth to c.g. divided by $W^{1/3}$ where W is the equivalent TNT weight in pounds) and, with decreasing values of λ_c, the possibility of a base surge decreased so that there is a good chance of no base surge occurring at $\lambda_c = 0.17$. This is shown diagrammatically in Figure 1.1.

The series of HE tests at the Nevada Test Site was designed primarily to obtain, under similar conditions, data to be used as a basis for making predictions concerning the phenomena to be studied during the nuclear tests of Operation JANGLE.

Originally a series of four HE explosions was planned. However, before this series was completed, it was decided to continue the tests with a second series with particular attention to the study of craters and base surges since plans called for the underground shot to be fired at $\lambda_c = 0.135$ and TNT charges HE-1 and HE-2 in the first series, with $\lambda_c = 0.15$, had not produced base surges. The course of action for the second series of shots outlined in Table 1.1 was developed in consultation with Dr. Herbert Scoville Jr., AFSWP, Dr. Pete Swift, NOL, and CAPT Frank I. Minant, USN, SWC.

1.2 LAYOUT OF TESTS

The original series of high explosive tests (HE-1 through HE-4) was conducted in the JANGLE area of upper Yucca Flat at a location midway between points S and U. The second series of tests was conducted in Frenchman Flat about one mile west of the northern half of the dry lake. Soil conditions appeared to be similar in the two regions and primarily consisted of a powdery sand mixed with some gravel. The Frenchman Flat site had a greater number of rocks and boulders.

[redacted]

[redacted]

PROJECT 1(9)-3

TABLE 1.1

Base Surge Studies

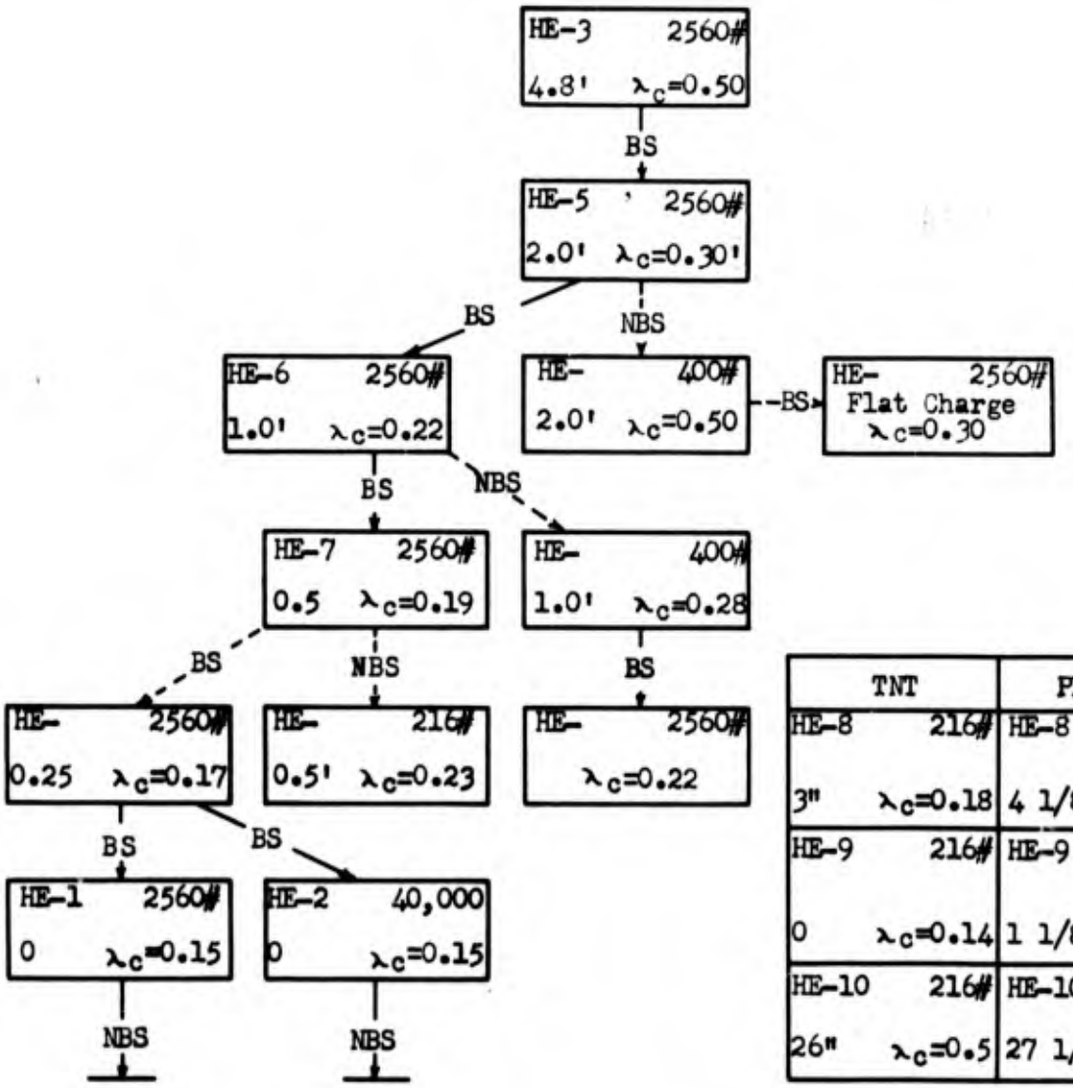

TNT		PENTOLITE	
HE-8	216#	HE-8	177#
3"	λc=0.18	4 1/8"	λc=0.18
HE-9	216#	HE-9	177#
0	λc=0.14	1 1/8"	λc=0.14
HE-10	216#	HE-10	177#
26"	λc=0.5	27 1/8"	λc=0.5

The HE-number indicates the number assigned to actually conducted shots. Number in upper right hand corner is the charge weight. Lower left hand corner is the dirt cover from the top of the charge to the surface. Values for λ_c are given in the lower right.

W = 40,000 lb - $W^{1/3}$ = 34.2
W = 2560 lb —— $W^{1/3}$ = 13.68
W = 400 lb —— $W^{1/3}$ = 7.4
W = 216 lb —— $W^{1/3}$ = 6.0

[redacted]

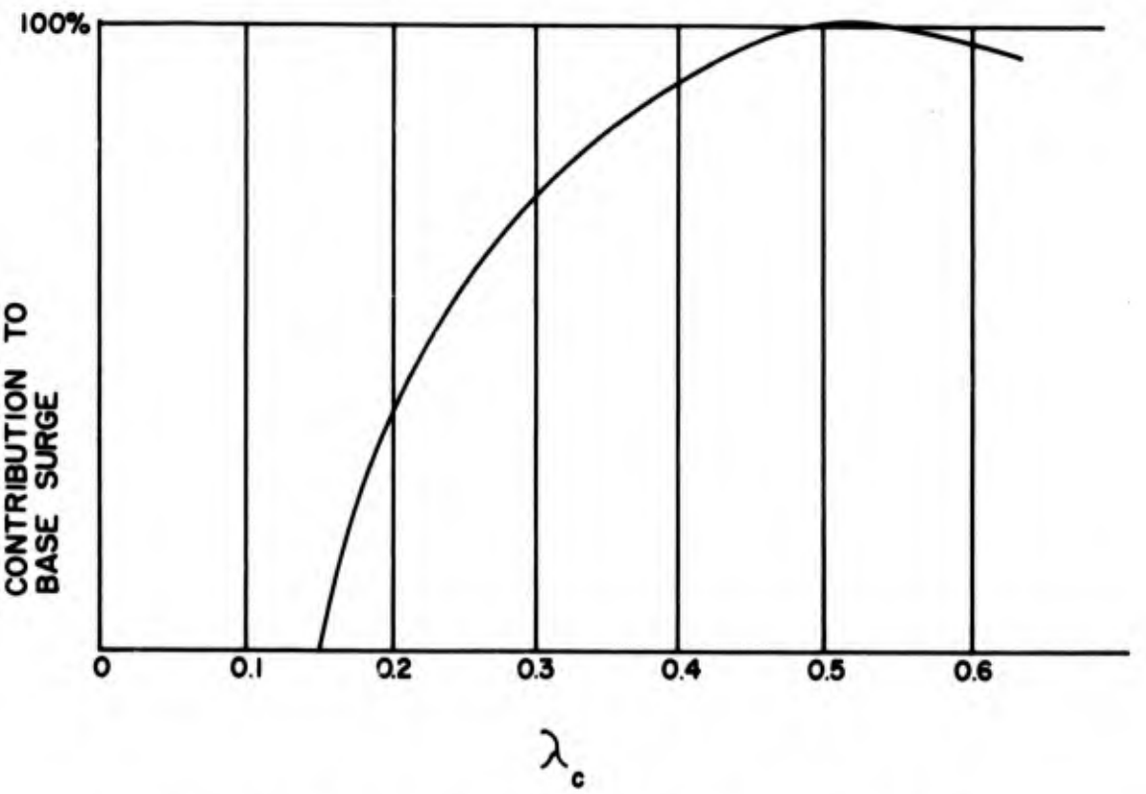

Fig. 1.1 Base Surge Formation as a Function of λ_c

[redacted]

SECTION 2

THE HE SHOTS

2.1 SHOT HE-1 ($\lambda_c = 0.15$)

This shot consisted of 2560 pounds of TNT with the center of gravity at a depth of 2.01 feet below the ground surface. It was fired on 25 August at 0915 PST. The detonation was of high order and completely successful.

During the period immediately following the explosion the surface wind averaged approximately 8 mph from N 60° E. The surface temperature was 86.5° F. The relative humidity at the Air Force Weather Station, 18 miles from the site, was 12 per cent. Immediately following the detonation there was observed a throw-out of streamers which appeared to travel several hundred feet radially outward. A considerable fall-out of dirt occurred in the immediate vicinity of the crater. A cloud of dust rose to a height of approximately 1500 feet and drifted in a southwest direction. This cloud dissipated within 45 minutes.

With a few minor exceptions, all instrumentation apparently performed in a satisfactory manner. Ground acceleration measurements appeared to run from 2 to 20 times the values predicted from theory. The factor increased with increasing distance. This was of considerable interest in setting gage ranges for subsequent HE and nuclear shots. This information was also of interest in the layout of Program Three structures.

2.2 SHOT HE-2 ($\lambda_c = 0.15$)

This charge of 40,000 pounds of TNT, with the center of gravity 4.63 feet below the ground surface and the upper edge tangent to the earth surface, was fired at 0900 PST on 3 September 1951. The detonation was of a high order and completely successful. A considerable throw-out was observed. A number of streamers appeared to travel out on trajectories having elevations between 30° and 45°. The majority of the throw-out fell within 500 feet of ground zero. A large cloud of dust, starting with a 500-foot diameter rose to an estimated height of 2,000 to 3,000 feet. This cloud moved slowly north and was observed over the underground site one hour and fifteen minutes after firing. A considerable fall-out occurred in the immediate vicinity of ground zero and continued along the path of the cloud movement. A definite darkening of the ground was observed out to 2,500 feet in a

[redacted]

[redacted]

PROJECT 1(9)-3

TABLE 2.1

Permanent Displacements, Shot HE-1

Radial Distance	S 50° E		N 80° E		S 85° W		N 5° W	
	ΔR	ΔT	ΔR	ΔT	ΔR	ΔT	ΔR	ΔT
28.00	.34	0.03	0.21	-0.12	0.53	0.15	0.43	0
32.00	.19	0.06	0.09	-0.12	0.42	0.13	0.29	0.04
36.00	.18	0.04	0.02	-0.13	0.18	0.15	0.13	0.09
40.00	.15	0.03	0.01	-0.13	0.12	0.17	0.05	0.10
44.00	.15	0	0.01	-0.08	0.09	0.19	0.02	0.05
48.00	D	D	0.01	-0.02	0.09	0.19	0.04	0.08
52.00	.20	0	-0.01	-0.08	0.04	0.19	-0.07	0.09
56.00	.12	0	-0.01	-0.06	0	0.24	-0.11	0.10
60.00	.10	-0.01	-0.02	-0.05	-0.02	0.25	-0.06	0.07
64.00	.10	0	-0.03	-0.05	D	D	-0.06	0.08
68.00	.11	0	-0.03	-0.04	-0.01	0.22	-0.11	0.12
72.00	.11	0	-0.02	-0.04	-0.03	0.22	-0.07	0.07
76.00	.11	0.02	0	-0.04	0	0.22	-0.08	0.08
80.00	.10	0.02	0	-0.03	-0.02	0.24	-0.11	0.09
84.00	.10	0	0	-0.05	-0.02	0.26	-0.10	0.09

Δ R = Radial Displacements - Positive in direction away from ground zero in feet. Δ T = Tangential Displacements - Positive is left of radial line in feet. D = Damaged Stake.

TABLE 2.2

Crater Data, Shot HE-1

R	S 40° E		N 40° W		S 50° W		N 50° E	
	Ea	Er	Ea	Er	Ea	Er	Ea	Er
0	-6.8	-7.6	-6.8	-7.6	-6.8	-7.6	-6.8	-7.6
3	-5.4	-6.5	-6.7	-7.5	-3.8	-5.6	-5.0	-6.0
5	-4.5	-6.1	-6.1	-7.0	-2.8	-4.8	-4.4	-5.7
8	-3.1	-5.3	-5.5	-6.0	-1.5	-3.7	-2.2	-5.0
10	-3.0	-4.5	-3.5	-5.7	-1.3	-3.5	-1.6	-4.7
14	-2.1	-3.0	-2.4	-3.9	-9.7	-2.5	-0.8	-2.5
18	-0.6	-1.5	-0.5	-2.5	-0.1	1.6	-0.2	-1.2
20	0.8	-0.2	1.9	-1.8	0	3.1	1.0	-0.8
21	1.2	0	2.5	-0.7	0	3.7	2.5	-0.6
23	0.8	0	2.0	-0.5	0	0	2.0	0.1
25	0	0	1.5	-0.1	0	0	1.2	0.2
29	0	0	0	0	0	0	0.2	0

R = Radial distance from zero in feet. Ea = Apparent Crater elevation in feet. Er = Real crater elevation in feet.

[redacted] [redacted]

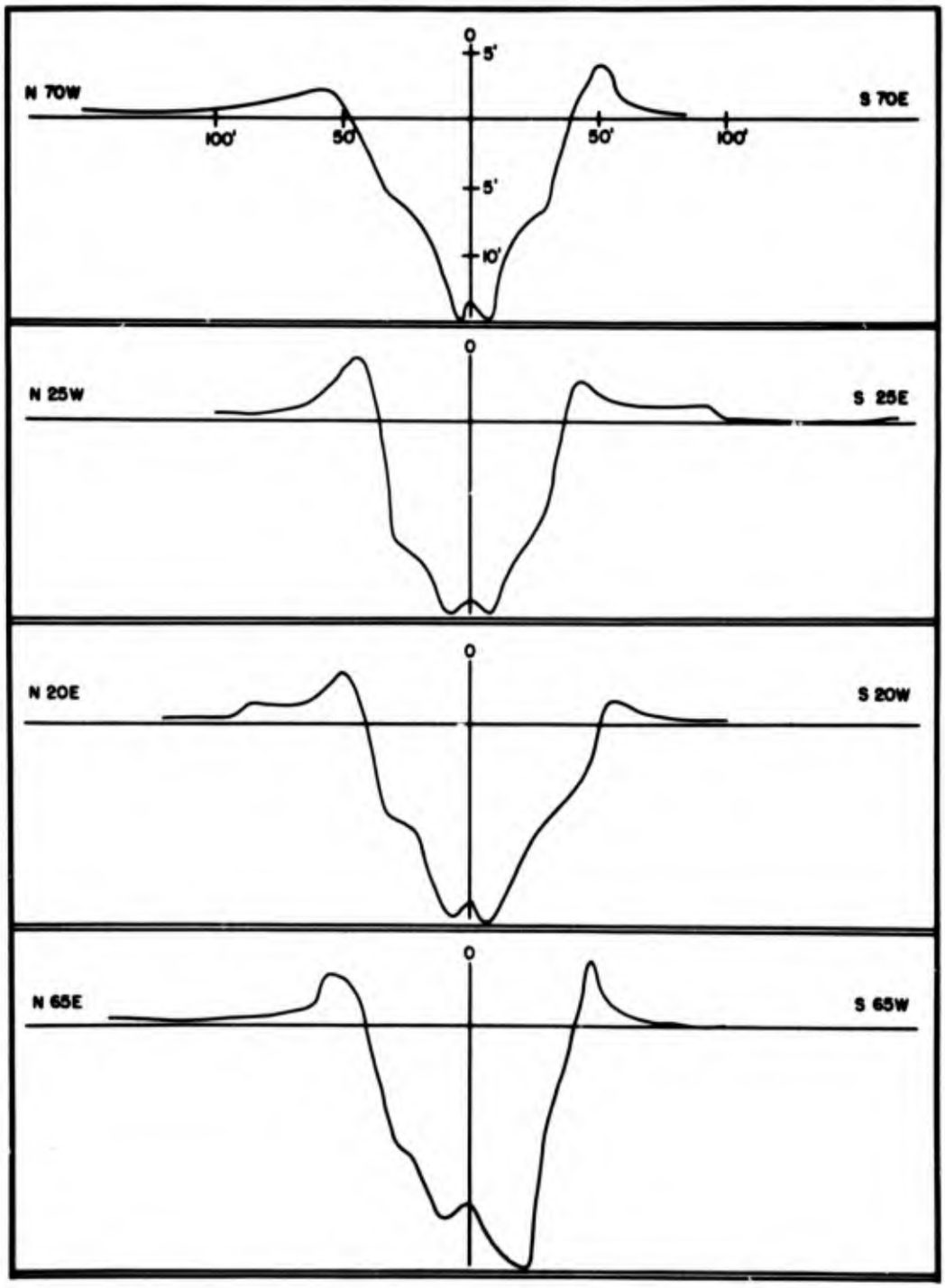

Fig. 2.1 Average Crater Contours for 40,000 Pounds of TNT on Shot HE-2

northerly direction. A crater remained which had a diameter of approximately 80 feet and a depth of 15 feet. A careful excavation was made to remove the fall-back material, however, the earth shattered to such an extent that no good data could be obtained. One hard spot was located at the center approximately 11½ feet below the level of the apparent crater.

Information on winds aloft at the test site just prior and after the detonation is given in Table 2.3.

TABLE 2.3

Wind Data, Shot HE-2

TIME - 0845			TIME - 0915		
Altitude Above Ground (Feet)	Velocity mph	Wind From	Altitude Above Ground (Feet)	Velocity mph	Wind From
0	5	S	0	6	S
1300	7	S	1000	6	S 20° E
2300	4	S	2200	4	S 10° E
3600	3	S	3400	3	S 20° E
4600	9	S 30° E	5600	14	S 40° E
5600	12	S 30° E	7800	7	S 20° E
			10,600	15	S 45° W

The surface temperature at the time of the explosion was 80.6° F and the relative humidity was 14 per cent.

As a last minute attempt to obtain some crude information on the close-in fall-out, 36 pie pans were distributed around the target area. Information from the pie pans as well as the observed distance of the ground discoloration (carbon fall-out) is given in Table 2.7.

Instrumentation performance was excellent as there were practically no failures. Performance was such that the Naval Ordnance Laboratory and the Ballistic Research Laboratories did not require additional tests (HE-3 and HE-4) prior to the nuclear shots. The Stanford Research Institute fully instrumented the remaining tests.

Results are reported by the participating agencies[1]. However, some tentative indications follow:

a. The ground acceleration phenomenon falls at a different attenuation factor than anticipated in the predictions from Lampson's work. This factor more nearly fits a square function than a fourth power law.

[1] See project reports of the Naval Ordnance Laboratory, the Ballistic Research Laboratories, Stanford Research Institute, and the David Taylor Model Basin published in the JANGLE report series.

TABLE 2.4

Permanent Displacements
(Hubs on S 20° W Blast Line)
Shot HE-2

Radial Distance From Zero, Pre-Blast	Final Position, Post-Blast		
	North	East	Elev (+Up)
59.09	-1.03	0.22	0.38
71.06	-0.53	-0.09	0.28
86.05	-0.10	0.29	0.07
102.67	-0.08	-0.40	0.04
123.20	0.05	0.14	0.03
147.61	0.08	0.08	0.03
177.86	0.07	0.05	0.02
217.03	0.03	0.05	0.03
262.17	0.01	-0.02	0.03
314.98	0.01	-0.04	0.03
378.25	-0.02	-0.10	0.02

b. There is good agreement between the HE-1 and HE-2 results and it should be possible to extrapolate from HE to the nuclear.

c. Air blast has scaled from 1 pound of TNT to the large HE shots and should continue to the nuclear range. Air pressure measurements showed a true blast wave. Considerable underground shock can be anticipated from the air blast.

d. The various methods of measurement between different agencies were in excellent agreement. There should be no question concerning the measurement technique on the nuclear tests.

e. HE-2 crater contours are shown in Figure 2.1.

2.3 SHOT HE-4 (λ_c=-0.15)

This charge, the third in order of firing, consisting of 2560 pounds of TNT, was fired at 0940 PST on 9 September 1951. Its center of gravity was 24½ inches above the ground surface with the lower edge tangent to the earth surface. The detonation was of a high order.

A cloud of dust was raised from the earth's surface to heights estimated by observers to be between 1,000 and 1,500 feet. This cloud traveled in a southerly direction and was dissipated within a half hour. The prevailing winds which have been observed by test personnel in this location are from the south. On two occasions the wind has been from

TABLE 2.5

Apparent Crater, Shot HE-2

N 70° W		N 25° W		N 20° E		N 65° E		S 70° E		S 25° E		S 20° W		S 65° W	
R	E	R	E	R	E	R	E	R	E	R	E	R	E	R	E
0	-13.4	0	-13.4	0	-13.4	0	-13.4	0	-13.4	0	-13.4	0	-13.4	0	-13.4
6	-14.0	7	-14.6	6	-14.2	9	-14.5	8	-14.8	9	-14.4	5	-14.7	7	-15.3
20	- 7.3	18	-16.4	23	- 7.5	21	-10.1	23	- 7.5	20	- 9.5	22	-18.0	20	-10.5
30	- 5.8	27	- 9.4	31	- 7.2	26	- 9.4	30	- 6.5	27	- 7.9	33	- 5.4	28	- 7.7
55	2.1	44	4.8	49	3.7	45	2.5	42	1.5	43	3.1	45	3.5	45	3.9
85	1.0	48	4.5	61	1.4	54	3.9	51	4.0	48	3.1	47	4.8	55	1.8
150	0.5	58	1.7			59	1.5	56	1.9	59	1.3	51	2.8	68	0.7
200	0.0	72	0.5	84	1.4	100	0.3	75	0.6	94	1.3	60	0.9	100	0.2
		100	0.5	91	0.4	140	0.3			100	0.2	100	0		
		200	0.1	100	0.2					165	- 0.1				
				117	0.1										

R = Radial Distance in feet.

E = Elevation in feet (+ up).

TABLE 2.6

Permanent Displacements, Shot HE-2

Radial Distance	N 25° W			N 65° E			S 25° E			S 65° W		
	ΔR	ΔT	ΔE	ΔR	ΔT	ΔE	ΔR	ΔT	ΔE	ΔR	ΔT	ΔE
50.00	2.79	0.04	1.15	2.25	0.00	0.94	3.18	-0.05	2.02	1.95	-0.05	1.23
60.00	1.66	0.10	0.55	1.12	0.00	0.31	1.44	0.01	0.33	0.62	-0.12	0.32
70.00	0.80	0.07	0.21	0.96	0.00	0.08	1.07	0.15	0.13	0.35	-0.02	0.16
80.00	0.58	0.02	0.14	0.63	0.03	0.05	0.57	0.09	0.10	0.16	-0.02	0.13
90.00	0.34	0.06	0.12	0.45	-0.02	0.05	0.49	0.07	0.07	0.02	-0.04	0.04
100.00	0.23	0.06	0.04	0.20	-0.03	0.02	0.28	0.03	0.00	-0.17	-0.03	0.04
110.00	0.22	0.01	0.05	0.02	-0.04	0.02	0.09	0.03	0.00	-0.24	-0.04	0.02
120.00	0.10	0.05	0.03	-0.02	-0.08	0.01	0.02	0.05	0.00	-0.33	-0.03	0.00
130.00	0.10	0.04	0.01	-0.07	-0.06	0.00	-0.02	0.05	-0.01	-0.35	-0.05	0.01
140.00	0.10	0.04	0.00	-0.13	-0.07	0.00	-0.03	0.05	-0.02	-0.42	-0.06	0.01
150.00	0.04	0.03	0.00	-0.10	-0.09	-0.01	-0.03	0.05	-0.02	-0.36	-0.02	-0.02
160.00	0.05	0.07	-0.01	0.10	-0.01	0.00	-0.03	0.06	-0.03	-0.25	-0.01	0.00
170.00	0.02	0.03	0.00	0.05	0.00	-0.01	-0.02	0.05	-0.03	-0.26	-0.04	0.00
180.00	0.05	0.02	0.01	0.08	0.02	-0.02	-0.02	0.05	-0.03	-0.22	-0.02	0.00
190.00	0.02	0.03	-0.02	0.14	0.02	-0.02	-0.04	0.06	-0.03	-0.28	-0.02	-0.01
200.00	0.05	0.03	-0.01	0.27	0.00	-0.04	-0.04	0.05	-0.02	-0.28	-0.03	-0.01
210.00	0.10	0.02	-0.02	0.10	-0.14	-0.02	0.00	0.09	-0.03	-0.07	-0.04	-0.02

Δ R = Radial Displacements - Positive is direction away from charge in feet.
Δ T = Tangential Displacements - Positive is to left of radial line in feet.
Δ E = Vertical Displacements - Positive is up in feet.

TABLE 2.7

Pie Pan Dust Collectors
Shot HE-2

Dist. From Zero (Ft.)	N		N 60° W		S 60° W		S		S 60° E		N60° E	
	A	B	A	B	A	B	A	B	A	B	A	B
400	48.3*	10% to ½" 90% silt	14.6*	few to 3/8"	16.7*	100% silt	3.1*	Part to 3/8"	23.0**	Part to ½"	96.0	50% to ½" 50% silt
600	29.2#	few to 3/8"	upended		0.9#	100% silt	0.3	Part to 3/8"	2.7#	Part to 3/8"	20.8	few to ½"
800	30.3#	100% silt	3.0#	1 - 3/8" rest silt	0.7#	100% silt	2.4	Part to ¼"	0.6	100% silt	8.1	1 - ¼" rest silt
1000	25.7#	100% silt	4.5	1 - 3/4" rest silt	0.3	100% silt	0.1*	100% silt	0.2	100% silt	3.4	100% silt
1500	8.0	100% silt	0.1	100% silt	0.1	100% silt	0.1	100% silt	0.1	100% silt	0.3	100% silt
2500	1.4	100% silt	0.1	100% silt	0.1	100% silt	0.1	100% silt	0.1	100% silt	0.1	100% silt
Dist. to Edge at Darkened Area	2500 ft.		850 ft.		450 ft.		250 ft.		650 ft.		1200 ft.	

* = Displaced but not overturned
\# = Overturned (Measurement off bottom)
** = Bent, displaced but not overturned

A = Weight of contents of pan in grams
B = Nature of contents of pans
Pie plate area = 430 cm^2

TABLE 2.8

Wind Data, 0 to 11,010 Feet Altitude, Shot HE-4[a]

Altitude[b]	TIME - 0930		TIME - 0950	
	Wind[c] Direction	Wind[d] Velocity	Wind Direction	Wind Velocity
0	090	15	020	13
1170	020	21	020	16
2310	020	24	010	14
3450	020	21	350	10
4560	360	15	300	15
5670	310	16	300	19
6700	290	17	310	21
7830	290	21	310	22
8910	290	23	320	16
9960	300	18	350	9
11,010	320	10	340	9

TABLE 2.9

Wind Data, 12,030 to 19,800 Feet Altitude, Shot HE-4[a]

Altitude[b]	TIME - 0930		TIME - 0950	
	Wind[c] Direction	Wind[d] Velocity	Wind Direction	Wind Velocity
12,030	330	8	340	9
13,020	340	13	340	9
14,010	340	15	350	16
15,000	340	26	340	23
15,960	340	30		
16,920	350	25		
17,880	350	34		
18,840	360	34		
19,800	010	30		

[a]The surface temperature at the time of the explosion was 84.2° F and the relative humidity was 12 per cent.
[b]Expressed in feet above ground surface.
[c]360° = N, 90° = E.
[d]Expressed in miles per hour.

TABLE 2.10

Pie Pan Dust Collectors
Shot HE-4

Distance From Zero (Feet)	N	N30°E	N60°E	E	S60°E	S30°E	S	S30°W	S60°W	W	N60°W	N30°W
400	4.5	1.4	0.6	1.8	1.7	0.5	1.0	1.7	0.4	12	12.6	3.5
600	4.2	0.5	1.0	0.1	0.5	0.2	0.1	2.7	4.9	0.7	4.8	0.2
800	1.0	0.3	0.05	0.05	0.05	0.05	0.1	0.2	1.3	0.2	0.6	0.4
1000	0.5	0.2	0.2	0.05	0.1	0.1	0.05	0.6	0.05	0.2	0.5	1.6
1500	0.1	0.05	0.1	0.05	0.2	0.05	0.1	0.1	0.2	0.1	0.05	0.1
2000	0.1	0.0	0.0	0.0	0.0	0.3	0.1	8.1	0.05	0.4	0.0	0.1

Pie Pan Area [illegible] (?)

Readings are in grams.

the north. By coincidence, these were the days of tests HE-1 and HE-4. Since the winds were gusty, any individual set of observations may not give a completely true picture, however, some readings taken just prior and after the detonation are given in Tables 2.8 and 2.9.

Some aerial dust samples were collected by a C-47 equipped with Stanford Research Institute filters. Pie pan collectors were used for ground fall-out measurements. Results are given in Table 2.10. There appears to be no consistency in these measurements and this may be attributed to the nature of the wind at the time of the test and between the time of the test and collection.

The Stanford Research Institute performed all medium instrumentation. Recording was 100 per cent successful with the exception of one air pressure gage which was damaged by the blast. A hasty examination of the records indicated that there may have been a larger coupling than was anticipated.

TABLE 2.11

Permanent Displacements
(Hubs on S 50° W Blast Line)
Shot HE-4

Radial Distance From Zero, Pre-Blast	Final Position, Post-Blast		
	North	East	Elev (+Up)
23.48	0.06	-0.14	-0.04
28.56	0.03	0.05	-0.04
33.93	0	0.02	-0.06
41.17	0.02	-0.08	-0.06
44.59	0.03	-0.06	-0.04
59.06	-0.01	-0.01	-0.06
71.08	-0.01	0.10	-0.05
85.82	0.02	-0.03	-0.05
102.63	0	-0.02	-0.03
148.32	0.05	-0.06	-0.05

2.4 SHOT HE-3 ($\lambda_c = 0.5$)

Shot HE-3 (the fourth in order of firing) was a charge of 2560 pounds of TNT with the center of gravity 6 feet 9½ inches below ground surface and the upper edge 4 feet 9 inches below the ground surface. It was fired at 0840 PST on 15 September 1951. The detonation was of a high order and completely successful.

TABLE 2.12

Permanent Displacements, Shot HE-4

Radial Distance	S 5° W			N 5° E			S 85° E			N 85° W		
	ΔR	ΔT	ΔE	ΔR	ΔT	ΔE	ΔR	ΔT	ΔE	ΔR	ΔT	ΔE
28.00	S	S	S	S	S	S	S	S	S	S	S	S
32.00	S	S	S	S	S	S	S	S	S	S	S	S
36.00	S	S	S	0	0.04	-0.06	S	S	S	S	S	S
40.00	0.03	-0.06	?	0	0.03	-0.07	S	S	S	0.07	0.03	-0.04
44.00	S	S	S	0.01	0.04	-0.07	-0.05	0.02	-0.03	0.06	0.04	-0.01
48.00	0.06	-0.06	-0.03	0.01	0.03	-0.05	-0.07	0.03	-0.05	0.08	0.04	-0.02
52.00	0.05	-0.06	-0.03	0.01	0.04	-0.04	-0.06	0.03	-0.01	0.06	0.04	-0.02
56.00	S	S	S	0.02	0.03	-0.04	-0.06	0.03	-0.02	0.07	0.04	-0.02
60.00	S	S	S	0.02	0.04	-0.05	-0.06	0.03	-0.03	0.07	0.05	-0.02
64.00	0.06	-0.05	-0.01	0	0.04	-0.07	-0.06	0.04	-0.02	0.07	0.04	-0.02
68.00	0.06	-0.06	-0.02	0.02	0.02	-0.05	S	S	-0.02	0.10	0.04	-0.02
72.00	0.07	-0.06	-0.02	0	0.01	-0.05	-0.05	0.03	-0.03	0.11	0.05	-0.01
76.00	0.07	-0.06	-0.02	0	0.01	-0.05	-0.05	0.03	-0.02	0.10	0.06	-0.01
80.00	0.06	-0.06	-0.05	0	0.01	-0.03	-0.09	0.01	-0.01	0.11	0.03	-0.01
84.00	0.07	-0.06	-0.02	-0.03	0.02	-0.03	0	0.03	-0.03	0.13	0.03	-0.03

Δ R = Radial Displacements - Positive is direction away from charge in feet.
Δ T = Tangential Displacements - Positive is to left of radial line in feet.
Δ E = Vertical Displacements - Positive is up in feet.
S = Shattered Stake.

TABLE 2.13

Crater Data, Shot HE-4

R	N 5° E		R	N 50° E		R	S 85° E		R	S 40° E	
	Ea	Er		Ea	Er		Ea	Er		Ea	Er
0	-1.9	-2.1	0	-1.9	-2.1	0	-1.9	-2.1	0	-1.9	-2.1
2	-1.9	-2.1	2	-1.9	-2.0	2	-1.9	-2.0	2	-2.0	-2.2
5	-0.1	-1.5	5	-0.3	-0.9	5	-0.2	-1.1	6	-0.1	-0.4
8	0.2	0.2	8	0.2	0	7	0.7	0.4	9	0.2	0.1
25	-0.1		14	0.3	0.2	27	0.2		31	-0.2	
51	-0.1		30	0.2		47	-0.7		55	0	
84	-0.1		87	0.4							

R	S 5° W		R	S 50° W		R	N 85° W		R	N 40° W	
	Ea	Er		Ea	Er		Ea	Er		Ea	Er
0	-1.9	-2.1	0	-1.9	-2.1	0	-1.9	-2.1	0	-1.9	-2.1
2	-2.1	-2.2	2	-1.8	-1.9	3	-1.6	-1.8	2	-1.9	-2.0
6	-0.2	-1.2	6	-0.4	-1.2	5	-0.4	-0.6	6	-0.3	-1.3
9	0.2	0.1	8	0.1	-0.1	8	0.1	-0.2	7	0	-0.2
24	0		22	0.1		28	-0.1		23	-0.2	
61	0					56	0		50	-0.2	

R = Radial distance in feet.

Ea = Apparent crater elevation (+ up)

Er = Real crater elevation (+ up)

[redacted]

[redacted]

PROJECT 1(9)-3

Information on winds aloft at the test site just prior and after the detonation of HE-3 is given in Table 2.14.

TABLE 2.14

Wind Data, Shot HE-3[a]

Altitude[b]	TIME 0930		TIME 0950	
	Wind[c] Direction	Wind[d] Velocity	Wind[c] Direction	Wind[d] Velocity
0	050	16	030	18
1,170	050	17	030	27
2,310	070	13	050	24
3,450	090	8	070	17
4,560	080	9	080	10
5,670	080	9	080	6
6,750	090	7	070	6
7,830	110	7	080	7
8,910	130	6	150	7
9,960	140	7	130	7
15,000	-	-	150	12
16,920	-	-	130	2
20,760	-	-	260	7

a The surface temperature at the time of the explosion was 76.4° F and the relative humidity was 32 per cent.
b Expressed in feet above ground surface.
c 360° = N, 90° = E.
d Expressed in miles per hour.

A considerable throw-out was observed as the result of shot HE-3 with trajectories between 30° and 45°. The majority of this throw-out appeared to fall within a few hundred feet of ground zero. A crude examination of the ground around point zero after the shot gave the large particle count per square foot as shown in Table 2.15.

A number of rocks fell at distances greater than 280 feet. One rock, approximately 1½ inches in diameter and weighing 114.9 grams, was observed to fall 3,500 feet from ground zero.

[redacted] [redacted]

TABLE 2.15

Large Particle Count Around Zero, Shot HE-3

Max. Dimension	Inside 70 ft	70 ft-140 ft	140 ft-210 ft	210 ft-280 ft
4 inches	7	1/10	None	None
2 inches	16	2	1/5	1/10
1 inch	27	6	1	1/5

The explosion appeared to break through the ground in a manner similar to that observed for the previous tests (HE-1, HE-2, Dugway, etc.). The plume rose to approximately 500 feet. At a time between 10 and 20 seconds after the explosion, a base surge formation appeared through the throw-out dust. Initially, this base surge had equal dimensions around the zero point, however, in short order the upwind travel ceased and the surge moved with the wind in a southwest direction. The plume almost immediately descended into the surge so that the height of the dust cloud was approximately 100 feet. The downwind (leading edge) of the base surge reached the 2,000 foot mark 50 seconds after the detonation and reached 5,000 feet 2 minutes and 20 seconds after the zero time. Between one and two minutes after the detonation, the surge expanded so that the top was roughly at 500 feet as the cloud passed the 5,000 foot mark. Travel in a direction normal to the direction of the wind was similar on both radii. By the time the surge reached the 5,000 foot mark, the "normal" diameter was estimated by observers to be between 3,500 and 4,000 feet. The upwind face of the surge followed the cloud movement and was estimated to be approximately 750 feet in the direction downwind from ground zero at 2 minutes and 20 seconds after zero time. The base surge eventually became an appreciably sized cloud of dust. It was 500 feet high at 5 minutes after zero time and was moving in the southwest direction. It was observed in a somewhat diffused condition 30 minutes after the blast.

Some samples of dust were collected on shot HE-3 by a C-47 equipped with Stanford Research Institute filters. Eighty four pie pan collectors, such as those used for shots HE-2 and HE-4, were used for ground fall-out measurements. Results are given in Table 2.16.

The Stanford Research Institute performed all medium instrumentation on shot HE-3.

TABLE 2.16

Fall-Out Study with Pie Pan Dust Collectors, Shot HE-3

Distance From Zero (Feet)	N	N30°E	N60°E	E	S60°E	S30°E	S	S30°W	S60°W	W	N30°W	N60°W
400	1.9	0.2	1.4	1.6	0.05	24.5	5.5	32.8	11.5	8.9	0.8	0.3
600	0.3	0.2	0.05	0.1	0.05	0.1	3.8	13.6	33.7	0.1	0.2	0.05
800	0.05	0.2	0.3	0.05	0.1	0	0.9	8.0	7.8	0.05	0.05	0.05
1000	0.2	0.05	0.3	0.05	0	0	0.05	4.3	7.1	0	0.2	0.05
1500	0.05	0.1	0.0	0	0.05	0	0.05	1.8	1.5	0.1	0.05	0
2000	0	0	0.2	0	0.2	0	0.05	0.9	0.4	0	0.05	0
2500	0	0	0	0	0	0	0	0.1	0.5	0.5	0	0

Pie Pan Area 430 cm.²(?)

Readings are in grams.

[redacted]

PROJECT 1(9)-3

TABLE 2.17

Crater Data, Shot HE-3

R	N 5° E		N 50° E		S 85° E		S 40° E	
	Ea	Er	Ea	Er	Ea	Er	Ea	Er
0	-10.8	-11.0	10.8	11.0	10.8	11.0	10.8	11.0
3	-10.8	---	-10.8	--	-10.9	--	-10.9	--
9	- 8.0	- 8.3	---	--	---	--	---	--
13	---	---	- -	--	- 5.5	- 5.9	---	--
15	---	---	- 4.9	- 5.6	---	---	- 5.9	- 6.3
23	2.1	1.0	1.3	0.7	1.8	1.4	0.8	- 0.3
36	0.1	0.1	0	0	0.1	0.1	0.1	0.1

R	S 5° W		S 50° W		N 85° W		N 40° W	
	Ea	Er	Ea	Er	Ea	Er	Ea	Er
0	-10.8	11.0	-10.8	-11.0	-10.8	-11.0	-10.8	-11.0
3	-10.8	--	- 10.5	---	---	---	---	---
9	---	--	--	---	---	---	- 6.9	- 7.6
13	---	--	- 6.1	- 6.8	---	---	---	---
15	- 5.9	- 6.5	---	---	- 5.2	-5.9	- 5.5	- 6.1
23	0.8	- 1.2	1.6	- 0.3	1.0	- 0.1	1.1	0.5
36	0.1	0.1	--	---	0.1	0.1	--	---

R = Radial Distance From Zero In Feet.

Ea - Apparent Crater Elevation In Feet.

Er = Real Crater Elevation In Feet.

[redacted]

TABLE 2.18

Permanent Displacements
(Hubs on S 50° W Blast Line)
Shot HE-3

Radial Distance From Zero, Pre-Blast	Final Position, Post-Blast		
	North	East	Elev (+ Up)
28.70	-1.59	-0.56	0.58
34.04	-0.02	-0.31	0.12
41.17	-0.01	-0.05	0.07
49.30	0.01	0.02	0.03
59.04	-0.04	0	0.04
71.17	-0.02	-0.09	0.01
85.53	-0.07	0.02	0.01
102.68	0	-0.01	-0.01
148.13	-0.05	0.01	0.01
178.22	0	-0.01	0

TABLE 2.19

Permanent Displacements, Shot HE-3

Radial Distance	N 5° E			S 85° E			S 5° W			N 85° W		
	ΔR	ΔT	ΔE	ΔR	ΔT	ΔE	ΔR	ΔT	ΔE	ΔR	ΔT	ΔE
28.00	1.13	0.13	0.43	0.49	0.09	0.44	S	S	S	0.94	-0.16	0.42
32.00	0.42	0.15	0.37	0.26	0.03	0.21	0.36	0.23	0.20	0.32	-0.11	0.21
36.00	0.35	0.06	0.12	0.22	0.09	0.14	0.32	0.17	0.10	0.24	-0.05	0.13
40.00	0.19	0.04	0.08	0.14	0.06	0.10	0.21	0.12	0.07	0.07	-0.04	0.07
44.00	0.13	0.05	0.02	0.09	0.06	0.04	0.17	0.13	0.04	0.02	-0.03	0.05
48.00	0.06	0.03	0.02	0.02	0.08	0.05	0.04	0.11	0.03	-0.01	-0.01	0.03
52.00	0.05	0.03	0.01	0	0.05	0.06	0.03	0.09	0.03	-0.04	-0.02	0.03
56.00	0.03	0.04	0.01	0.01	0.05	0.04	0	0.08	0.01	-0.02	-0.03	0.03
60.00	0	0.04	0.01	-0.03	0.04	0.01	0	0.09	0	0	-0.03	0.03
64.00	0.02	0.02	0	-0.03	0.02	0	0.01	0.07	0	-0.02	0	0.02
68.00	0	0	0.02	-0.02	0.01	0.01	0	0.07	0.01	--	--	0.01
72.00	0.01	0.02	-0.01	-0.02	0.01	0.01	0.09	0.10	0	-0.03	0	0.01

Δ R = Radial Displacements - Positive is direction away from charge in feet.
Δ T = Tangential Displacements - Positive is to left of radial line when looking away from charge.
Δ E = Vertical Displacements - Positive is up in feet.
S = Shattered Stake.

[redacted]

PROJECT 1(9)-3

2.5 SHOT HE-5 (λ_c=0.30)

Shot HE-5 was the first of the second series of shots since only four were planned originally. The first four shots were fired in upper Yucca Flat and this second series was fired in Frenchman Flat.

On 30 September 1951 at 0800 PST, shot HE-5, consisting of 2560 pounds of TNT, was fired. Observers noted a considerable throw-out of streamers in the initial phases. A column of dust estimated to be 80 feet in diameter rose to between 450 and 500 feet. At 10 seconds after the detonation a base surge was observed to form. This surge traveled outward reaching a 500 feet radius in 30 seconds and a 750 feet radius at one minute. The central plume appeared to form one mammoth cloud of dust which floated away with the wind.

Camera stations were placed 5,000 feet east and 5,000 feet south of the center point of the explosion area. HE-5 was fired 100 feet S 22° E of the center of the explosion area.

Camera targets consisting of boards 8 feet square having alternating two feet squares were placed on lines through the center of the explosion area and at right angles to the line of camera sight as follows: 1,000 feet north; west and east; 1,615 feet south.

Crater and weather data are shown in Tables 2.20 and 2.21.

2.6 SHOT HE-6 (λ_c=0.22)

At 0800 PST on 2 October 1951, shot HE-6 consisting of 2560 pounds of TNT was fired. As in previous shots, a considerable throw-ou out was noted in the initial phases. A number of six to ten inch boulders was found up to 200 feet from the crater. A careful examination of the photographic records will be required to differentiate the degree of throw-out between shots HE-5 and HE-6#. The dust column rose to between 600 and 700 feet in the first 10 to 15 seconds. At eight seconds after the detonation a base surge was observed through the throw-out. This surge was of less magnitude than those previously produced. The actual travel, as a base surge, was something over 500 feet which was reached in 50 seconds. The ultimate height, as a base surge cloud, was about 200 feet. The central plume remained above the base surge. A horizontal shear was noted at an altitude of approximately 450 feet with the surge cloud moving in one direction and the top of the plume in another.

Camera stations were placed 5,000 feet east and 5,000 feet south of the center point of the explosion area.

This information is reported in the report of JANGLE Project 1(9)-4.

[redacted]

TABLE 2.20

Crater Data, Shot HE-5

From North to South			From West to East			From N45°W to S45°E			From S45°W to N45°E		
Radial Distance	Apparent Depth	Real Depth	Radial Distance	Apparent Depth	Real Depth	Radial Distance	Apparent Depth	Real Depth	Radial Distance	Apparent Depth	Real Depth
56.6	0	0	46.9	0	0	40.0	0	0	42.0	0	0
32.6	-0.3	0	35.0	-0.2	0	30.0	-0.8	0	31.4	-0.2	1.9
22.7	-1.8	-0.9	30.0	-0.7	0.2	22.0	-1.3	0.8	24.1	-2.3	2.6
20.0	-1.3	0	27.0	-1.1	1.0	15.0	1.9	4.3	20.0	-0.3	3.2
15.0	1.2	2.8	23.0	-1.3	2.7	9.3	5.9	6.0	14.0	4.2	6.5
10.3	5.5	6.1	20.0	-0.6	3.6	7.2	5.9	7.5	10.0	4.3	5.1
8.2	5.5	6.6	15.0	3.0	5.2	5.0	7.0	9.1	3.1	7.8	8.9
5.0	6.8	8.0	11.0	5.2	6.1	3.3	7.3	9.6	0	7.5	9.5
3.0	8.1	10.1	7.0	6.0	6.5	0	7.5	9.5	3.1	7.9	10.2
0	7.5	9.5	3.3	7.4	9.2	3.3	7.4	9.3	7.0	6.9	8.6
2.7	7.8	10.2	0	7.5	9.5	7.0	6.0	7.9	11.3	7.4	5.4
5.0	6.0	8.7	3.3	7.8	11.1	10.1	4.4	6.3	20.0	-0.1	2.2
9.0	5.1	6.8	7.0	6.1	7.9	14.0	4.0	5.5	24.7	-1.7	1.5
11.7	3.7	5.5	9.6	5.3	6.6	15.5	3.1	5.4	32.0	-0.6	0.5
13.6	3.8	5.5	24.3	-0.8	2.5	20.0	1.0	3.7	44.0	0	0
20.0	0	2.0	30.0	-0.3	0.5	23.4	-0.4	2.4			
23.3	-1.1	1.3	35.0	-0.1	0.1	26.5	0	1.6			
30.0	-0.8	0.5	50.0	0	0	46.0	0	0			
35.0	-0.4	0.5									
60.0	0	0									

W = 2560 Pounds of TNT. $W^{1/3}$ = 13.68.
λ_c =0.30. Earth Over Charge = 2.0 Feet.
All Values Are in Feet. Minus Indicates Above Grade.

TABLE 2.21

Weather Data, Shot HE-5[a]

Altitude[b]	TIME - 0740		TIME - 0815	
	Wind[c] Direction	Wind[d] Velocity	Wind[c] Direction	Wind[d] Velocity
Surface	Calm	Calm	Calm	Calm
1170	290	6	150	5
2310	190	14	180	10
3450	170	23	180	16
4560	180	24	190	26
5670	190	30	190	31
6750	200	33	190	32
7830	190	33	200	39
8910	200	29	200	47
9960	200	29		
11,010	210	33		

[a]Temperature at Ground Level - 56° F. Relative Humidity at Ground Level was 51%.

TABLE 2.22

Weather Data, Shot HE-6[a]

Altitude[b]	TIME - 0755		TIME - 0805	
	Wind[c] Direction	Wind[d] Velocity	Wind[c] Direction	Wind[d] Velocity
Surface	180	4	180	4
1170	230	11	230	10
2310	230	13	230	7
3450	210	7	230	18
4560	230	4	220	8
5670	240	6	190	6
6750	210	5	190	7

[a]Temperature at Ground Level - 54° F. Relative Humidity at Ground Level was 51%.
[b]Expressed in feet above ground surface.
[c]360° = N, 90° = E.
[d]Expressed in miles per hour.

[redacted] [redacted]

TABLE 2.23

Crater Data, Shot HE-6

From South to North			From East to West			From S45°E to N45°W			From S45°W to N45 E		
Radial Distance	Apparent Depth	Real Depth	Radial Distance	Apparent Depth	Real Depth	Radial Distance	Apparent Depth	Real Depth	Radial Distance	Apparent Depth	Real Depth
40.0	0	0	45.0	0	0	40.0	0	0	40.0	0	0
29.5	-0.2	0.6	36.0	-0.2	0.3	33.0	-0.3	0.2	30.0	-0.2	0.1
23.0	-1.2	1.8	30.0	1.0	0.8	30.0	-0.6	0.9	23.3	-2.0	2.1
15.0	2.3	4.8	24.3	1.6	1.5	25.3	-1.3	1.8	20.0	-0.6	2.4
12.0	3.4	6.0	20.0	0.5	2.1	20.3	-2.5	2.0	16.0	1.9	4.2
9.5	3.9	7.0	12.4	4.2	5.3	16.0	1.1	3.9	11.5	4.3	5.8
6.0	5.0	7.0	9.2	4.8	5.9	11.2	4.7	5.9	7.0	5.0	6.3
3.5	6.4	9.0	4.0	7.0	9.6	7.7	5.3	6.6	4.0	6.2	8.5
0	6.1	10.1	0	6.1	10.1	3.8	7.6	8.8	0	6.1	10.1
4.0	6.3	8.4	1.2	5.8	9.0	0	6.1	10.1	4.5	6.5	8.0
8.4	4.2	6.3	4.5	6.2	8.4	1.1	5.9	9.1	9.1	4.2	5.4
12.7	4.2	5.4	7.8	5.1	7.0	4.5	6.4	9.0	11.3	4.4	5.2
20.0	-0.1	2.0	10.9	4.9	6.0	9.0	4.7	6.0	16.6	2.5	3.3
24.0	-1.5	0.9	16.0	1.3	4.1	12.2	4.3	5.6	19.0	1.2	1.8
30.0	-0.9	0.3	20.0	-1.0	3.1	18.0	0.8	3.0	22.0	-0.7	0.8
35.0	-0.3	0.1	22.0	-1.6	2.8	24.0	-1.6	1.8	26.1	-1.2	1.1
40.0	-0.1	0	32.0	-0.3	0.2	30.0	-0.5	1.1	30.0	-0.7	0.6
			50.0	0	0	35.0	-0.1	0.1	35.0	0.3	0.1
						40.0	0	0	40.0	0	0

W = 2560 Pounds of TNT. $W^{1/3} = 13.68$.
$\lambda_c = 0.22$. Earth Over Charge = 1.0 Foot.
All Values in Feet. Minus Indicates Above Grade.

HE-6 was fired 75 feet N 23° W of the center of the explosion area.

Camera targets consisting of boards 8 feet square having alternating two feet squares were placed on lines through the center of the explosion area and at right angles to the line of camera sight as follows: 1,000 feet north, west and east; 1615 feet south.

Weather and crater data are given in Tables 2.22 and 2.23.

2.7 SHOT HE-7 (λ_c=0.19)

At 0700 PST on 4 October 1951, shot HE-7 was fired. A large column of dust was thrown more than 1,000 feet in the air. At 20 seconds after the detonation there was a feeble indication of a base surge in the throw-out area at the bottom of the column. The top of the plume started moving with the wind and at 3 minutes after zero time had drifted 5,000 feet with the wind. One hour after the shot the remains of the dust cloud were still visible five to six miles to the southwest.

Camera stations were placed 5,000 feet east and 5,000 feet south of the center point of the explosion area.

HE-7, 2560 pounds of TNT, was fired 150 feet west of the center of the explosion area.

Camera targets consisting of boards 8 feet square having alternating two feet squares were placed on lines through the center of the explosion area and at right angles to the line of camera sight as follows: 1,000 feet north, south, east and west.

Crater and weather data are given in Tables 2.24 and 2.25.

The base surge formation from shot HE-7 was so slight that it was not considered necessary to fire any additional shots to confirm the curve given in Figure 1.1.

2.8 SHOT HE-8 (λ_c=0.18)

At 0700 PST on 13 October 1951, shot HE-8 was fired. The TNT was an assembly of 216 pounds while the Pentolite weighed 177 pounds. (See Figures 3.1 and 3.2.) The Pentolite explosion was of high order, sending a slender column of smoke and dust high into the air and producing a magnificent smoke ring. A minor base surge was formed which, to observers, appeared similar to that produced by shot HE-6 with λ_c = 0.22. The priming was not adequate on the TNT portion of the test

TABLE 2.24

Crater Data, Shot HE-7

From South to North			From East to West			From S45° E to N45° W			From N45°E to S45°W		
Radial Distance	Apparent Depth	Real Depth	Radial Distance	Apparent Depth	Real Depth	Radial Distance	Apparent Depth	Real Depth	Radial Distance	Apparent Depth	Real Depth
50.0	0	0	45.0	-0.5	0	40.0	0	0	50.0	0	0
35.0	-0.1	0.3	35.0	-0.9	0	33.4	-0.6	0.3	40.0	-0.3	0
30.0	-1.0	0.6	33.6	-1.8	0	24.0	-1.8	1.7	26.6	-1.8	0
23.3	-2.2	0.8	30.5	-0.6	0	19.0	0	2.1	22.4	-1.1	0.6
18.0	0.2	2.8	23.6	-1.8	2.2	13.6	2.8	3.2	14.0	2.8	3.2
13.8	3.4	4.9	20.0	0	2.8	9.7	4.0	5.6	7.7	4.1	5.0
8.2	5.1	6.0	15.3	3.0	3.8	3.9	6.0	7.4	3.1	5.5	8.0
3.2	7.1	8.0	9.1	3.5	4.1	0	6.7	8.6	0	6.7	8.4
0	6.7	8.6	5.4	5.0	6.9	2.8	6.8	8.4	2.3	7.3	8.6
2.2	6.9	8.5	1.6	6.1	7.5	7.8	4.2	5.5	8.0	4.9	6.6
6.8	5.0	6.1	0	6.7	8.6	13.6	3.3	4.2	11.5	4.0	5.9
10.0	4.8	5.5	1.8	7.3	8.7	17.0	1.7	3.6	18.0	0	1.5
12.1	4.2	5.1	7.0	4.6	5.5	20.8	-1.1	2.4	20.0	-1.5	1.2
17.0	1.0	4.0	12.9	3.0	4.5	26.1	-0.7	0.3	23.1	-1.9	0.7
22.4	-1.5	2.4	18.0	0	2.6	28.8	-1.4	0.3	27.8	-0.9	0.2
29.0	-0.3	0.5	21.3	-1.5	2.0	31.2	-0.3	0.2	33.0	-0.2	0
36.0	0	0	26.6	-1.6	0.3	40.0	0	0	40.0	0	0
			34.2	-0.3	0						
			40.0	0	0						

W = 2560 Pounds of TNT. $W^{1/3}$ = 13.68.
λ_c = 0.19. Earth Over Charge = 0.5 Foot.
All Values in Feet. Minus Indicates Above Grade.

TABLE 2.25

Weather Data, Shot HE-7[a]

Altitude[b]	TIME - 0655		TIME - 0705	
	Wind[c] Direction	Wind[d] Velocity	Wind[c] Direction	Wind[d] Velocity
Surface	Calm	Calm	Calm	Calm
1170	010	13	020	13
2310	020	15	020	15
3450	020	15	020	15
4560	020	15	010	15
5670	020	11	020	8
6750	020	7	030	3
7830	340	6	300	5
8910	320	8	280	10
9960			270	16
11,010			270	24
12,030			280	28
13,020			280	31
14,010			280	42
15,000			280	50

[a]Temperature at Ground Level - 56° F. Relative Humidity - 46%.

TABLE 2.26

Weather Data, Shot HE-8[a*]

Altitude	TIME - 0655		TIME - 0705	
	Wind[c] Direction	Wind[d] Velocity	Wind[c] Direction	Wind[d] Velocity
Surface	140	3	080	6
720	020	7	010	7
1380	020	14	010	12
2040	030	15	020	12
2670	050	10	050	11
3300	050	10	040	11
3700	050	8	050	11

[a*]Temperature at Ground Level - 56° F. Relative Humidity - 51%.
[b]Expressed in feet above ground surface.
[c]360° = N, 90° = E.
[d]Expressed in miles per hour.

[redacted]

[redacted]

PROJECT 1(9)-3

TABLE 2.27

Crater Data, Shot HE-8 (Pentolite)

From North to South			From East to West		
Radial Distance	Apparent Depth	Real Depth	Radial Distance	Apparent Depth	Real Depth
24.0	0	0	23.0	0	0
15.5	-0.3	0.1	16.1	-0.1	0.1
13.0	-0.8	0.9	12.1	-0.3	0.1
11.2	-1.0	1.7	10.7	-0.9	1.7
8.4	0.6	2.2	8.5	0	2.7
5.1	2.3	3.4	5.5	1.9	3.7
4.0	2.6	3.8	4.1	2.7	3.8
1.6	3.3	3.6	3.1	2.8	3.5
0	3.3	4.3	1.6	3.2	3.7
2.0	3.1	4.3	0	3.2	4.3
3.0	2.8	4.0	1.8	3.4	4.5
6.3	0.9	3.0	4.0	2.6	4.2
8.5	0.1	3.3	5.3	2.3	4.2
10.9	-0.8	2.8	7.5	0.6	3.1
13.2	-0.1	0.3	9.3	-0.5	2.6
19.0	0	0	10.5	-0.7	2.2
			14.7	-0.3	0.6
			22.8	0	0

[redacted]

and explosion of roughly one half of the charge resulted. Weather data will be found in Table 2.26. The TNT crater was not measured but data on the Pentolite crater will be found in Table 2.27.

For shot HE-8, the center point of the area was moved 1,000 feet south of the center of the area used for shots HE-5, 6, and 7.

Shot HE-8 (TNT) was fired 100 feet east of the center of the explosion area and shot HE-8 (Pentolite) was fired 100 feet west of the center of the explosion area.

One camera station was placed 4,000 feet south of the center point of the area. The camera targets (same type as used for HE-5, 6 and 7) were located on an east-west line at right angles to the line of camera sight as follows: 500 feet east, center, and 500 feet west.

2.9 SHOT HE-9 (λ_c=0.14)

At 0705 PST on 14 October 1951, shot HE-9 was fired. Both Pentolite and TNT produced high order explosions. The above ground activity appeared similar for both explosions. A considerable throw-out was noted which produced a cloud around the base of the plume. The cloud had some expansion and a careful examination of the photographic records will be required to determine if there was any base surge contribution, (Refer to JANGLE Report 1(9) - 4, "Base Surge Analysis for HE Tests".) It is certain that a large plume remained above the base activity. Crater and weather data are given in Table 2.28, 2.29 and 2.30.

Shot HE-9 was fired in the same explosion area used for HE-8.

Shot HE-9 (TNT) was fired 200 feet east of the center of the explosion area and shot HE-9 (Pentolite) was fired 200 feet west of the center of the explosion area.

One camera station was placed 4,000 feet south of the center point of the area.

The camera targets (same type as used for HE-5 through HE-8) were located on an east - west line at right angles to the line of camera sight as follows: 500 feet east, center, and 500 feet west.

2.10 SHOT HE-10 (λ_c=0.5)

At 1130 PST on 14 October 1951, shot HE-10 was fired. Both the Pentolite and TNT produced high order explosions. A massive base surge was produced by each explosion. The TNT produced what was virtually 100 per cent base surge just as it was in shot HE-3. Some

[redacted]

PROJECT 1(9)-3

TABLE 2.28

Crater Data, Shot HE-9 (Pentolite)

From North to South			From East to West		
Radial Distance	Apparent Depth	Real Depth	Radial Distance	Apparent Depth	Real Depth
18.4	0	0	18.6	0	0
12.9	-0.4	0.7	12.4	-0.4	0.7
10.5	-0.8	2.5	10.2	-0.9	2.6
9.9	-0.6	2.8	8.0	0.5	2.7
7.5	0.8	3.2	3.9	2.3	3.5
4.8	1.5	3.5	1.0	3.5	4.4
2.4	2.7	4.1	0	3.4	4.0
0	3.4	4.0	1.4	3.3	3.9
1.8	3.1	3.9	4.0	2.0	3.2
5.9	1.4	3.6	6.4	1.2	3.1
7.1	1.0	2.4	10.7	-1.2	1.8
10.2	-0.8	2.9	11.8	0	1.0
11.3	-0.5	2.5	16.0	0	0
13.0	-0.2	0.3			
20.5	0	0			

[redacted]

[redacted]

TABLE 2.29

Crater Data, Shot HE-9 (TNT)

From North to South			From East to West		
Radial Distance	Apparent Depth	Real Depth	Radial Distance	Apparent Depth	Real Depth
17.5	0	0	18.0	0	0
12.9	-0.7	0	13.0	-0.3	0.5
10.3	-0.5	2.5	10.5	-0.7	2.5
7.9	0.1	2.1	9.7	-0.6	2.6
6.2	1.0	3.0	6.0	1.1	3.2
4.5	1.5	4.0	1.5	3.3	4.5
3.4	2.4	3.7	0	4.0	3.5
2.1	2.6	3.7	1.5	4.0	3.5
0.9	3.5	4.1	3.6	2.5	3.0
0	3.5	4.0	4.9	2.1	3.4
1.8	3.0	4.0	8.1	0.2	2.3
4.7	1.9	3.0	10.4	-0.7	1.5
6.1	1.7	2.7	13.9	-0.2	0.5
10.4	-0.6	1.9	22.0	0	0
12.7	-0.1	0.7			
19.8	0	0			

[redacted]

PROJECT 1(9)-3

TABLE 2.30

Weather Data, Shot HE-9[a]

Altitude[b]	TIME - 0700		TIME - 0710	
	Wind[c] Direction	Wind[d] Velocity	Wind[c] Direction	Wind[d] Velocity
Surface	320	7	300	5
720	020	7	030	6
1380	040	9	050	9
2040	060	9	060	9
2670	080	8	080	7
3300	090	6	100	6
3900	090	6	100	5
4500	090	4	100	4
5100			120	4

[a] Temperature at Ground Level - 48° F.
Relative Humidity at Ground Level - 62%.

TABLE 2.31

Weather Data, Shot HE-10[a*]

Altitude[b]	TIME - 1128		TIME - 1133	
	Wind[c] Direction	Wind[d] Velocity	Wind[c] Direction	Wind[d] Velocity
Surface	090	3	100	3
720	150	4	170	5
1380	170	5	180	5
2040	180	6	180	6
2670	170	5	170	6
3300	150	7	160	8
3900	150	8	160	10
4500	160	6	160	8
5100	160	6	170	7

[a*] Temperature at Ground Level - 68° F.
Relative Humidity at Ground Level - 55%.
[b] Expressed in feet above ground surface.
[c] 360° = N, 90° = E.
[d] Expressed in miles per hour.

[redacted]

[redacted]

PROJECT 1(9)-3

TABLE 2.32

Crater Data, Shot HE-10 (Pentolite)

From North to South			From East to West		
Radial Distance	Apparent Depth	Real Depth	Radial Distance	Apparent Depth	Real Depth
22.0	0	0	23.2	0	0
16.2	-0.2	0.7	16.0	-0.4	0.1
13.2	-1.0	1.9	13.5	-1.0	0.5
12.1	-1.0	2.5	11.6	-0.7	1.5
9.7	0.2	2.7	8.1	2.0	2.8
8.6	1.7	2.9	4.4	3.5	4.1
6.3	2.6	3.8	2.3	3.7	4.7
5.6	3.4	4.3	1.7	4.1	4.8
3.9	3.9	5.0	0	4.1	5.4
2.1	5.0	5.2	1.5	4.5	5.3
1.1	3.5	5.4	4.4	3.4	4.6
0	4.1	5.5	5.4	3.1	4.2
0.9	4.3	4.9	6.3	3.0	3.6
2.8	3.5	4.6	8.4	1.8	2.7
5.2	3.4	4.3	9.8	0.3	2.8
10.2	-0.5	2.8	12.5	-0.9	2.0
11.7	-0.7	2.2	14.9	-0.4	0.1
15.2	-0.3	0.3	21.3	0	0
21.3	0	0			

[redacted]

[redacted]

PROJECT 1(9)-3

TABLE 2.33

Crater Data, Shot HE-10 (TNT)

From North to South			From East to West		
Radial Distance	Apparent Depth	Real Depth	Radial Distance	Apparent Depth	Real Depth
22.0	0	0	21.2	0	0
16.2	-0.2	0.3	19.0	-0.5	0.2
12.9	-0.8	3.0	16.9	-0.5	1.9
12.0	-0.7	3.0	13.0	-0.5	2.5
6.6	2.6	4.1	6.8	2.9	3.5
2.5	4.7	5.9	5.6	3.0	4.9
0	5.5	6.3	1.8	5.0	5.6
1.7	5.1	6.1	0	5.5	6.3
7.2	3.3	3.6	1.4	4.9	6.4
11.6	0.5	3.5	6.1	2.7	3.5
12.8	-0.8	2.6	10.5	0.7	2.9
17.2	-0.1	0.2	12.1	-0.8	2.4
26.5	0	0	13.3	-1.2	1.8
			16.8	-0.5	0.3
			24.0	0	0

[redacted] [redacted]

minor plume remained in the air above the Pentolite base surge. The contribution to the surge was estimated by observers to be greater than that produced on HE-5 with λ_c=0.3. Weather and crater data are given in Tables 2.31, 2.32 and 2.33.

Shot HE-10 was fired in the same explosion area used for shots HE-8 and 9.

Shot HE-10 (TNT) was fired 450 feet east of the center of the explosion area. Shot HE-10 (Pentolite) was fired 450 feet west of the center of the explosion area.

One camera station was placed 4,000 feet south of the center of the area.

The camera targets (same type as used for HE-5 through HE-9) were located on an east - west line at right angles to the line of camera sight as follows: 500 feet east, center, and 500 feet west.

[redacted]

PROJECT 1(9)-3

SECTION 3

RESULTS

3.1 RELATIVE GROUND ACTIVITY PRODUCED BY TNT AND PENTOLITE

One is inclined toward a tentative conclusion that there is little difference in the above ground activity produced by TNT and by Pentolite, which occupied 76 per cent of the TNT volume (V_{TNT} = 3823 in^3 and V_P = 2936 in^3), when both explosives were fired with the center of gravity at the same depth.

3.2 EFFECTS OF SIZE OF CHARGE

Since the nuclear explosion will present virtually a point source when compared to the equivalent energy of a 34 foot diameter ball of TNT, an investigation of the effect of size was conducted. Three simultaneous explosions of 216 pounds of TNT and the equivalent energy in 177 pounds of Pentolite were conducted as shown in Table 3.1.

TABLE 3.1

Relative Energy of Pentolite and TNT

Shot	Depth to c.g. (inches)	λ_c	Earth Cover Over Charge (inches)	
			TNT	Pentolite
HE-8	13	0.18	3	4-1/8
HE-9	10	0.14	0	1-1/8
HE-10	36	0.5	26	27-1/8

The TNT charge was built up with 1, 5, 20 and 100 pound blocks as shown in Figure 3.1. The vertical dimension of the charge was 20 inches. The Pentolite charge was made up of two hemispheres having diameters of 17 and 3/4 inches as shown in Figure 3.2

3.3 OBSERVING AND RECORDING DATA

All information on the above ground action is based on eye witness observations and is subject to modifications based on careful analysis of the photographic data. Some comparative photographs of base surge formation are shown in Figures 3.3 through 3.12. The Sandia Corpora-

[redacted] [redacted]

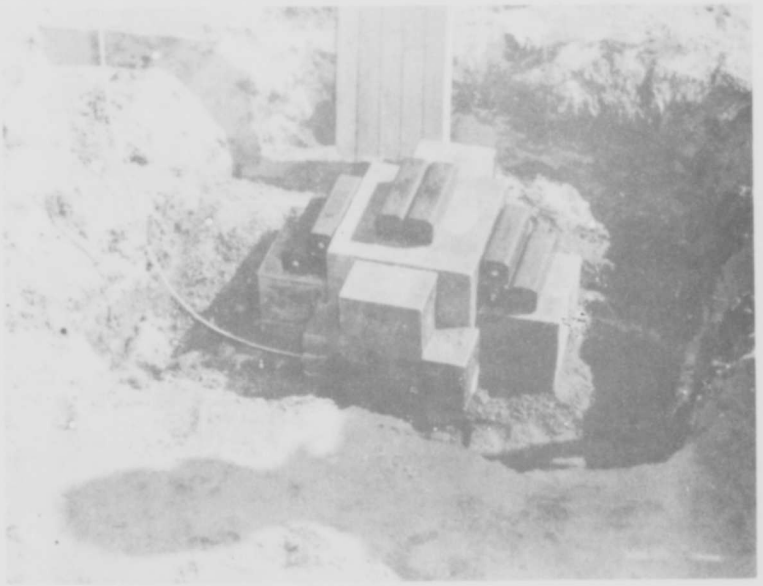

Fig. 3.1 216 Pound TNT Assembly

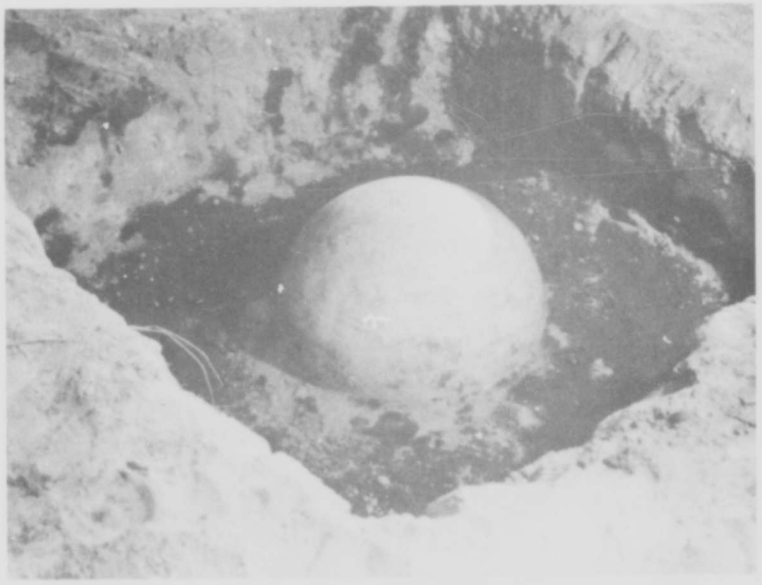

Fig. 3.2 177 Pound Pentolite Sphere

Fig. 3.3 HE-3. Time between zero and 1 second. 2560 Pounds of TNT with $\lambda_c = 0.5$.

Fig. 3.4 HE-2. Time between zero and 1 second. 40,000 Pounds of TNT with $\lambda_c = 0.135$.

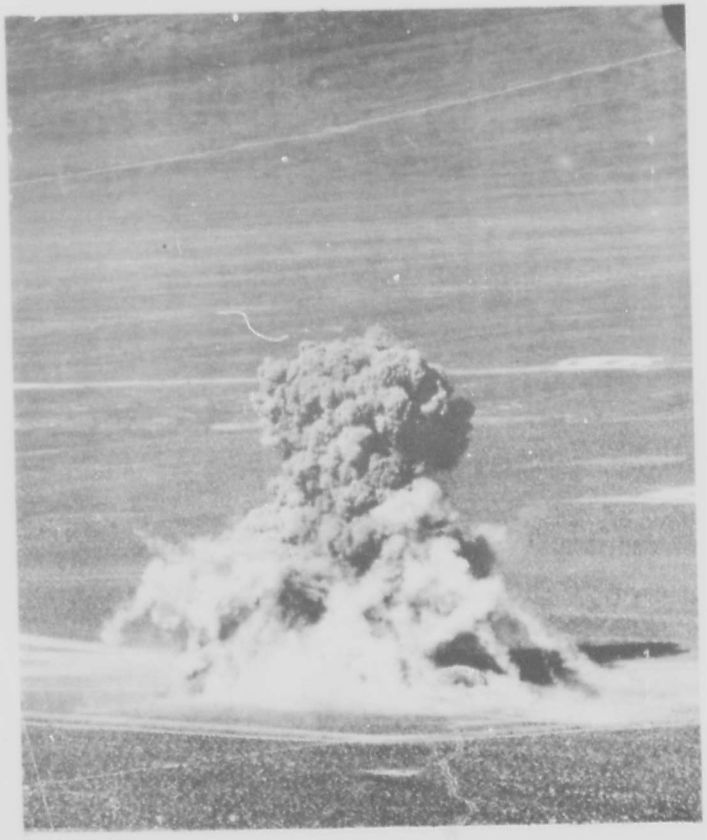

Fig. 3.5 HE-3. Time plus 10 seconds.

Fig. 3.6 HE-2. Time plus 10 seconds.

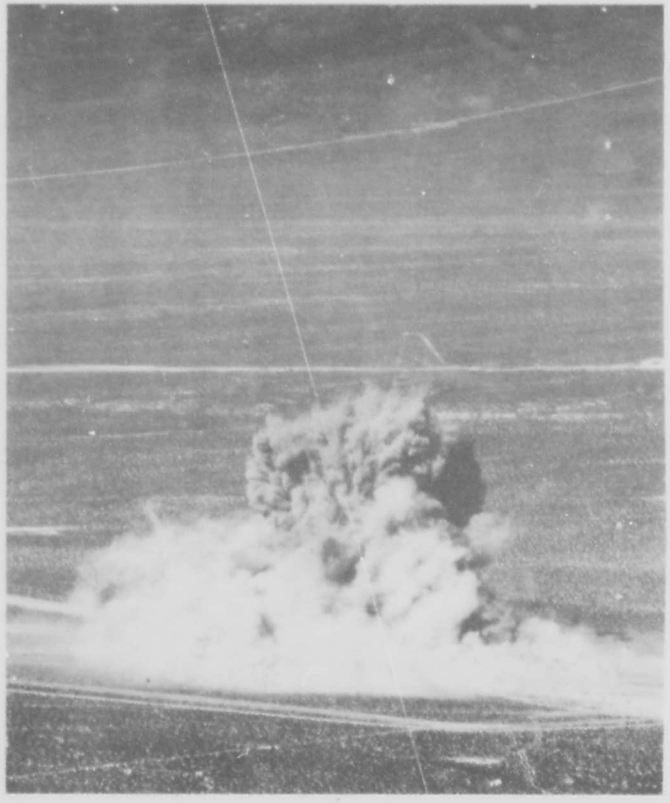

Fig. 3.7 HE-3. Time plus 20 seconds. Base surge in initial phases.

Fig. 3.8 HE-2. Time plus 20 seconds. Roughly one-half of the volume is shown.

Fig. 3.9 HE-3. Time plus 30 seconds. Plume falling into base surge.

Fig. 3.10 HE-2. Time plus 30 seconds. Plume still rising.

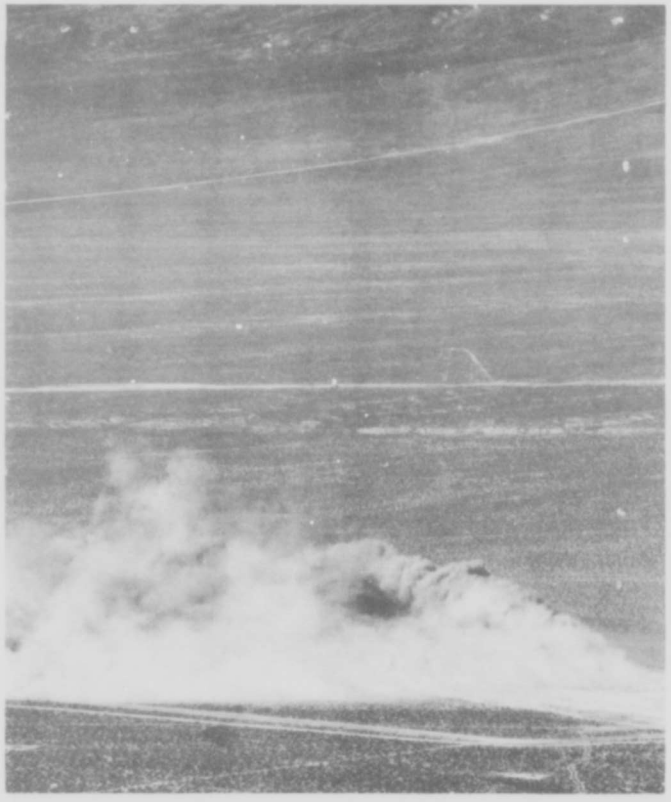

Fig. 3.11
HE-3. Time plus 40 seconds. 100 per cent base surge formation moving with wind toward left side of picture.

Fig. 3.12
HE-2. Time plus 40 seconds. Roughly one-half of the plume is shown. Plume is still rising. Little, if no, base surge was formed. Some throwout is still visible.

tion, through Program Four, has been requested to make measurements[1] from the 35mm motion pictures of the various HE shots as follows:

a. Rate of rise of plume. Rate of descent into base surge.
b. Diameter of plume, at several elevations, as a function of time.
c. Time and location of first appearance of base surge.
d. Radial travel of base surge as a function of time.
e. Height of base surge as a function of time and distance.
f. From aerial pictures of Shot HE-3, determine shape and volume of base surge as a function of time.

3.4 BEHAVIOR OF BASE SURGE AND CRATER SIZE PHENOMENA

Lacking the photographic analysis, it is possible only to make some rough estimations as to the mechanism producing the base surge and what can be predicted to occur during the nuclear tests. It is certain that some minimum density of soil is required in the plume in order to produce the downward sweep of dust which, at ground level, moves outward as the base surge. The density is produced by blowing a large volume of earth a relatively short distance up into the air. The closer the charge to the surface (smaller values of λc), the smaller the crater and greater the height of plume, hence, lower density and less base surge contribution. Average crater contours are given in Figures 3.13 through 3.17 and are summarized in Tables 3.1 and 3.2. It is known from the work of Dr. Curtis Lampson and others that a large number of tests are required to obtain data that is good to within 35 per cent, therefore, only generalities can be obtained from this crater data.

Crater radii may be calculated from the following equation:

$$R = 1.3\ C\ E\ k^{1/12} \qquad (3.3\text{-}1)^2$$

Where

R = the radius in feet
C = 0.4 (for $\lambda c = 0.135$)[3]
k = 11,000 (for a seismic velocity of 4,000 feet per second)

A comparison of calculated and observed values of radii is given in Table 3.2 and is plotted in Figures 3.18 and 3.19. It will be noted that there is some difference between the values of the crater radius as calculated, extrapolated from observed data, and that previously predicted in the WINDSTORM Handbook. A plot of crater depth and lip height is given in Figure 3.20.

---

[1] This analysis is reported in Project 1(9)-4
[2] The Effects of Atomic Weapons, Washington, GPO, June 1950, App. B, p. 421.
[3] Ibid., Figure B29, p. 421.

TABLE 3.2

Comparative Crater Data

2560 Pounds of TNT ($W^{1/3} = 13.68$)								
Depth to c.g. (inches)	Cover Over Charge (inches)	λc	Crater Volume (Ft^3)			Crater Depth (Feet)		Apparent Crater Radius (Feet) d
			Apparent a	Real	Fall Back b	Real c	Apparent c	
24	0	0.15	2200	4100	3200	6.8	7.6	18.4
30	6	0.19	3300	6180	5400	6.7	8.6	19.0
36	12	0.22	3600	8800	7200	6.1	10.1	19.8
48	24	0.30	4000	8700	7000	7.5	9.5	19.4
81.6	57.6	0.50	6000	7600	3000	10.8	11.0	19.8

216 Pounds of TNT and 177 Pounds of Pentolite[e]									
Depth (inches)			λc	Crater Volume (Ft^3)			Crater Depth (Feet)		Apparent Crater Radius (Feet) d
Charge	c.g.	Top of Charge		Apparent a	Real	Fall Back b	Real c	Apparent c	
P	10	1-1/8	0.14	290	1310	1020	4.0	3.4	8.6
TNT	10	0	0.14	270	1120	980	4.0	3.5	8.3
P	13	4-1/8	0.18	380	1310	1130	4.3	3.3	8.7
P	36	27-1/8	0.5	520	1460	1330	5.5	4.1	9.6
TNT	36	26	0.5	860	2600	1370	6.3	5.5	11.3

a = Volume below original ground level.
b = Difference between real and apparent crater volume plus lip volume.
c = Depth from original ground level.
d = Radius at original ground level.
e = $W^{1/3} = 6$

TABLE 3.3

Observed and Calculated Crater Radii

W	$W^{1/3}$	Radius in Feet	
		Calculated	Observed
216	6	6.8	6.3
2560	13.7	15.5	18.5
40000	34.2	38.5	38.5
1 KT	126	150	——

$\lambda_c = 0.135$

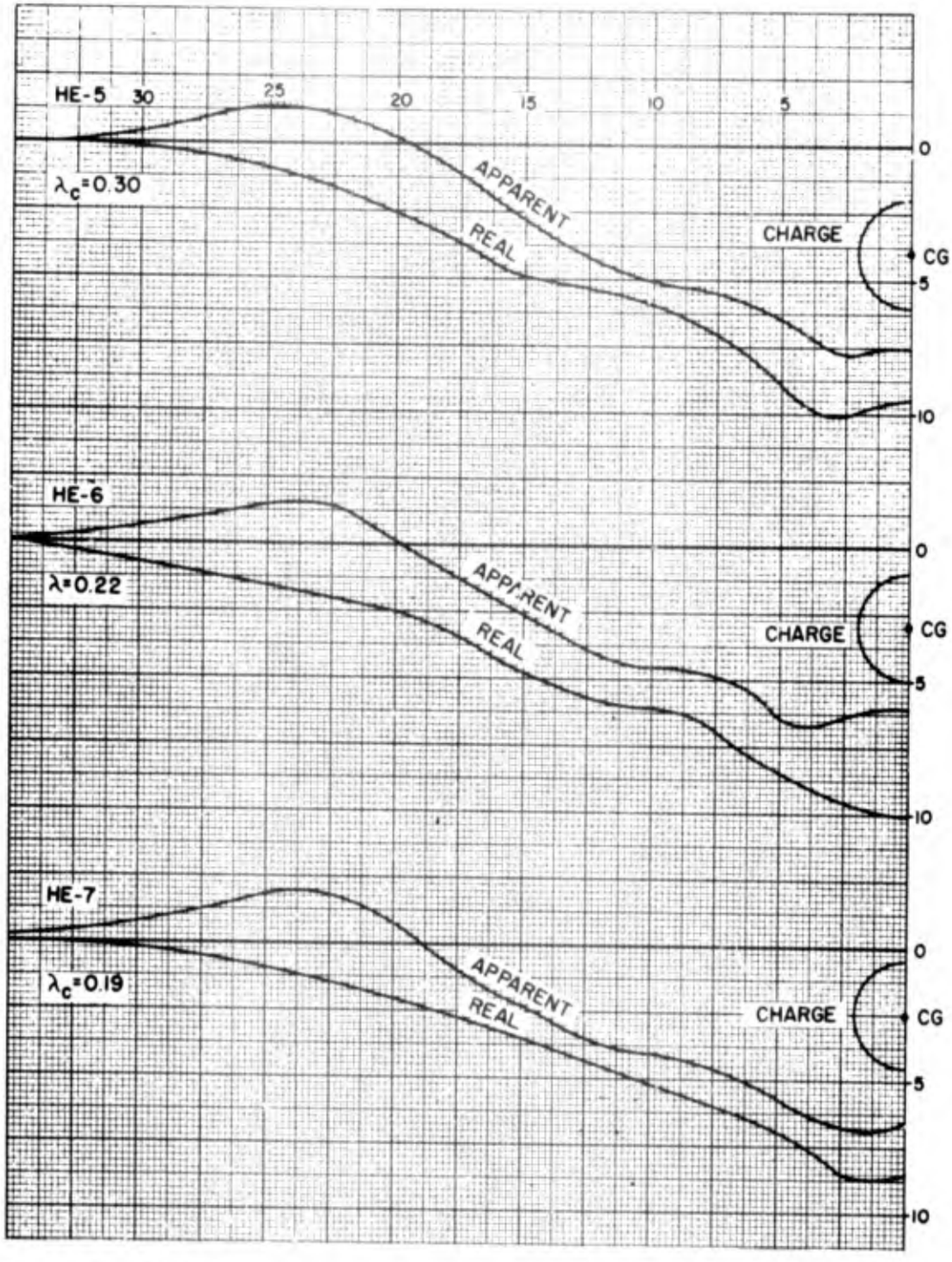

Fig. 3.13 Average Crater Contours for 2560 Pounds of TNT in Shots HE-5, HE-6, and HE-7

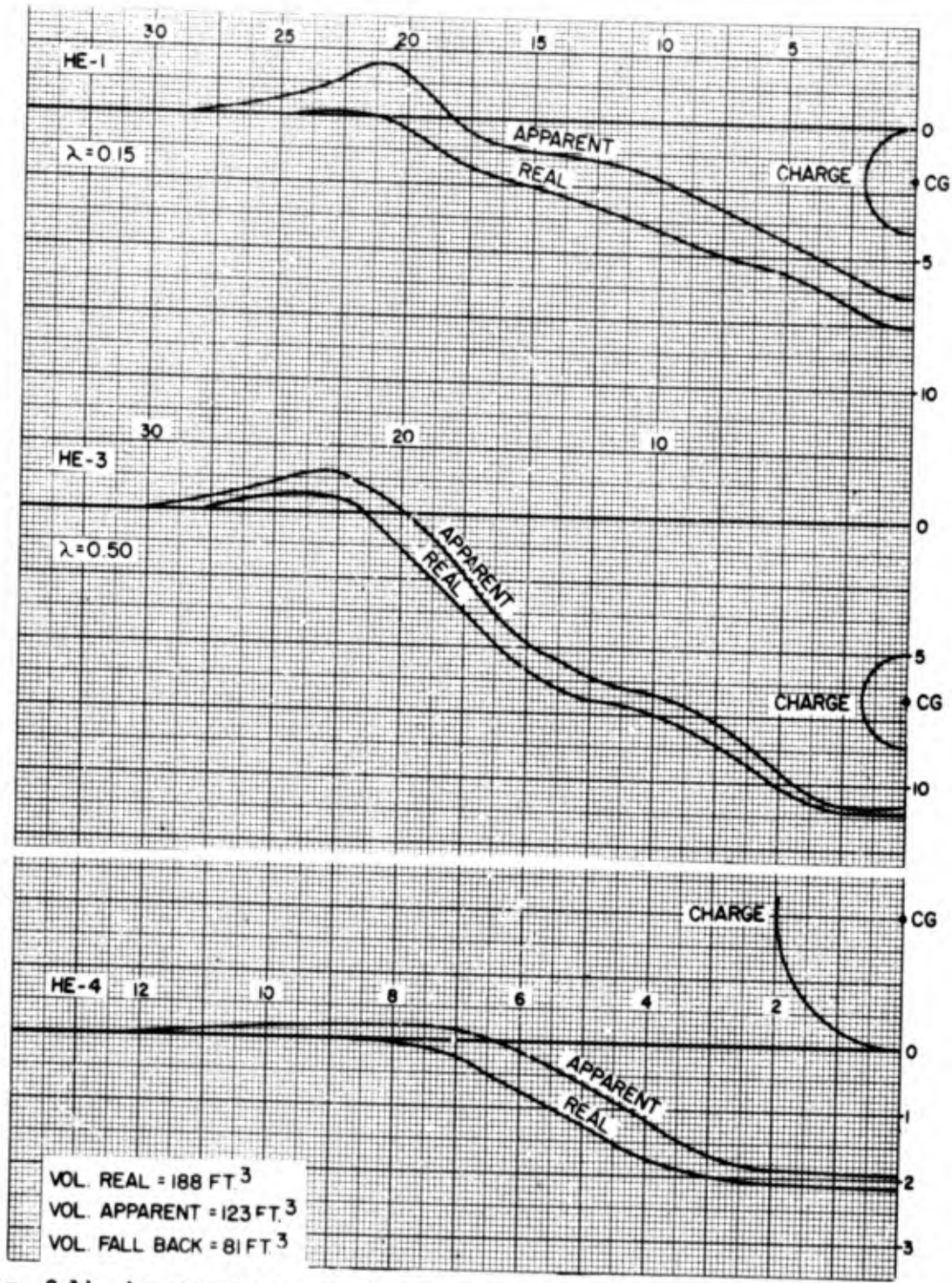

Fig. 3.14 Average Crater Contours for 2560 Pounds of TNT in Shots HE-1, HE-3 and HE-4

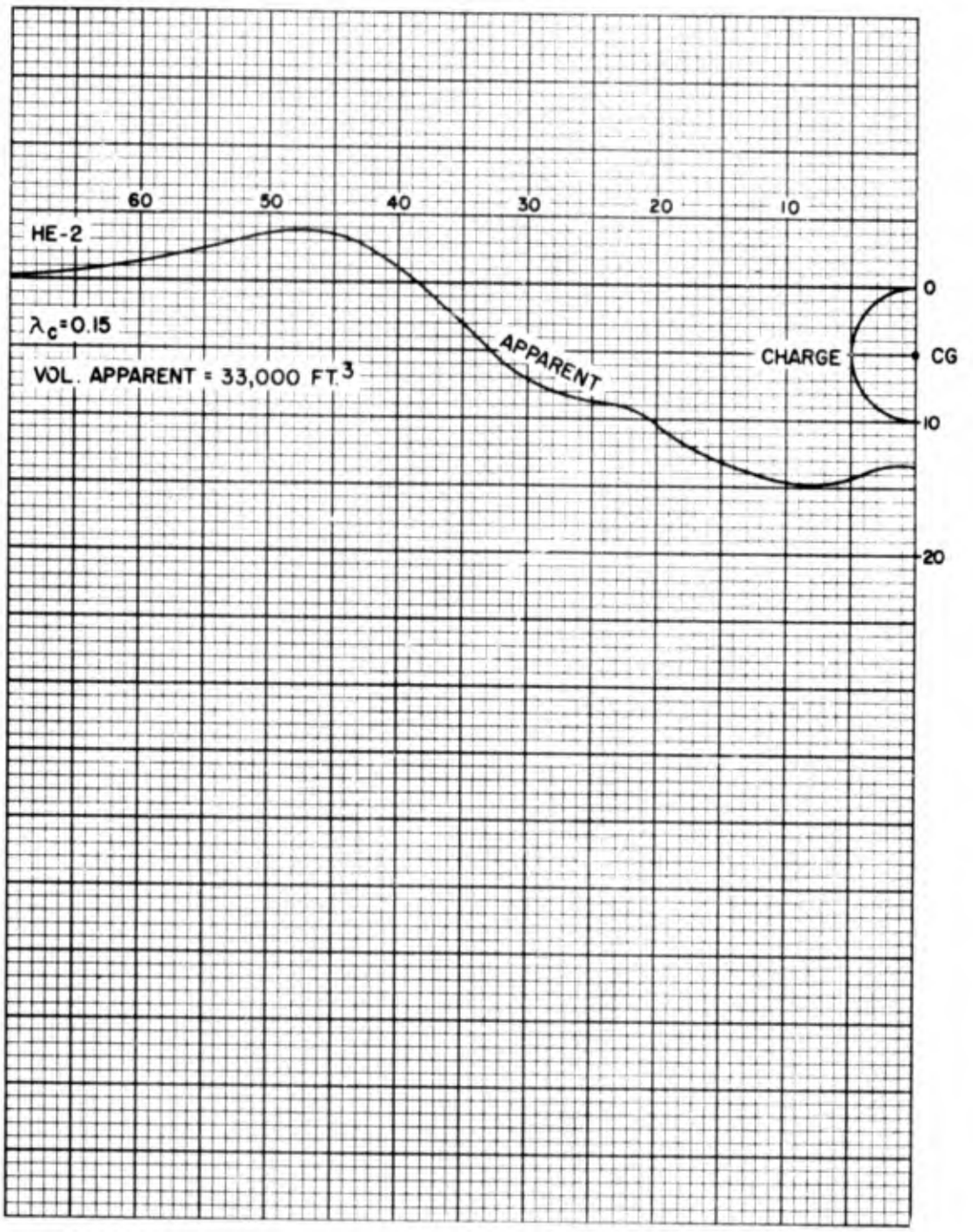

Fig. 3.15 Average Crater Contours for 40,000 Pounds of TNT in Shot HE-2

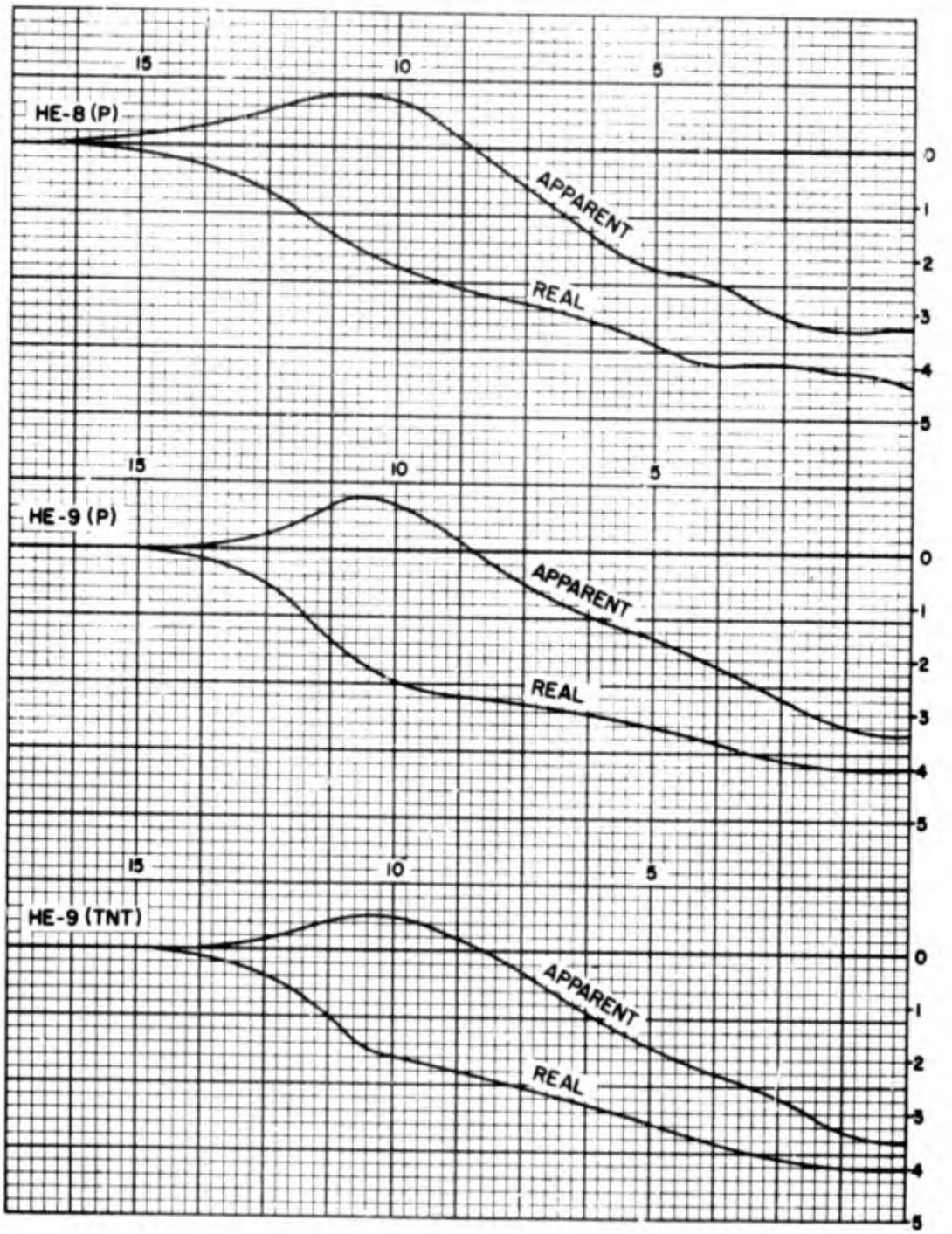

Fig. 3.16 Average Crater Contours for 21.6 Pounds of TNT and 177 Pounds of Pentolite in Shots HE-8 (P), HE-9 (P) and HE-9 (TNT)

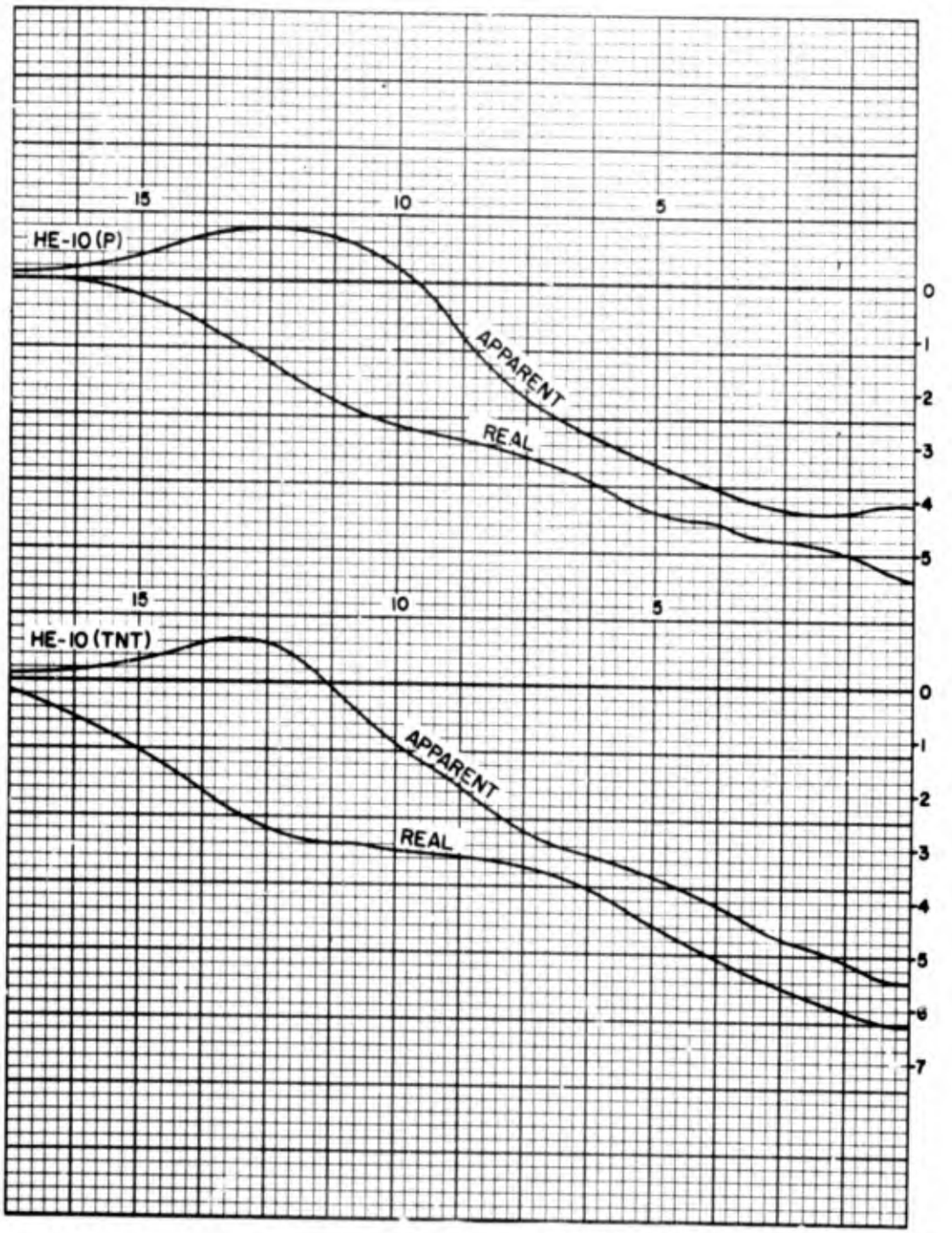

Fig. 3.17 Average Crater Contours for 216 Pounds of TNT and 177 Pounds of Pentolite in Shots HE-10 (P) and HE-10 (TNT)

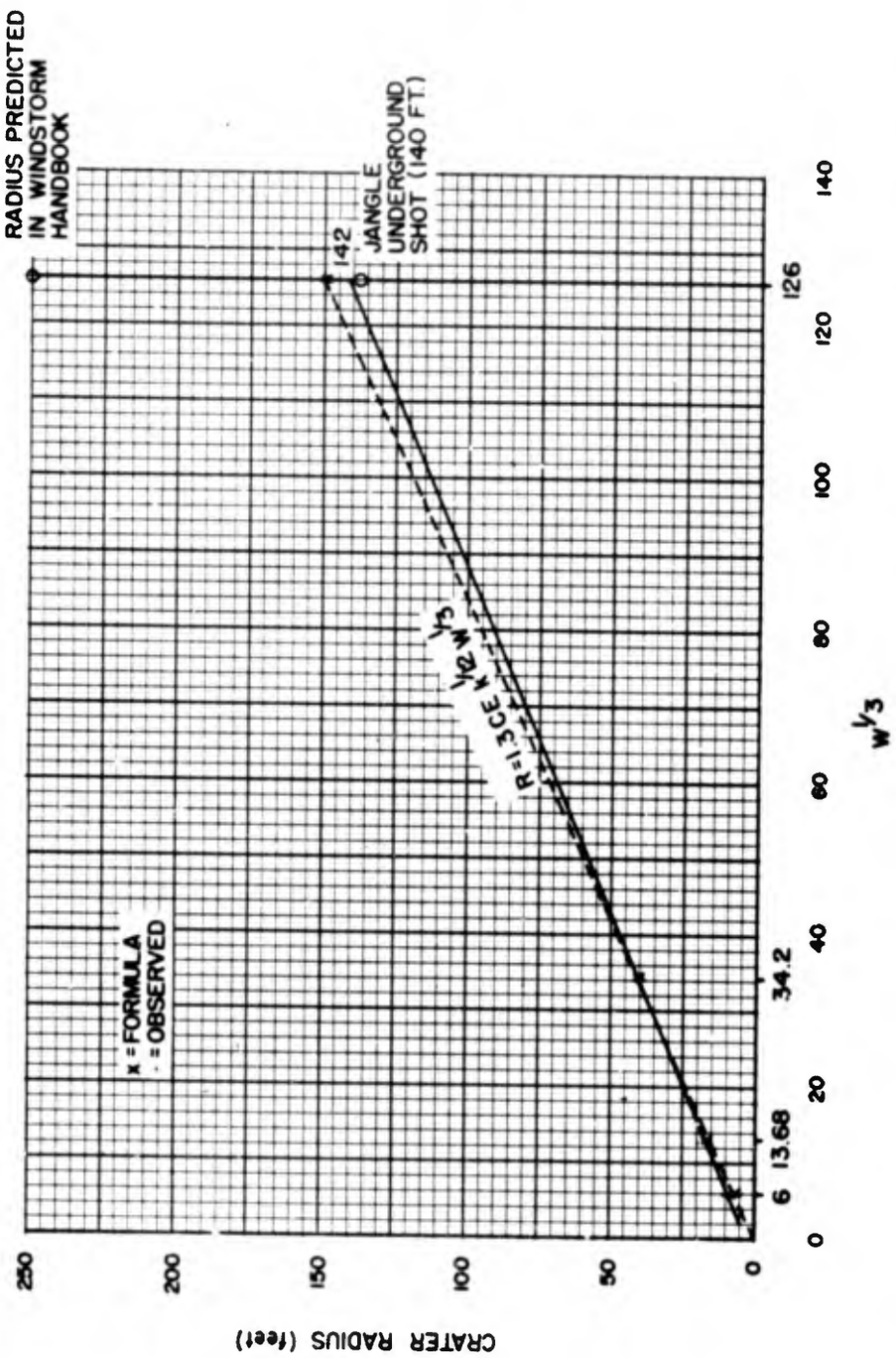

Fig. 3.18 Calculated and Observed Values of Crater Radius for Charge CG Underground

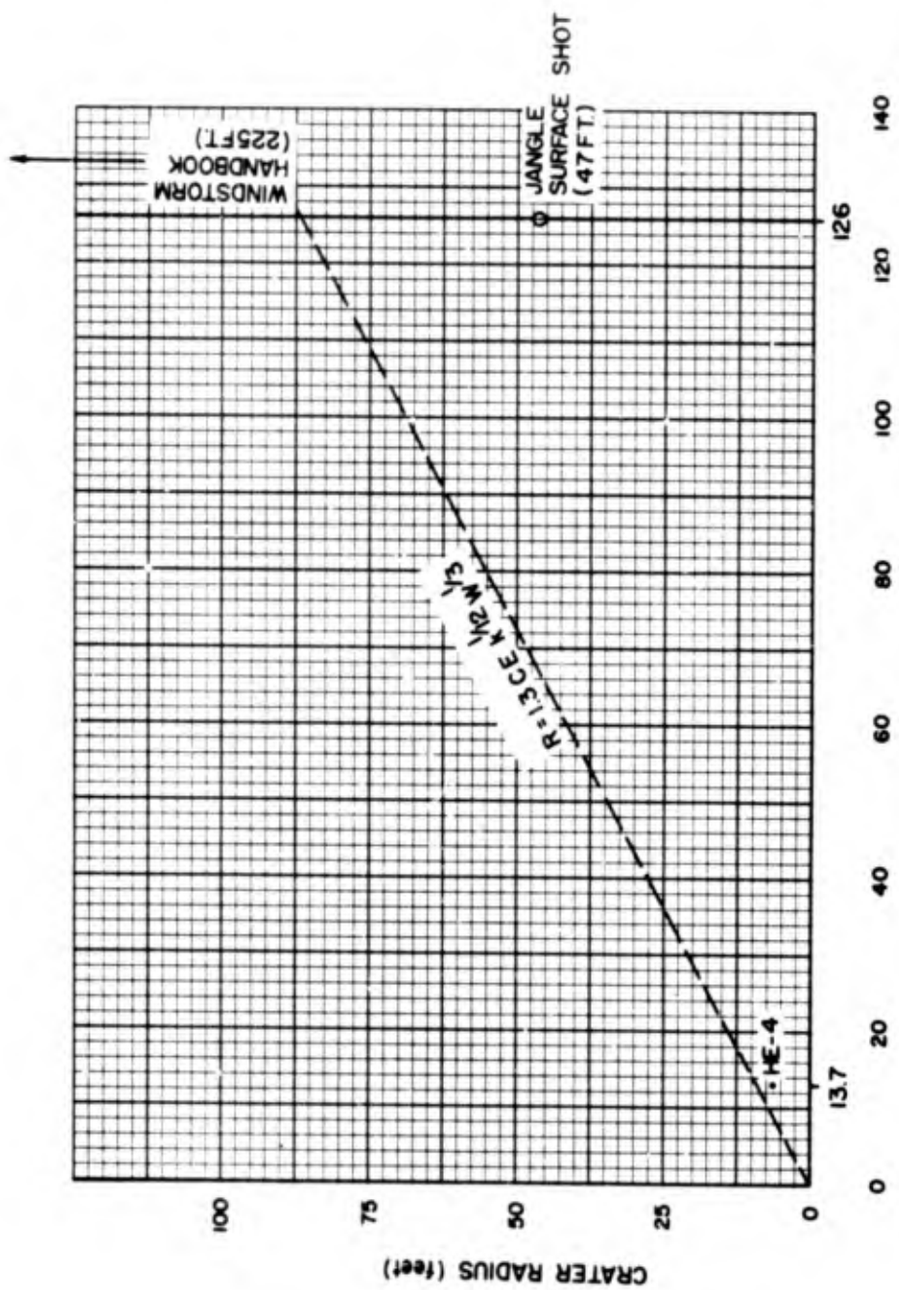

Fig. 3.19 Calculated and Observed Values of Crater Radius for Charge CG at Surface

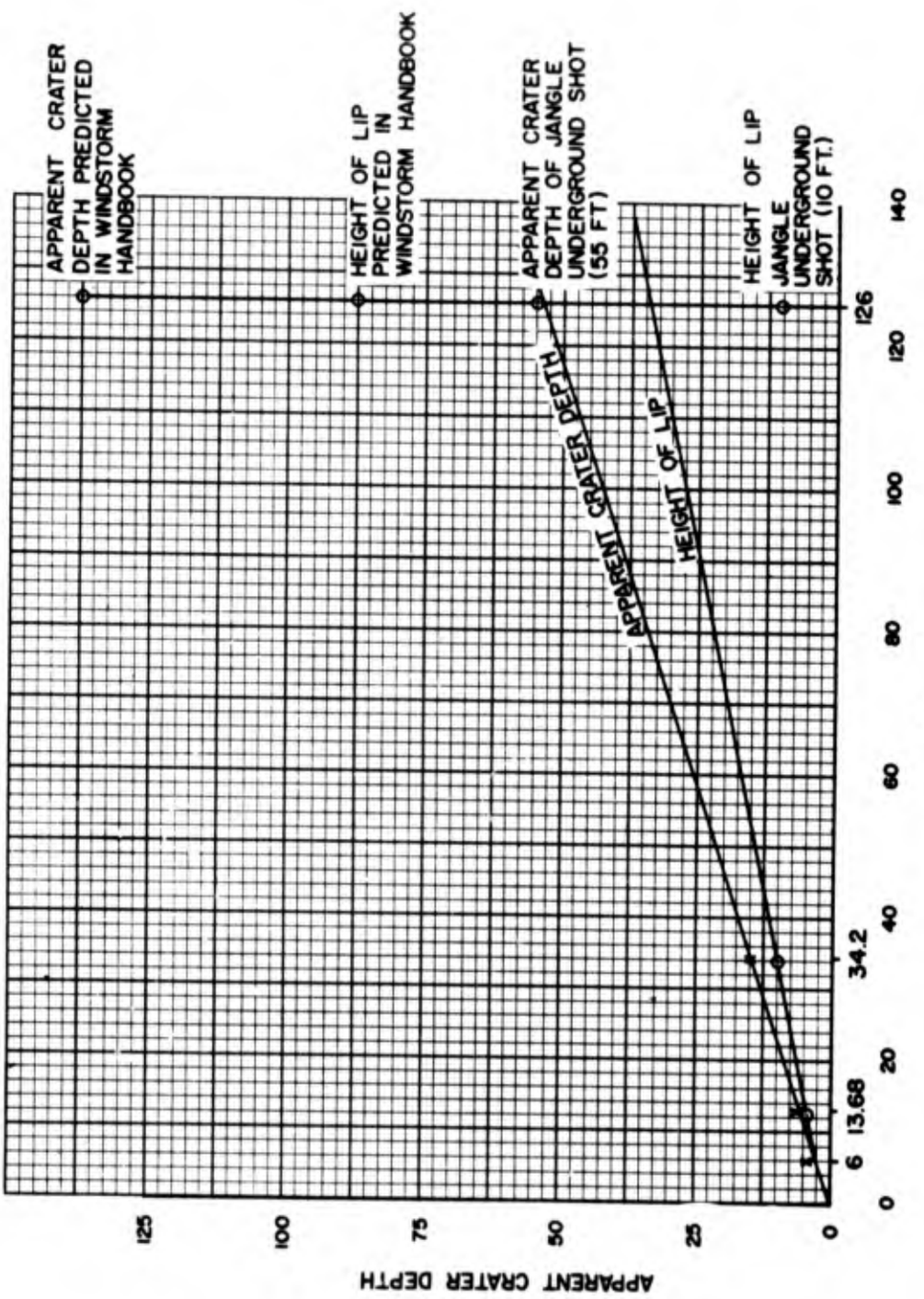

Fig. 3.20 Crater Depth and Height of Lip for Charge CG Underground

[redacted]

PROJECT 1(9)-3

SECTION 4

CONCLUSIONS AND RECOMMENDATIONS

4.1 GENERAL

From the information presented herein, the interested reader can form his own opinion as to what can be anticipated from the nuclear tests. The phenomenology is so complex that limited tests, based primarily on eye witness observations, cannot lead to any clear cut set of conclusions. However, the following guesses are the best that the writer can make.

4.2 SURFACE NUCLEAR SHOT

a. A base surge appears very unlikely.
b. There will be a good sized cloud produced at ground level by the passage of the air blast wave which may be mistaken for a base surge.
c.

Crater Radius	80-90 feet
Crater Depth	25-30 feet
Crater Area	25,000 feet^2
Crater Volume	25,000 cubic yards
Lip Radius	170 feet
Lip Height	7 feet
Maximum Altitude of Cloud	12,000 feet

4.3 UNDERGROUND NUCLEAR SHOT

a. There will be a considerable throw-out at the base of the plume which may be mistaken for a base surge.
b. The probability of a base surge appears very small. If a base surge forms the magnitude will be small.
c. A ground level dirt cloud will be produced by the air blast wave but will probably not cause as much interference with photography as that which occurred at GREENHOUSE.
d.

Crater Radius	140-150
Crater Depth	50-60 feet
Crater Area	60,000 feet^2
Crater Volume	60,000 cubic yards
Lip Radius	375 feet
Lip Height	14 feet
Maximum Altitude of Cloud	6,000 feet

e. Since it is an observed fact that the crater diameter is a

[redacted] [redacted]

readily scaled parameter for underground TNT explosions, then the immediate observation (photographic or otherwise) of the underground crater diameter may be a simple and reliable method for determining equivalent TNT mechanical yield of the nuclear weapon.

4.4 RECOMMENDATIONS

Of course, if predictions were always right there would be no need for experimental programs and field tests. The writer is inclined to believe that the firing of one underground and one surface atomic weapon will not give sufficient information on which to make reliable predictions for either offensive or defensive planning. A large number of well planned HE tests, all required to lead into a smaller number of nuclear tests, are necessary in order to produce reliable results.

Fig. 4.1 Crater from Shot HE-4. On a small scale, this is probably an indication of the crater on the Surface Shot.

Fig. 4.2 Crater from Shot HE-2. The Underground Shot will probably be very similar with the diameter increased 3 1/3 times.

[redacted]

OPERATION JANGLE

PROJECT 1(9)-4

BASE SURGE ANALYSIS - HE TESTS

by

GEORGE A. YOUNG

20 MAY 1952

U. S. NAVAL ORDNANCE LABORATORY WHITE OAK, MARYLAND

[redacted]

[redacted]

PROJECT 1(9)-4

PREFACE

The purpose of this report is to present a compilation and analysis of data concerning the behavior of the base surge and related surface phenomena produced by underground explosions in the Dugway Tests in Soils and the Operation JANGLE HE Tests. These two sets of data were combined in order to provide a wide range of charge weight and charge depth and to determine some of the effects of soil properties on surface phenomena.

The formulas and conclusions presented herein were obtained almost entirely from records of TNT charges weighing from 320 to 320,000 lb fired at scaled depths ranging from zero to 3.07 $ft/lb^{1/3}$ in dry clay, dry sand, and wet clay. Extension of the results beyond this range of variables may not be justified.

ACKNOWLEDGMENTS

The author wishes to acknowledge the cooperation of Mr. H. B. Zackrison of the Protective Construction Branch, Office of the Chief of Engineers, in forwarding prints of the dust cloud photographs and pertinent data for the 1951 Dugway Tests in Soils. Sincere thanks are due to Dr. E. Swift, Jr. for useful comments and suggestions during the program of investigation and the preparation of this report. Mrs. M. L. Milligan's thorough and careful analysis of the material and her valuable comments on the results were extremely helpful in the writing of this report. Mrs. M. M. Lyttle's conscientious preparation of the manuscript is gratefully acknowledged.

[redacted]

[redacted]

PROJECT 1(9)-4

CONTENTS

[redacted]

ILLUSTRATIONS

CHAPTER 2 SURFACE PHENOMENA

CHAPTER 3 BASE SURGE

TABLES

[redacted]

PROJECT 1(9)-4

ABSTRACT

Base surge and related surface phenomena were measured on photographic records of the 1951 Underground Explosion Tests in Soils at Dugway, Utah and the Operation JANGLE HE Tests. Data concerning groundrise, smoke crown, column, jet, and base surge behavior are presented.

A base surge is produced by TNT explosions at scaled depths (λ_c) ranging from zero to 3.07 ft/lb$^{1/3}$, the greatest depth in these programs, but is small and tenuous at scaled depths less than 0.2 ft/lb$^{1/3}$. The surge has the highest velocity and greatest extent at a λ_c of about 1.0 ft/lb$^{1/3}$.

Base surges were formed in the three Dugway soil types; explosions in dry sand produced the largest, wet clay the smallest surges. Explosions in dry clay were intermediate in effectiveness. Thus, it appears that soils with low seismic velocities have the physical characteristics best suited for the formation of a base surge.

Froude scaling is adequate for reducing the surge radial growth data at scaled depths from about 0.2 to 2.0 ft/lb$^{1/3}$. At a λ_c of 0.508 ft/lb$^{1/3}$, comparison with liquid model results indicates a 1.9 ratio of column density to atmospheric density. Similarities between the base surges formed by underwater and underground explosions are noted.

Areas of dust deposit and crater dimensions also indicate that a scaled depth of 1.0 ft/lb$^{1/3}$ is near the optimum for base surge formation.

TNT and Pentolite charges with different volumes but equivalent energy formed similar base surges in a small-scale test.

[redacted]

[redacted]

CHAPTER 1

ANALYSIS OF DATA

1.1 SOURCES OF DATA

The data presented in this report were obtained from photographic records of the Underground Explosion Tests in Soils at the Dugway Proving Ground, Utah[1] in 1951 and the series of underground high explosive tests conducted in Nevada in 1951 as part of Operation JANGLE.[2]

Motion picture records of the Dugway Dry Clay Tests were obtained for the Naval Ordnance Laboratory by Charles H. Bradley, Jr. Timing marks (100 per second) were placed on the margin of 35 mm film by an electronic timer, and a length scale was established from markers placed a known distance apart at the location of the charge or by the use of the lens focal length and the distance from the camera to the explosion. Measurements were made from continuous prints of the 35 mm film, enlarged 5 times. A 16 mm kodachrome record without timing was obtained.

Prints of the dust cloud photographs of the Dry Clay, Dry Sand, and Wet Clay Tests at Dugway were provided by the Protective Construction Branch of the Office of the Chief of Engineers, Washington, D. C. This photographic work was carried out by the Institute of Industrial Research of the University of Denver, by subcontract to Engineering Research Associates, Inc.[3] The dust cloud was photographed with still cameras from two positions with an initial angle of 90° between the respective camera lines-of-sight. A clock reading in minutes and seconds was included in the field of view of each camera and the movement of the dust cloud was followed by the operators. Measurements were made from the prints, using the focal length of the camera lens and the distance from the camera to the charge to establish a scale factor.

---

[1] Underground Explosion Tests, Program "A" - Tests in Soils, Protective Construction Branch, Engineering Division, Office, Chief of Engineers, Nov. 1950, pp 1-9.

[2] D. C. Campbell, LCDR, USN, Tests and Observations on Craters and Base Surges, JANGLE Report 1(9)-3, 1 Nov. 1951.

[3] Instrumentation for Underground Explosion Test Program, Interim Technical Report No. 1, Dry Clay, Engineering Research Associates, Inc., Contract No. DA-04-167-eng-298, 1 Aug. 1951, pp 5-2 to 5-4.

[redacted]

Ground photography of the Nevada HE tests was conducted by the Sandia Corporation with motion picture and still cameras from as many as five camera stations. Timing records were made, and targets in the field of view were used to establish length scales. Photographic analysis was performed by the Sandia Corporation and data sheets and films were forwarded to NOL for additional study and measurement. Aerial photographs of shots HE-2 and HE-3 in the Nevada series were provided by Major Victor Bloecker of the Office of the Director, Effects Tests.

The rounds for which data are available for this report are summarized in Tables 1.1 and 1.2. For comparison of charges of different weights, a scaled depth of burial, λ_c, is used:

$$\lambda_c = \frac{d}{W^{1/3}} \qquad (1.1)$$

where d = depth to center of charge, ft
W = weight of charge, lb (TNT)

It should be noted that the Dugway Tests include shots with λ_c ranging from zero to 3.07 ft/lb$^{1/3}$, while the Nevada work was confined to the relatively shallow depths ranging between λ_c values of -0.149 and 0.500 ft/lb$^{1/3}$.

The TNT charges fired at Utah and Nevada consisted of cast blocks of various sizes, stacked to approximate spheres in shape. The pentolite charges used at Nevada were spherical. The vertical dimensions are important for the scaling of depth and are listed in Table 1.3.

1.2 MEASUREMENT OF RECORDS

Wherever possible, measurements were made of overall height of the dust cloud, column height and diameter, and base surge height and radius as functions of time. This was done by the Sandia Corporation for the Nevada high explosive tests and by NOL for the Dugway tests. The Sandia analyses were checked for consistency with NOL methods of measurement.

On the longer Dugway records a scale correction for cloud motion toward or away from the camera was computed by using the mean low-level wind velocity for the period during which photographs were obtained.

The initial surface breakthrough of explosion gases from an underground charge is extremely rapid, and high-speed photography is required for its analysis, but the subsequent formation and expansion of the dirt column can usually be resolved with a camera speed of 24 frames per second. Since the base surge does not appear until a few seconds after detonation,

TABLE 1.1

Underground Explosion Tests in Soils
Dugway, Utah, 1951

Round	Date	Soil Type	Charge Weight W (lb TNT)	Charge Depth d (ft)	Scaled Depth λ_c ($ft/lb^{1/3}$)	Records Used	
						NOL Motion Picture	E.R.A. Still Prints
302	3/29	Dry Clay	320	0	0	x	x
303	4/2	Dry Clay	320	1.3	0.190	x	x
304	4/4	Dry Clay	320	3.5	0.512	x	x
305	4/6	Dry Clay	320	7.0	1.02	x	x
306	4/12	Dry Clay	320	14.0	2.05	x	x
307	4/10	Dry Clay	320	21.0	3.07	x	x
308	4/16	Dry Clay	2560	2.6	0.190	x	x
309	4/18	Dry Clay	2560	7.0	0.512		x
310	4/23	Dry Clay	320	3.5	0.512		x
312	5/4	Dry Clay	2560	7.0	0.512		x
315	5/10	Dry Clay	40,000	17.5	0.512	x	x
318	5/22	Dry Clay	320,000	35.0	0.512	x	x
102	6/7	Dry Sand	320	0	0		x
103	6/7	Dry Sand	320	1.3	0.190		x
105	6/19	Dry Sand	320	7.0	1.02		x
106	6/27	Dry Sand	320	14.0	2.05		x
108	7/10	Dry Sand	2560	2.6	0.190		x
110	8/13	Dry Sand	320	3.5	0.512		x
112	7/27	Dry Sand	2560	7.0	0.512		x
115	8/8	Dry Sand	40,000	17.5	0.512		x
402	8/23	Wet Clay	320	2.5	0.366		x
403	8/11	Wet Clay	2560	5.0	0.366		x
404	8/21	Wet Clay	320	2.5	0.366		x

[redacted]

PROJECT 1(9)-4

TABLE 1.2

Underground Explosion Tests in Nevada
Operation JANGLE, 1951

Round	Date	Charge Weight W (lb)	Charge Depth d (ft)	Scaled Depth λ_c ($ft/lb^{1/3}$)	Charge Composition
HE-1	8/25	2,560	2.01	0.147	TNT
HE-2	9/3	40,000	4.63	0.135	TNT
HE-3	9/15	2,560	6.79	0.496	TNT
HE-4	9/9	2,560	-2.04	-0.149	TNT
HE-5	9/30	2,560	4.04	0.295	TNT
HE-6	10/2	2,560	3.04	0.222	TNT
HE-7	10/4	2,560	2.54	0.185	TNT
HE-8a	10/13	216	1.08	0.181	TNT
HE-8b	10/13	177	1.08	*0.181	Pentolite
HE-9a	10/14	216	0.83	0.139	TNT
HE-9b	10/14	177	0.83	*0.139	Pentolite
HE-10a	10/14	216	3.00	0.500	TNT
HE-10b	10/14	177	3.00	*0.500	Pentolite

* The 177 lb Pentolite charge is assumed to have the energy equivalent of 216 lb of TNT.

TABLE 1.3

Vertical Dimensions of Charges

Charge Weight (lb)	Charge Composition	Charge Height (inches)
177	Pentolite	17.75
216	TNT	20.0
320	TNT	24.5
2,560	TNT	49.0
40,000	TNT	117.0
320,000	TNT	234.0

[redacted]

its growth can be measured satisfactorily with a slower rate of exposure.

The NOL cameras at Dugway were operated at 24 frames per second and provided excellent coverage of the column and surge formation but the records did not always extend for a sufficient period to cover the complete cycle of growth and dissipation of the surge cloud.

The ERA dust cloud photographs of the Dugway tests were taken at varying intervals of time, though seldom less than 5 seconds apart. This proved inadequate for studying the formation of columns but permitted the tracking of the surge clouds for a long period, particularly after their growth had become relatively slow. In some cases, hills, trucks, or large trees obstructed the view of the surge cloud and made accurate measurement impossible.

The Sandia cameras were operated at different speeds, but the combination of a 24 frame per second 35 mm motion picture camera and an F-56 aerial camera making one exposure per second provided the most satisfactory coverage for record analysis. Greater camera speeds for base surge studies usually proved wasteful of film.

In general, the manual operation of equipment and the following of the dust cloud by the photographer proved superior to the use of remotely-controlled cameras.

Many times at Dugway and Nevada the passage of the shock wave in air raised a layer of surface dust which obscured much of the formation and development of the base surge. With shallow charges this dust layer was sometimes high enough to obscure the initial formation of the entire surge cloud. In these arid regions, cameras at elevated positions provide better records than those operated at ground level. The aerial photographs made in Nevada showed the surge growth more clearly than any surface camera when surface dust obscuration occurred, and in some cases provided measurements that would have been unobtainable from ground level cameras. Aerial photography is probably the best method of tracking a moving surge cloud and also shows some of the changes taking place in the interior of the column and surge. However, ground markings should be provided to establish a distance scale.

1.3 SCATTER OF DATA

Experience in studying the effects of underwater explosions has shown that considerable scatter must be expected in the measurements of surface phenomena. It is usually necessary to fire a large number of charges and treat all results statistically in order to obtain consistent relationships between the important variables. For example: the records of a series of 18 one hundred pound charges fired on a river bottom at a 30

inch depth show coefficients of variation of 10.8% for maximum column diameter, 30.3% for maximum surge radius, and 21.6% for maximum surge height.[4] Sufficient data are not available to determine in like manner the degree of dispersion of the data from underground explosions, but charges fired under seemingly identical conditions have produced dissimilar results.

Some of the factors responsible for the scatter of data points are the following:

1.3.1 Non-homogeneity of Soil

The soil surrounding a buried charge is almost never homogeneous. Layers of different types of soil and gravel and variations of moisture content with depth all affect the total result. Excavating and filling operations probably affect the density and moisture content of the soil close to the charge. Day-to-day variations in moisture content will also occur during rainy periods. This variation in soil properties is probably responsible in part for the lack of symmetry of the dust clouds produced by most of the explosions studied. In many cases radial throwout and base surge development is pronounced on one side of the charge and relatively minor on the other. Unless camera coverage is extensive or aerial photography is available the true shape of the surge cloud is difficult to determine.

1.3.2 Turbulence

The base surge flow is never smooth in appearance. The cloud is in a continual turbulent state, with tongues of material flowing outward at speeds greater than the main cloud mass. Both horizontal and vertical turbulent motion are present and the surge is quite irregular in shape. The erratic motion decreases with time until the dynamic flow has ceased, and measurements of the flow often require considerable smoothing. As the base surge loses its momentum, turbulent atmospheric motion becomes increasingly important and the surge cloud is gradually diluted by the surrounding air. This reduces the sharpness of the outer boundary of the cloud and it becomes tenuous and difficult to see. Objective measurement of the details of the various parts of the jet, column, and base surge become impossible when this diffuse condition is reached.

---

[4] A. B. Arons, G. A. Young and M. L. Milligan, Further Investigation of the Base Surge, Interim Report No. 3 of NOL Project 152, NAVORD Report 2144, 1 June 1951, pp 15-18.

1.3.3 Accuracy of Measurements

Although every effort is made to obtain accurate time and length scales for the photographic records, minor differences in lens focal lengths, faulty or incomplete timing, and possible errors in measurement of distances may reduce the accuracy of measurements of surface phenomena and contribute to the scatter of the resulting data. In some cases the distance between the cameras and charge is too great for precise measurement of the surface phenomena. The changes in scale due to movement of the entire dust cloud are difficult to estimate because of the generally irregular variation of wind speed and direction. On the shallow charge records, careful study is required to separate the dust produced by the radial throwout and the passage of the shock wave from the true surge cloud.

1.4 ANALOGY WITH UNDERWATER EFFECTS

The appearance of the surface phenomena produced by underground explosions is similar to the visible surface effects of underwater explosions and the physical processes of formation are probably somewhat analogous. In this report, the same nomenclature is used for the phenomena produced in soils that was previously applied to the surface phenomena from underwater charges,[5] in order to facilitate comparison of results and to make use of the same scaling procedures in studying the base surge flow.

---

[5] J. S. Coles and G. A. Young, Investigations of Base Surge Phenomena by Means of High Explosives and a Liquid Model, Interim Report No. 2 of NOL Project 152, NAVORD Report 1744, 1 Sept. 1950.

[redacted]

CHAPTER 2

SURFACE PHENOMENA

2.1 DESCRIPTION AT SCALED DEPTH OF 0.5 FT/LB$^{1/3}$

The appearance and structure of the surface phenomena produced by high explosive charges fired underground are markedly dependent upon charge depth and the character of the soil. As an introduction, it will be useful to describe briefly the sequence of events above the ground level at an intermediate scaled depth (λ_c = 0.5 ft/lb$^{1/3}$ in dry clay) at which all of the important features are relatively large and clearly defined. The 320,000 lb "full scale" charge at Dugway was fired at this scaled depth.

The first visible surface effect is the bulging of the earth above the charge into a smooth dome-shaped mound. Explosion gases start to vent through the upper surface of the elevated ground and the entire earth mound appears to explode into a roughly spherical cloud of smoke and dust, which expands rapidly. The diameter of the earth dome continues to increase, and the ground is lifted to form a cylindrical column, which becomes visible beneath the rising smoke cloud. These features are shown in Figure 2.1, which was obtained from the photographic records of Round HE-3 at Nevada.

The rounded top of a central jet appears at the center of the expanding smoke cloud and rushes upward at a high velocity, pushing the initially spherical cloud upward and outward into a smoke crown. The jet of explosion gases appears to be rising through the center of the earth column, and contributing to its outward radial expansion. The column then settles and the surge appears at its base while the jet continues to rise and expand. Initially the surge cloud is almost white in appearance and is irregular and turbulent. The smoke crown and jet then fall and flow outward along the ground to contribute additional material to the surge cloud, though, if light winds prevail, some of the upper dust and smoke will remain airborne. Figure 2.2 illustrates this development for Round 304 at Dugway.

The base surge continues to grow in height and diameter, maintaining the shape of a torus, or doughnut, with a shallow central dust layer. The surge cloud moves downwind, its bulk density decreasing due to expansion and mixing with the surrounding air. It gradually rises from the ground and is dispersed by atmospheric turbulence, as shown in the aerial photographs of Round HE-3 in Fig. 2.3.

[redacted]

3.50 MILLISEC

5.33 MILLISEC

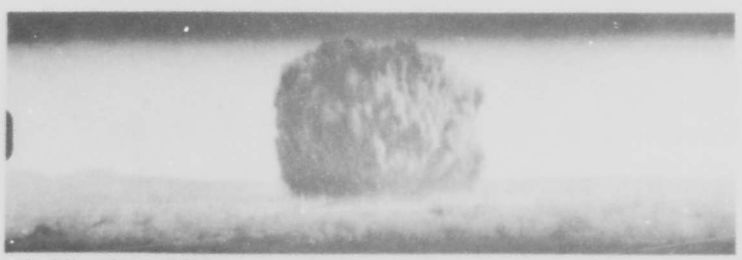

12.33 MILLISEC

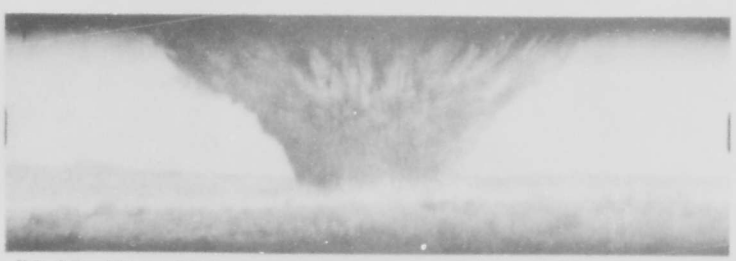

58.33 MILLISEC

CHARGE WEIGHT = 2560 LB SCALED DEPTH = 0.496 FT/LB$^{1/3}$

CHARGE DEPTH = 6.79 FT

Fig. 2.1 Rise of Ground and Formation of Smoke Crown and Column
Round HE-3

Fig. 2.2 Formation of Jet and Base Surge - Round 304

PROJECT 1(9)-4

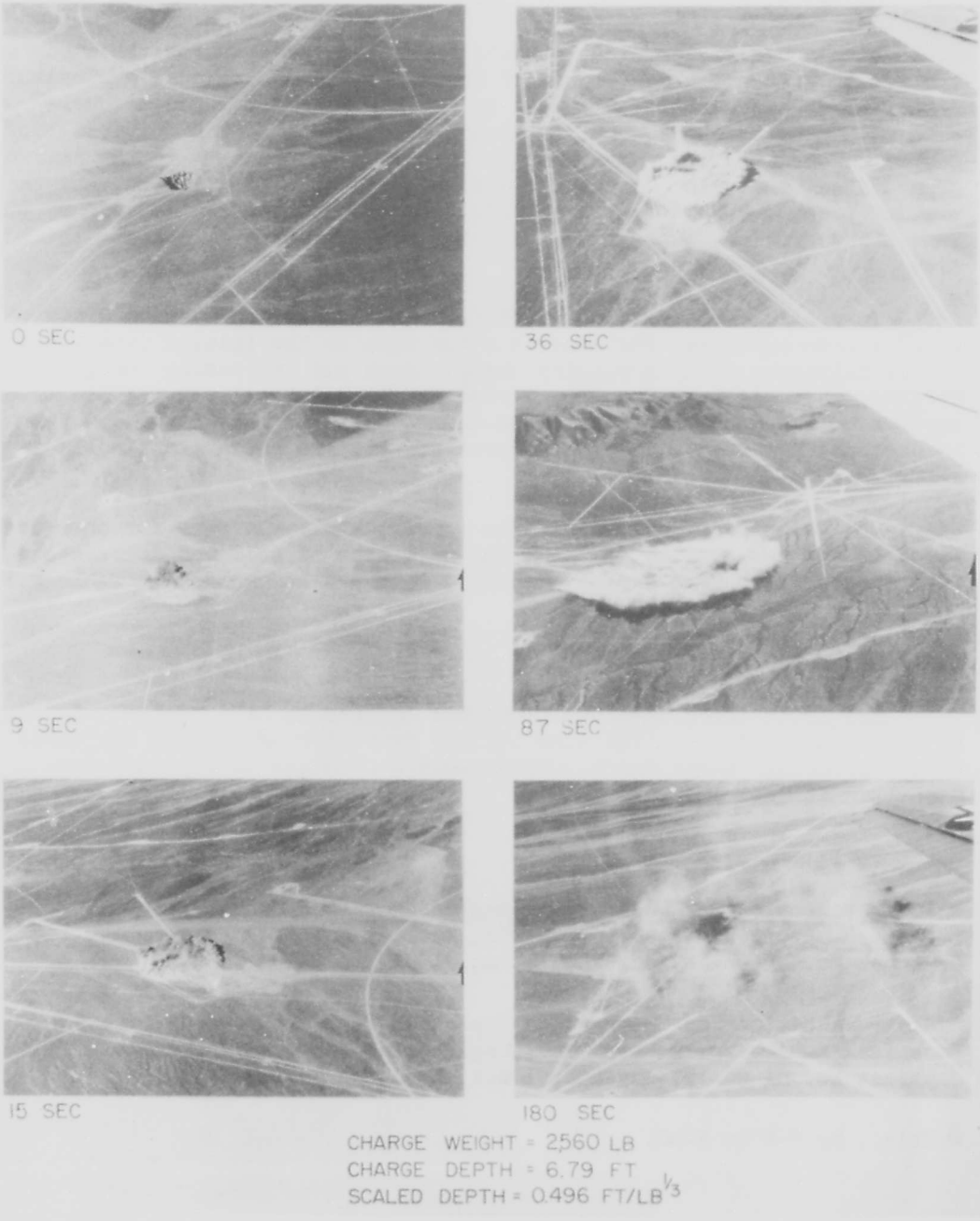

Fig. 2.3 Aerial Photographs - Round HE-3

2.2 GROUND-RISE

High-speed motion picture photography is necessary for the study of the ground rise and breakthrough of gases from an underground explosion. Fastax cameras, operated at speeds up to 1540 frames per second, were used at Dugway by the Industrial Research Institute of the University of Denver. When possible, measurements were made of the time to the initial ground rise, the velocity and maximum height of the ground rise, and the time of breakthrough. Fastax records were also obtained at Nevada by the Sandia Corporation, but similar measurements are not available at this time.

In general, the data obtained from the Dugway dry clay[1] and dry sand[2] photographic records show that the time to the initial rise of the ground increases with increasing charge depth and increasing charge weight. The height of the ground rise at which initial venting occurs appears to increase with increasing charge depth to a maximum, and then to decrease for deeper charges. These results are shown graphically in Figure 2.4.

The velocity of ground-rise is approximately the same for charges fired at the same scaled depth in the same type of soil and decreases with increasing charge depth. Velocity data are summarized in Table 2.1.

2.3 SMOKE CROWN

The smoke crown develops from what appears to be a partial venting of explosion products. The time to this initial breakthrough increases with increasing charge depth. Measurements obtained in dry sand are presented in Table 2.2.[3]

---

[1] Instrumentation for Underground Explosion Test Program, Interim Technical Report No. 1, Dry Clay, Engineering Research Associates, Inc., Contract No. DA-04-167-eng-298, 1 Aug. 1951, pp 5-1 to 5-11.

[2] Instrumentation for Underground Explosion Test Program, Interim Technical Report No. 2, Dry Sand, Engineering Research Associates, Inc., Contract No. DA-04-167-eng-298, 1 Oct. 1951, pp 5-1 to 5-16.

[3] Ibid., pp 5-4 to 5-10.

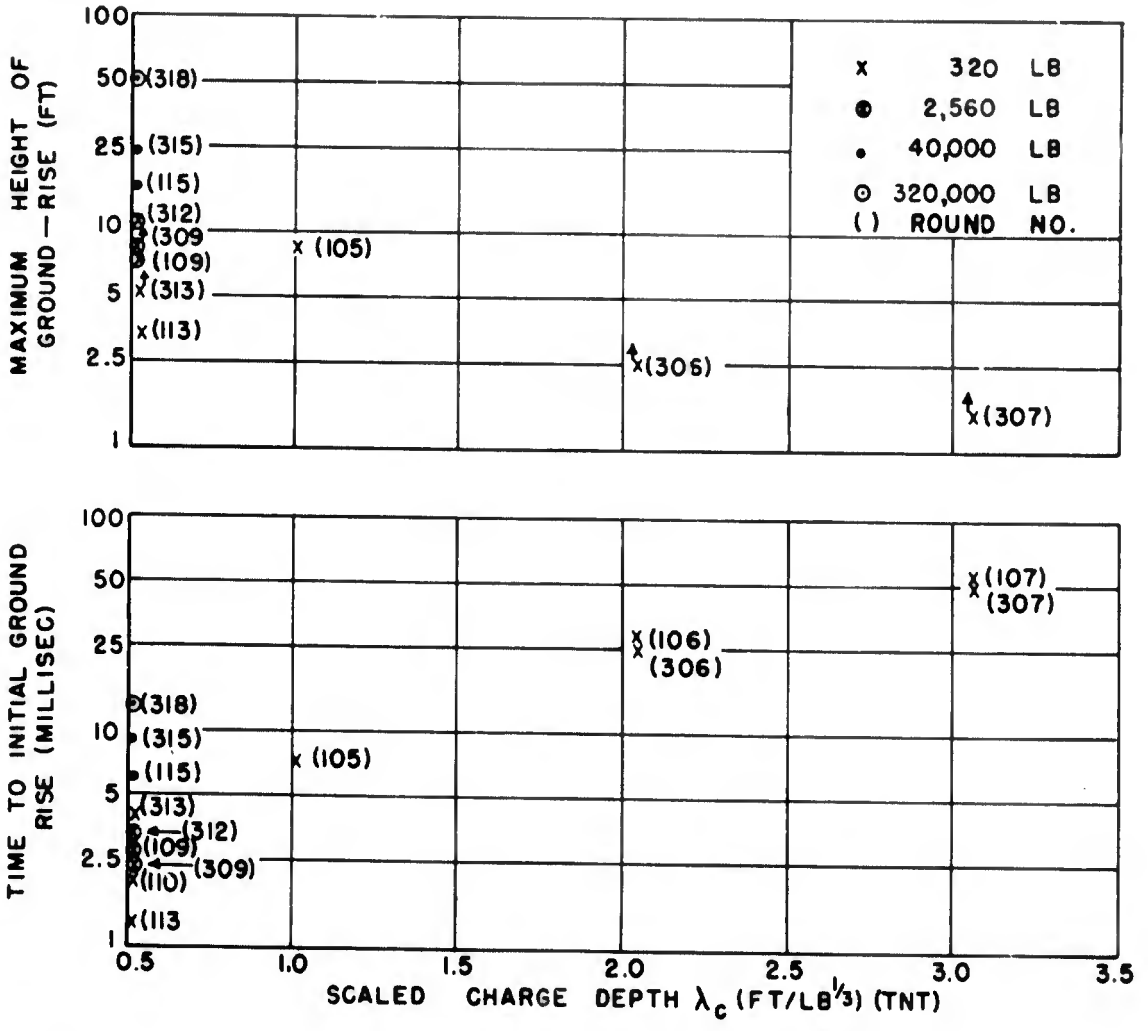

Fig. 2.4 Time to Initial Ground-Rise and Maximum Height of Ground-Rise vs Scaled Charge Depth

TABLE 2.1

Velocity of Ground-Rise in Dry Clay and Dry Sand

Round	Soil Type	Charge Wt. (lb TNT)	Scaled Depth ($ft/lb^{1/3}$)	Velocity of Ground-Rise (ft/sec)
110	Dry Sand	320	0.512	730
113	Dry Sand	320	0.512	680
109	Dry Sand	2,560	0.512	510
115	Dry Sand	40,000	0.512	710
105	Dry Sand	320	1.02	220
106	Dry Sand	320	2.05	70
107	Dry Sand	320	3.07	30
313	Dry Clay	320	0.512	770
309	Dry Clay	2,560	0.512	780
312	Dry Clay	2,560	0.512	834
315	Dry Clay	40,000	0.512	770
318	Dry Clay	320,000	0.512	780
306	Dry Clay	320	2.05	57.6
307	Dry Clay	320	3.07	18.8

TABLE 2.2

Time of Breakthrough for Charges Fired in Dry Sand

Round	Charge Weight (lb TNT)	Scaled Depth ($ft/lb^{1/3}$)	Breakthrough (millisec)
113	320	0.512	5.8
105	320	1.02	42
106	320	2.05	700
107	320	3.07	>1300
109	2,560	0.512	15.4
115	40,000	0.512	31

The smoke crown seems to consist of a mixture of dust and smoke particles and behaves like an aerosol with a relatively low density. It falls and mixes with the surge cloud when charges are fired at $\lambda_c = 0.5$ $ft/lb^{1/3}$ with a moderate wind (see Section 2.5) and for all deeper shots.

At λ_c = 2.0 ft/lb$^{1/3}$ and at greater depths, the jet does not break through the smoke crown and its general appearance is that of a dome-shaped dust and smoke cloud. It is difficult to distinguish the smoke crown from the dirt column beneath it at these scaled charge depths.

For charges fired at a scaled depth less than 0.5 ft/lb$^{1/3}$ (and rounds fired at a λ_c of 0.5 ft/lb$^{1/3}$ with a light wind), the smoke crown does not fall appreciably but becomes diffuse and moves downwind, mixing with the rising surge cloud until they become indistinguishable.

The initial rise of the smoke crown for Round HE-3 in Nevada is shown in Figure 2.5.

2.4 COLUMN

The dirt column rises from the ground following the initial smoke cloud. For charges fired at scaled depths of 1.0 ft/lb$^{1/3}$ or less the column is initially narrower at the base than at the top, but expands radially until the walls are almost vertical. The column walls are relatively smooth until this time, but develop a spiky appearance and then become diffuse and less sharply defined. Dirt clods are thrown out radially through the column and follow a downward trajectory. In dry hard-packed soils, such as at the Nevada test site, dust trails from the soil conglomerates may obscure the further behavior of the column. The assumptions are made that the dust aerosol in the column drops vertically and flows outward radially along the ground as the base surge and that the heavy radial throwout does not contribute to the surge flow.

For charges fired at scaled depths of 2.0 ft/lb$^{1/3}$ or more, the column is initially dome-shaped, reaching its greatest diameter at the base. The column expands until the walls are approximately vertical and little or no radial throwout is observed.

At all depths studied, the rate of expansion of the column base is approximately linear until the walls become spiky and diffuse. For scaling purposes, the maximum column diameter at the base (D_{max}) is defined as the size attained when the linear horizontal growth ends. (The column subsequently <u>appears</u> to grow rapidly because of throwout and dust obscuration.) Column height (C) is measured to the base of the smoke crown and, for scaling, the assumption is made that any part of the column extending into the smoke crown is diffuse and has a negligible effect on the growth of the base surge.

As accurate measurements of maximum column height and diameter can be obtained solely from motion picture records, such data are not available for all of the Dugway tests.

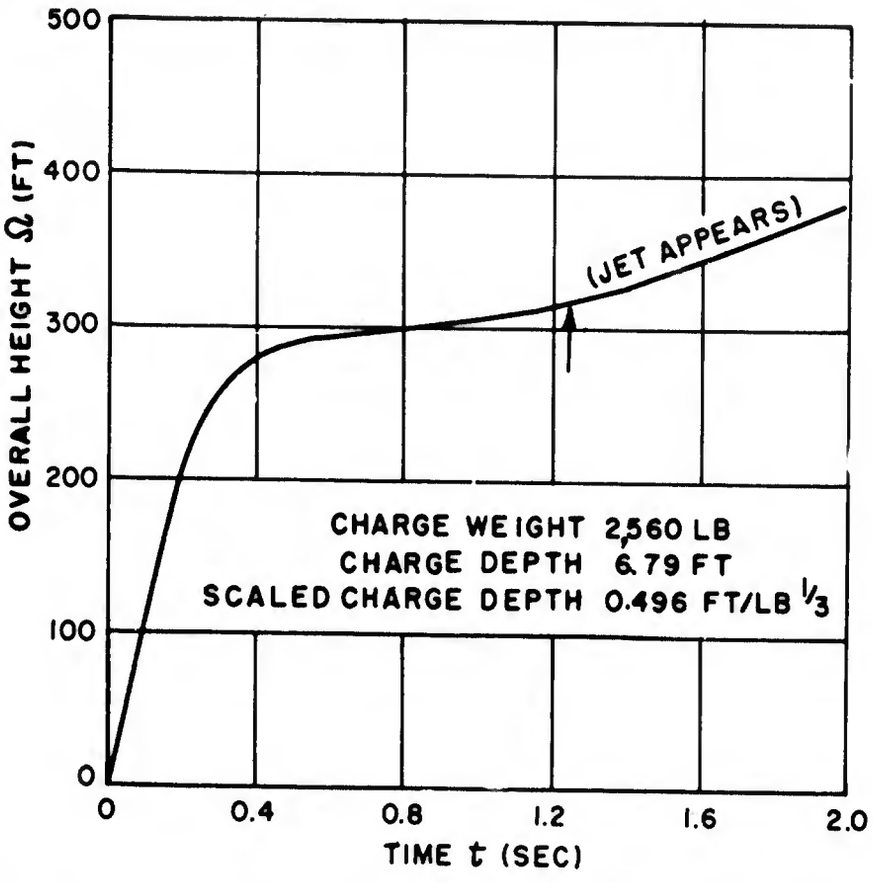

Fig. 2.5 Height of Smoke Crown vs Time - Round HE-3

As shown in Figure 2.6, the relation between D_{max} and charge weight may be expressed by a power formula for buried charges fired at the same scaled depth. Column diameter apparently reaches a maximum when the charge is half underground ($\lambda_c = 0$) or near that depth. For rounds fired with the upper surface of the charge tangent to the ground and for deeper shots, D_{max} increases with increasing depth to a maximum at about $\lambda_c = 1.0$ and decreases from there on.

The relation between maximum column diameter and charge weight for a scaled depth of $\lambda_c = 0.512$ ft/lb$^{1/3}$ in dry clay may be expressed as:

$$D_{max} = 10.9\ W^{0.304} \quad (\lambda_c = 0.512 \text{ ft/lb}^{1/3}) \tag{2.1}$$

where D_{max} = maximum column diameter, ft
W = charge weight, lb (TNT)

At a scaled depth of 0.135 ft/lb$^{1/3}$ in dry clay, the shallowest depth at which the charge was not exposed to the air, the relation is:

$$D_{max} = 8.38\ W^{0.304} \quad (\lambda_c = 0.135 \text{ ft/lb}^{1/3}) \tag{2.2}$$

Similar expressions can be obtained for C_{max}. (See Fig. 2.7.) As maximum column height and maximum column diameter are equal at scaled depths of 0.512 ft/lb$^{1/3}$, the formulas are the same. However, since column height changes more rapidly with charge depth than does column diameter, agreement is not obtained at other values of λ_c. The formulas for scaled depths of 0.512 and 0.135 ft/lb$^{1/3}$ in dry clay are:

$$C_{max} = 10.9\ W^{0.304} \quad (\lambda_c = 0.512 \text{ ft/lb}^{1/3}) \tag{2.3}$$

$$C_{max} = 5.71\ W^{0.304} \quad (\lambda_c = 0.135 \text{ ft/lb}^{1/3}) \tag{2.4}$$

where C_{max} = maximum column height, ft
W = charge weight, lb (TNT)

Column heights reach a maximum at about $\lambda_c = 1.0$ ft/lb$^{1/3}$ and are less for charges shallower or deeper than this.

The ratio of maximum column height to maximum column diameter is important for scaling the radial growth of the base surge. (See Chap. 4.) Average values of C_{max}/D_{max} are given in Fig. 2.8, for the range of scaled

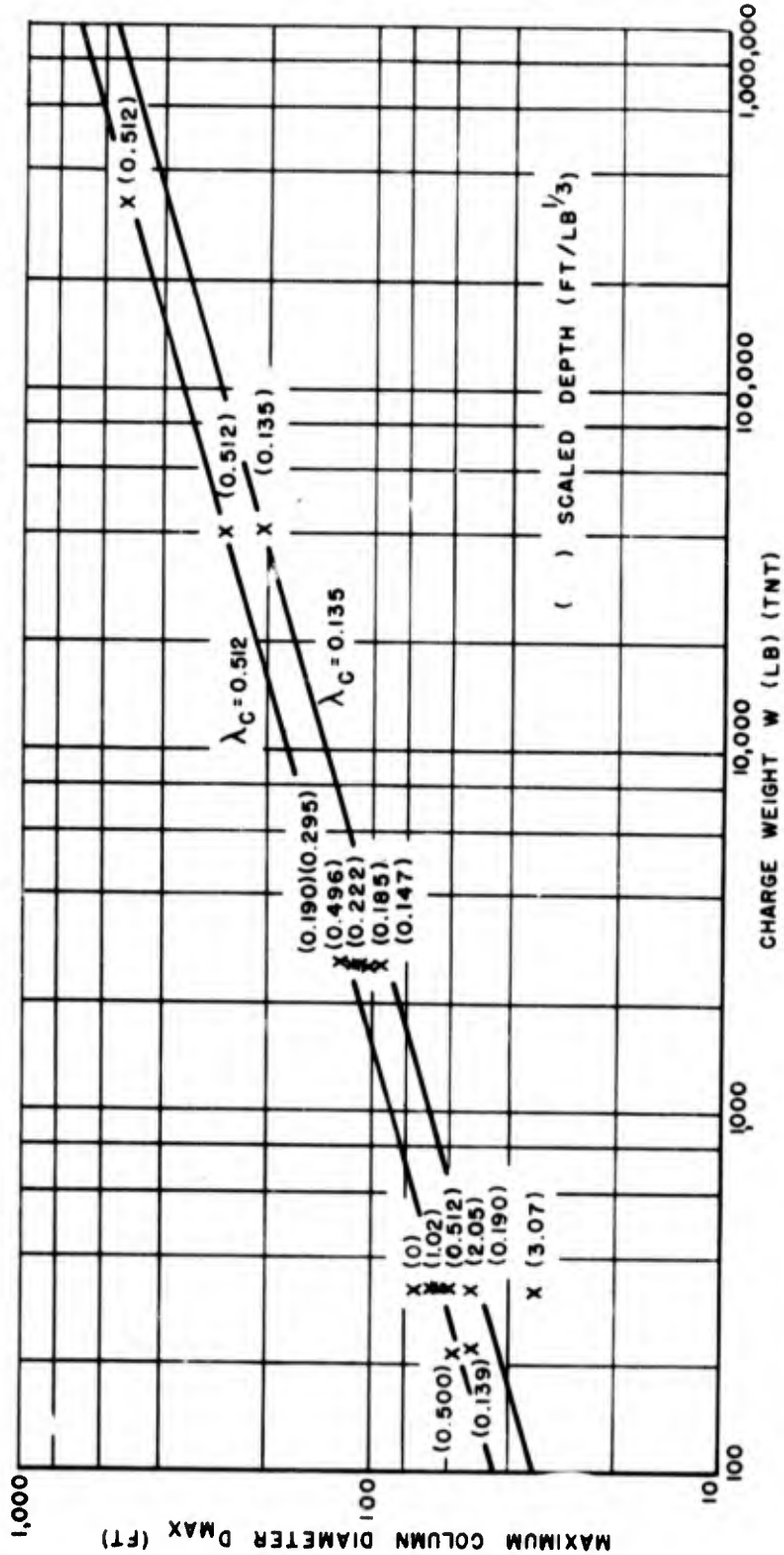

Fig. 2.6 Maximum Column Diameter vs Charge Weight

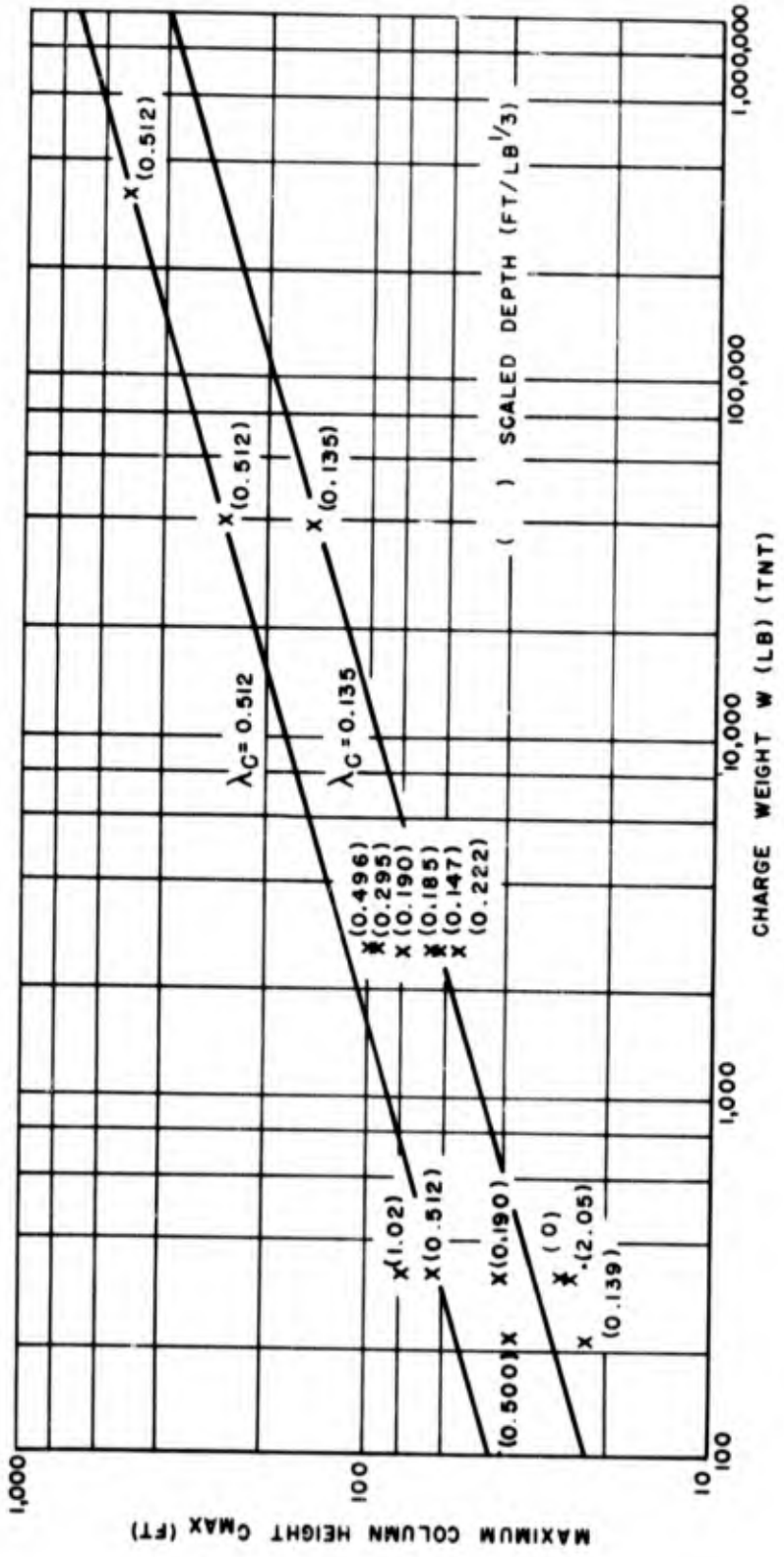

Fig. 2.7 Maximum Column Height vs Charge Weight

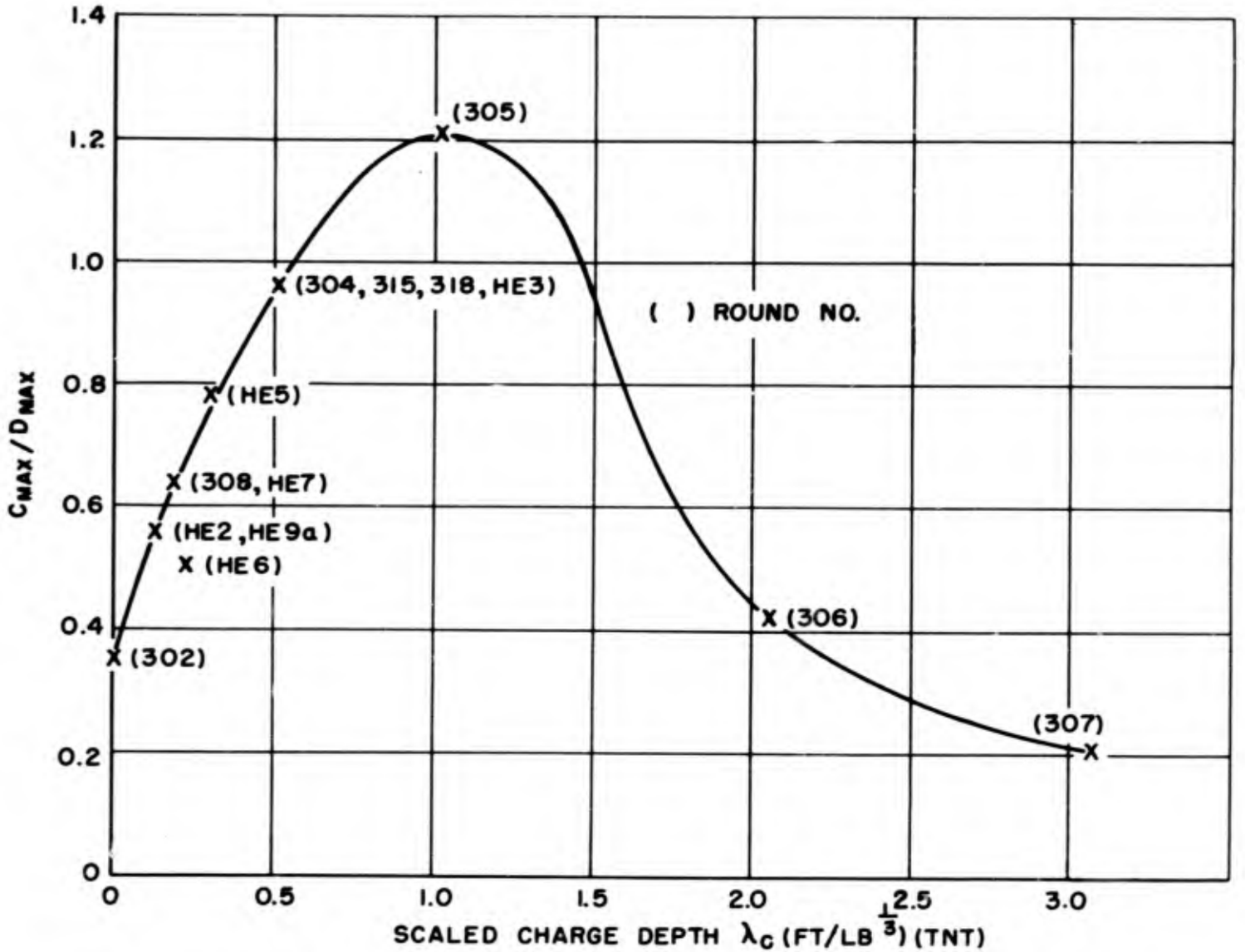

Fig. 2.8 Ratio of Maximum Column Height to Maximum Column Diameter vs Scaled Charge Depth

depths available in dry clay at Dugway and at Nevada, and indicate a maximum value of this ratio at about λ_c = 1.0 ft/lb$^{1/3}$.

The general structure of the visible surface phenomena indicates that the column is a hollow cylinder,[4] except possibly at charge depths of 2.0 ft/lb$^{1/3}$ or more, when the central jet does not vent through the ground surface. It is difficult to distinguish the column from the smoke crown at these depths.

2.5 JET

A central jet of explosion gases and smoke appears for charges fired at scaled depths ranging from zero to a depth somewhat greater than 1.0 ft/lb$^{1/3}$, though the jet is relatively low and narrow at the deeper positions in this range. When charges are fired at scaled depths of 2.0 ft/lb$^{1/3}$ and deeper, the jet does not appear.

TNT charges produce a black jet, which is clearly defined at first and rises at a high velocity, due to the rapid expansion of the explosion gases. The outline of the black cloud is sharp and it has a turbulent appearance.

The rate of rise then decreases, due to turbulent mixing with the surrounding air, and the outer edges become diffuse. However, the jet continues to rise at a fairly high rate, as a result of its buoyancy.

When the buoyant lifting ceases, the jet cloud may rise or fall, depending upon its density and atmospheric conditions. If the bulk density is high enough and the smoke and soil particles are of the proper size and spacing, a downward density flow will be started and the cloud will drop and flow outward along the ground into the base surge. If the bulk density is nearly the same as the density of the air, the jet cloud will be subject to lift and dispersal by atmospheric convection and turbulence.

The scaled depth of 0.5 ft/lb$^{1/3}$ appears to be critical in this regard. At this firing condition, the jet remains partially airborne if the wind is light, but falls almost completely with a strong wind. The contribution of the jet to the base surge decreases as charges are fired in relatively shallower positions, and at λ_c = zero, the jet remains

---

[4] V. Salmon, Throw-Out Phenomena in Underground Explosions, Status Report No. 6, Contract N7onr32104, Stanford Research Institute Project 317, 29 March 1951, p 2.

completely airborne and is dispersed by turbulent atmospheric motion.

For charges fired at scaled depths greater than 0.5 ft/lb$^{1/3}$, virtually the entire jet deposits on the ground or enters the base surge in a short time. The contribution of the jet to the surge cloud decreases with increasing depth and is unknown when the jet does not vent completely through the smoke crown.

For scaling purposes, the maximum jet height (J_{max}) is defined as the limit of the buoyant rise of the jet. This is measured, somewhat subjectively, by examination of motion picture records, but may sometimes be obtained from plotted data of jet height vs time. For shallow charges J_{max} may coincide with the point at which the jet growth becomes linear, beyond which the growth is due to turbulent diffusion. With deeper charges, J_{max}, as defined herein, should be approximately equal to the greatest height attained by the jet.

The maximum jet heights for the Dugway dry clay tests and the Nevada HE tests are shown in Fig. 2.9 as functions of charge weight. For the scaled depth of 0.512 ft/lb$^{1/3}$ the relation between J_{max} and charge weight may be expressed by the following formula:

$$J_{max} = 116\ W^{0.224} \quad (\lambda_c = 0.512 \text{ ft/lb}^{1/3}) \tag{2.5}$$

where J_{max} = maximum jet height, ft
W = charge weight, lb (TNT)

J_{max} does not vary greatly for shallow charges, and the same formula may be applied to obtain an approximate maximum jet height, with about a 15% possible error, for charges fired between the scaled depths of zero and 0.6 ft/lb$^{1/3}$ in dry clay.

If maximum overall height is plotted against λ_c, as in Fig. 2.10, a good relation can be obtained for the maximum heights reached by the surface phenomena produced by the deeper 320 lb charges in dry clay (scaled depth greater than 0.5 ft/lb$^{1/3}$), although overall height coincides with jet height at scaled depths of 0.5 and 1.0 ft/lb$^{1/3}$ and represents height of the smoke crown for deeper charges. The formula is:

$$\Omega_{max} = 774\ e^{-1.13\ \lambda_c} \quad (320 \text{ lb, dry clay, } \lambda_c > 0.5 \text{ ft/lb}^{1/3}) \tag{2.6}$$

where Ω_{max} = maximum overall height, ft
λ_c = scaled charge depth, ft/lb$^{1/3}$

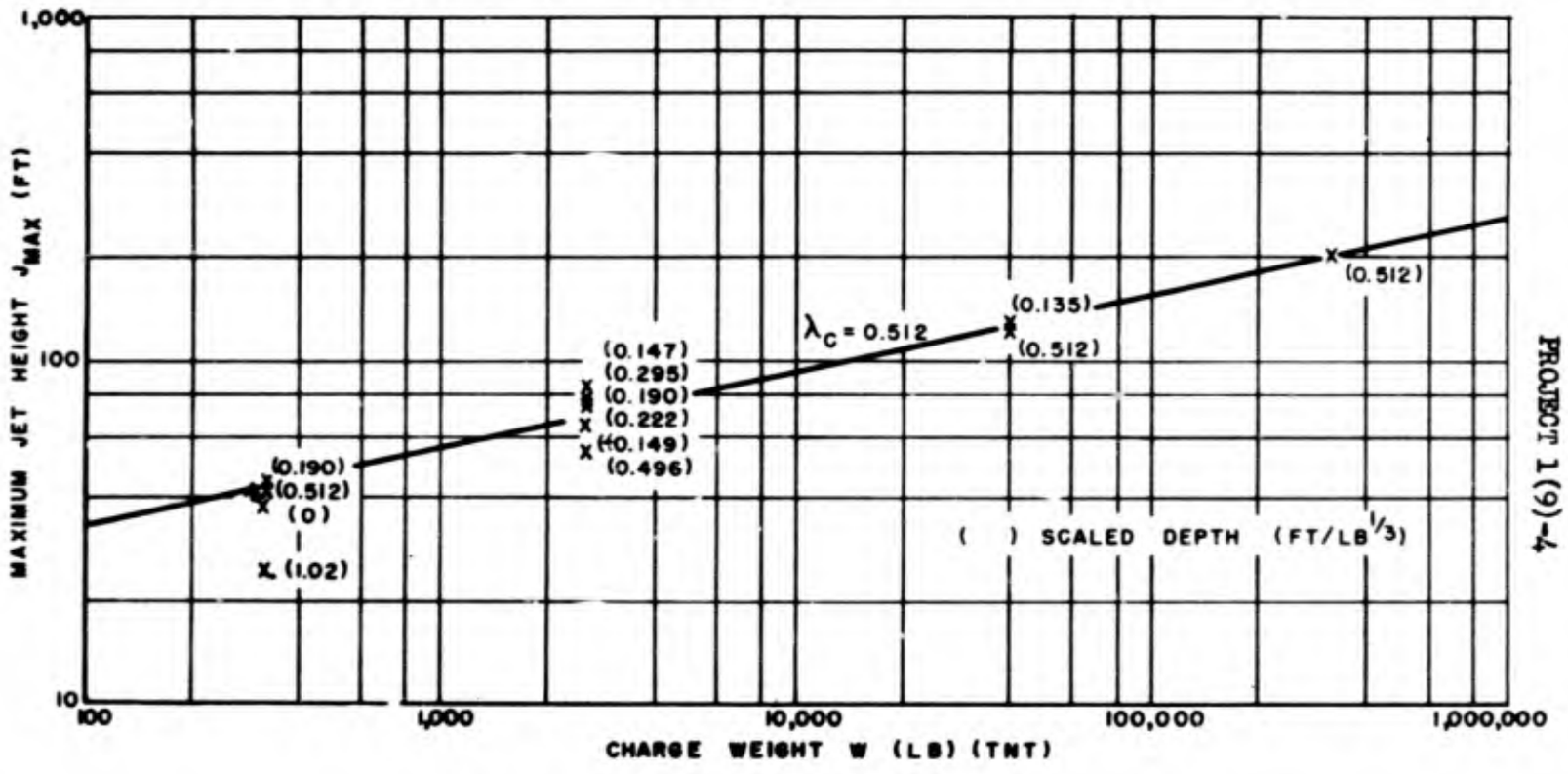

Fig. 2.9 Maximum Jet Height vs Charge Weight

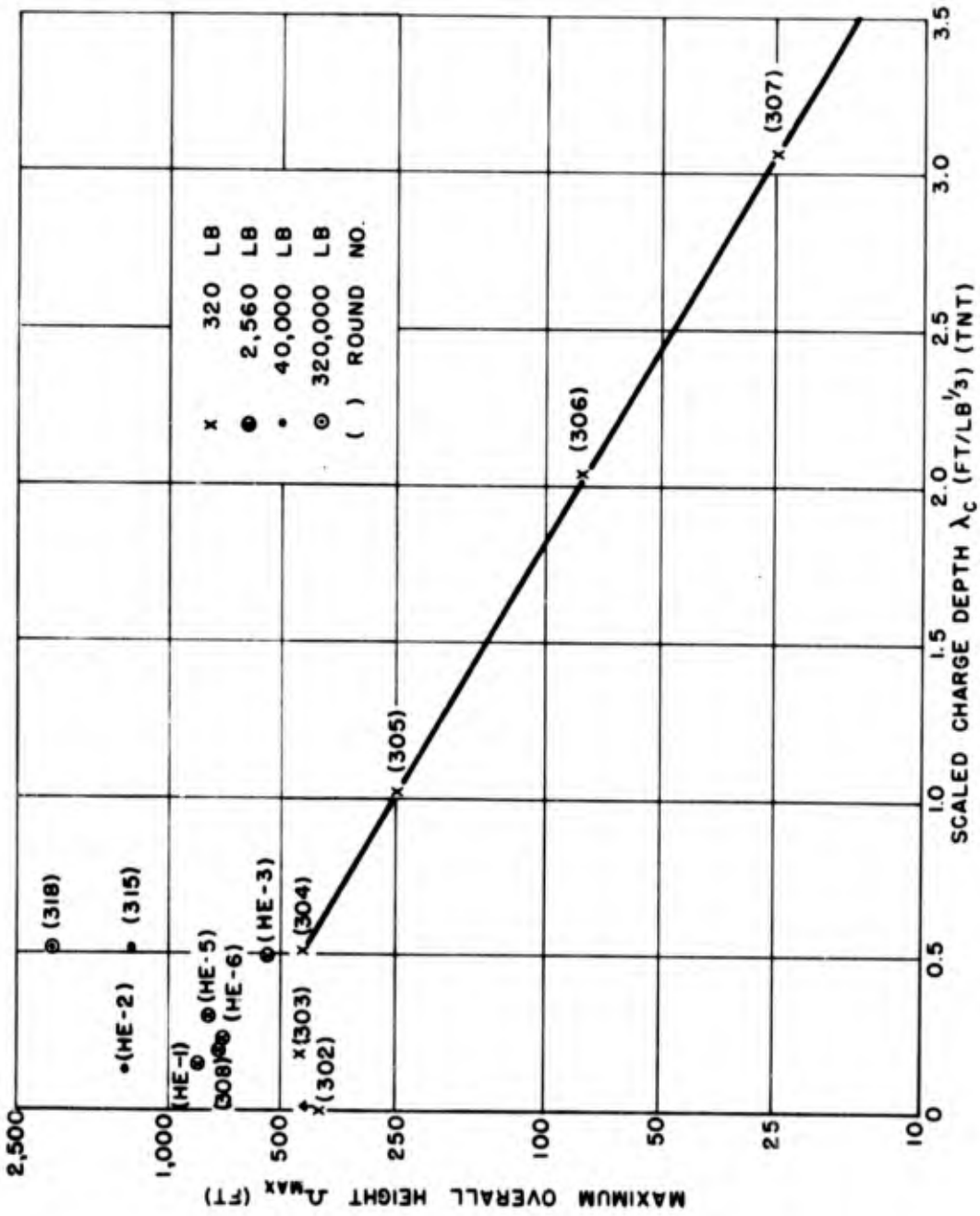

Fig. 2.10 Maximum Overall Height vs Scaled Charge Depth

The data indicate that the maximum scaled depth for the formation of such surface phenomena increases with increasing charge weight.

The vertical growth of jets from 320 lb and 2560 lb charges is presented in Figs. 2.11 and 2.12 and a comparison of the jets from charges of different weights at the same scaled depth is shown in Fig. 2.13. When possible, the ends of the growth curves indicate J_{max}, as defined herein. As the initial rapid rise of the jet can only be resolved with motion picture photography, jet records are not available for the dry sand and wet clay programs.

The available data show that the jet velocity is greatest for charges fired at a scaled depth of about 1.0 ft/lb$^{1/3}$ and decreases for charges placed at shallower or deeper positions. The records of Rounds 306 and 307 represent height of the smoke crown, but are included in Fig. 2.11 for comparison with shallower shots. Initial jet velocity increases with increasing charge weight, for charges fired at the same scaled depth.

After the buoyant rise of the jet has ended, the top of the jet cloud represents the overall height (Ω) of the surface phenomena. Records of the changes in overall height are given in Figs. 2.14, 2.15 and 2.16. Overall heights of dry sand and wet clay rounds are included in these charts.

When charges were fired at the same scaled depth in different types of soil, the wet clay rounds produced the most rapidly rising jet clouds and dry clay the slowest rising jet clouds, with charges in dry sand generally intermediate between the two.

However, the overall height is greatly affected by atmospheric conditions, as indicated by the different curves shown for charges fired at the same scaled depth in the same soil type. Both jet height and overall height are influenced by wind and atmospheric turbulence. The effects of wind and its variations in time and space are complex but, in general, strong winds have the effect of holding the jet down. Probably a surface wind of at least 15 mph, accompanied by gustiness and an increase of speed with height, is needed to hold back the jet and force it down rapidly, when charges are fired at scaled depths of 0.5 ft/lb$^{1/3}$ or greater. (See Fig. 3.11.) Atmospheric conditions may have effects of different relative importance for charges greater than 320,000 lb or less than 320 lb.

Wind effects are discussed further in Section 5.2.

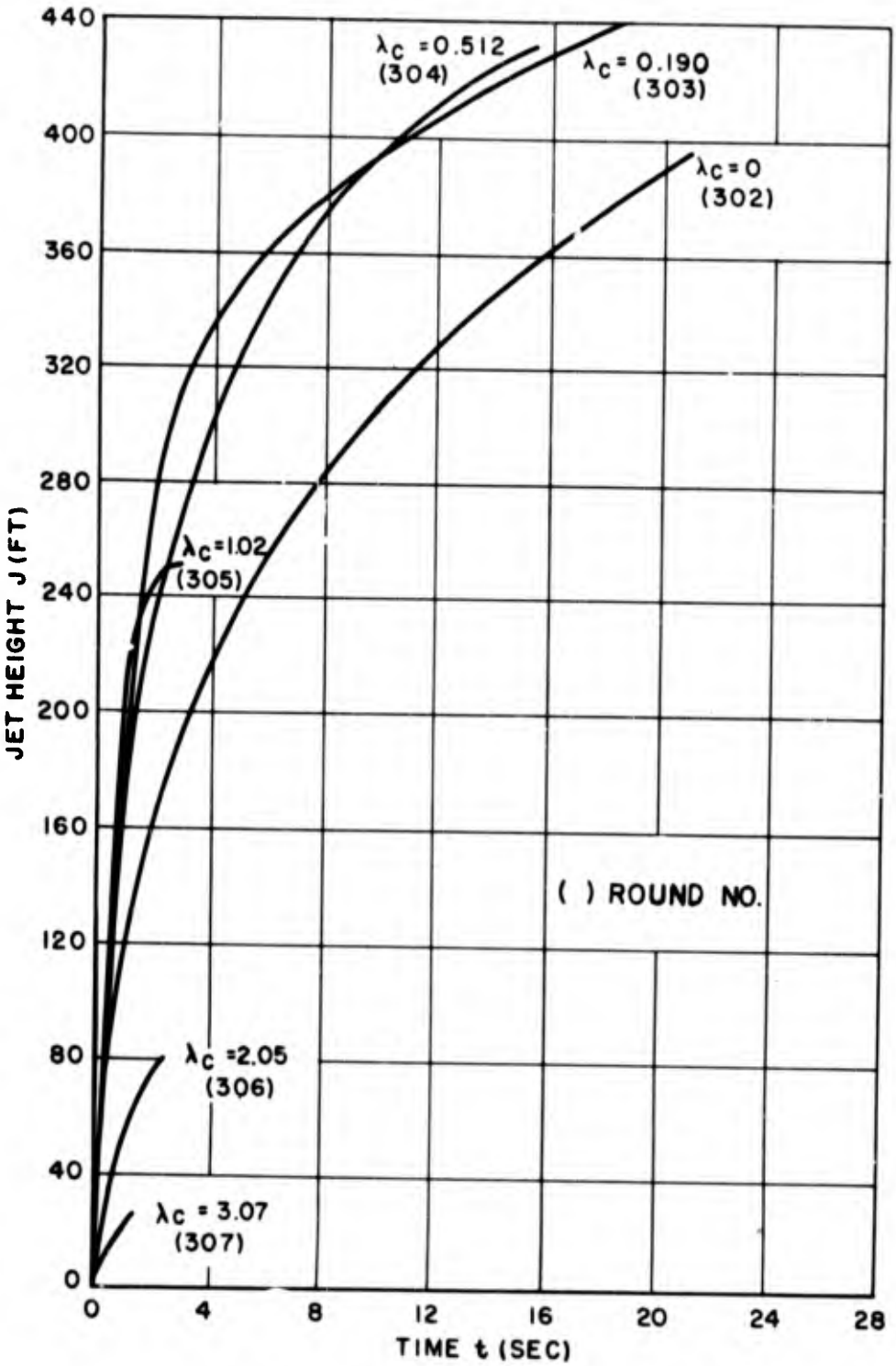

Fig. 2.11 Jet Height vs Time - 320 Lb TNT Charges

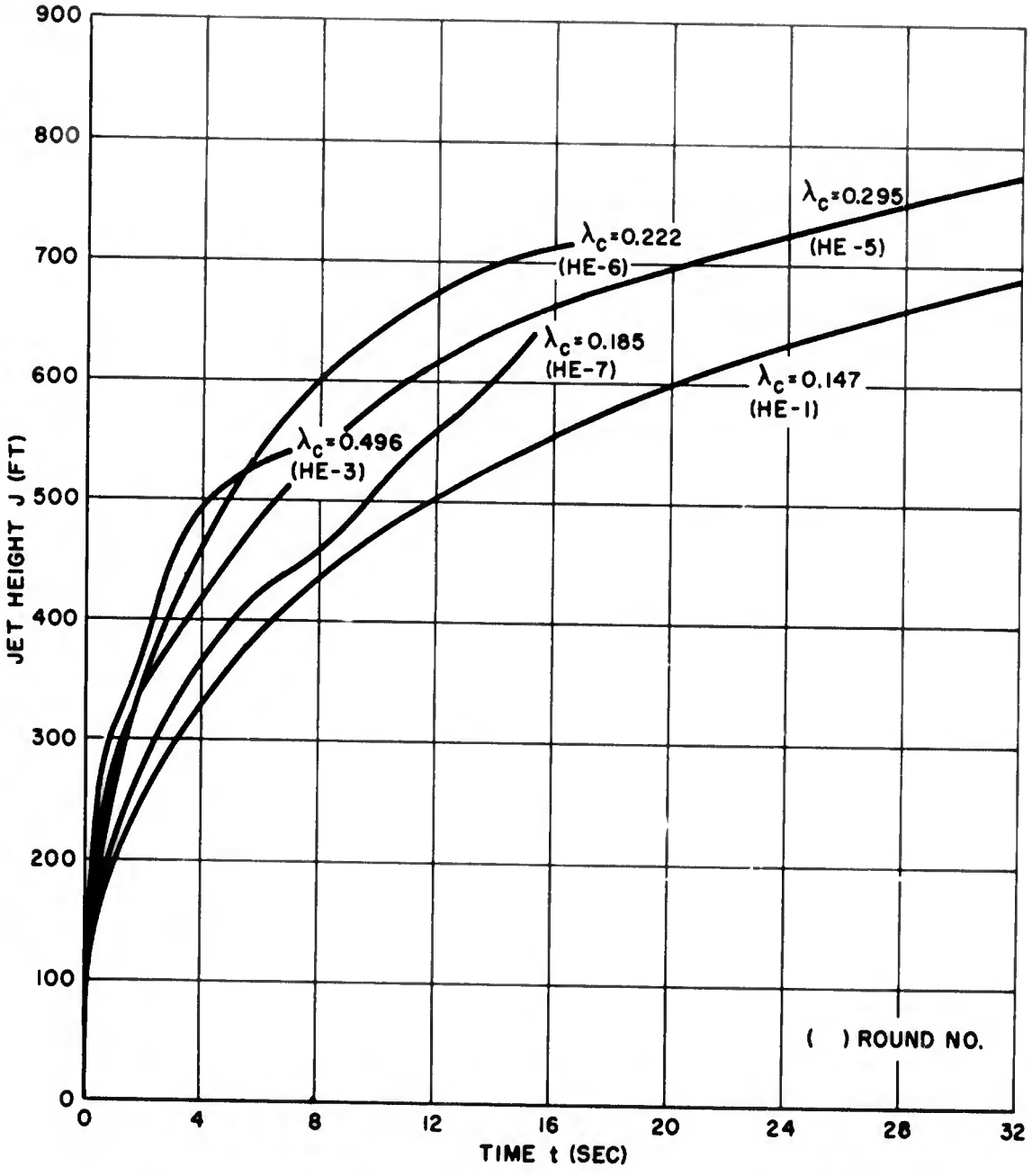

Fig. 2.12 Jet Height vs Time - 2,5600 Lb TNT Charges

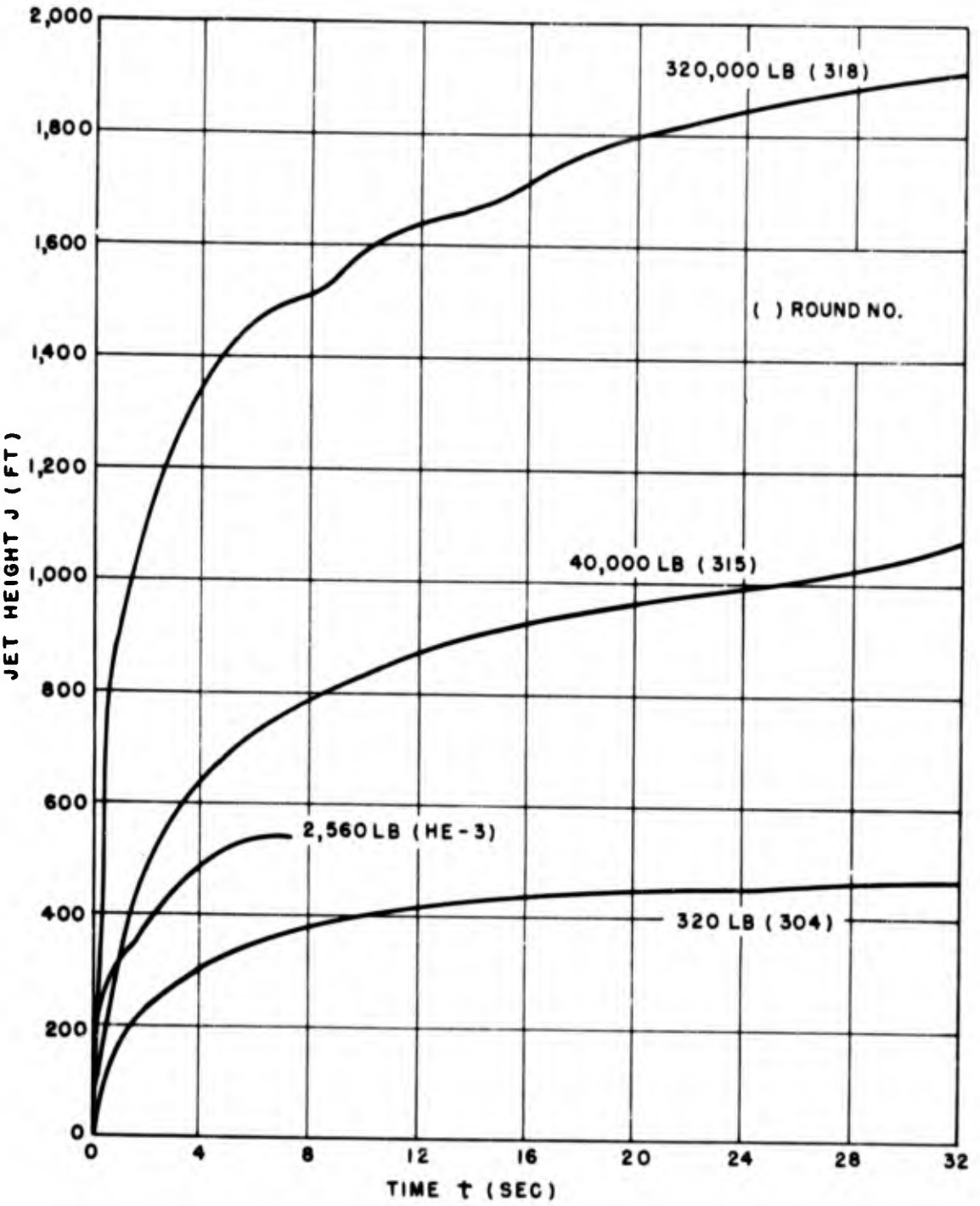

Fig. 2.13 Jet Height vs Time - Scaled Depth = 0.5 Ft/Lb$^{1/3}$ (TNT)

[redacted]

PROJECT 1(9)-4

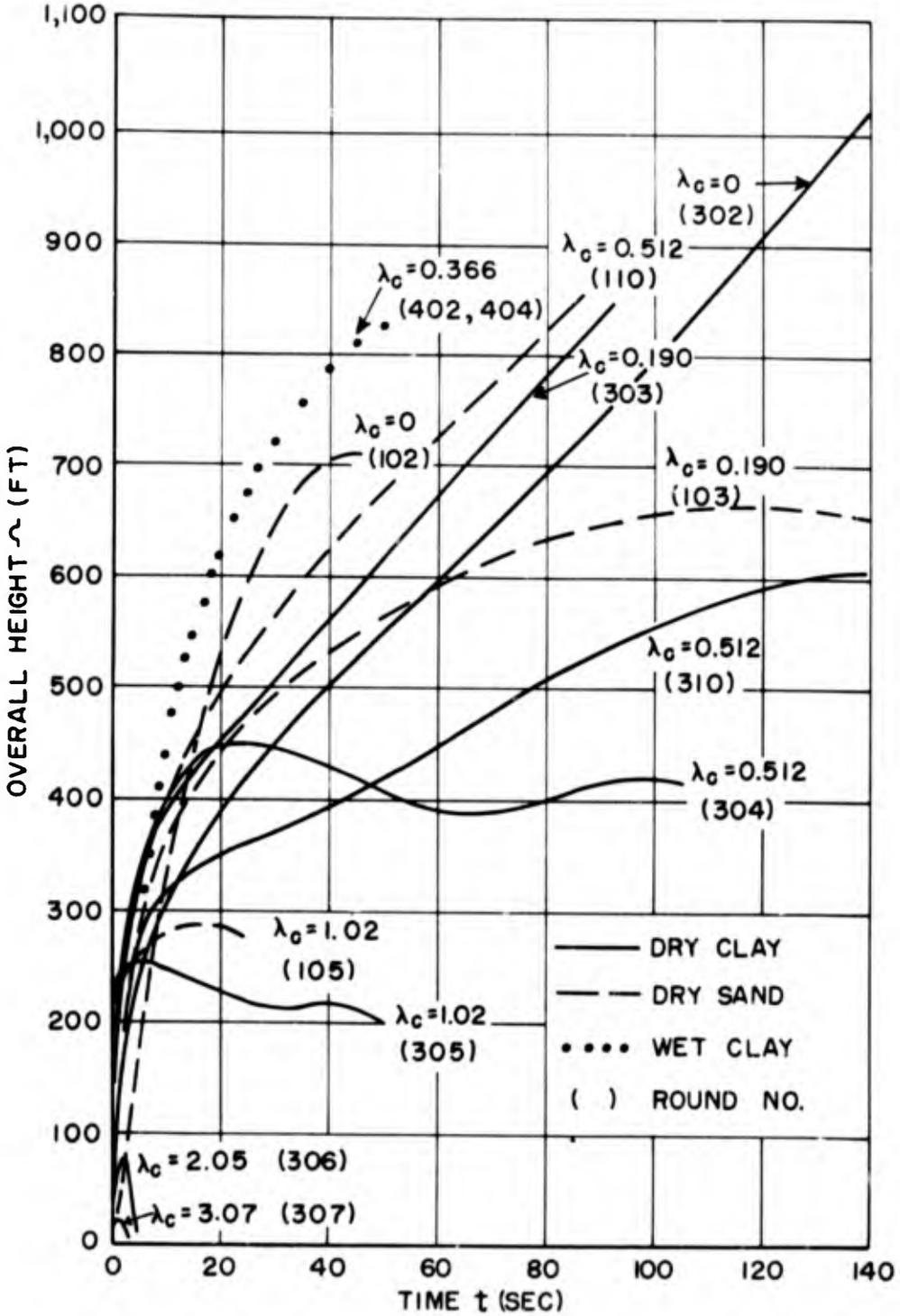

Fig. 2.14 Overall Height vs Time - 320 Lb TNT Charges

[redacted]

PROJECT 1(9)-4

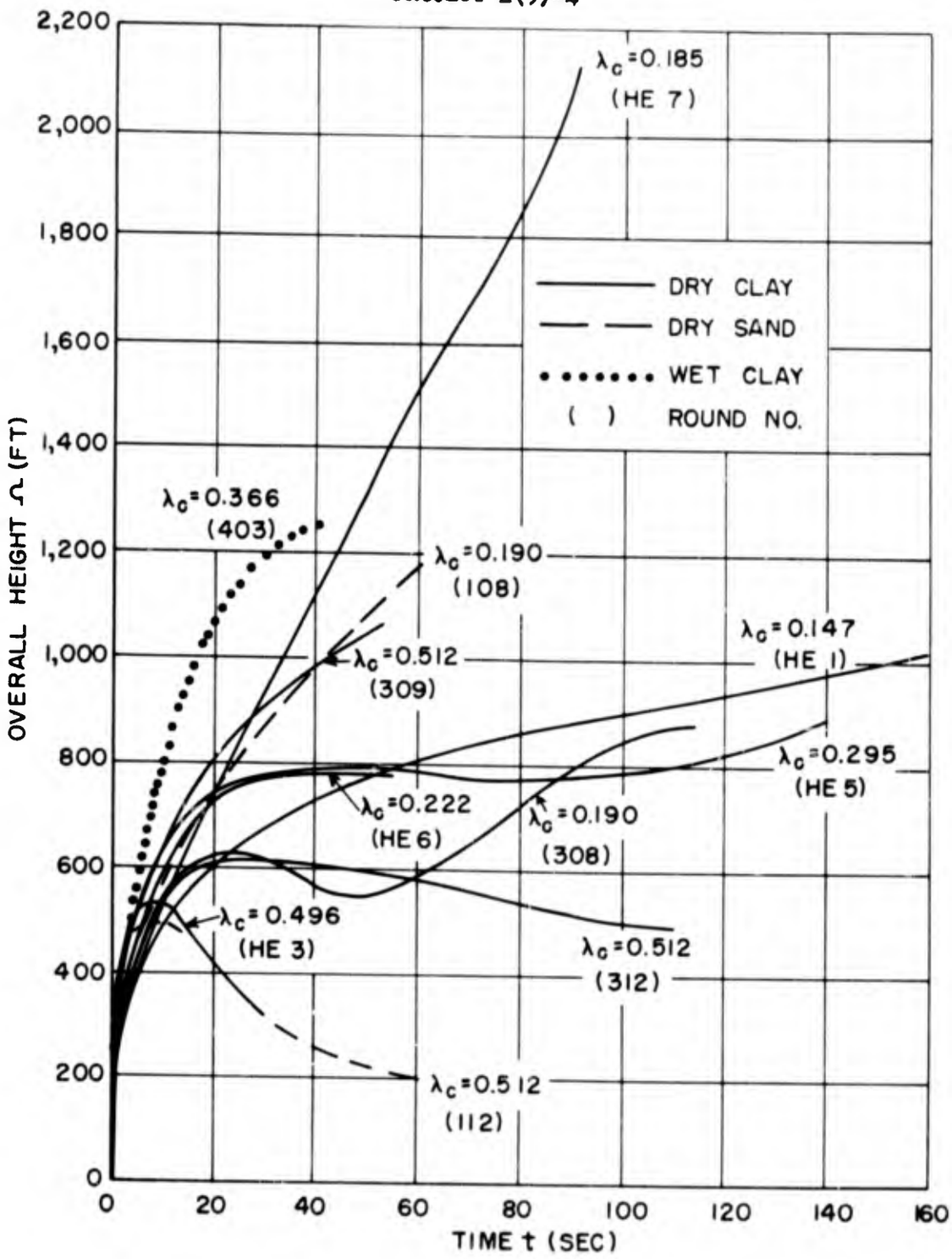

Fig. 2.15 Overall Height vs Time - 2,560 Lb TNT Charges

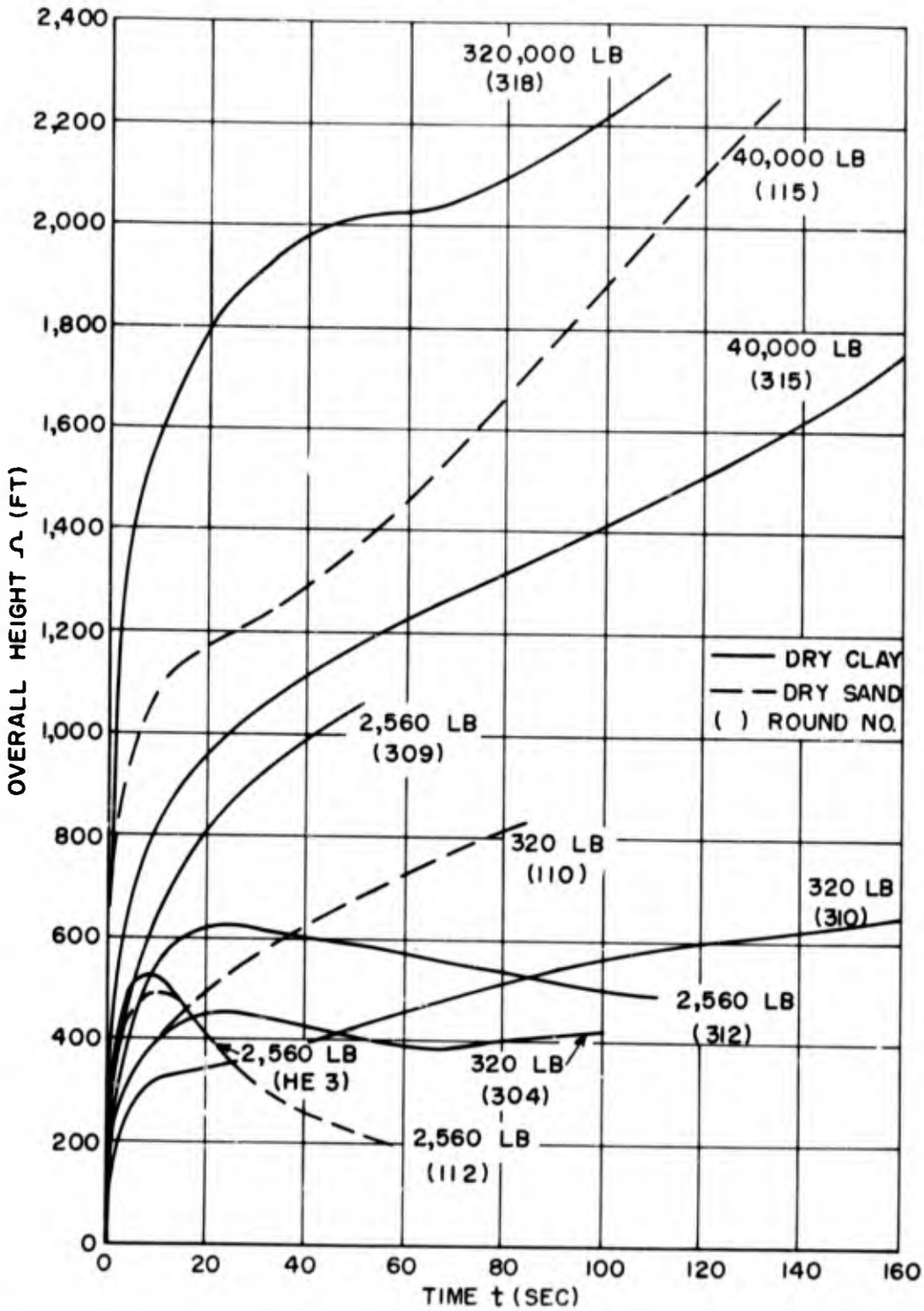

Fig. 2.16 Overall Height vs Time - Scaled Depth = 0.5 Ft/Lb$^{1/3}$ (TNT)

2.6 CHARGES ON THE SURFACE

One record is available for a charge fired on the surface of the ground: Round HE-4, at Nevada, was a 2560 lb charge, detonated at $\lambda_c = -0.149$ ft/lb$^{1/3}$.

The explosion scooped out a shallow crater, about 2 ft deep and 16 ft in diameter,[5] and the surface shock wave raised considerable surface dust. An irregularly shaped cloud formed and rose relatively slowly, while a thin pillar of dust trailed beneath it. The upper cloud was divided into two distinct portions, a black smoke cloud and a light dust cloud, which gradually merged into a single diffuse mass. The trailing dust pillar soon became tenuous and the whole cloud dissipated within a half hour. No base surge formed at this charge position.

Some of the important features of the surface phenomena are shown in Fig. 2.17.

---

[5] D. C. Campbell, LCDR, USN, Tests and Observations on Craters and Base Surges, JANGLE Report 1(9)-3, 1 Nov. 1951.

0.10 SEC

2.0 SEC

10 SEC

20 SEC

CHARGE WEIGHT = 2,560 LB
CHARGE ON SURFACE OF THE GROUND

SCALED DEPTH = 0.149 FT/LB $^{1/3}$

Fig. 2.17 Surface Phenomena - Round HE-4

[redacted]

CHAPTER 3

BASE SURGE

3.1 METHOD OF FORMATION AND DISSIPATION

The roughly cylindrical earth column that is formed above the ground when the explosive gases vent consists of a mixture of soil particles of a wide range of size. The larger clods or aggregates drop back but the smaller particles entrain air because of their high concentration and do not fall individually. It is assumed that the dense aerosol falls at a rate considerably greater than the terminal velocities of the individual particles and flows outward radially at the base of the column to form the base surge. The entire suspension of dust in air behaves in the manner of a homogeneous fluid with a mean density somewhat higher than the density of the surrounding air.

This type of phenomenon is not confined to explosions and is known as bulk subsidence. It has been investigated on a laboratory scale at the Woods Hole Oceanographic Institution[1] and Stanford University.[2] The limited data available indicate that the ratio of current velocity to particle velocity is greatest for very small particles at a high concentration and was as large as 10,000 with smoke containing one million particles of ammonium chloride per cc (particle radius 0.1 micron).[3]

When the falling aerosol changes its direction of flow from vertical to horizontal at the base of the column, the larger particles do not follow the sudden bending of the streamlines but continue their downward path and are deposited upon the ground. A tall dense column will fall rapidly and deposit particles of a wide range of size in this manner, but a shallow column of low density will deposit only the relatively large particles.

---

[1] A. B. Arons, G. Wertheim, and M. Krumholz, Density Currents Induced by Streams of Falling Particles, Woods Hole Oceanographic Institution, Woods Hole, Mass., NAVORD Report 485, 21 March 1951, pp 1-29.

[2] S. W. Grinnell, W. A. Perkins and F. X. Webster, Bimonthly Report 3 of Chemical Warfare Service Research and Development Program, Contract No. W-18-035-CWS-1256, Stanford Univ., Calif., May - June 1946, pp 15-24.

[3] Ibid., p 16.

[redacted]

After the column has settled and flowed outward, the clouds of dust and smoke particles constituting the jet and smoke crown may fall and propagate into the surge. These clouds are lighter than the column and drop more slowly, but contribute additional material to the base surge.

The successful use of Froude scaling in the study of the base surges produced by underwater[4] and underground explosions (see Chap. 4) indicates that the initial radial growth of the base surge is controlled by gravitational and inertial forces. When the particle concentration is reduced by expansion of the surge, further growth is controlled by eddy diffusion. The point at which the latter mechanism becomes the more important of the two depends upon meteorological as well as firing conditions.

As the rate of radial growth of the base surge decreases, the heavier particles settle under gravity until a relatively stable aerosol remains. At this stage, the particles are probably less than a few microns in size and the Stokes' Law rate-of-fall is small. The tenuous dust cloud is then subject to atmospheric turbulence and may remain airborne for a considerable period of time.

3.2 EFFECTS OF SOIL AND CHARGE DEPTH

The rate of growth and maximum extent of the base surge depend upon charge weight, charge depth, character of soil, and meteorological conditions.

As the base surge is often irregular in shape initially and is further distorted by wind and atmospheric turbulence, mean values of the radius are used in the following pages to indicate the growth of the surge. Similar records of two or more rounds are averaged. Figure 3.1 shows that the maximum average rate of surge growth and probably the greatest surge extent for 320 lb charges in dry clay or dry sand occurs at a 7 ft charge depth (λ_c = 1.02 ft/lb$^{1/3}$). A similar trend is indicated in Figure 3.2 for 2560 lb charges, though no rounds were fired at scaled depths greater than 0.512 ft/lb$^{1/3}$. The effect of charge weight is shown for rounds fired at λ_c = 0.5 ft/lb$^{1/3}$ in Fig. 3.3.

The base surge produced by shallow charges (scaled depth less than 0.2 ft/lb$^{1/3}$) is relatively small and difficult to distinguish from

---

[4] A. B. Arons, G. A. Young, and M. L. Milligan, Further Investigation of the Base Surge, Interim Report No. 3 on NOL Project 152, NAVORD Report 2144, 1 June 1951, pp 1-15.

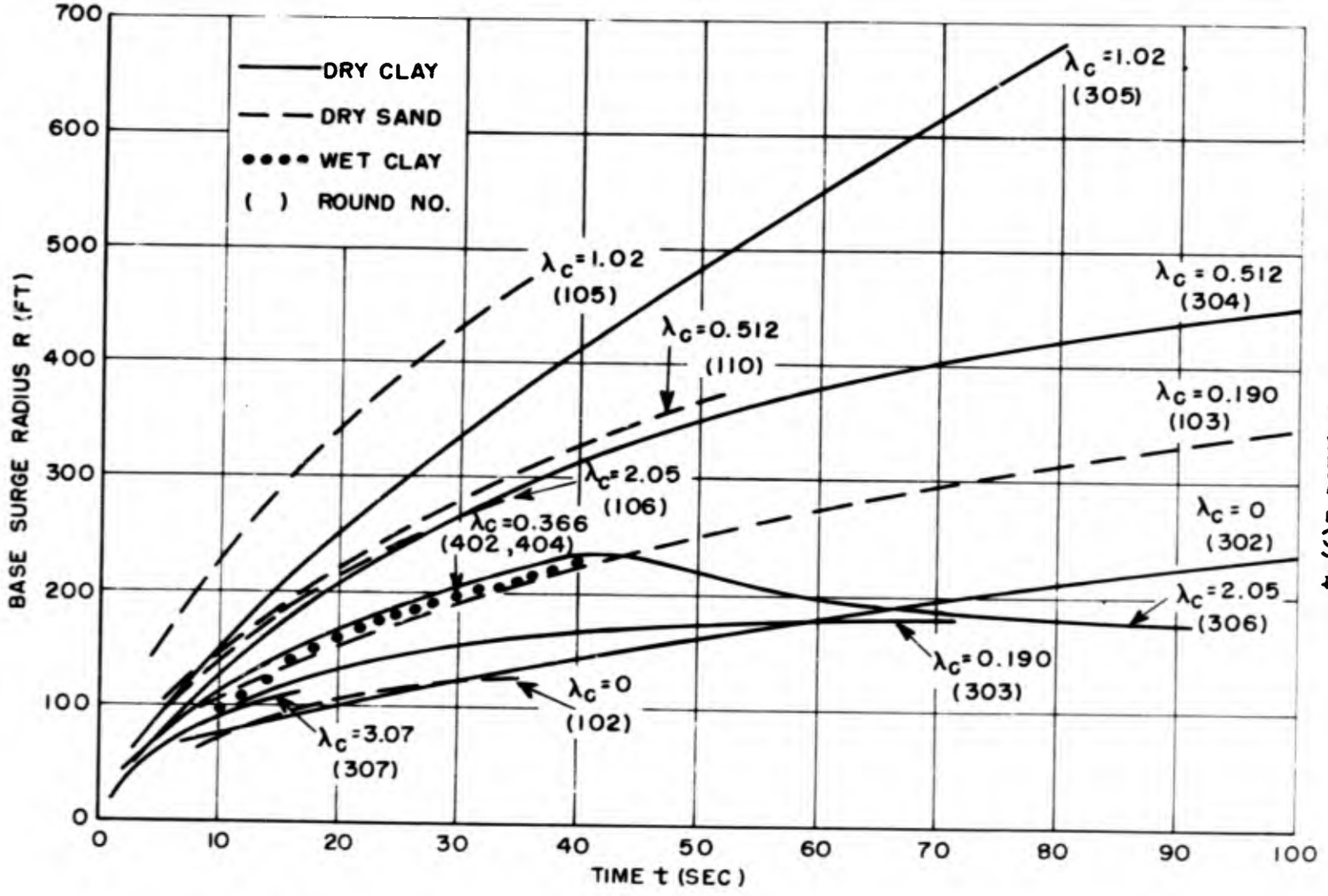

Fig. 3.1 Base Surge Radius vs Time - 320 Lb TNT Charges

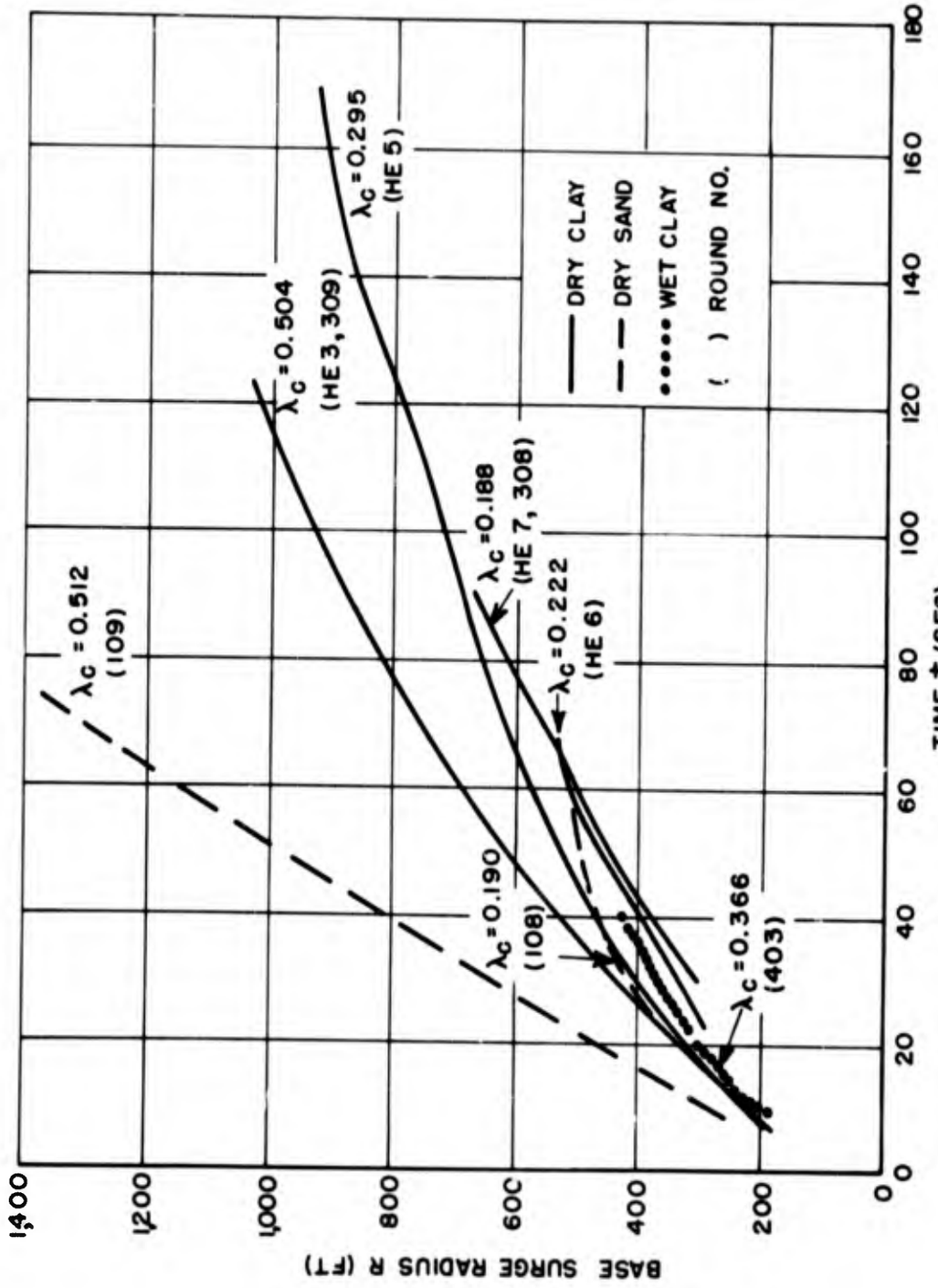

Fig. 3.2 Base Surge Radius vs Time - 2,560 Lb TNT Charges

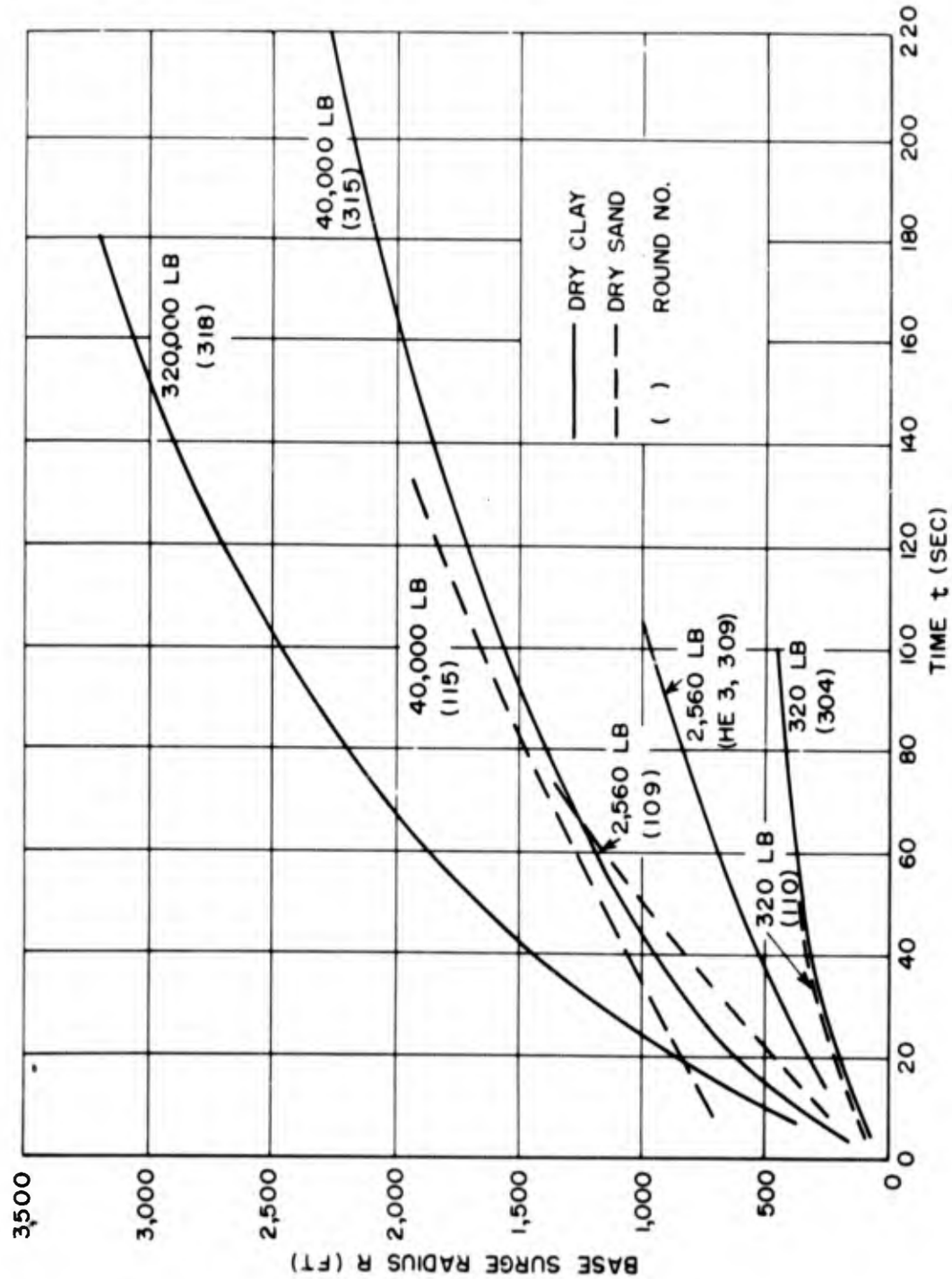

Fig. 3.3 Base Surge Radius vs Time - Scaled Depth = 0.5 Ft/Lb$^{1/3}$ (TNT)

surface dust. It is usually tenuous and has a limited radial growth. The low initial velocity and general appearance indicate that the surge density must be almost equal to that of the surrounding air at zero scaled depth. It is most probable that no recognizable surge would occur when more than half of a charge is exposed to the air at detonation.

The base surge produced by relatively deep charges (scaled depth greater than 2.5 ft/lb$^{1/3}$) is also small, but the high initial rate of spread indicates a pronounced density difference between the surge and surrounding air. The surge clouds are clearly defined, though small in size, at these depths.

In almost every case, charges fired in dry sand produced a larger, faster-moving base surge than the equivalent charges fired in dry clay. The limited data indicate that wet clay is the least effective of the three soil types for the production of a base surge.

The ends of the radius-time curves do not generally indicate the maximum radial extent of the surge cloud, but represent the limit of the available data. No objective measurement of maximum size can be made because the surge cloud grows by mixing with the surrounding air until the concentration has been reduced to a level at which the cloud is no longer visible. In cases where the growth curve indicates expansion to a maximum radius followed by a decrease in size (e.g., Round 306), the surge cloud has thinned and lifted, changing to a tall cylindrical dust cloud.

Examples of the base surge from shallow and deep charges in dry clay are shown in Figs. 3.4 and 3.5. Some dry sand and wet clay surges are presented in Figs. 3.6 and 3.7.

Surge heights are difficult to determine because of the billowy nature of the upper surface. Sometimes great differences in height occur between parts of the base surge, probably due to the lack of symmetry of the initial breakthrough of explosion gases and the subsequent irregular fallout. Theory indicates that the upper surface of a density current, such as the base surge, is subject to the formation of waves which may become unstable and lead to mixing with the air above.[5] In a dense current of this type, mixing is generally at a minimum at the leading edge. Mean values of surge height for each round are used in this presentation, but the data are subject to considerably more scatter than the measurements of surge radius.

---

[5] J. S. Coles and G. A. Young, Investigations of Base Surge Phenomena by Means of High Explosives and a Liquid Model, Interim Report No. 2 of NOL Project 152, NAVORD Report 1744, 1 Sept. 1950, p 53.

PROJECT 1(9)-4

Fig. 3.4 Formation of Base Surge by Shallow Explosion in Dry Clay

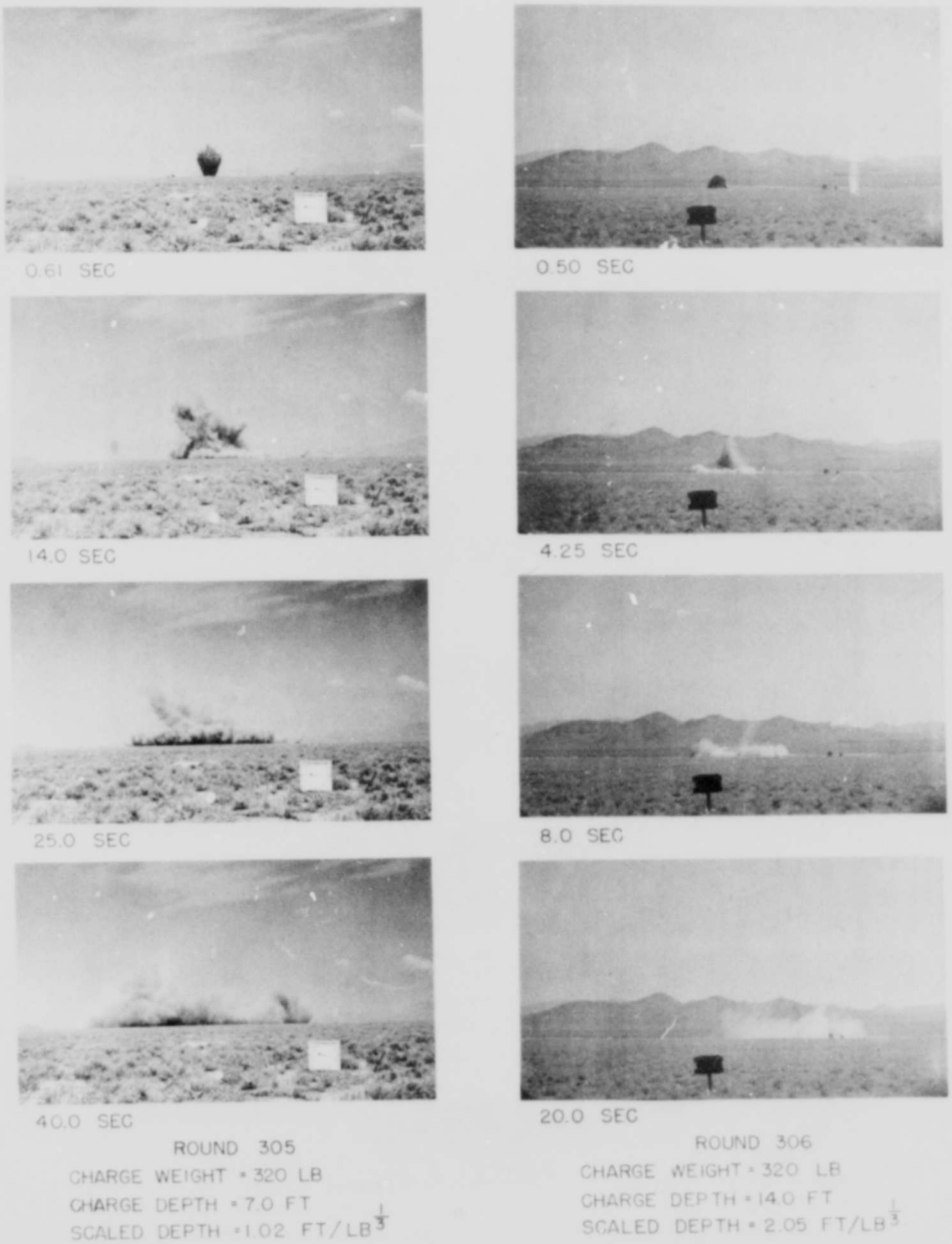

Fig. 3.5 Formation of Base Surge by Deep Explosions in Dry Clay

Fig. 3.6 Formation of Base Surge by Explosions in Dry Sand

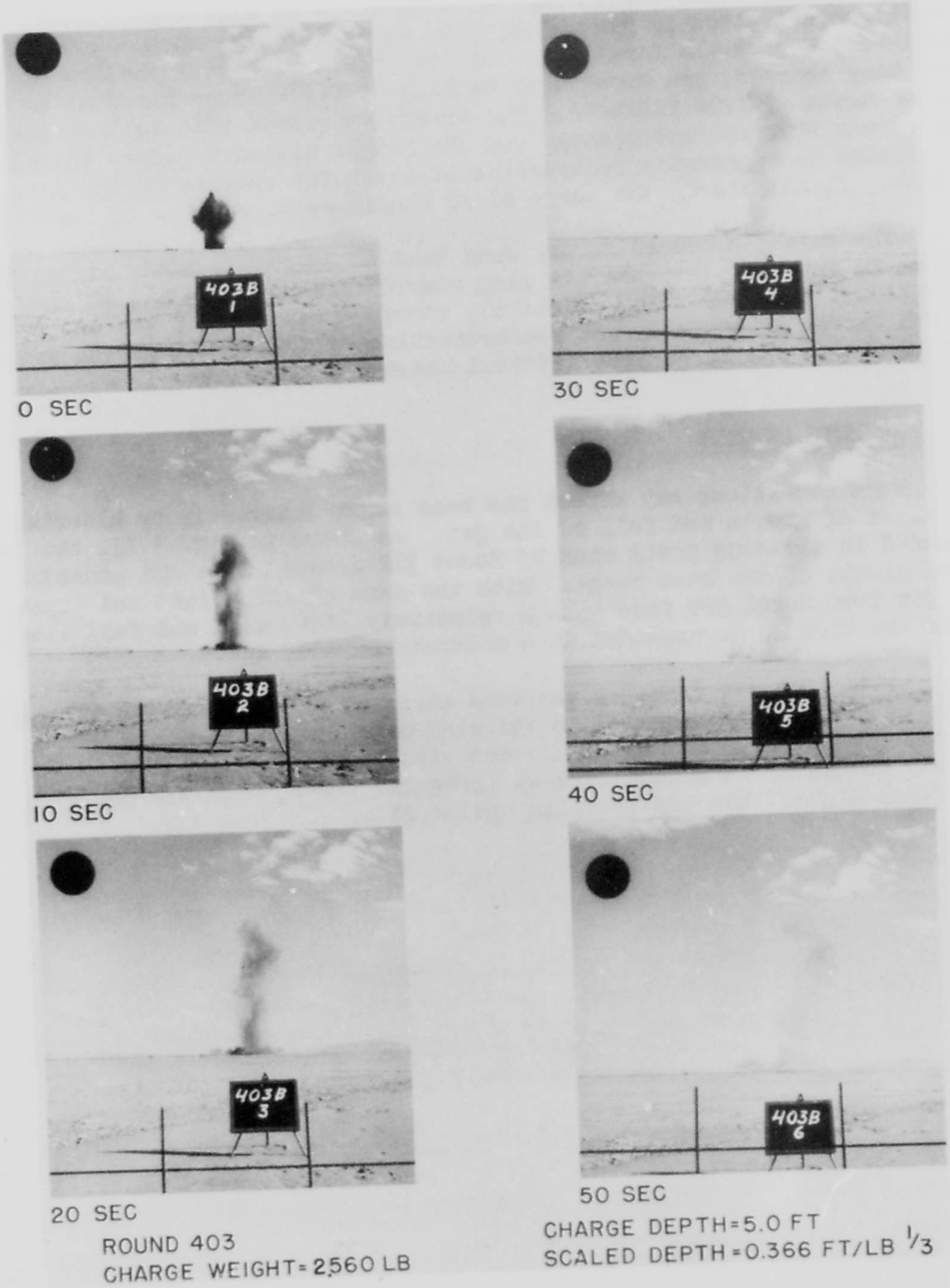

Fig. 3.7 Formation of Base Surge by Explosion in Wet Clay

The height-time curves for the base surge at different firing conditions are given in Figs. 3.8, 3.9, and 3.10. The surge cloud is shallowest during the first stage of its growth with very shallow and very deep charges, and appears to be highest for charges fired at a scaled depth of 1.02 $ft/lb^{1/3}$. The irregular growth that follows shows the effect of turbulent mixing, and the height attained before the surge dissipates is apparently independent of depth for charges of the same weight. In all cases, the surge cloud continues to rise as it expands.

The surges produced in dry sand tend to be consistently higher than surges in dry clay, but the wet clay records are not adequate to show a significant tendency. The relatively smooth appearance of the dry sand growth curves is probably not representative of the actual growth process, but is due to the large time interval between data points.

3.3 EFFECTS OF WIND

Wind conditions may affect the base surge indirectly by altering the rates of growth and fall of the jet. As shown in Fig. 3.11, the jet produced in a strong gusty wind by Round 312 dropped fast and caused a rapid growth of the base surge. With the same charge weight and depth, the jet from Round 309 rose into a relatively light wind and fell slowly, while the base surge expanded at a moderate rate of speed.

Aside from jet effects, the wind shortens the diameter of the surge cloud in a direction parallel to the wind direction so that the surge becomes ovoid before moving bodily downwind. When the surge is completely formed it is shaped like an irregular torus, with the downwind edge much higher than the trailing upwind side.

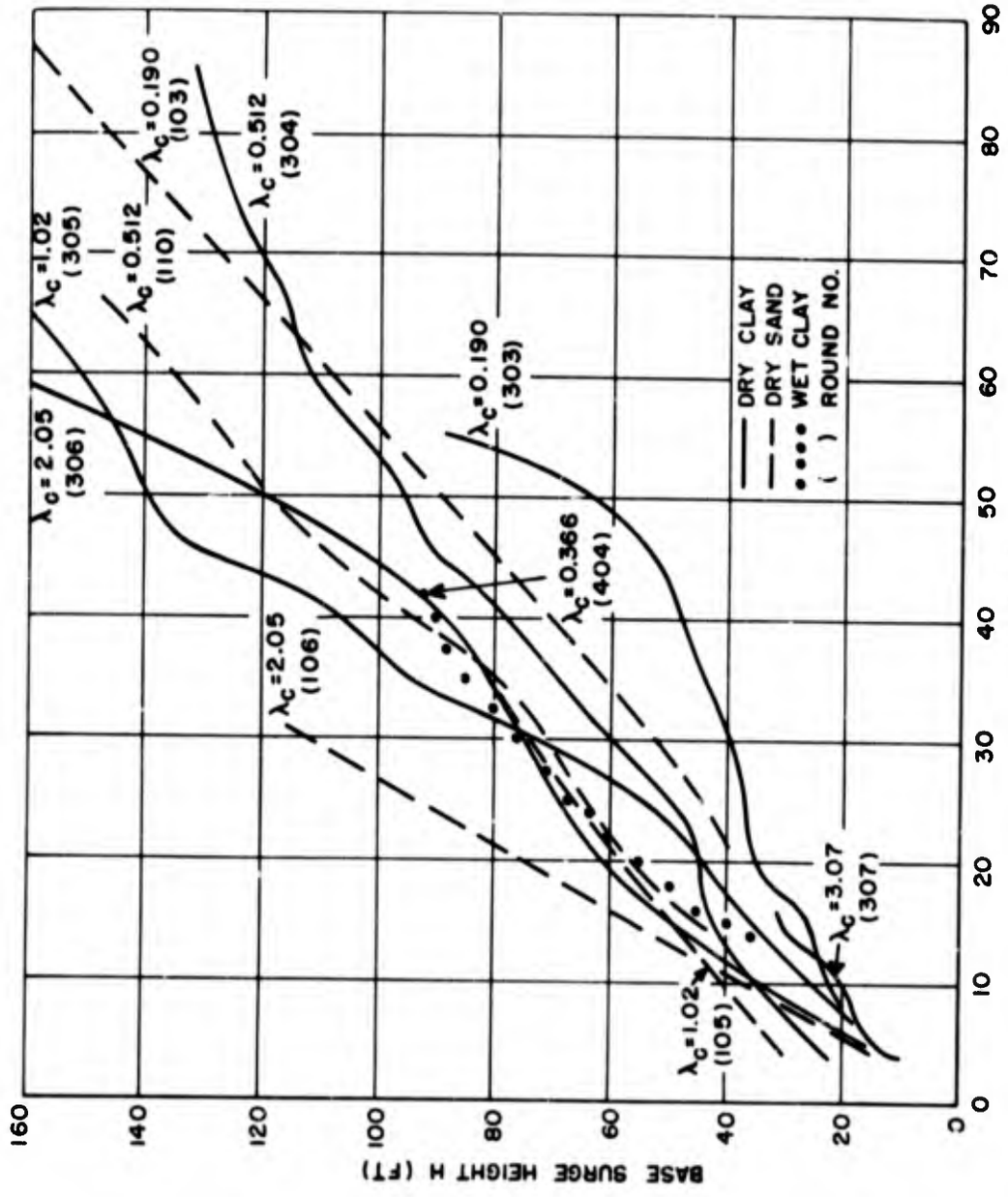

Fig. 3.8 Base Surge Height vs Time - 320 Lb TNT Charges

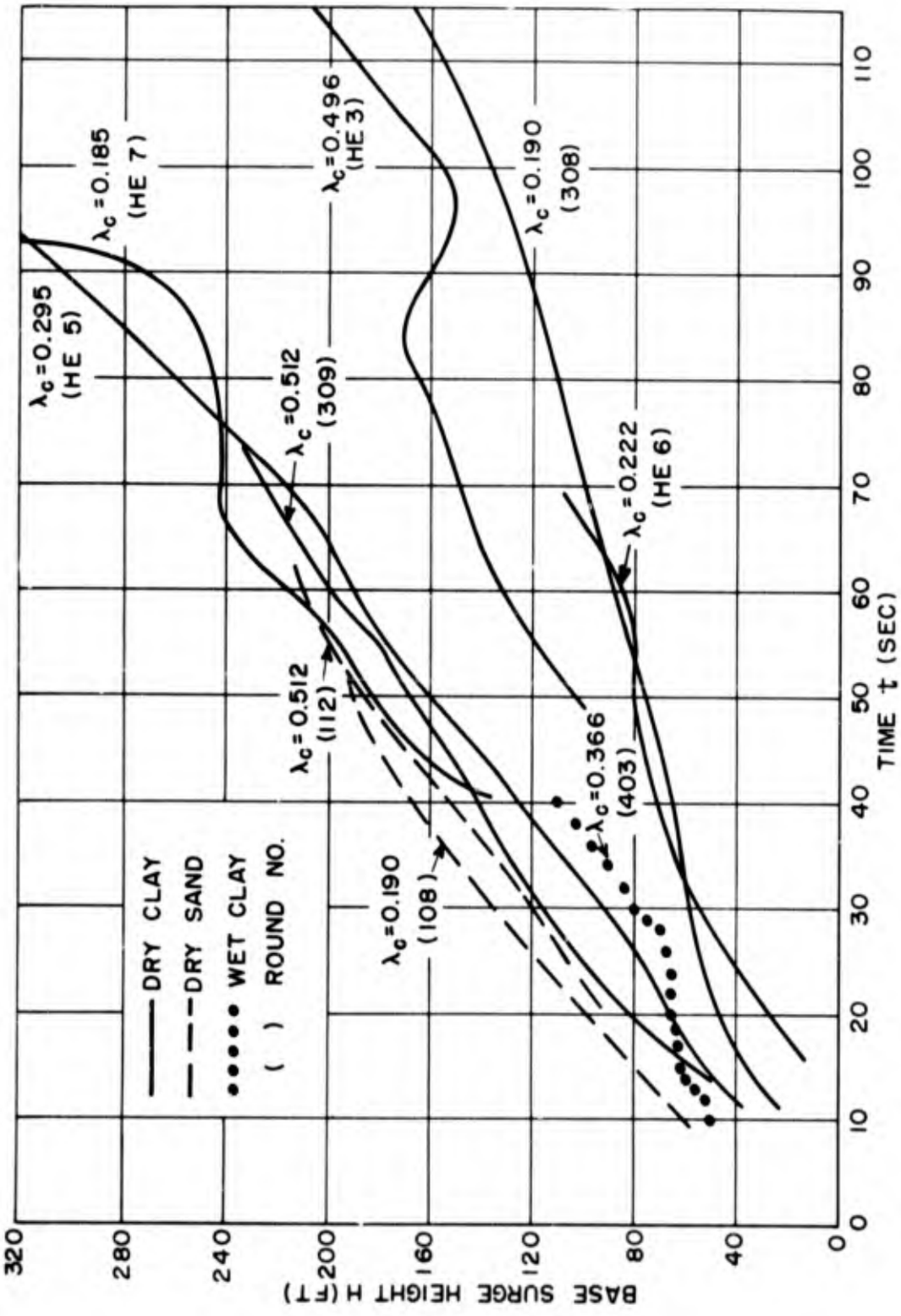

Fig. 3.9 Base Surge Height vs Time - 2,560 Lb TNT Charges

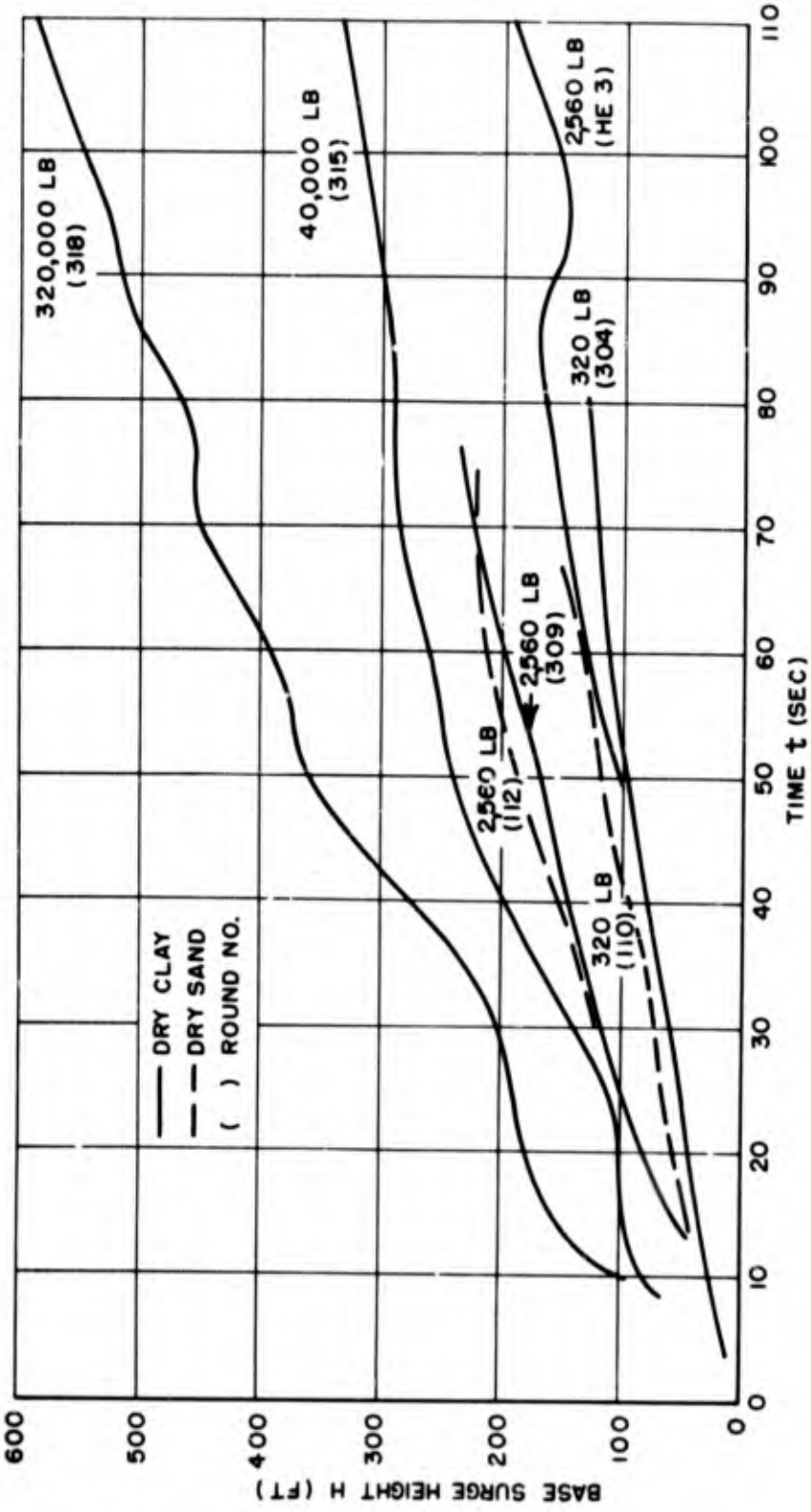

Fig. 3.10 Base Surge Height vs Time - Scaled Depth = 0.5 $Ft/Lb^{1/3}$(TNT)

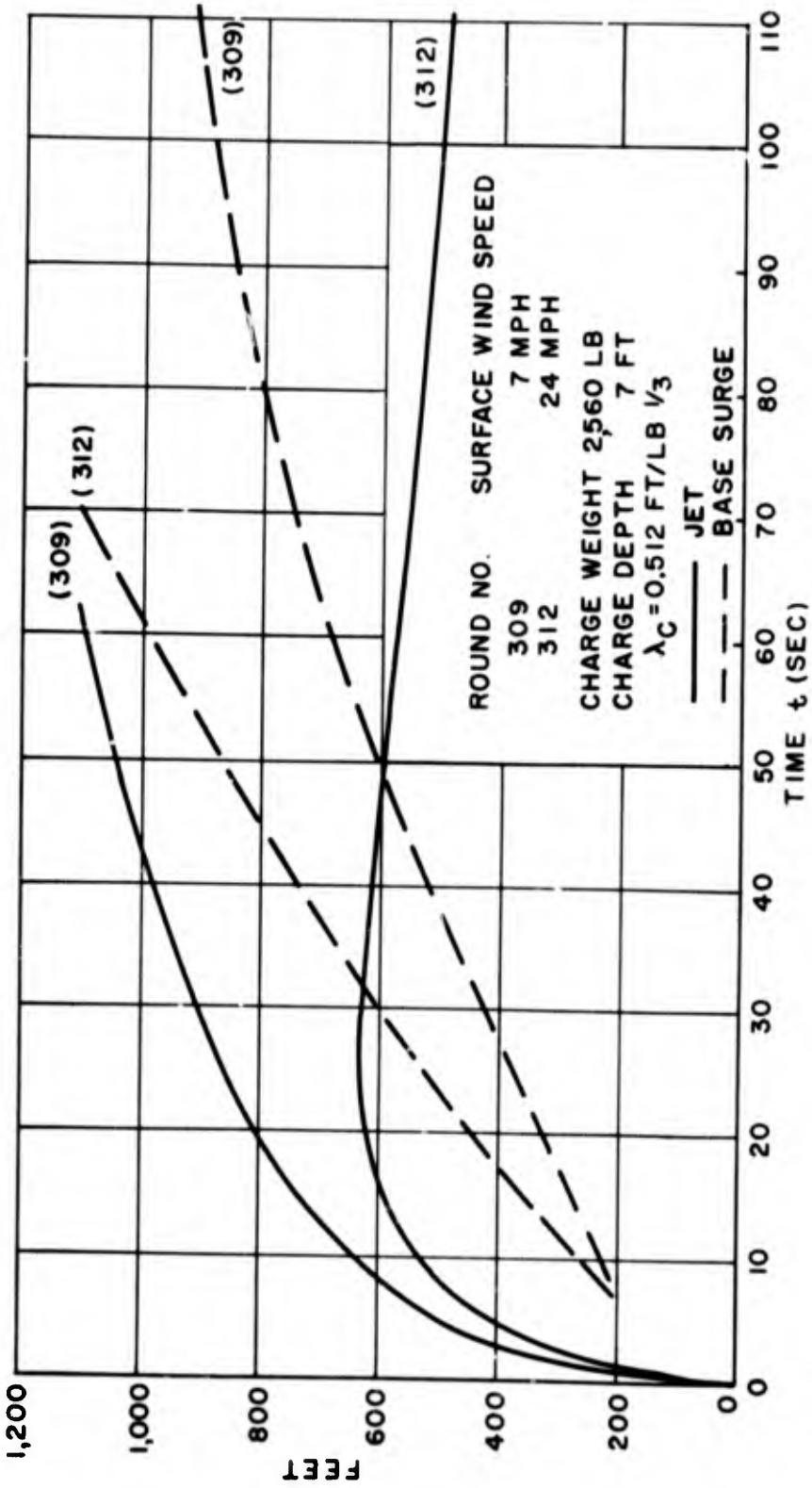

Fig. 3.11 Effect of Wind Speed on Jet and Base Surge

[redacted]

CHAPTER 4

SCALING METHODS

4.1 MODELS

The concept of the bulk subsidence and radial outflow of the aerosol that constitutes the base surge implies that the suspension of dust particles in air can be treated as a fluid, somewhat heavier than air. Consequently it is possible to use some of the techniques of fluid dynamics and apply the laws of similarity to the flow phenomena produced by underground explosions.

The concepts of similarity and models may be applied to base surge phenomena in two possible ways. If complete similarity exists between the surge flow produced by charges of different weights fired at the same scaled depths, the effects of large charges may be predicted by applying appropriate scaling rules to small charge results. Secondly, a better understanding of surge phenomena in general can be obtained if it is possible to simulate the base surge on a laboratory scale with dense liquids or aerosols.

A liquid model has been used with success in the study of the base surges produced by underwater explosions.[1] The model consists of a metal cylinder retaining a column of dense colored solution in the center of a tank of water. When the cylinder is removed suddenly the column descends vertically and flows outward horizontally along the bottom of the tank. Both homogeneous and hollow columns were studied, and the inner and outer diameters, column height, and fluid density were varied.

4.2 FROUDE SCALING OF BASE SURGE RADIAL GROWTH

As equivalence of Froude numbers is a necessary condition for similarity in all cases of flow with a free surface, Froude scaling was used for the initial flow of the surge both in the liquid model and in underwater explosions. It proved to be adequate for comparing the initial rates of growth, indicating that gravitational and inertial forces play the dominant role in establishing the character of the flow. It is

---

[1] A. B. Arons, Experimental Investigations of Base Surge Phenomena, Interim Report No. 1 of NOL Project 152, NAVORD Report 1501, 13 July 1950, pp 6-7.

[redacted]

significant that the explosion results give best agreement with the hollow core liquid models.

A. B. Arons[2] has derived scaling laws for the initial radial propagation velocity of the surge front, obtaining the following parameters:

$$r = \frac{R}{D_{max}} \qquad (4.1)$$

$$\tau = \frac{t}{D_{max}^{1/2}} \qquad (4.2)$$

where r = scaled surge radius (dimensionless)
R = surge radius, ft
D_{max} = maximum column diameter, ft
τ = scaled time, sec/ft$^{1/2}$
t = time, sec

The maximum diameter of the column is used as the characteristic length for scaling purposes. Reducing lengths by the first power of D_{max} and time by the square root of D_{max}, as indicated above, corresponds to Froude scaling. If this procedure is adequate, measurements of the radial growth of the base surge produced by charges fired at the same scaled depth should lie on the same curve when scaled in this manner.

For complete geometrical similarity, the ratios between corresponding lengths in model and prototype should be the same. Therefore, the effective column height and the diameter of the core must be directly proportional to maximum column diameter for this method to be applicable. This proved to be true in the study of underwater explosions, and good agreement was obtained between the scaled surge radius vs scaled time curve for Test Baker at Bikini and the curves obtained from high explosives fired at the same or similar scaled depths, out to about $\tau = 1.5$ sec/ft$^{1/2}$.

The radial growth of the base surges produced by underground explosions in the Dugway dry clay tests and in the Nevada HE program is shown in Fig. 4.1, reduced according to the same Froude scaling parameters.

---

[2] Ibid., pp 2-3.

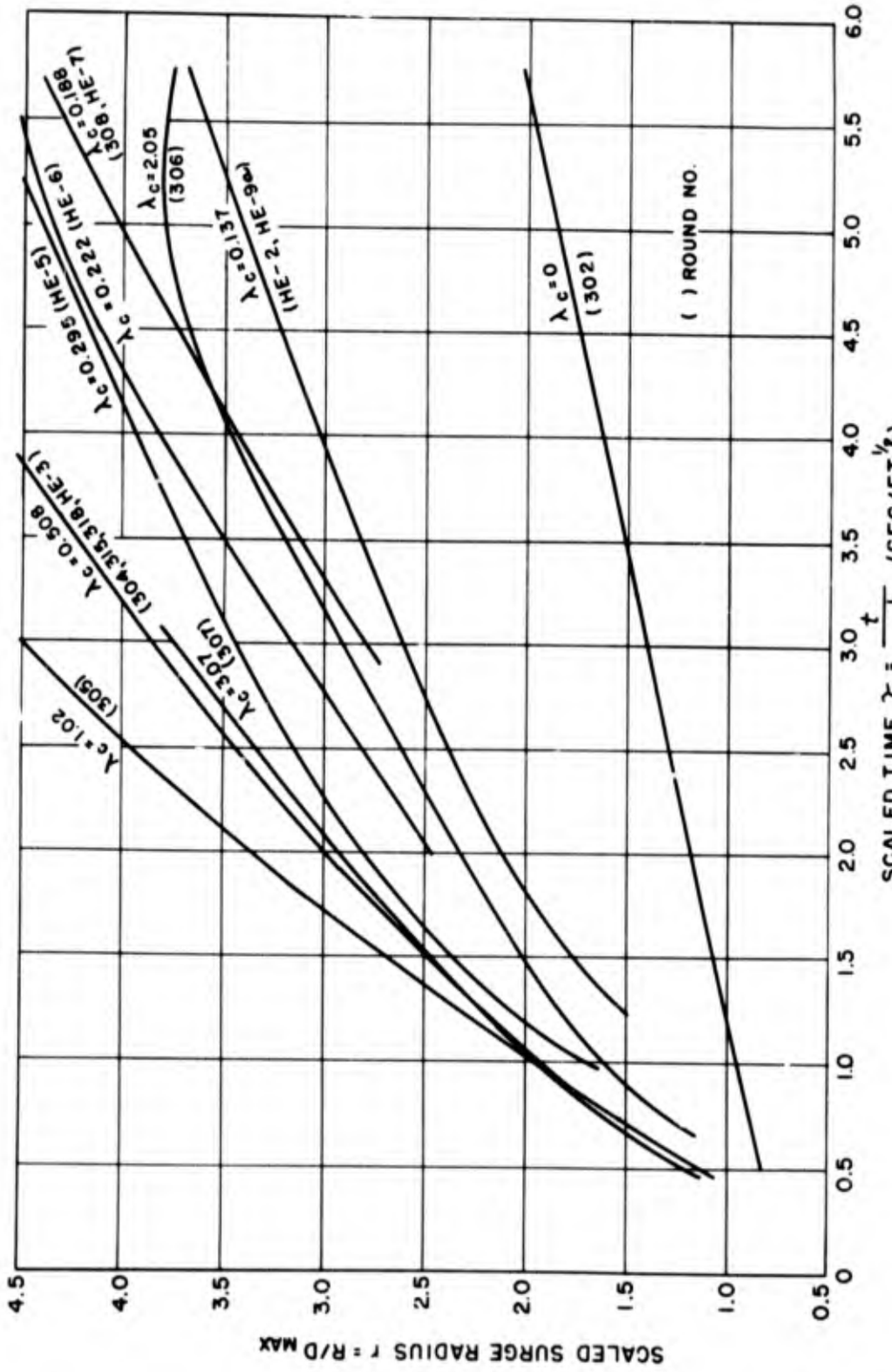

Fig. 4.1 Preliminary Scaling of Radial Growth of Base Surge in Dry Clay

Where available, data for different rounds fired at the same scaled depths were averaged. As the ratio of maximum column height to maximum column diameter is the same (see Section 2.4) for charges fired at the same scaled depth in the same type of soil, the corresponding scaled surge radius vs scaled time curves are similar. Thus it appears that the diameter of the core of the column is directly proportional to the outer diameter for all charges fired at the same scaled depth in the same soil.

Figure 4.1 shows a gradual increase of scaled radial surge growth with increasing values of λ_c to a maximum at 1.02 ft/lb$^{1/3}$, with lower values at greater scaled depths. This is consistent with the measurements of C_{max} in indicating a high initial velocity for the tallest columns. The later portions of the curves show atmospheric effects.

The reason for the apparent inconsistency of the record for Round 307 (λ_c = 3.07 ft/lb$^{1/3}$) is not known, but may be due to differences between the internal structure of the column and the structure of the columns produced by shallower charges.

As the above scaling procedure is not complete, Arons[3] has derived more generalized Froude scaling criteria, defining scaled radius as before and scaled time in the following manner:

$$\tau^* = \frac{t\ (\sigma C_{max})^{1/2}}{D_{max}} \qquad (4.3)$$

where τ^* = scaled time, sec/ft$^{1/2}$

$$\sigma = \frac{\rho - \rho_o}{\rho}$$

ρ = density of moving fluid
ρ_o = density of ambient fluid
C_{max} = maximum column height, ft
D_{max} = maximum column diameter, ft

---

[3] A. B. Arons, G. A. Young, and M. L. Milligan, Further Investigation of the Base Surge, Interim Report No. 3 of NOL Project 152, HAVORD Report 2144, 1 June 1951, pp 4-5.

This more complete scaling does not provide for hollow columns but permits the comparison of records when density ratios and column heights are varied. However, measurements of radial surge growth when reduced in the form of r vs τ^*, should fall on a single curve for all tests with the same ratio of core to outer column diameter.

The modified scaling law does not take into account all of the physical effects of differences between the densities of the moving and ambient fluids. However, when applied to liquid model results, it proved extremely useful in the study of the simulated base surge.[4] The resulting scaled curves are reproduced in Fig. 4.2 and show the following:

(a) For any given σ and ratio of core to column diameter (D_c/D) there is a separate r vs τ^* curve embracing the effects of variation of C_{max} and D_{max}.

(b) The r vs τ^* curves show a lower slope with decreasing ρ (or σ) and increasing D_c/D.

(c) The slope is more sensitive to density changes of a fixed value in the lower density region.

The following relation between τ and τ^* can be obtained:

$$\tau^* = \tau \left(\frac{\sigma C_{max}}{D_{max}} \right)^{1/2} \qquad (4.4)$$

It is also convenient to define a scaled time parameter, which does not include a density term, as follows:

$$\tau' = \tau \left(\frac{C_{max}}{D_{max}} \right)^{1/2} \qquad (4.5)$$

In the scaling of underwater explosion results, the r vs τ data for the initial portion of the Bikini base surge flow was computed, and the values of τ were multiplied by various assumed values of $(\sigma C_{max}/D_{max})^{1/2}$. The resulting curves were compared with similarly scaled liquid model curves and the agreement of slopes proved best

---

[4] Ibid., pp 5-8.

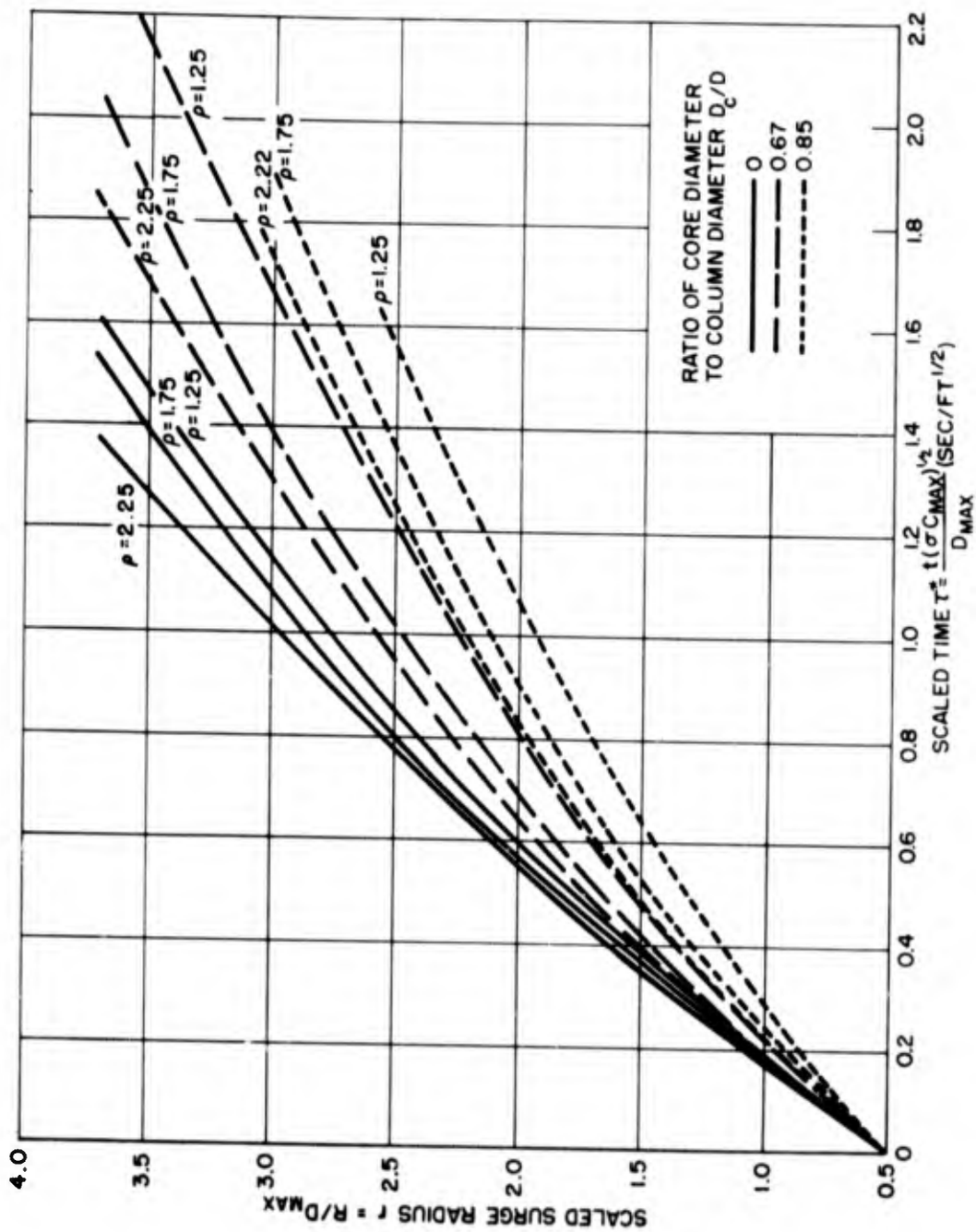

Fig. 4.2 Scaled Liquid Model Results

with liquid models having a water core ratio of about 0.7. The appropriate value of $(\sigma C_{max}/D_{max})^{1/2}$ lay somewhere between 0.77 and 0.88. Since $D^{1/2}$ was equal to 45.1 for Test Baker, the corresponding values of $(\sigma C)^{1/2}$ for the Baker column were between 35 and 39. This permitted a calculation of the probable range of density and height of the Baker column, and the estimate was made that the ratio of column density to ambient density was about 1.5, with an effective column height of about 4000 ft and a core ratio of about 0.7.[5]

As the values of maximum column height are known for the underground explosion data plotted in Fig. 4.1, a first step toward a more complete scaling is the multiplication of the known values of τ by the square root of the ratio of C_{max} to D_{max} for each scaled depth. (See Fig. 2.8.) As the measured ratio for Round HE-6 ($\lambda_c = 0.222$) appeared to be doubtful, a value of 0.685 was obtained from the smoothed curve and substituted for the recorded ratio. The resulting r vs τ' curves are shown in Fig. 4.3.

The separation in these partially scaled curves should be due only to differences in D_c/D and the bulk density of the material in the column that forms the base surge. Neither of these quantities has been measured, but if one could be determined it might be possible to estimate the magnitude of the other, for a particular scaled depth.

If the assumption is made that the diameter of the core is equal to the true crater diameter, it is possible to estimate the ratio of core to outer column diameter (D_c/D) for the rounds used to obtain the curves shown in Figs. 4.1 and 4.3. The mean values of the ratios of true crater diameter to maximum column diameter given in Fig. 6.3 are generally intermediate between the values of D_c/D for which liquid model results are available. As the crater-column ratio is equal to 0.46 for charges scaled to 0.508 ft/lb$^{1/3}$, interpolated liquid model curves for $D_c/D = 0.46$ are presented in Fig. 4.4 for comparison with the scaled explosion surge curves.

If column heights, column diameters, core diameters, and ratios between the densities of the earth columns and the surrounding air were known accurately, the scaled curves for explosion base surge growth would be identical with scaled curves obtained from geometrically similar liquid models with the same ratios between column and ambient densities, providing that the use of Froude scaling is valid.

This ideal situation does not exist, and many simplifying assumptions have been made, but by applying the trial-and-error process of assuming

---

[5] Ibid., pp 12-13.

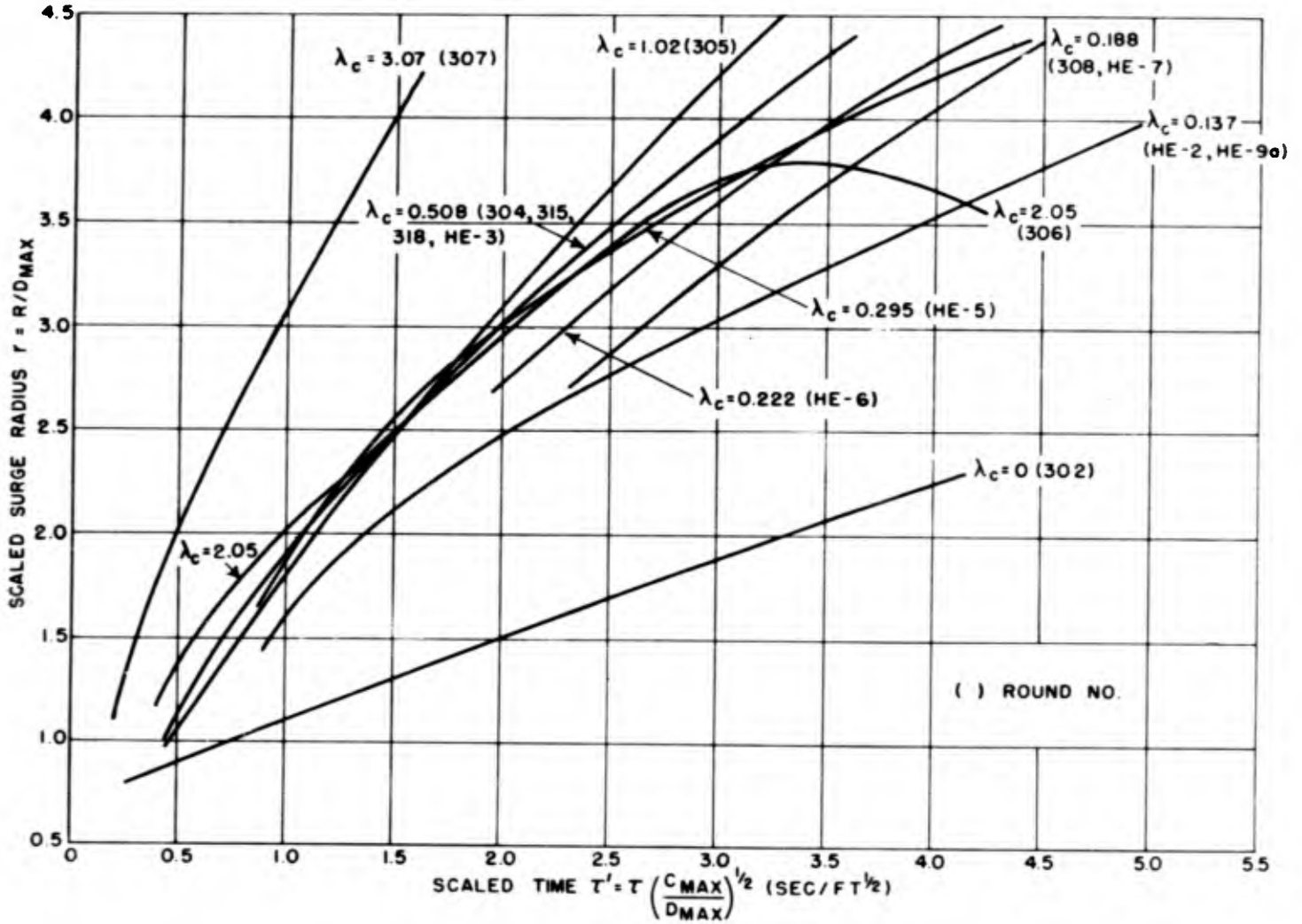

Fig. 4.3 Scaling of Radial Growth of Base Surge in Dry Clay with Column Height Effect Included

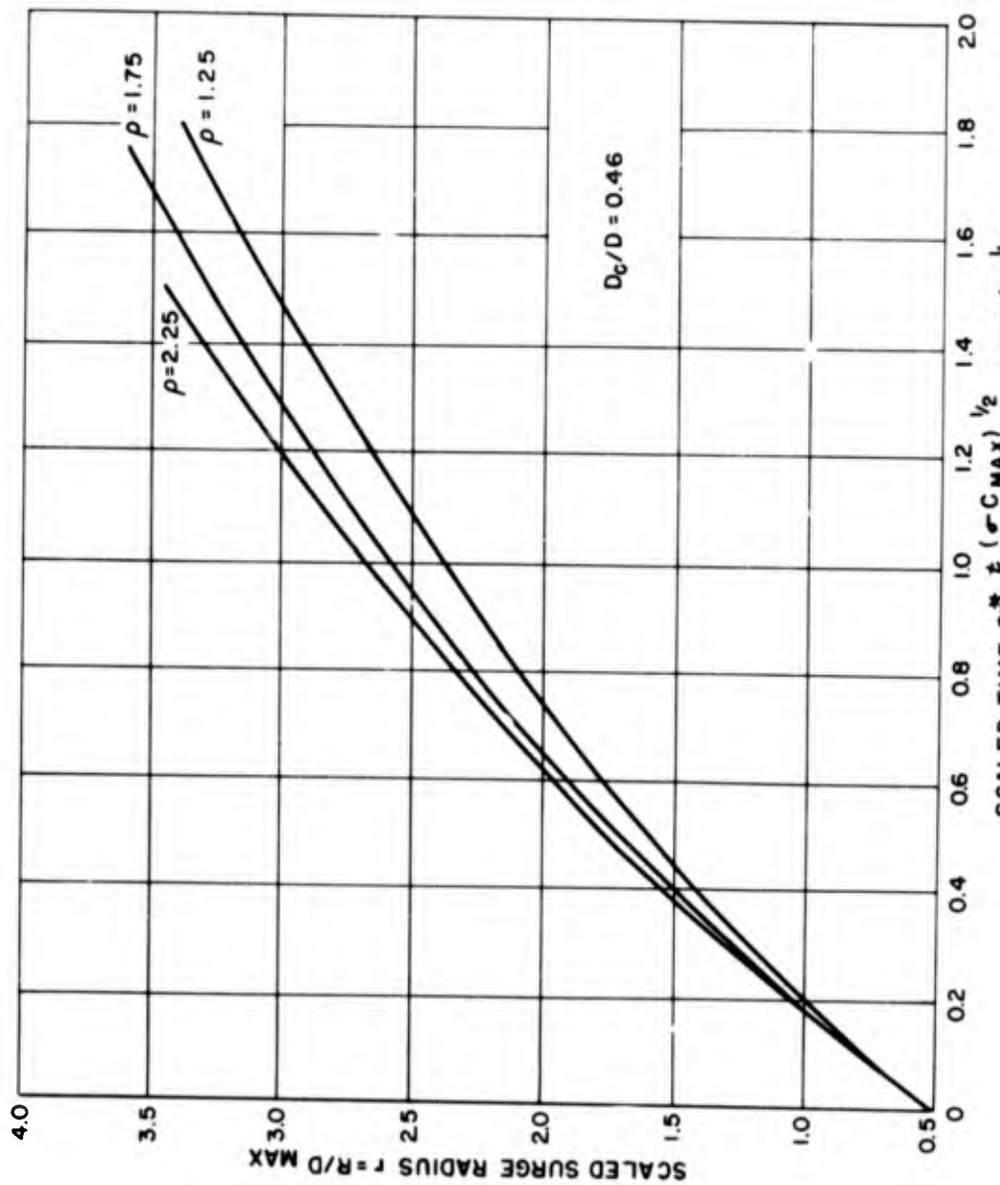

Fig. 4.4 Interpolated Scaled Liquid Model Curves for a 0.46 Ratio of Core Diameter to Column Diameter

different density values for the earth columns and multiplying the values of τ' in Fig. 4.3 by the computed values of $\sigma^{1/2}$ it is possible to obtain r vs τ^* curves for the explosions to compare with the liquid model curves. As the origin of time for the liquid model curves in Figs. 4.2 and 4.4 is the instant at which the surge emerges from the base of the column, the partially scaled curves in Fig. 4.3 should be extrapolated to find the time at which the scaled surge radius is equal to 0.5 and this time used as the actual origin for τ^*.

The corrected scaled curve for a scaled depth of 0.508 ft/lb$^{1/3}$ is given in Fig. 4.5 with derived curves for several possible values of column specific gravity. The most consistent agreement between curves with the same density ratio in liquid model and prototype occurs with an assumed ρ/ρ_0 of about 1.9. This would indicate that the aerosol in the earth column which contributes to the formation of the base surge has about 1.9 times the density of the surrounding air, when high explosive charges are fired at a scaled depth of about 0.5 ft/lb$^{1/3}$.

The mean scaled radius vs scaled time data for this value of λ_c was obtained from measurements of Rounds 304, HE-3, 315, and 318. Atmospheric density was computed for the time of firing of these rounds, using meteorological data obtained at Dugway[6] and Nevada,[7] and was found to be 0.0657, 0.0632, 0.0645, and 0.0632 lb/cu ft respectively. In accordance with the density ratio of 1.9 obtained from the comparison of scaled curves, the bulk densities of the aerosols in the columns were approximately 0.125, 0.120, 0.123, and 0.120 lb/cu ft. Using mean densities of 0.122 lb/cu ft for columns and 0.0642 lb/cu ft for the atmosphere, and the column dimensions presented previously, it is possible to compute the approximate weight of finely divided soil in the columns formed by these rounds that produced the base surge. These values are listed in Table 4.1.

---

6 Instrumentation for Underground Explosion Test Program, Interim Technical Report No. 1, Dry Clay, Engineering Research Associates, Inc., Contract No. DA-04-167-eng-298, 1 Aug. 1951, pp 4-9 to 4-85.

7 D. C. Campbell, LCDR, USN, Tests and Observations on Craters and Base Surges, JANGLE Report 1(9)-3, 1 Nov. 1951.

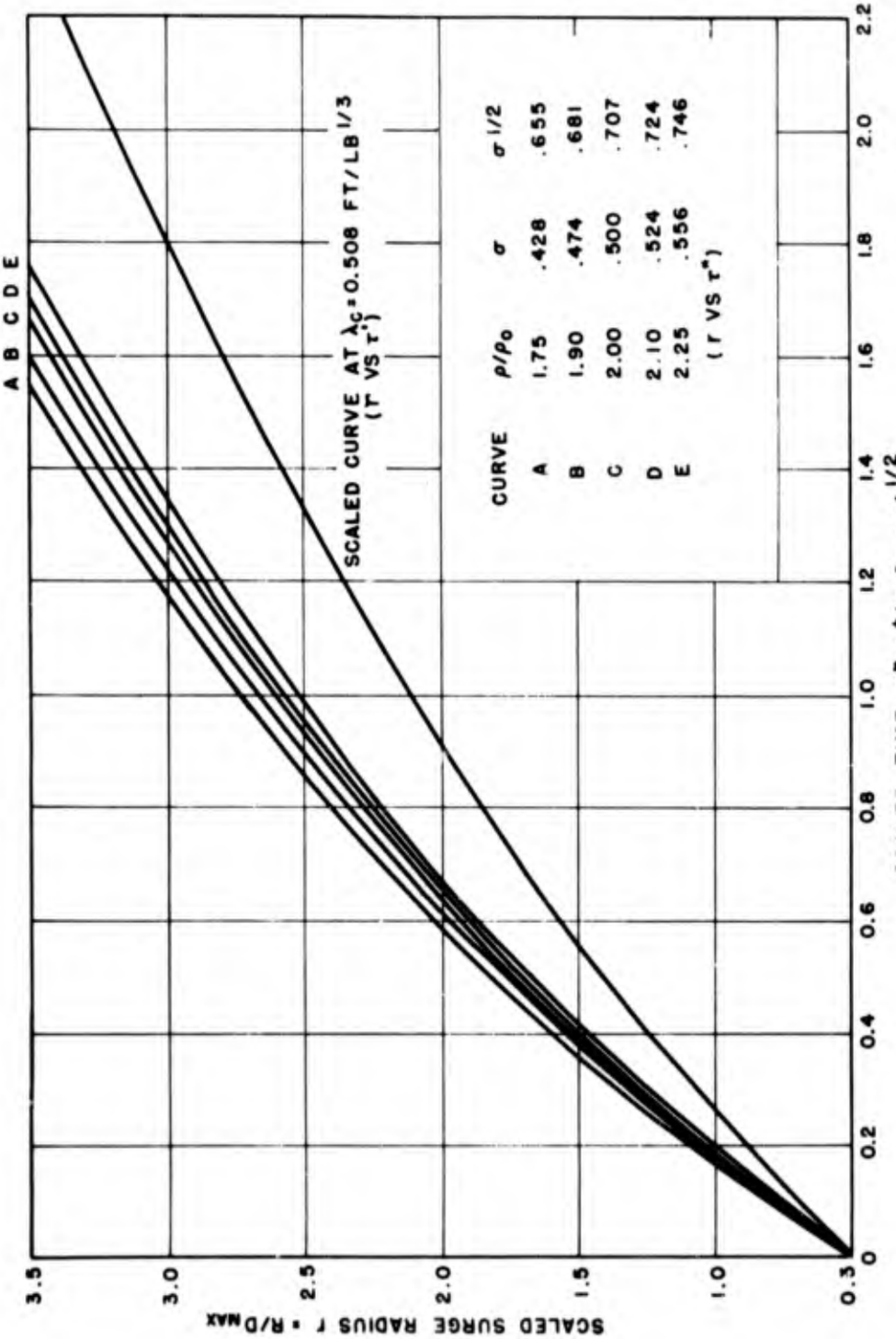

Fig. 4.5 Scaled Radial Growth of Base Surge in Dry Clay at Scaled Depth of 0.508 Ft/Lb$^{1/3}$ with Assumed Values of Column Density

TABLE 4.1

Estimated Weights of Soil in Base Surges for Rounds Fired at a Scaled Depth of 0.5 ft/lb$^{1/3}$

Round	Charge Weight (lb TNT)	Soil Weight (lb)
304	320	8,950
HE-3	2,560	53,400
315	40,000	529,000
318	320,000	2,980,000

The relation between weight of soil in the column aerosols produced by charges fired at λ_c = 0.5 ft/lb$^{1/3}$ and charge weight may be expressed in the following manner:

$$S = 77.4\ W^{0.833} \quad (\lambda_c = 0.5\ \text{ft/lb}^{1/3}) \tag{4.6}$$

where S = weight of soil that forms the base surge, lb
W = charge weight, lb (TNT)

The scaled curves for λ_c = 1.02 and 0.295 ft/lb$^{1/3}$ given in Fig. 4.3 are similar to the curve for λ_c = 0.508 ft/lb$^{1/3}$ to a scaled surge radius of about 3.0, and the ratios of true crater diameter to maximum column diameter are not greatly different. Therefore the ratio of the bulk density of the column aerosols to atmospheric density for charges at these scaled depths is probably approximately equal to 2.0 also. In view of the scarcity of data at these scaled depths and the assumptions necessary in the application of the scaling method, an attempt to compute the density ratio more closely would not be justified.

The shapes of the curves and probable values of D_c/D indicate that the column and initial surge density increase with increasing charge depth. The inconsistency of the scaled curve at λ_c = 3.07 ft/lb$^{1/3}$ indicates that this scaling method is not applicable at relatively great depths, without additional knowledge of column structure.

The rapid decrease in the slope of the scaled curve for a λ_c value of 0.137 ft/lb$^{1/3}$ in Fig. 4.3 indicates that frictional drag becomes effective very soon after the base surge forms at this scaled depth. A

more elaborate scaling technique would be required to study this type of flow.

The relatively straight curve for λ_c = zero shows that the gravity flow is relatively brief and ineffective and that almost all of the growth of the surge cloud at this shallow position is probably due to turbulent mixing with the surrounding air.

4.3 SIMILARITY TO UNDERWATER RESULTS

It is of interest to note that the r vs τ curves for underground explosions at λ_c = 0.508 agree very closely with the scaled curve for the growth of the base surge produced by the underwater atomic test (Baker) at Bikini out to about r = 2.0. The base surge formed by the underwater atomic explosion expanded at a relatively slower rate from there on.

Arons' estimate of a column density of 1.5 times the density of the surrounding air for Test Baker and the estimate by Martin and Moyce[8] of a ρ/ρ_o of 1.75 for the same test are not significantly different from the ρ/ρ_o value of 1.9 calculated for the soil columns produced at a scaled depth of 0.508 ft/lb$^{1/3}$.

These results indicate a similarity between the physical processes of base surge formation by underwater and underground explosions and show that liquid model experiments can be used successfully in the study of both types. Thus, theoretical and experimental results obtained in the investigation of one form of surge will be of value in the study of analogous phases of the other.

---

[8] J. C. Martin and W. J. Moyce, "An Experimental Study of the Collapse of Fluid Columns on a Rigid Horizontal Plane, in a Medium of Lower, but Comparable, Density", Philosophical Transactions of the Royal Society of London, Series A, No. 882, Vol 244, 4 March 1952, p 333.

[redacted]

CHAPTER 5

AREA OF DUST DEPOSIT

5.1 ANALYSIS OF DATA

The Armour Research Foundation of the Illinois Institute of Technology investigated the dispersion of dust from underground explosions at Dugway under subcontract to Engineering Research Associates, Inc.[1] As part of the instrumental program, settlement gages were placed at a number of points surrounding the explosion sites, in order to obtain a record of dust-fall distribution by weight. Polar graphs of settlement data were presented in Interim Technical Reports No. 1,[2] 2,[3] and 3[4] showing lines of constant dust-fall weights around the point of the explosion for three types of soil. The lines represent values of 0.5, 1.0, 5.0, 10, 50, 100, 500, 1000, 3000 and 6000 grams per square meter.

In most cases the graphs showed a roughly circular dust distribution around the crater with a tongue of deposited dust extending downwind. Considerable smoothing and extrapolation were necessary in the preparation of the charts; and the size and shape of the areas of dust fall and the uniformity of dust coverage were greatly affected by wind and atmospheric turbulence. Because of these effects, the data presented are subject to considerable scatter and are not always comparable, but are considered adequate for showing the important trends.

Although these data represent total dust deposit from the radial throwout and all parts of the dust cloud, the maximum extent of deposit

---

[1] Instrumentation for Underground Explosion Test Program, Interim Technical Report No. 1, Dry Clay, Engineering Research Associates, Inc., Contract No. DA-04-167-eng-298, 1 Aug. 1951, pp 4-1 to 4-7.

[2] Ibid., pp 4-86 to 4-108.

[3] Instrumentation for Underground Explosion Test Program, Interim Technical Report No. 2, Dry Sand, Engineering Research Associates, Inc., Contract No. DA-04-167-eng-298, 1 Oct. 1951, pp 4-47 to 4-57.

[4] Instrumentation for Underground Explosion Test Program, Interim Technical Report No. 3, Wet Clay, Engineering Research Associates, Inc., Contract No. DA-04-167-eng-298, 1 Nov. 1951, pp 4-31 to 4-37.

[redacted]

probably coincides closely with the limit of radial surge growth along the ground, except possibly in the downwind direction when the upper winds are strong. As the determination of the absolute boundaries of dust-fall is probably impossible, particularly when a small amount of airborne dust is present, greater objectivity is attained by measuring the area containing a dust deposit equal to or greater than some fixed low value. It seems justified to assume that the area enclosed by a line of low dust-fall, such as 0.5 grams per square meter, is closely related to the size of the surge cloud. However, correlating these dust data with surge extent is not valid when the base surge is relatively small and poorly defined, as occurs with shallow charges (scaled depths less than 0.2 $ft/lb^{1/3}$).

To compare these data with the base surge analysis, the areas inside the lines representing dust deposits of 0.5 and 50 grams per square meter were measured at NOL with a planimeter, using the A.R.F. analysis. The areas obtained from the A.R.F. charts are listed in Table 5.1. Data for the 320 lb and 2560 lb charges are shown in Fig. 5.1 as a function of scaled depth (λ_c). The plotted data for the 320 lb dry clay and dry sand series are consistent with base surge growth data in showing the greatest area of deposit when $\lambda_c = 1.0$.

Charges fired in dry sand produced greater areas of dust-fall than charges fired at the same scaled depths in dry clay, and the two data points for Rounds 402 and 404 indicate that charges fired in wet clay yield the smallest areas of dust-fall. These results are consistent with base surge measurements and support the hypothesis that dry sand is the most favorable of the three Dugway soils for producing a base surge and wet clay the least.

The relatively large areas for Rounds 102 and 302 can not be considered to represent surge growth but are due chiefly to the broad dust columns of low density which fell slowly and were easily transported by the wind.

A careful analysis of data from a dense network of settlement gages should show a heavy fallout of large particles near the crater and in the downwind path of the jet and column and a more uniform light deposit in the area traversed by the surge. A complete analysis of this type is not possible with the available data, but a plot of deposit weights against area for Rounds 309 and 312 ($\lambda_c = 0.512$) on rectilinear graph paper shows a pronounced change in slope between the dust-fall values of 10 and 50 grams per square meter. Assuming that the 30 gram per square meter line marked the approximate extent of the heavy vertical fallout from the jet and column, the data show that this fallout accounted for less than 15% of the total area of deposit in both cases. At this scaled depth, the passage of the surge cloud and the gradual settlement of finer particles from the jet and smoke crown probably were responsible for over 85% of

TABLE 5.1

Areas of Dust Deposit for Dugway Underground Explosion Tests

Round	Charge Weight (lb TNT)	Soil Type	Area of Dust-fall		Wind Speed (mph)
			≥ 50 gm/sq m (sq ft)	≥ 0.5 gm/sq m (sq ft)	
302	320	Dry Clay	44,800	1,230,000	13
303	320	Dry Clay	47,900	386,000	4
304	320	Dry Clay	92,500	1,860,000	6
305	320	Dry Clay	135,000	2,720,000	7
306	320	Dry Clay	23,000	213,000	8
308	2,560	Dry Clay	500,000	17,200,000	3
309	2,560	Dry Clay	---	38,200,000	7
310	320	Dry Clay	102,000	1,720,000	10
312	2,560	Dry Clay	534,000	13,600,000	24
313	320	Dry Clay	122,000	1,690,000	15
315	40,000	Dry Clay	3,980,000	35,100,000	3
318	320,000	Dry Clay	21,500,000	223,000,000	4
102	320	Dry Sand	48,400	---	4
103	320	Dry Sand	95,800	---	2
105	320	Dry Sand	229,000	5,250,000	5
106	320	Dry Sand	39,900	408,000	2
108	2,560	Dry Sand	530,000	16,900,000	11
110	320	Dry Sand	130,000	5,210,000	5
112	2,560	Dry Sand	530,000	---	6
115	40,000	Dry Sand	5,960,000	---	12
402	320	Wet Clay	238,000	---	16
404	320	Wet Clay	200,000	---	22

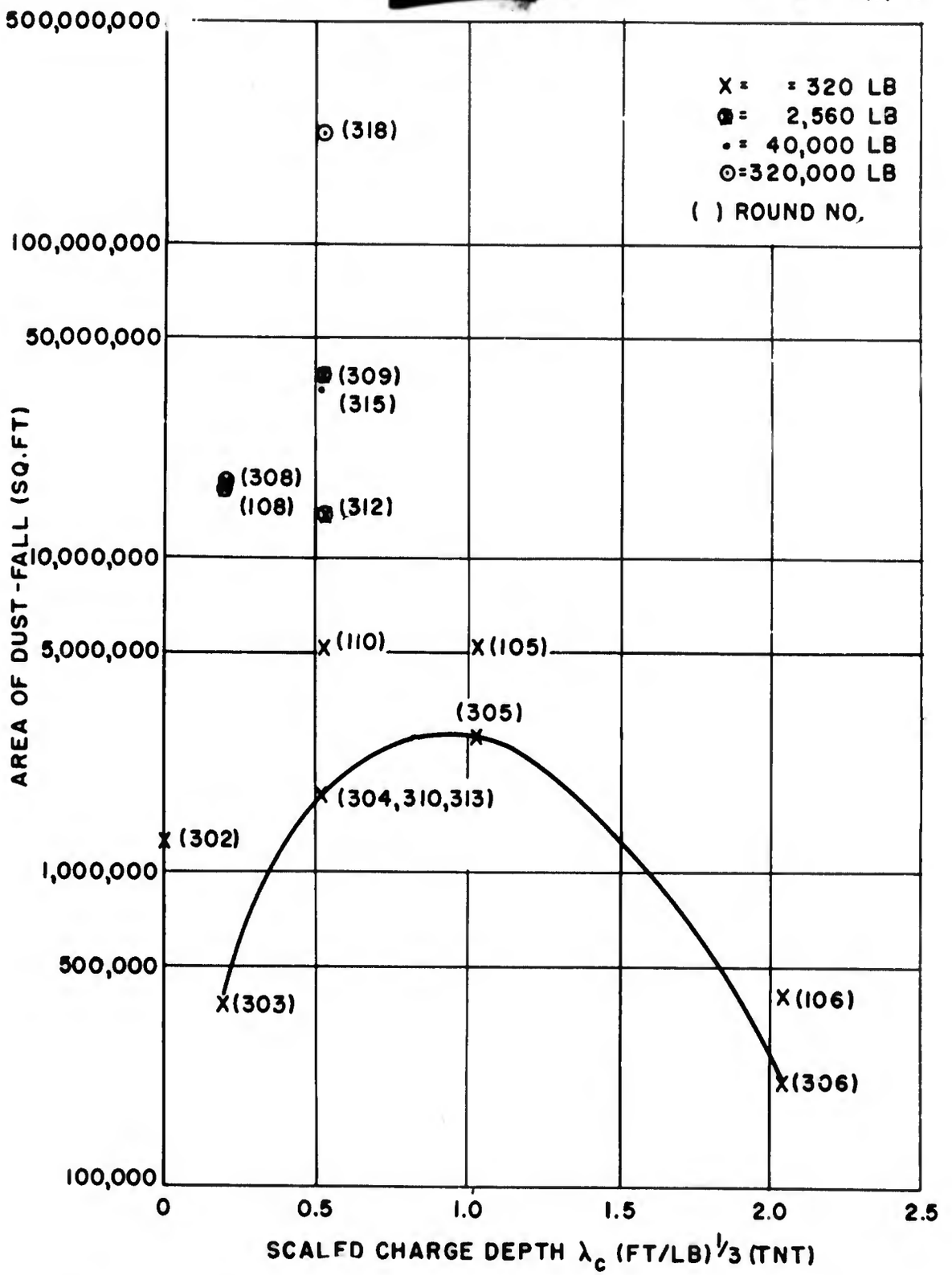

Fig. 5.1 Area of Dust-Fall = 0.5 gm/sq m vs Scaled Charge Depth

the dust-fall area.

5.2 METEOROLOGICAL EFFECTS

The available data are not adequate for a complete study of the effects of wind and atmospheric stability on the dispersal of the various parts of the surface phenomena and the consequent areas of dust-fall, but some purely qualitative results can be obtained.

In general, an increase in wind speed indicates a decrease in the area traversed by the surge cloud and an increase in the area of fall-out from the column. This effect is shown by the data in Table 5.1 for Rounds 304, 310, and 313 (320 lb charges at a 3.5 ft depth in dry clay; $\lambda_c = 0.512$ ft/lb$^{1/3}$), assuming that the area covered by more than 50 grams per square meter of dust is roughly indicative of the fallout region and the area between the 0.5 and 50 grams per square meter lines is representative of the base surge settlement.

The same effect appears for Rounds 309 and 312, both 2560 lb charges fired at a 7 ft depth in dry clay ($\lambda_c = 0.512$ ft/lb$^{1/3}$). Rounds 309 and 312 were fired with 7 and 24 mph surface winds respectively. For Shot 309 the line of 0.5 gram per square meter dust-fall enclosed a broad tongue extending 9430 ft downwind from the crater with a total area of 1.37 sq mi, while Shot 312 produced a relatively narrow tongue with the same dust-fall, extending 7390 ft downwind and including a total area of 0.489 sq mi. In this case the area covered by dust weighing 0.5 grams per square meter or more was about three times as great with a relatively light wind as with a strong wind. However, the area of heavy dust-fall was greater for 312 than 309, indicating a greater uniformity of deposit with the stronger wind. The distribution of dust-fall by weight for both rounds is shown in Fig. 5.2.

These results are consistent with the experience of the Chemical Warfare Service in the study of the behavior of clouds of heavy toxic gases.[5] The CWS data show a decrease in contaminated area with increasing wind speed but also show a dependence upon atmospheric stability. At the same wind speed, contaminated areas are greater when the air is stable than when it is unstable. The effect of wind speed on deposit area is greater when the air is stable.

---

[5] W. M. Latimer, "Behavior of Gas Clouds", Military Problems with Aerosols and Nonpersistent Gases, Summary Technical Report of Division 10, NDRC, Vol 1, Washington, D. C., 1946, pp 260-283.

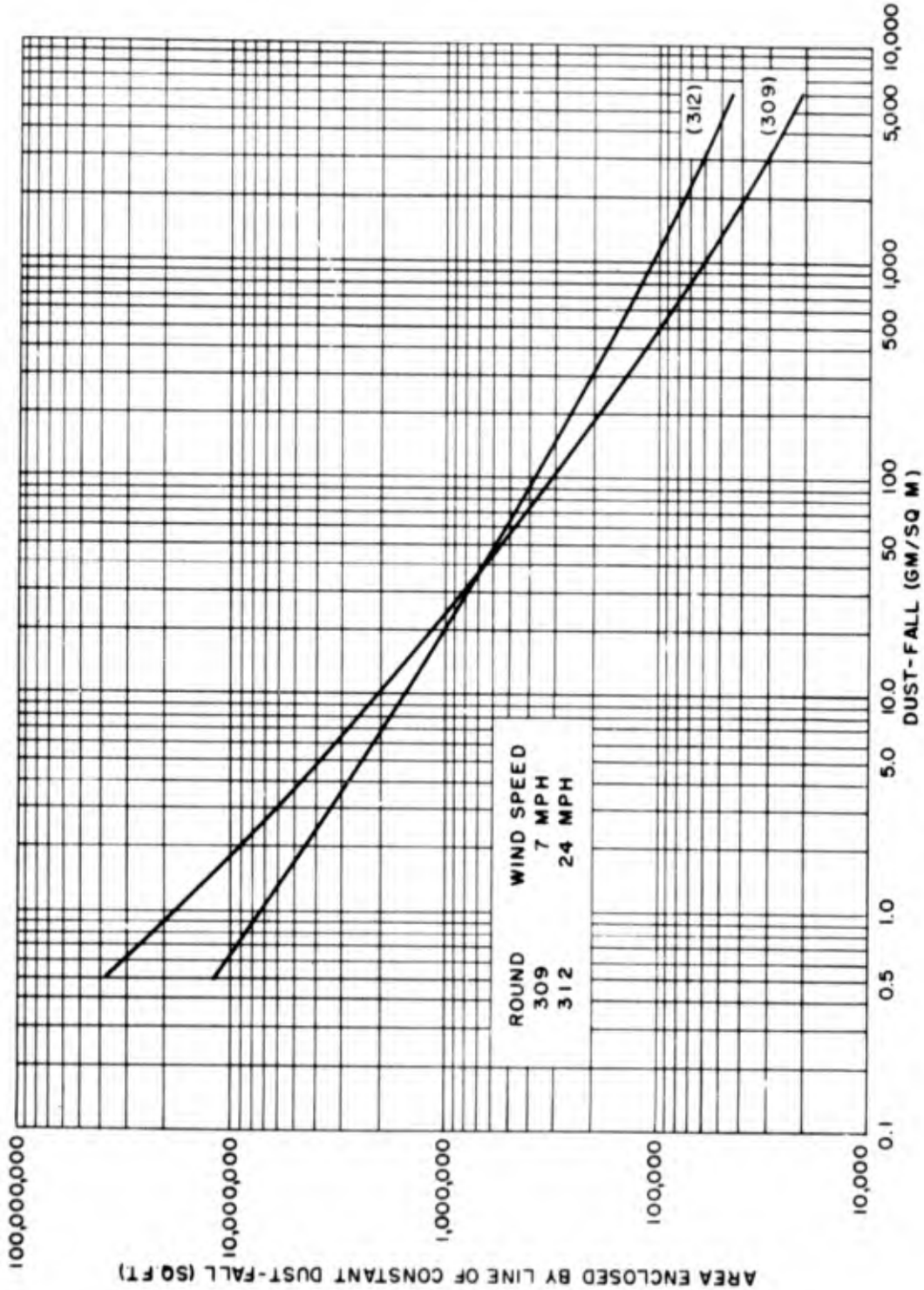

Fig. 5.2 Effect of Wind Speed on Distribution of Dust-Fall

As the correlation of areas of dust-fall from underground explosions with a single observation of wind speed is an oversimplification, it will be helpful to examine the character of the wind and the general state of local weather for Rounds 309 and 312 in order to gain some insight into the character of atmospheric stability and turbulence when the charges were fired.

Round 309 was exploded at 1106:30 MST on 18 April 1951. The surface wind direction varied from 140° to 50° about the time of the shot but a pilot balloon ascension after the burst indicated a surface wind from 280° at 7 mph and a 1000 ft wind from 280° at 6 mph. The U. S. Weather Bureau Daily Weather Map showed a weak low pressure area in the Utah region on 18 April, with showers and thunderstorms starting in the late evening. These wind and weather conditions show a slowly varying light wind and probable thermal instability in the Dugway region.

Round 312 was fired at 1621:20 MST on 4 May 1951. The surface wind instruments were not operating but a pilot balloon ascension at 1322 MST showed a surface wind from 180° at 30* mph and a 1000 ft wind from 190° at 40 mph. After the shot no release was made, due to the high and gusty surface winds. The photographs of the shot show an altocumulus overcast at Dugway. The gustiness and pronounced wind shear in the vertical combined with the overcast sky indicate considerable mechanical turbulence with little or no thermal instability.

The fluctuations of wind velocity indicate directly the turbulent motion of the atmosphere and provide information on the nature and size of the eddies which form in the turbulent air. In general the low frequency components of the velocity fluctuations indicate large diameter eddies and the higher-frequency components represent small eddies, or those in more rapid eddy-motion.[6] The dispersal of a particulate cloud depends upon the relative size of the predominant eddies.

The wind data and probable vertical convection on the day Round 309 was fired indicate the presence of relatively large, slowly-moving eddies, which were able to disrupt the dust cloud after gravitational

---

* The value of 24 mph assigned to the time of the shot was obtained by triangulation of the dust cloud movement shown by E.R.A. still photographs.

[6] S. W. Grinnell, W. A. Perkins and F. X. Webster, Bimonthly Report No. 3 of Chemical Warfare Service Research and Development Program, Contract No. W-18-035-CWS-1256, Stanford Univ., Calif., May - June 1946, p 26.

flow had effectively ceased and spread it over a wide area. The path of an airborne particulate cloud is difficult to predict in this type of meteorological condition. The atmospheric eddies on 4 May were probably smaller than the Round 312 dust cloud and did not have the same effect.

The base surge and resulting dust clouds for Rounds 309 and 312 are shown in Fig. 5.3. The jet produced by Shot 309 rose to a great height and became diffuse, contributing only part of its material to the base surge. The surge cloud ultimately rose from the ground and gradually mixed with the air. The jet from Round 312 was shorter and fell rapidly, probably contributing all of its material to the base surge, which grew at an exceptionally fast rate and tended to hug the ground surface without rising appreciably. The strong wind and turbulence caused a more uniform distribution of dust than for Round 309.

Jet height and surge radius for the two rounds are shown as functions of time in Fig. 3.11.

Fig. 5.3 Effect of Wind Speed on Surface Phenomena

[redacted]

CHAPTER 6

CRATER ANALYSIS

6.1 EFFECT OF SCALED CHARGE DEPTH ON CRATER DIMENSIONS

A study of the size of the true and apparent craters formed by underground explosions gives some insight into the mechanism of ejection of soil into the air and its subsequent fall-back. In particular, the weight of soil that enters the airborne dust cloud can be estimated fairly directly by using crater dimensions.

Crater measurements for the Dugway Tests were obtained from E.R.A. Interim Technical Reports No. 1,[1] 2,[2] and 3[3] and data on the Nevada high-explosive tests from JANGLE Report 1(9)-3, by LCDR. D. C. Campbell.[4]

To study some of the effects of charge weight and depth, the assumption can be made that the volume of the apparent crater remaining after a charge is fired indicates the approximate amount of soil that is ejected from the crater and enters the column, jet, smoke crown, and base surge. Inaccuracies are introduced by changes in soil density, and probably only a small percentage of this ejected soil remains aloft for more than a few seconds, but a comparison of the soil volumes ejected at different scaled depths gives an indication of the relative effectiveness of various charge positions for producing dust-cloud phenomena. The amount of soil falling directly back into the crater and lip can be

---

[1] Instrumentation for Underground Explosion Test Program, Interim Technical Report No. 1, Dry Clay, Engineering Research Associates, Inc., Contract No. DA-04-167-eng-298, 1 Aug. 1951, pp 2-12.

[2] Instrumentation for Underground Explosion Test Program, Interim Technical Report No. 2, Dry Sand, Engineering Research Associates, Inc., Contract No. DA-04-167-eng-298, 1 Oct. 1951, pp 2-18.

[3] Instrumentation for Underground Explosion Test Program, Interim Technical Report No. 3, Wet Clay, Engineering Research Associates, Inc., Contract No. DA-04-167-eng-298, 1 Nov. 1951, pp 2-8.

[4] D. C. Campbell, LCDR, USN, Tests and Observations on Craters and Base Surges, JANGLE Report 1(9)-3, 1 Nov. 1951.

[redacted]

estimated by obtaining the difference between the real and apparent crater volumes and adding the lip volume, but it is assumed that this direct fall-back has a negligible effect on the surface flow phenomena.

Figure 6.1 is a plot of apparent crater volume vs scaled depth and shows a maximum volume of about λ_c = 1.0 ft/lb$^{1/3}$ for 320 lb charges fired in dry sand. The remaining data is consistent in showing a similar trend for greater charge weights but does not cover a sufficient range of depth to indicate a maximum value.

A second way of assessing the effectiveness of a charge in producing an airborne dust cloud is to examine the ratio of the depth of the apparent crater to the charge depth. As shown in Fig. 6.2, the apparent crater depth is considerably greater than charge depth for shallow shots, but becomes equal to charge depth at scaled depths somewhat greater than 1.0 ft/lb$^{1/3}$ and decreases to considerably less than charge depth for deeper charges, particularly in dry clay. Physically, this indicates that with deeper charges, much of the soil in the column and jet drops back into the relatively deep true crater and remains there.

It is of interest to compare the ratios of the diameter of the true crater to maximum column diameter, as the true crater may indicate the size of the rising jet. Fig. 6.3 shows that the column is about twice the crater size for charges fired between scaled depths of 0.135 and 1.02 ft/lb$^{1/3}$, but approaches crater diameter when charges are fired at deeper positions. When the column expands only slightly beyond the limits of the crater, much of the falling soil will drop down into the crater and remain there. For scaled depths greater than λ_c = 3.07 ft/lb$^{1/3}$, column diameter probably becomes equal to crater diameter, to the maximum depth at which craters will form (about λ_c = 5.0 ft/lb$^{1/3}$).[5]

Probably the optimum condition for base surge formation is obtained when the rising column attains a diameter twice the crater diameter, at about λ_c = 1.0 ft/lb$^{1/3}$. When the charge is very shallow, the relatively wide column formed has a bulk density too low to set up the pronounced density current needed for the formation of a large clearly-defined base surge.

The crater measurements presented here are consistent with the measured areas of dust deposit in indicating that a maximum volume of airborne soil is produced by a charge fired at a scaled depth of about

---

[5] C. W. Lampson, "Underground Explosions", Appendix B, The Effects of Atomic Weapons, U. S. Atomic Energy Commission, Washington, D. C., Sept. 1950, p 421.

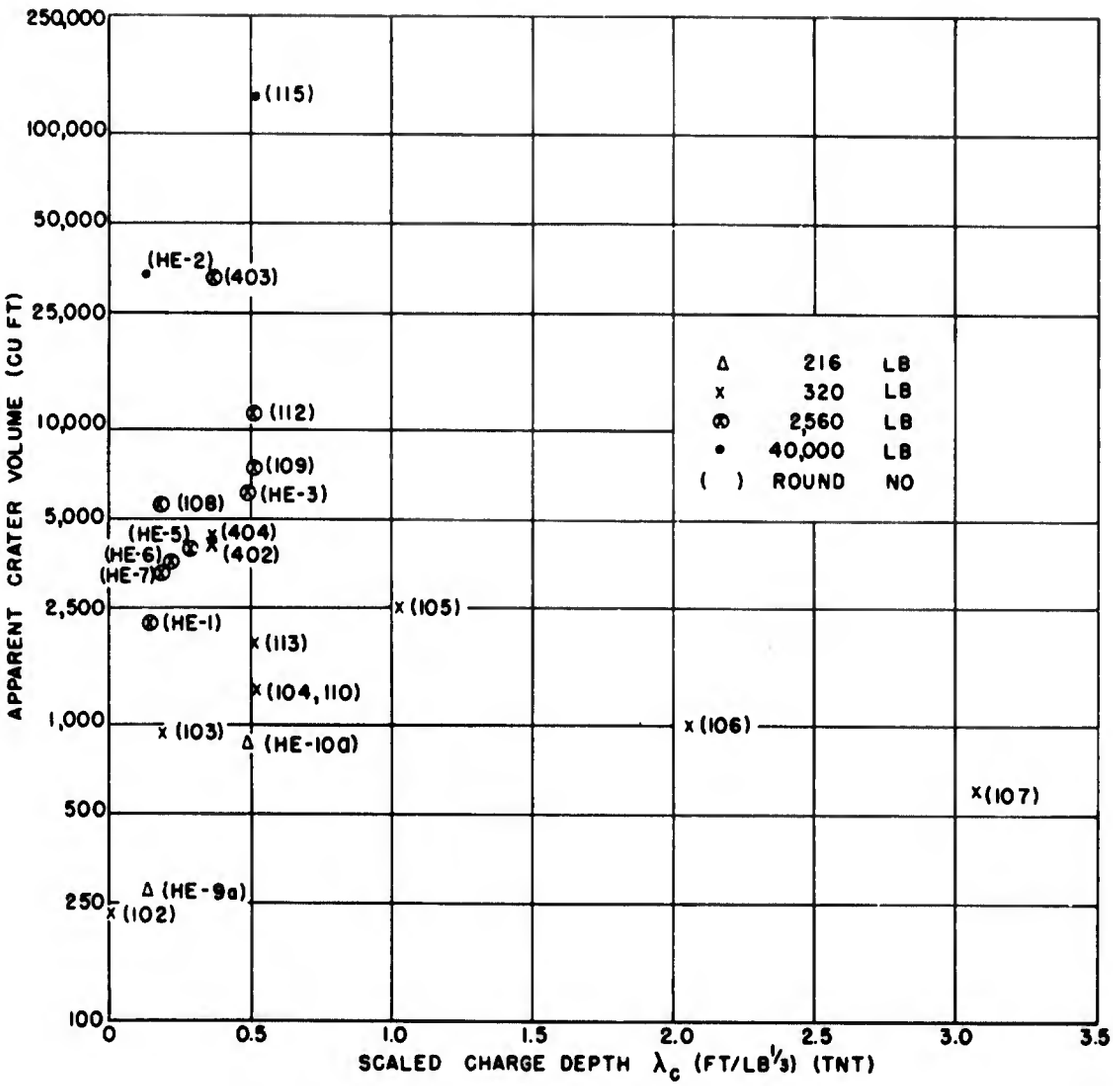

Fig. 6.1 Apparent Crater Volume vs Scaled Charge Depth

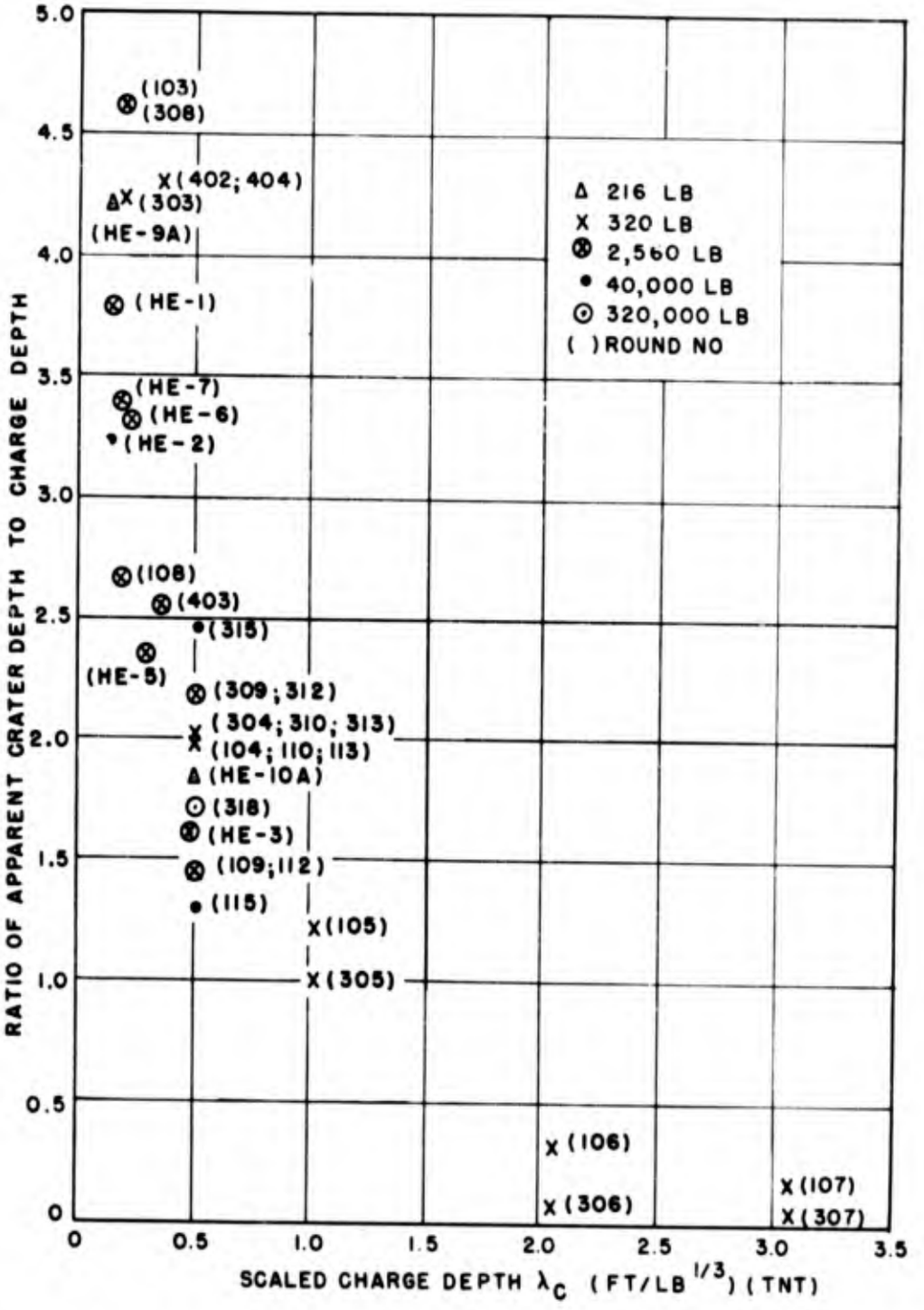

Fig. 6.2 Ratio of Apparent Crater Depth to Charge Depth vs Scaled Charge Depth

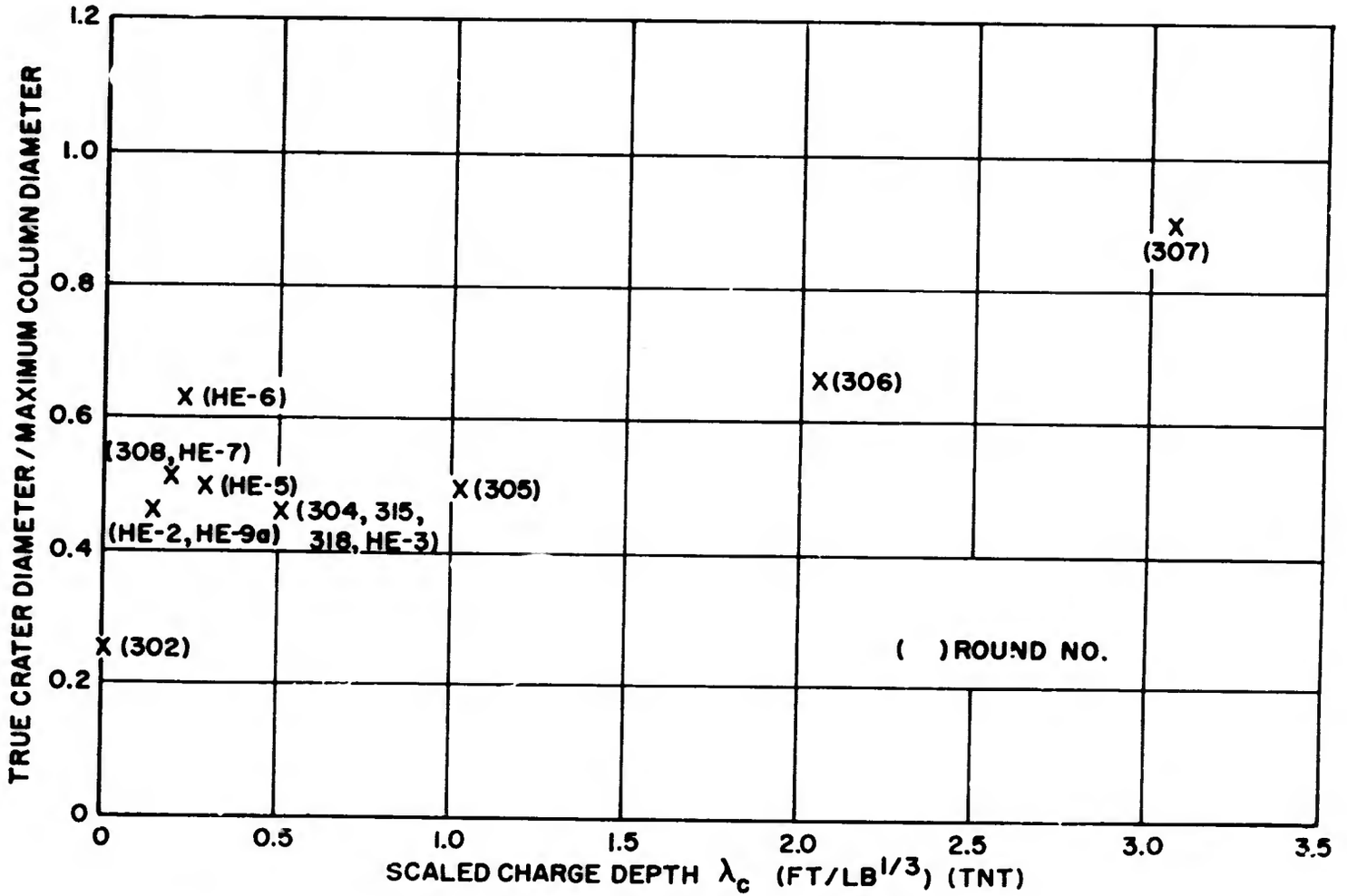

Fig. 6.3 Ratio of True Crater Diameter to Maximum Column Diameter vs Scaled Charge Depth

$\lambda_c = 1.0$ ft/lb$^{1/3}$.

In these studies, the largest craters were produced in wet clay, indicating that crater size alone is not a good criterion of the effectiveness of the charge in producing a base surge. Crater size will aid in the estimation of the amount of soil raised into the air, but the behavior of the ejected soil depends upon its physical characteristics, such as moisture content, particle size and cohesiveness.

[redacted]

CHAPTER 7

SOIL EFFECTS

7.1 SOIL CHARACTERISTICS FAVORABLE FOR BASE SURGE FORMATION

The size and rate of growth of the base surge produced by an underground explosion is obviously dependent upon the nature of the soil. The amount of data available is not adequate for a quantitative study of the soil effect, but the records of the Dugway series in three soil types indicate that well-developed surges are formed in dry sand, dry clay, and wet clay, with the largest surge clouds resulting from the dry sand tests and the smallest from the wet clay. The surge clouds produced in the Nevada high explosive tests were similar to those in the Dugway dry clay rounds, though the soil appeared to be a mixture of limestone, sand, and clay.[1]

It may be significant that the seismic velocities ranged from 750 to 2000 fps at the dry sand site,[2] from 2500 to 3500 fps at the dry clay site,[3] and from 5000 to 6000 fps in the wet clay.[4] The seismic velocity at the Nevada test site was 3000 fps.[5]

---

[1] R. D. Cadle and A. G. Wilder, Composition of Clouds Formed by TNT Explosions, (HE Tests-Operation JANGLE), Technical Report No. 3, Stanford Research Institute, Stanford, Calif., ONR Project NR 350-023, SRI Project 412-317, Oct. 1951, p 5.

[2] Instrumentation for Underground Explosion Test Program, Interim Technical Report No. 2, Dry Sand, Engineering Research Associates, Inc., Contract No. DA-04-167-eng-298, 1 Oct. 1951, p 2-19.

[3] Underground Explosion Tests, Program "A", Tests in Soils, Protective Construction Branch, Engineering Division, Office, Chief of Engineers, Nov. 1950, p 2.

[4] Instrumentation for Underground Explosion Test Program, Interim Technical Report No. 3, Wet Clay, Engineering Research Associates, Inc., Contract No. DA-04-167-eng-298, 1 Nov. 1951, pp 2-49 to 2-51.

[5] Interim Report - HE Tests - Operation JANGLE, Project 1(9), Stanford Research Institute, Stanford, Calif., Oct. 1951, p 3.

[redacted]

It appears, therefore, that the size of the base surge formed by an underground explosion is related inversely to the velocity of propagation of seismic waves in the soil. This seems reasonable, as heavy plastic wet clays are good transmitters of seismic waves while light loamy soils are very poor in this respect.[6] The highly cohesive clays do not separate easily into the fine particles needed to establish a downward density current and radial base surge, while the powdery low-cohesive soils are favorable for the formation of such a density flow and the development of a light particulate cloud which will propagate for a long distance. In general, wet soils would be less suited to base surge formation than dry soils.

Thus, the available data indicate that a single soil characteristic - the seismic velocity - might be used as an indicator of the probable success of a soil type as a base surge producer. If this point of view is correct, a soil type such as dry loess would be one of the most favorable for the production of a large, long-persisting base surge.

---

[6] C. W. Lampson, "Underground Explosions", Appendix B, The Effects of Atomic Weapons, U. S. Atomic Energy Commission, Washington, D. C., Sept. 1950, pp 410-416.

[redacted]

CHAPTER 8

EFFECT OF CHARGE SIZE

8.1 GENERAL

The data presented in this report were obtained from records of TNT explosions. Results were fairly consistent for similar soil types and scaling was generally satisfactory for charges weighing from 320 to 320,000 lb at scaled depths ranging from 0.185 to 2.05 ft/lb$^{1/3}$. However, the simple scaling methods used were not adequate for very shallow and very deep charges and possibly would not apply outside the range of weights used. In addition, the possibility exists that explosives other than TNT might produce somewhat different surface phenomena, due to differences in explosion products, energy per unit volume, heat of detonation, or other factors.

The effects of charge size and shape might become important for shallow explosions, when part or all of the charge is exposed to the air at detonation. The scaled depth of 0.135 ft/lb$^{1/3}$ is probably transitional for spherical TNT charges, because the top of the charge is tangent to the surface of the ground at this position. The characteristics of the surface phenomena change markedly in this shallow zone, and the base surge becomes very tenuous and difficult to detect, though a true, but weak, density flow exists at λ_c = 0.135 ft/lb$^{1/3}$.

The size and rate of growth of a base surge depend upon the volume of earth ejected from the ground and the size and concentration of the soil particles in the earth column. As shown in Fig. 8.1, the volume of the true crater decreases rapidly with decreasing charge depth in the shallow range, indicating that considerably less soil is thrown into the air by shallow charges, and the relatively wide columns at λ_c = zero indicate that the soil particles are widely separated.

The lack of a soil covering above the charge probably reduces the efficiency of the explosion as a producer of a base surge, though it should not be inferred that only the soil above the charge enters the base surge. Visual study of the films of underground explosions shows that the ground surrounding a charge is lifted into an earth column which drops and flows outward to form the base surge. The earth directly above the charge is probably carried upward by the rising jet.

The effect of the thickness of the earth covering (overburden) above a charge might be determined by firing explosives with a greater energy per unit volume than TNT at the same scaled depths as the equivalent TNT charges. Another possible experimental approach would be

[redacted]

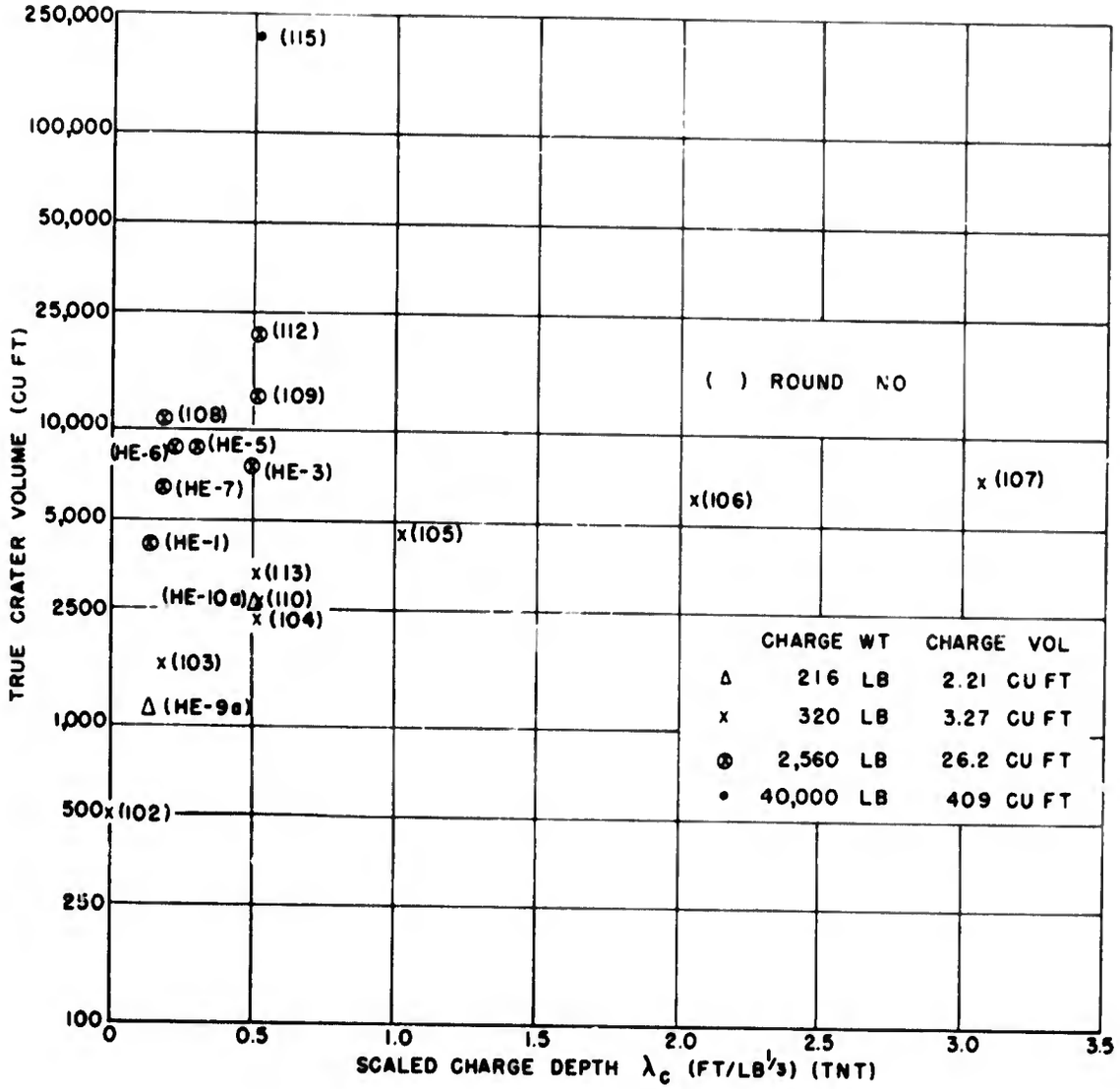

Fig. 8.1 True Crater Volume vs Scaled Charge Depth

the use of a series of TNT charges of different shapes but the same weight, with the center of gravity at the same depth.

If an explosive with the equivalent energy of a charge of TNT, but smaller in size, produces a crater equal in size to the TNT crater, it might be assumed that the additional volume of soil displaced would favor the formation of a larger surge. However, within the range of energy density of conventional high explosives, differences in charge volume are insignificant when compared to the total volume of soil ejected from the crater.

8.2 COMPARISON OF TNT AND PENTOLITE

A test of the effect of charge volume on the base surge was conducted as part of the HE program at Nevada.[1] The experiment consisted of simultaneous detonations of 216 lb of TNT and 177 lb of Pentolite, with equivalent energies, fired at scaled depths of 0.181, 0.139, and 0.500 ft/lb$^{1/3}$. (See Table 1.2.)

Round HE-8 (λ_c = 0.181) was not satisfactory, due to inadequate priming of the TNT charge and an anomalous behavior of the Pentolite jet, which rose to an exceptionally great height.

Rounds HE-9 (λ_c = 0.139) and HE-10 (λ_c = 0.500) produced clearly defined base surges. The surge radii and heights are given in Figs. 8.2 and 8.3, and overall heights are shown in Fig. 8.4, as functions of time. Unsmoothed surge data is shown for both shots, and two camera records are given for HE-9, to illustrate the degree of scatter and lack of consistent trends. There appears to be no significant difference between the radial growth and extent of the surge clouds produced by the two explosives, but considerable difference appears in the growth of the jet. The pentolite jets rose to greater heights in both cases and were whitish in appearance, while the jets formed by TNT were black. Following Round HE-9, both jets remained airborne and drifted with the wind but for HE-10 the jet produced by TNT fell rapidly while part of the Pentolite jet remained aloft. Some of these effects are illustrated in Fig. 8.5.

This test showed how above-ground activity might vary with different explosives, but did not show any significant effect of charge volume on the size of the base surge. The earth cover was 1-1/8 inches over

---

[1] D. C. Campbell, LCDR, USN, Tests and Observations on Craters and Base Surges, JANGLE Report 1(9)-3, 1 Nov. 1951.

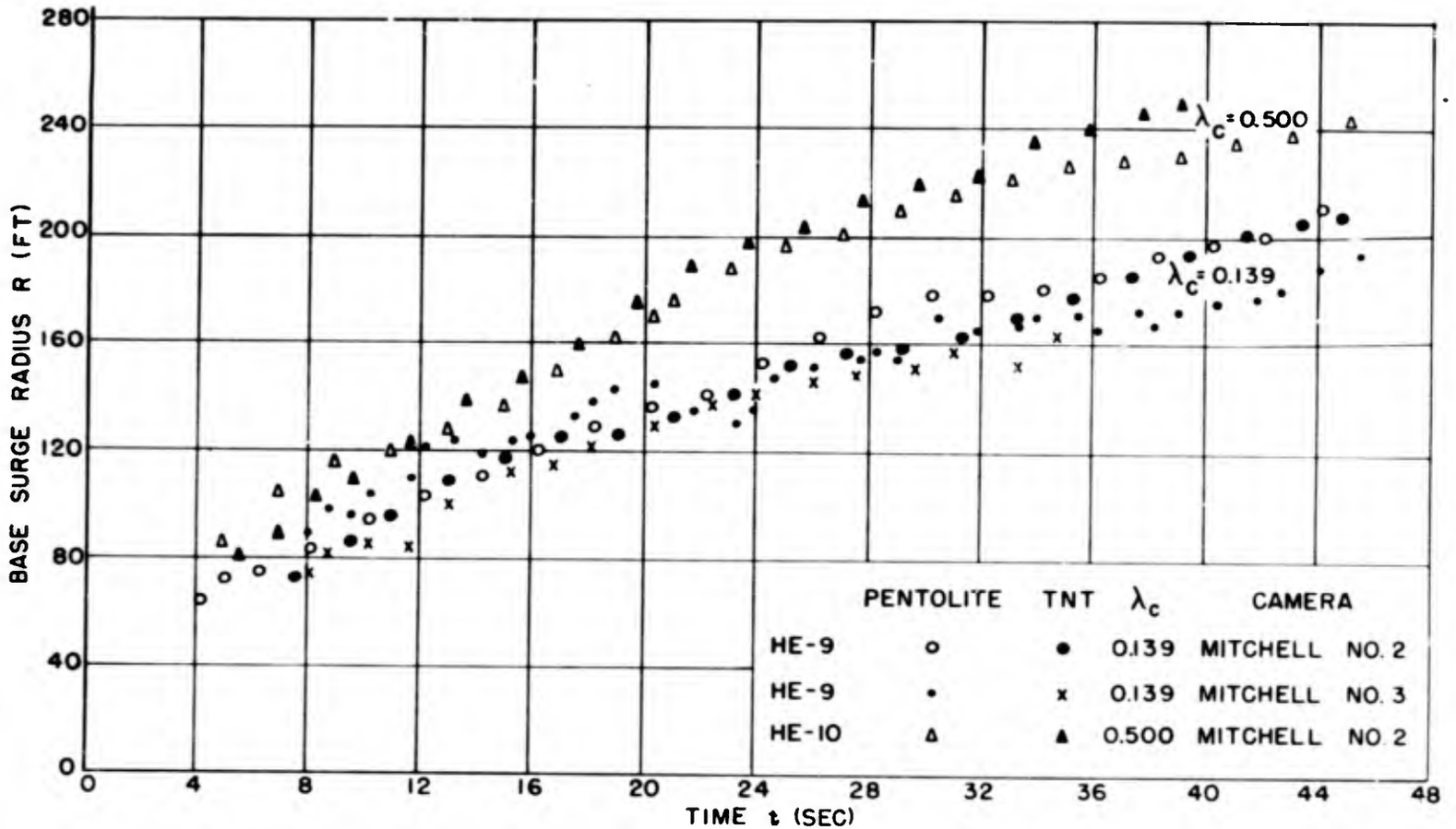

Fig. 8.2 Base Surge Radius vs Time - TNT and Pentolite Comparison

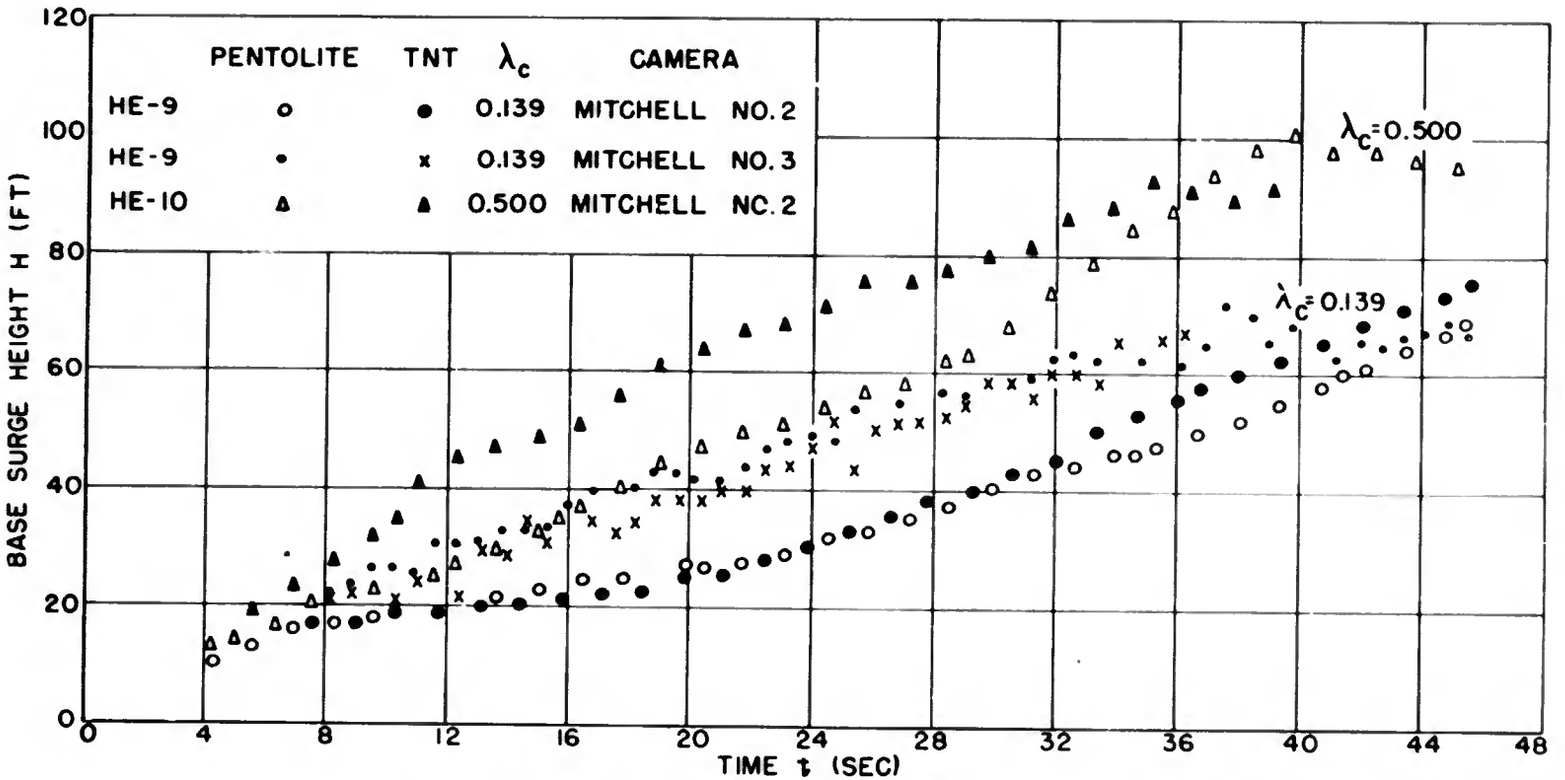

Fig. 8.3 Base Surge Height vs Time - TNT and Pentolite Comparison

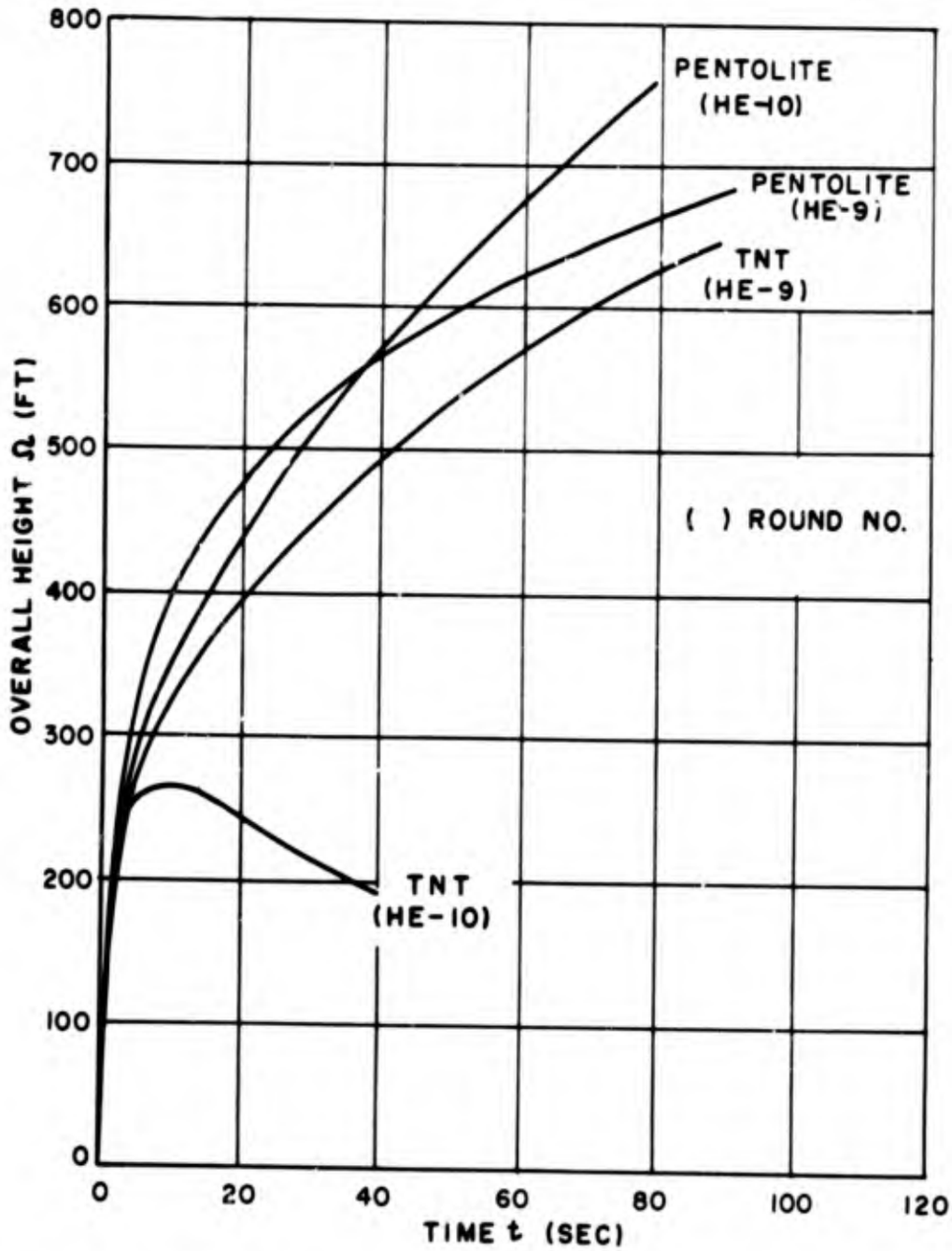

Fig. 8.4 Overall Height vs Time - TNT and Pentolite Comparison

PROJECT 1(9)-4

0.5 SEC

10 SEC

2.0 SEC

20 SEC

5.0 SEC

40 SEC

CHARGE WEIGHTS:
PENTOLITE (LEFT EXPLOSION)
= 177 LB
TNT (RIGHT EXPLOSION)
= 216 LB

CHARGE DEPTH = 3 FT
SCALED DEPTH = 0.500 FT/LB $^{1/3}$

Fig. 8.5 Surface Phenomena Produced by TNT and Pentolite - Round HE-10

the Pentolite charge and zero over the TNT charge for Round HE-9 but surge growth was essentially the same. For this round the volume of the true crater formed by Pentolite was 1310 cu ft and the TNT true crater volume was 1120 cu ft. The difference between charge volumes was 0.52 cu ft.

[redacted]

PROJECT 1(9)-4

BIBLIOGRAPHY

A. B. Arons, Experimental Investigations of Base Surge Phenomena, Interim Report No. 1 of NOL Project 152, NAVORD Report 1501, 13 July 1950.

A. B. Arons, G. Wertheim, and M. Krumholz, Density Currents Induced by Streams of Falling Particles, Woods Hole Oceanographic Institution, Woods Hole, Mass., NAVORD Report 485, 21 March 1951.

A. B. Arons, G. A. Young, and M. L. Milligan, Further Investigation of the Base Surge, Interim Report No. 3 of NOL Project 152, NAVORD Report 2144, 1 June 1951.

R. D. Cadle and A. G. Wilder, Composition of Clouds Formed by TNT Explosions (HE Tests-Operation JANGLE), Technical Report No. 3, Stanford Research Institute, Stanford, Calif., ONR Project NR350-023, SRI Project 412-317, Oct. 1951.

D. C. Campbell, LCDR, USN, Tests and Observations on Craters and Base Surges, JANGLE Report 1(9)-3, 1 Nov. 1951.

J. S. Coles and G. A. Young, Investigations of Base Surge Phenomena by Means of High Explosives and a Liquid Model, Interim Report No. 2 of NOL Project 152, NAVORD Report 1744, 1 Sept. 1950.

S. W. Grinnell, W. A. Perkins, and F. X. Webster, Bimonthly Report No. 3 of Chemical Warfare Service Research and Development Program, Contract No. W-18-035-CWS-1256, Stanford University, Calif., May-June 1946.

Instrumentation for Underground Explosion Test Program, Interim Technical Report No. 1, Dry Clay, Engineering Research Associates, Inc., Contract No. DA-04-167-eng-298, 1 Aug. 1951.

Instrumentation for Underground Explosion Test Program, Interim Technical Report No. 2, Dry Sand, Engineering Research Associates, Inc., Contract No. DA-04-167-eng-298, 1 Oct. 1951.

Instrumentation for Underground Explosion Test Program, Interim Technical Report No. 3, Wet Clay, Engineering Research Associates, Inc., Contract No. DA-04-167-eng-298, 1 Nov. 1951.

Interim Report - HE Tests - Operation JANGLE, Project 1 (9), Stanford Research Institute, Stanford, Calif., Oct. 1951.

[redacted]

[redacted]

PROJECT 1(9)-4

C. W. Lampson, "Underground Explosions", Appendix B, The Effects of Atomic Weapons, U. S. Atomic Energy Commission, Washington, D. C., Sept. 1950, pp 410-423.

W. M. Latimer, "Behavior of Gas Clouds", Military Problems with Aerosols and Nonpersistent Gases, Summary Technical Report of Division 10, NDRC, Vol 1, Washington, D. C., 1946, pp 260-283.

J. C. Martin and W. J. Moyce, "An Experimental Study of the Collapse of Fluid Columns on a Rigid Horizontal Plane, in a Medium of Lower, but Comparable, Density", Philosophical Transactions of the Royal Society of London, Series A, No. 882, Vol 244, 4 March 1952, pp 325-334.

V. Salmon, Throw-Out Phenomena in Underground Explosions, Status Report No. 6, Contract N7onr32104, Stanford Research Institute Project 317, 29 March 1951.

Underground Explosion Tests, Program "A" - Tests in Soils, Protective Construction Branch, Engineering Division, Office, Chief of Engineers, Nov. 1950.

[redacted]

[redacted]

DISTRIBUTION

	Copy No.
ARMY ACTIVITIES	
Asst. Chief of Staff, G-1, Department of the Army, Washington 25, D. C.	1
Asst. Chief of Staff, G-2, Department of the Army, Washington 25, D. C.	2
Asst. Chief of Staff, G-3, Department of the Army, Washington 25, D. C.	3- 6
Asst. Chief of Staff, G-4, Department of the Army, Washington 25, D. C.	7- 11
Chief of Ordnance, Department of the Army, Washington 25, D. C.	12- 14
Chief Chemical Officer, Temp. Bldg. T-7, Room G-522, Gravelly Point, Va.	15- 18
Chief of Engineers, Temp. Bldg. T-7, Room G-425, Gravelly Point, Va.	19- 21
The Quartermaster General, Second and T Sts. SW, Room 1139A, Washington 25, D. C.	22- 26
Chief of Transportation, Temp. Bldg, T-7, Room G-816, Gravelly Point, Va.	27- 28
Chief Signal Officer, Department of the Army, Washington 25, D. C.	29- 31
The Surgeon General, Main Navy Bldg., Room 1651, Washington 25, D. C.	32- 34
Provost Marshal General, Main Navy Bldg., Room 1065, Washington 25, D. C.	35- 37
Chief, Army Field Forces, Fort Monroe, Va.	38- 41
President, Army Field Forces Board No. 1, Fort Bragg, N. C.	42
President, Army Field Forces Board No. 2, Fort Knox, Ky.	43
President, Army Field Forces Board No. 3, Fort Benning, Ga.	44
President, Army Field Forces Board No. 4, Fort Bliss, Tex.	45
Commandant, The Infantry School, Fort Benning, Ga.	46- 47
Commandant, The Armored School, Fort Knox, Ky.	48- 49
President, The Artillery School Board, Fort Sill, Okla.	50- 51
Commandant, The AA&GM Branch, The Artillery School, Fort Bliss, Tex.	52- 53
Commandant, Army War College, Carlisle Barracks, Pa.	54- 55
Commandant, Command and General Staff College, Fort Leavenworth, Kans.	56- 57
Commandant, Army General School, Fort Riley, Kans.	58

[redacted] [redacted]

[redacted]

DISTRIBUTION (Continued)

	Copy No.
Commanding General, First Army, Governor's Island, New York 4, N. Y.	59- 60
Commanding General, Second Army, Fort George G. Meade, Md.	61- 62
Commanding General, Third Army, Fort McPherson, Ga.	63- 64
Commanding General, Fourth Army, Fort Sam Houston, Tex.	65- 66
Commanding General, Fifth Army, 1660 E. Hyde Park Blvd., Chicago 15, Ill.	67- 68
Commanding General, Sixth Army, Presidio of San Francisco, Calif.	69- 70
Commander-in-Chief, European Command, APO 403, c/o Postmaster, New York, N. Y.	71- 72
Commander-in-Chief, Far East, APO 500, c/o Postmaster, San Francisco, Calif.	73- 74
Commanding General, U. S. Army, Pacific, APO 958, c/o Postmaster, San Francisco, Calif.	75- 76
Commanding General, U. S. Army, Caribbean, APO 834, c/o Postmaster, New Orleans, La.	77- 78
Commanding General, U. S. Army, Alaska, APO 942, c/o Postmaster, Seattle, Wash.	79- 80
Director, Operations Research Office, 6410 Connecticut Ave., Chevy Chase, Md.	81- 83
Commanding Officer, Ballistic Research Laboratories, Aberdeen Proving Ground, Aberdeen, Md.	84- 85
Commanding Officer, Engineer Research and Development Laboratory, Fort Belvoir, Va.	86- 87
Commanding Officer, Signal Corps Engineering Laboratories, Fort Monmouth, N. J.	88- 89
Commanding Officer, Evans Signal Laboratory, Belmar, N. J.	90- 91
Commanding General, Army Chemical Center, Md. ATTN: Chemical and Radiological Laboratory	92- 93

NAVY ACTIVITIES

Chief of Naval Operations, Department of the Navy, Washington 25, D. C. ATTN: Op-36	94- 95
Chief, Bureau of Ships, Department of the Navy, Washington 25, D. C.	96- 99
Chief, Bureau of Ordnance, Department of the Navy, Washington 25, D. C.	100
Chief, Bureau of Medicine and Surgery, Department of the Navy, Washington 25, D. C.	101-102
Chief, Bureau of Aeronautics, Department of the Navy, Washington 25, D. C.	103-104
Chief, Bureau of Supplies and Accounts, Department of the Navy, Washington 25, D. C.	105-106
Chief, Bureau of Yards and Docks, Department of the Navy, Washington 25, D. C.	107-109

[redacted]

[redacted]

DISTRIBUTION (Continued)

	Copy No.
Chief of Naval Personnel, Department of the Navy, Washington 25, D. C.	110
Commandant of the Marine Corps, Washington 25, D. C.	111-113
Commander-in-Chief, U. S. Pacific Fleet, Fleet Post Office, San Francisco, Calif.	114
Commander-in-Chief, U. S. Atlantic Fleet, Fleet Post Office, New York, N. Y.	115
President, U. S. Naval War College, Newport, R. I.	116
Commandant, Marine Corps Schools, Quantico, Va.	117-118
Chief of Naval Research, Department of the Navy, Washington 25, D. C.	119-120
Commander, U. S. Naval Ordnance Laboratory, Silver Spring 19, Md.	121
Commander, U. S. Naval Ordnance Laboratory, Silver Spring 19, Md. ATTN: Aliex	122
Director, U. S. Naval Research Laboratory, Washington 25, D. C.	123
Commanding Officer and Director, U. S. Naval Electronics Laboratory, San Diego 52, Calif.	124
Commanding Officer, U. S. Naval Radiological Defense Laboratory, San Francisco 24, Calif.	125-128
Commanding Officer and Director, David Taylor Model Basin, Washington 7, D. C.	129
Commander, Naval Material Laboratory, New York Naval Shipyard, Naval Base, New York 1, N. Y.	130
Officer-in-Charge, U. S. Naval Civil Engineering Research and Evaluation Laboratory, U. S. Naval Construction Battalion Center, Port Hueneme, Calif.	131-132
Commanding Officer, U. S. Naval Medical Research Institute, National Naval Medical Center, Bethesda 14, Md.	133
Commander, U. S. Naval Ordnance Test Station, Inyokern, China Lake, Calif.	134

AIR FORCE ACTIVITIES

Assistant for Atomic Energy, Headquarters, United States Air Force, Washington 25, D. C.	135-136
Director of Operations, Headquarters, United States Air Force, Washington 25, D. C. ATTN: Operations Analysis Division	137-138
Director of Plans, Headquarters, United States Air Force, Washington 25, D. C. ATTN: AFOPD-P1	139
Director of Requirements, Headquarters, United States Air Force, Washington 25, D. C.	140
Director of Research and Development, Headquarters, United States Air Force, Washington 25, D. C.	141-142
Director of Intelligence, Headquarters, United States Air Force, Washington 25, D. C. ATTN: Phys. Vul. Branch, Air Targets Division	143-144

[redacted] [redacted]

[redacted]

DISTRIBUTION (Continued)

	Copy No.
Director of Installations, Headquarters, United States Air Force, Washington 25, D. C.	145
Asst. for Development Planning, Headquarters, United States Air Force, Washington 25, D. C.	146
Asst. for Materiel Program Control, Headquarters, United States Air Force, Washington 25, D. C	147
The Surgeon General, Headquarters, United States Air Force, Washington 25, D. C.	148
Commanding General, Strategic Air Command, Offutt Air Force Base, Nebr.	149-151
Commanding General, Air Research and Development Command, P.O. Box 1395, Baltimore 3, Md.	152-161
Commanding General, Air Materiel Command, Wright-Patterson Air Force Base, Dayton, Ohio	162-163
Commanding General, Air Materiel Command, Wright-Patterson Air Force Base, Dayton, Ohio. ATTN: Air Installations Division	164-165
Commanding General, Tactical Air Command, Langley Air Force Base, Va.	166-168
Commanding General, Air Defense Command, Ent Air Force Base, Colo.	169-171
Commanding General, Air Proving Ground, Eglin Air Force Base, Fla.	172-173
Commanding General, Air Training Command, Scott Air Force Base, Belleville, Ill.	174-176
Commanding General, Air University, Maxwell Air Force Base, Montgomery, Ala.	177-179
Commanding General, Special Weapons Center, Kirtland Air Force Base, N. Mex.	180-182
Commanding General, 1009th Special Weapons Squadron, 1712 G St. NW, Washington 25, D. C.	183
Commanding General, Wright Air Development Center, Wright-Patterson Air Force Base, Dayton, Ohio	184-187
Commanding General, Air Force Cambridge Research Center, 230 Albany St., Cambridge 39, Mass.	188-189
Commanding General, U. S. Air Forces in Europe, APO 633, c/o Postmaster, New York, N. Y.	190-191
Commanding General, Far East Air Forces, APO 925, c/o Postmaster, San Francisco, Calif.	192-193
Commanding General, Air Force Missile Center, Patrick Air Force Base, Cocoa, Fla.	194
Commandant, USAF School of Aviation Medicine, Randolph Air Force Base, Randolph Field, Tex.	195
Asst. to the Special Asst., Chief of Staff, United States Air Force, Washington 25, D. C. ATTN: David T. Griggs	196
The RAND Corporation, 1500 Fourth St., Santa Monica, Calif.	197-198

[redacted] [redacted]

DISTRIBUTION (Continued)

	Copy No.
AFSWP ACTIVITIES	
Chief, Armed Forces Special Weapons Project, P.O. Box 2610, Washington 13, D. C.	199-207
Commanding General, Field Command, Armed Forces Special Weapons Project, P.O. Box 5100, Albuquerque, N. Mex.	208-210
Commanding Officer, Test Command, Armed Forces Special Weapons Project, P.O. Box 5600, Albuquerque, N. Mex.	211-213
OTHER ACTIVITIES	
Chairman, Research and Development Board, Department of Defense, Washington 25, D. C.	214
Director, Weapons System Evaluations Group, Office of the Secretary of Defense, Washington 25, D. C.	215
Executive Director, Committee on Atomic Energy, Research and Development Board, Department of Defense, Washington 25, D. C. ATTN: David Beckler	216
Executive Director, Committee on Medical Sciences, Research and Development Board, Department of Defense, Washington 25, D. C.	217
U. S. Atomic Energy Commission, Classified Document Room, 1901 Constitution Ave., Washington 25, D. C. ATTN: Mrs. J. M. O'Leary	218-220
Los Alamos Scientific Laboratory, Report Library, P.O. Box 1663, Los Alamos, N. Mex. ATTN: Helen Challenger	221-223
Sandia Corporation, Classified Document Division, Sandia Base, Albuquerque, N. Mex. ATTN: Wynne K. Cox	224-243

AEC, Oak Ridge, Tenn., A31902

[redacted] [redacted]